# Enhancing the Bioavailability of Some Therapeutically Potent Plant Secondary Metabolites through Development of Novel Delivery Systems

**Thesis Submitted By**
**Ranjit Kumar Harwansh, M. Pharm**
Index No. 201/13/Ph

**Doctor of Philosophy (Pharmacy)**

**School of Natural Product Studies**
**Department of Pharmaceutical Technology**
**Faculty Council of Engineering & Technology**
**Jadavpur University**
**Kolkata, India**

**2016**

**JADAVPUR UNIVERSITY**
**KOLKATA – 700032, INDIA**

**Index No. 201/13/Ph**

**1. Title of the thesis:**

Enhancing the bioavailability of some therapeutically potent plant secondary metabolites through development of novel delivery systems

**2. Name, designation & institution of the supervisor:**

Prof. Pulok K Mukherjee, *M. Pharm, PhD, FRSC*
Director, School of Natural Product Studies
Department of Pharmaceutical Technology
Jadavpur University, 188, Raja S.C. Mullick Road,
Kolkata - 700032, India

**3. List of publications:**

**a)** Pulok K. Mukherjee, Ranjit K. Harwansh, Sauvik Bhattacharyya. Bioavailability of herbal products: approach toward improved pharmacokinetics, in: P.K. Mukherjee (Eds.), Evidence-based validation of herbal medicine, Elsevier, Amsterdam, 2015, pp. 217-245.

**b)** Ranjit K. Harwansh, Pulok K. Mukherjee, Shiv Bahadur, Rajarshi Biswas. Enhanced permeability of ferulic acid loaded nanoemulsion based gel through skin against UVA mediated oxidative stress. Life Sciences, Elsevier, 2015, 141, 202-211, doi: 10.1016/j.lfs.2015.10.001 (Impact Factor: 2.70).

**c)** Ranjit K Harwansh, Pulok K Mukherjee, Amit Kar, Shiv Bahadur, Naif Abdullah Al-Dhabi, V. Duraipandiyan. Enhancement of photoprotection potential of catechin loaded nanoemulsion gel against UVA induced oxidative stress. Journal of Photochemistry and Photobiology B: Biology, Elsevier, 2016, 160, 318-329, doi: 10.1016/j.jphotobiol.2016.03.026 (Impact Factor: 2.96).

**d)** Ranjit K Harwansh, Pulok K Mukherjee, Sayan Biswas. Nanoemulsion based nano-gel of genistein enhancing UVA protection efficacy and bioavailability by improving its pharmacokinetics through transdermal route. Journal of Pharmaceutical and Biomedical Analysis, Elsevier, 2016, Impact Factor: 2.82 (Communicated).

**4. List of patents:** Nil

**5. List of presentations in national and international conferences:**

**a)** Ranjit K Harwansh, Pulok K Mukherjee, Rajarshi Biswas, Sayan Biswas, Shiv Bahadur. Nanoemulsion based nano-gel of genistein enhancing UVA protection efficacy and bioavailability by improving its pharmacokinetics through transdermal delivery. 3rd International Congress of Society for Ethnopharmacology (SFEC - 2016) on *"Ethnopharmacology and Evaluation of Medicinal Plants – Global Perspective"*, at the Pt. Ravishankar Shukla University, Raipur, India, February 19-21, 2016.

**b)** Ranjit K Harwansh, Pulok K Mukherjee, Rajarshi Biswas, Joydeb Chanda, Amit Kar, Shiv Bahadur, Debayan Goswami. Enhanced bioavailability of ferulic acid through development of a novel drug delivery system using nanoemulsion based nanogel. 2nd National Convention of SFE-India on *"Integrated Approaches for Promotion and Development of Herbal Medicine"* at the Jadavpur University, Kolkata, India, December 5-6, 2015.

**c)** Ranjit K Harwansh, Pulok K Mukherjee, Rajarshi Biswas, Amit Kar, Shiv Bahadur. Enhanced bioavailability of catechin through nanoemulsion based nano-gel via transdermal route. UGC Sponsored National Seminar on *"Prospects of Pharmacy Education"* at the Pt. Ravishankar Shukla University, Raipur, India, November 19-21, 2015.

**d)** Ranjit K Harwansh, Pulok K Mukherjee. Enhancing transdermal delivery of catechin via nanoemulsion based novel delivery system. 1st National Convention of SFE-India on *"Opportunities in Medicinal Plant Research"*, at the Jadavpur University, Kolkata, India, November 29-30, 2014.

**e)** Ranjit K Harwansh, Joydeb Chanda, Pulok K Mukherjee. Enhancing topical effect of ferulic acid against UVA induced oxidative stress via nanoemulsion based novel delivery system. 53rd National Pharmacy Week Celebration, *"IPA's Platinum Jubilee Celebration"*, Indian Pharmaceutical Association (Bengal Branch) at the Jadavpur University, Kolkata, India, November 16, 2014.

**School of Natural Product Studies**
**Department of Pharmaceutical Technology**
**Jadavpur University**
**Kolkata 700032, India**

***CERTIFICATE FROM THE SUPERVISOR***

This is to certify that the thesis entitled "Enhancing the bioavailability of some therapeutically potent plant secondary metabolites through development of novel delivery systems" submitted by Shri Ranjit Kumar Harwansh, who got his name registered on November 27, 2013 for the award of Ph.D. (Pharmacy) degree of Jadavpur University is absolutely based upon his own work under the supervision of Prof. Pulok K. Mukherjee and that neither his thesis nor any part of the thesis has been submitted for any degree/diploma or any other academic award anywhere before.

**Prof. Pulok K Mukherjee,** *M. Pharm, PhD, FRSC*
Director, School of Natural Product Studies
Department of Pharmaceutical Technology
Jadavpur University
Kolkata - 700032, India

## Declaration

I hereby declare that my research work embodied in this Ph.D. thesis entitled “Enhancing the bioavailability of some therapeutically potent plant secondary metabolites through development of novel delivery systems” have been carried out by me in the School of Natural Product Studies, Department of Pharmaceutical Technology, Jadavpur University, West Bengal, Kolkata, India under the direct supervision of Prof. Pulok K. Mukherjee, Director, School of Natural Product Studies, Department of Pharmaceutical Technology, Jadavpur University, West Bengal, Kolkata, India. I also confirm that this work is original and has not been submitted partially or in full for any other degree or diploma to this or other University or Institute.

Date: Signature

Place: Kolkata **Ranjit Kumar Harwansh**

**CONTENTS** **PAGE NO.**


| | | |
|---|---|---|
| | Front page | i |
| | Title, list of publications & presentations | ii-iii |
| | Certificate | iv |
| | Declaration | v |
| | Contents | vi |
| | Financial support | vii |
| | List of figures | viii-x |
| | List of tables | xi-xii |
| | Abbreviations | xiii-xiv |
| | Dedication | xv |
| **Chapter - 1:** | Novel drug delivery systems (NDDS) for herbal drugs - enhancement of bioavailability | 1-52 |
| **Chapter - 2:** | Scope, objective and plan of work | 53-57 |
| **Chapter - 3:** | Formulation and evaluation of ferulic acid loaded nanoemulsion for its therapeutic benefit | 58-93 |
| **Chapter - 4:** | Catechin loaded nanoemulsion - formulation and its evaluation | 94-121 |
| **Chapter - 5:** | Development and evaluation of genistein loaded nanoemulsion for its therapeutic benefits | 122-147 |
| **Chapter - 6:** | Summary and conclusion | 148-158 |
| **Chapter - 7:** | References | 159-188 |
| | Acknowledgement | 189 |
| | Reprints of publications | |

## Financial support

I express my deep gratitude to the University Grant Commission, Govt. of India, New Delhi for awarding Rajiv Gandhi National Fellowship (UGC-RGNF) [Ref. No. F1-17.1/2014-15/ RGNF-2014-15-SC-CHH-63801/(SA-III/Website), February, 2015]

I am also thankful to the Department of Biotechnology, Govt. of India, New Delhi for financial support through DBT-Twinning project grant (Ref. No. BT/153/NE/TBP/2011 & Dt. 08/11/2011) for providing Senior Research Fellowship (SRF) at the School of Natural Product Studies, Department of Pharmaceutical Technology, Jadavpur University, Kolkata-700032, India.

## List of figures


| Figure No. | Title of figure | Page |
|---|---|---|
| 1.1. | Different novel delivery systems for herbal drugs | 23 |
| 1.2. | Salient features of novel herbal delivery system | 24 |
| 1.3. | Structure of liposome | 24 |
| 1.4. | Structure of noisome | 26 |
| 1.5. | Schematic representation of SLN | 28 |
| 1.6. | Structure of micelle | 29 |
| 1.7. | Schematic diagram of phytosome | 30 |
| 1.8. | Structure of microemulsion or nanoemulsion | 31 |
| 1.9. | A hypothetical pseudo-ternary phase diagram of an oil, water and surfactant/co-surfactant ($S_{mix}$) system with emphasis on nanoemulsion and emulsion phases | 34 |
| 1.10. | Schematic diagram of skin structure and major routes of drug penetration, (1) via the sweat ducts (intercellular pathway); (2) directly across the *stratum corneum* (intracellular pathway) and (3) through the hair follicles and sebaceous gland (folicullar pathway) | 44 |
| 2.1. | Work plan for the study | 57 |
| 3.1. | Schematic diagram of preparation of ferulic acid based nanoemulsion | 63 |
| 3.2. | Consequences of UV radiations on the skin | 71 |
| 3.3. | Solubility studies of FA in several excipients. Values were mean ± SEM (n = 6). $^{*}P$ & $^{**}P < 0.05$, $^{***}P < 0.01$ | 75 |
| 3.4 (A-E). | Pseudo-ternary phase diagrams of group I, indicating o/w nanoemulsion region at different Smix ratios | 76 |
| 3.5 (A-E). | Studies of pseudo-ternary phase diagrams for group II at various Smix | 77 |
| 3.6 (A-E). | Construction of pseudo-ternary phase diagrams for group III formulations at different Smix ratios | 78 |
| 3.7 (A-E). | Pseudo-ternary phase diagram studies for group IV formulations at Smix ratio (1:0-1:2) | 79 |
| 3.8. | Droplet size (a) and zeta potential (b) study of optimized formulation, FA-NE3 | 81 |
| 3.9. | Transmission electron microscope photograph (A) and UV spectra (B) of FA-NE3 nanoemulsion | 82 |
| 3.10. | HPTLC chromatogram of standard FA (A) and FA-NE3 formulation (B) | 83 |
| 3.11. | HPTLC plate (A) and 3D-chromatogram (BN) of standard ferulic acid and FA-NE3 formulation at 315 nm [S1-6 = Standard ferulic acid and F1-2 = FA-NE3 formulation] | 83 |

| | | |
|---|---|---|
| 3.12. | FTIR spectrum of ferulic loaded formulation, FA-NE3 (A), placebo formulation (B) and pure ferulic acid (C) | 85 |
| 3.13. | First order degradation kinetics of ferulic acid from FA-NE-3 at 40°C | 86 |
| 3.14. | Rheological behavior of placebo (a), FA-NG3 (b) where, $\eta$ = viscosity (Pa.s), $\gamma$ = shear rate (1/s) | 87 |
| 3.15. | Permeation study of ferulic acid from various nanoemulsions (A) FA-NE (1-5), (B) FA-CG, FA-NE3 and FA-NG3 through rat skin and (C) steady state flux of various formulations across rat skin [Values were mean ± SEM (n = 6), $^{c}P < 0.05$, $^{a, b}P < 0.01$] | 88 |
| 3.16. | Effect of FA loaded different gel formulations on (A) SOD, (B) GPX, (C) CAT and (D) TBARS levels in rat skin [Values were mean ± SEM (n = 6), $^{**}P < 0.05$, $^{***}P < 0.01$] | 90 |
| 3.17. | Plasma concentration profiles of ferulic acid in rats, after administration of oral suspension (~5 mg of FA) and FA-NG3 (~5 mg of FA), values were mean ± SD (n = 6) | 91 |
| 4.1. | Schematic presentation of preparation of catechin loaded nanoemulsion | 99 |
| 4.2. | Solubility studies of CA in several excipients<br>[Values were mean ± SEM (n = 6), $^{**}P < 0.05$, $^{***}P < 0.01$] | 105 |
| 4.3. | Construction of pseudo-ternary phase diagram for CA based formulations at Smix (1:0-1:2) | 106 |
| 4.4. | Droplet size (a) and zeta potential (b) analysis of CA-NE4 | 109 |
| 4.5. | TEM photograph (A) and UV spectra (B) analysis of CA-NE4 formulation | 110 |
| 4.6. | HPTLC chromatogram of pure CA (A) and catechin loaded nanoemulsion, CA-NE4 (B) | 110 |
| 4.7. | HPTLC plate (A) and 3D-chromatogram (B) of pure CA and CA-NE4 formulation at 280 nm [S1-6 = Standard catechin and F1-2 = CA-NE4 formulation] | 110 |
| 4.8. | FTIR spectrum of pure CA (A), placebo nanoemulsion (B) and CA-NE4 (C) | 112 |
| 4.9. | First order degradation kinetics of CA from CA-NE-4 at 40°C | 113 |
| 4.10. | Rheogram of placebo-NG4 (A) and CA-NG4 (B) where, $\eta$ = viscosity (Pa.s), $\gamma$ = shear rate (1/s) | 114 |
| 4.11. | Transdermal skin permeation profiles of CA from different nanoemulsions (A) CA-NE (1-5), (B) CA-CG, CA-NE4 and CA-NG4 through rat skin and (C) steady state flux of different formulations across rat skin [Values were mean ± SD (n = 3). $^{**}P < 0.05$, $^{***}P < 0.01$ when compared to the conventional group] | 115 |
| 4.12. | Effect of transdermal gel formulations of CA on different cutaneous antioxidant enzyme levels (A) SOD and GPX, (B) CAT and TBARS<br>[Values are mean ± SEM (n = 6), $^{**}P < 0.05$, $^{***}P < 0.01$ when compared to the control and UVA irradiated group] | 118 |

| | | |
|---|---|---|
| 4.13. | Plasma concentration profiles of CA in rats, after administration of oral suspension (~ 5 mg of CA) and CA-NG4 (~ 5 mg of CA) [Values were mean ± SD (n = 6)] | 119 |
| 5.1. | Schematic preparation techniques of GN based nanoemulsion formulation | 127 |
| 5.2. | Solubility studies of GN in several excipients<br>[Values were mean ± SEM (n = 6), $^{*}P$ & $^{**}P < 0.05$, $^{***}P < 0.01$] | 132 |
| 5.3. | Ternary phase diagrams indicating NEs (o/w) region at different $S_{mix}$ 1:0 (a), $S_{mix}$ 1:1 (b), $S_{mix}$ 1:2 (c), $S_{mix}$ 1:3 (d), $S_{mix}$ 2:1 (e), $S_{mix}$ 3:1 (f) and $S_{mix}$ 4:1 (g) | 133 |
| 5.4. | Analysis of droplet size (a) and zeta potential (b) of optimized formulation, GN-NE2 | 136 |
| 5.5. | TEM photograph (a) and UV spectrum of pure GN, placebo formulation and GN-NE2 formulation (b) | 136 |
| 5.6. | HPTLC chromatogram of pure GN (a) and GN loaded nanoemulsion, GN-NE2 (b) | 138 |
| 5.7. | HPTLC plate (a) and 3D-chromatogram (b) of pure GN and GN-NE2 formulation at 254 nm (S1-8 = Standard GN and F1-2 = GN-NE2 formulation) | 138 |
| 5.8. | FTIR spectrum of pure GN (a) and GN-NE2 (b) | 139 |
| 5.9. | Degradation kinetics of GN from GN-NE2 at 40°C | 140 |
| 5.10. | Rheogram of placebo-NG2 (a) and GN-NG2 (b) where, $\eta$ = viscosity (Pa.s), $\gamma$ = shear rate (1/s) | 141 |
| 5.11. | Skin permeability profiles of GN from different nanoemulsions (a) GN-NE1-4, (b) GN-CG and GN-NG2 through rat skin and (c) steady state flux of different formulations across rat skin<br>[Values were mean ± SEM (n = 3), $^{a,b}P < 0.01$, $^{c}P < 0.05$ when compared to the conventional group] | 142 |
| 5.12. | Cutaneous antioxidant enzyme levels (a) SOD and GPX, (b) CAT and TBARS after transdermal application of GN based gel formulations<br>[Values are mean ± SEM (n = 6), $^{a,b}P < 0.01$, $^{c}P < 0.05$ when compared to the control and UVA irradiated group] | 144 |
| 5.12. | Plasma profiles of GN in rats after administration of pure GN and GN-NG2 [Values were mean ± SEM (n = 6)] | 146 |

## List of tables


| Table No. | Title of tables | Page |
|---|---|---|
| 1.1. | The pharmacokinetics of different phytoconstituents after oral administration (Mean ± SD) | 12-13 |
| 1.2. | Example of oils (lipid Ingredients), surfactants and co-surfactants | 37-39 |
| 1.3. | Application of the target based NDDS for phytopharmaceuticals | 45-50 |
| 3.1. | Oil, surfactant and co-surfactant grouped in different combinations | 63 |
| 3.2. | Thermodynamic stability studies of various formulations selected from group I at a 5% w/w increasing amount of oil | 76 |
| 3.3. | Thermodynamic stability studies of group II formulations at increasing amount of oil (5% w/w) | 77 |
| 3.4. | Evaluation of thermodynamic stability test for group II formulations | 78 |
| 3.5. | Investigation of thermodynamic stability test for group IV formulations | 79 |
| 3.6. | Composition of optimized nanoemulsion formulations selected from group II | 80 |
| 3.7. | Characterization of various nanoemulsions | 84 |
| 3.8. | Degradation study of optimized ferulic acid loaded NE formulation, FA-NE3 | 86 |
| 3.9. | Transdermal steady state flux and permeability coefficient of formulations across rat skin | 88 |
| 3.10. | Model fitting of accumulated release data of different formulations | 89 |
| 3.11. | Pharmacokinetic parameters of ferulic acid in rats after administration of oral suspension and FA-NG3, values represented are mean ± SD (n = 6) | 92 |
| 4.1. | Analysis of thermodynamic tests of formulations | 107 |
| 4.2. | Compositions of CA based different nanoemulsion formulations | 108 |
| 4.3. | Characterization of catechin loaded different nanoemulsions | 111 |
| 4.4. | Degradation study of optimized CA-NE4 formulation | 113 |
| 4.5. | Transdermal steady state flux and permeability coefficient of CA nano formulations across rat skin, Mean ± SD | 116 |
| 4.6. | Release kinetics of data of CA based formulations | 117 |
| 4.7. | Analysis of pharmacokinetic parameters of CA in rats | 120 |
| 5.1. | Evaluation of thermodynamic stability of different formulations (5% w/w increasing amount of oil) | 134 |
| 5.2. | Compositions of GN encapsulated nanoemulsion formulations | 135 |
| 5.3. | Characterization of genistein loaded different nanoemulsions | 137 |
| 5.4. | Stability test of optimized GN-NE2 formulation | 140 |
| 5.5. | Transdermal steady state flux and permeability coefficient of formulations | 142 |

| | | |
|---|---|---|
| | across rat skin, Mean ± SEM | |
| 5.6. | Drug release kinetic profiles of GN loaded different formulations | 143 |
| 5.7. | Pharmacokinetic profiles of GN in rats after administration of pure GN oral suspension and GN-NG2 [Values represented were mean ± SEM (n = 6)] | 146 |

## Abbreviations

| | | |
|---|---|---|
| ξ | : | Zeta potential |
| 'Cos' | : | Co-surfactant |
| *'F'* | : | Relative bioavailability |
| 'S' | : | Surfactant |
| ABC | : | ATP-binding cassette |
| ALP | : | Serum alkaline phosphatase |
| ANOVA | : | Analysis of variance |
| AP | : | Andrographolide |
| ARW | : | Alcoholized red wine (13% ethanol) |
| AUC | : | Area under curve |
| BA | : | Betulinic acid |
| BCRP | : | Breast cancer resistance protein |
| BCS | : | Biopharmaceutical classification system |
| CA | : | Catechin |
| CA-CG | : | Conventional gel of catechin |
| CA-NE | : | Catechin encapsulated nanoemulsion |
| CA-NG | : | Nanoemulsion (CAT-NE4) based nano-gel |
| CAT | : | Catalase |
| Cent. | : | Centrifugation |
| CGA | : | Chlorogenic acid |
| $C_l$ | : | Clearance |
| $C_{max}$ | : | Peak of maximum concentration |
| CMC | : | Sodium carboxymethyl cellulose |
| Cond. | : | Conductivity |
| CPCSEA | : | Committee for the purpose of control and supervision of experiment on animals |
| CYP450 | : | Cytochrome 450 enzyme |
| DL | : | Drug loading |
| DMSO | : | Dimethyl sulfoxide |
| DNA | : | Deoxyribonucleic acid |
| DRW | : | Dealcoholized red wine |
| dTMP | : | Thymidine monophosphate |
| EA | : | Ellagic acid |
| EE | : | Drug entrapment efficiency |
| EIP | : | Emulsion inversion point |
| ELO | : | Eucalyptus oil |
| EO | : | Ethyl oleate |
| FA | : | Ferulic acid |
| FA-CG | : | Conventional gel of ferulic acid |
| FA-NE | : | Ferulic acid loaded nanoemulsion |
| FA-NG3 | : | Nanoemulsion (FA-NE3) based nano-gel |
| FDA | : | Food and drug administration |
| Freeze Tha. | : | Freeze-thaw cycle |
| FTIR | : | Fourier transform infrared spectroscopy |
| GA | : | Gallic acid |
| GI | : | Gastrointestinal |
| GIT | : | Gastrointestinal tract |
| GN | : | Genistein |
| GN-CG | : | Conventional gel of genistein |
| GN-NE | : | Genistein loaded nanoemulsion |
| GN-NG2 | : | Nanoemulsion (GN-NE2) based nano-gel |
| GPX | : | Glutathione peroxidase |
| GRAS | : | Generally regarded as safe |
| GSH | : | Glutathione |
| GTE | : | Green tea extract |
| H & C | : | Heating and cooling cycle |
| HLB | : | Hydrophilic-lipophilic balance |
| HPLC | : | High performance liquid chromatography |
| HPTLC | : | High performance thin layer chromatography |
| HSPC | : | Hydrogenated soy phosphatidylcholine |
| i.v. | : | Intravenous |
| ICH | : | International Conference on Harmonization |
| IPA | : | Isopropyl alcohol |
| IPM | : | Isopropyl myristate |
| ISIS | : | Isostearyl isostearate® |
| *Jss* | : | Stead state transdermal flux |

| | | |
|---|---|---|
| Kel | : | Elimination rate constant |
| *Kp* | : | Permeability coefficient |
| LLW | : | Labrafac™ lipophile WL1349 |
| LOD | : | Limit of detection |
| LOQ | : | Limit of quantification |
| LPH | : | Lactase phlorizin hydrolase |
| MDR | : | Multi drug resistance |
| MED | : | Minimally erythemogenic dose |
| MMPs | : | Matrix metalloproteinases |
| MRT | : | Mean residence time |
| NATs | : | Arylamine N-acetyltransferases |
| NCEs | : | New chemical entities |
| NDDS | : | Novel drug delivery systems |
| NE | : | Nanoemulsion |
| NEs | : | Nanoemulsions |
| NLCs | : | Nanostructured lipid carriers |
| NPs | : | Polymeric nanoparticles |
| o/w | : | Oil-in-water emulsion |
| OA | : | Oleic acid |
| OL | : | Olive oil |
| P.T. | : | Percentage transmittance |
| PAMAM | : | Poly-amido-amine |
| PBS | : | Phosphate buffer saline |
| PDA | : | Photo diode array detector |
| PDI | : | Polydispersity index |
| PEG 400 | : | Polyethylene glycol 400 |
| PG | : | Propylene glycol |
| P-gp | : | P-glycoprotein |
| PIS | : | Plurol isostearique® |
| PIT | : | Phase inversion temperature |
| PLA | : | Polylactic acid |
| PLGA | : | Copolymer of poly lactic acid and glycolic acid |
| PTA | : | Phosphotungstic acid |
| Q3G | : | Quercetin 3-O-β-glucoside |
| Q4'G | : | Quercetin 4-O-β-glucoside |
| QC | : | Quality control |
| R. I. | : | Refractive index |
| $R_f$ | : | Retardation factor |
| ROS | : | Reactive oxygen species |
| RP-HPLC | : | Reversed phase -High performance liquid chromatography |
| RSD | : | Relative standard deviation |
| $R_t$ | : | Retention time |
| SBO | : | Soybean oil |
| SC | : | *Stratum corneum* |
| SD | : | Standard deviation |
| SEDDS | : | Self-emulsifying drug delivery system |
| SEM | : | Standard error of mean |
| SLN | : | Solid lipid nanoparticle |
| SMEDDS | : | Self-microemulsifying drug delivery system |
| $S_{mix}$ | : | Surfactant/co-surfactant mixture |
| SNEDDS | : | Self-nanoemulsifying drug delivery system |
| SO | : | Sesame oil |
| SOD | : | Superoxide dismutase |
| SULTs | : | Sulfatransferase |
| $t_{1/2}$ | : | Half-life |
| $t_{1/2}$el | : | Elimination half-life |
| $t_{90}$ | : | Shelf-life |
| TBARS | : | Thiobarbituric acid reactive substances |
| TDDS | : | Topical/transdermal drug delivery systems |
| TEA | : | Triethanolamine |
| TEM | : | Transmission electron microscopy |
| $T_{max}$ | : | Time of peak concentration |
| UDP | : | Uridine diphosphate |
| UGTs | : | UDP-glucuronosyltransferase |
| UV | : | Ultraviolet rays |
| UVA | : | Ultraviolet A radiation |
| UVB | : | Ultraviolet B radiation |
| $V_d$ | : | Volume of distribution |
| w/o | : | Water-in-oil emulsion |
| Z.P. | : | Zeta potential |

## Dedication

This thesis is especially dedicated to my beloved mother and father: Smt. Chandrakanta Devi and Shri R. P. Harwansh for their love, blessings, inspiration and active support in all of my works.

# Chapter - 1

## Novel drug delivery systems (NDDS) for herbal drugs - enhancement of bioavailability

1.1. Approaches for formulation and development for herbal drugs
1.2. The bioavailability and pharmacokinetics of some phytoconstituents
1.3. Challenges in developing herbal formulations
1.4. Techniques for novel drug delivery system for herbal formulation
1.5. Application of the target based nanotechnology and NDDS with phytopharmaceuticals
1.6. Summary and conclusion
1.7. Publication

## 1.1. Approaches for formulation and development for herbal drugs

The therapeutic and phytochemical importance of herbal drug has been built for the improvement of human health, but its broader application is restricted due to low bioavailability. The nature of the molecule plays an essential role in enhancing the rate and extent of absorption of molecules when administered through any path. Generally, the problems come with poor lipid-soluble compounds due to limited membrane permeability (Rahman et al., 2011). Many herbal products demonstrated low therapeutic action due to their solubility problems which finally resulted in low bioavailability despite their extraordinary potential (Kesarwani and Gupta, 2013). The strength of any herbal product depends on the delivery of effective levels of the therapeutically active compound. To overcome these limitations of absorption, developing novel herbal drug delivery system with better absorption profile is of premier importance. The therapeutic indices of the associated drugs are improved by increasing the drug concentration at the site of action. On the other hand, their biodistribution is altered in favor of the diseased tissue (Mukherjee et al., 2009). In the past century, attention has been focused on the approaches toward improved bioavailability and pharmacokinetics of herbal drugs through development of a novel drug delivery system (NDDS).

The application of NDDS is an important approach toward solving bioavailability-related problems associated with phytomolecules. Several novel herbal drug delivery systems specifically liposomes, transfersomes, ethosomes, niosomes, phytosomes, herbosomes, dendrimers, micro/nanoparticles, micro/nanoemulsions (NEs), micelles, etc., have been successfully employed for the delivery of phytopharmaceuticals. The novel formulations have notable advantages compared to conventional formulations like enhancement of solubility and stability, membrane permeability and bioavailability, improved pharmacological activity through sustained-release profile, and reduced toxicity. The novel systems of herbal medicine have the capability to deliver the drug at a rate directed by the needs of the body for an extended period of time, and it should channel the bioactive molecule of herbal products to the site of action (Ajazuddin and Saraf, 2010). Therefore, the NDDS have a great future for enhancing the therapeutic activity and overcoming problems attributed with herbal medicine. Most of bioactive agents (e.g., nutraceuticals and pharmaceuticals) intended for oral administration are found as highly hydrophobic compounds with low water solubility and poor bioavailability. Furthermore, poor solubility also leads to lower absorption in the gastrointestinal tract (GIT) and therefore limited therapeutic activity (Li et al., 2012). The application of nanotechnology/nanoencapsulation to food, medical and pharmaceutical industries have received great attention from the scientific community. Forced back by the increasing consumer demand for quality and safer medicinal food products for the promotion of better health, researchers are currently concentrating on nanotechnology to address topics relevant to food as medication (Silva et al., 2012). The NDDS offers various advantages over conventional systems which including (i) stabilization in aqueous systems (foodstuffs) of lipophilic bioactive compounds with scarce solubility in

water, (ii) protection of herbal drugs against degradation reactions with food constituents and minimization of the revision of the food matrix, (iii) controlled release by engineering the delivery systems, (iv) enhancement of cell uptake and bioavailability. Especially, the pharmacokinetic profile of nanoencapsulated herbal drug enhanced due to their nanoparticle size distribution range. Cutting down the particle size to values below cell size (~500 nm) produces higher absorption of the active ingredient and higher particle uptake, by enhancing the mechanisms of passive transport through the intestinal membranes (Sessa et al., 2014). NDDS have been set up to be promising for the effective and efficacious herbal drug delivery. The present discussion highlights the current status of pharmacokinetics and bioavailability of herbal drugs or phytopharmaceuticals and implication of novel herbal drug delivery technology with particular emphasis on nanoemulsion based carrier system.

## 1.2. The bioavailability and pharmacokinetics of some phytoconstituents

Bioavailability is the degree and rate at which a drug substance (molecule) is absorbed into a living system or is made available at the site of physiological activity. In other hand, the rate and extent to which a drug is available to serve as a substrate, bind to a specific molecule or participate in biochemical reactions in a target tissue after administration. The term bioavailability is one of the main pharmacokinetic properties of drugs, is used to describe the fraction of an administered dose of unchanged drug that reaches the systemic circulation. For oral agents, bioavailability reflects the rate and extent of GI tract absorption. Bioavailability depends on the isoelectric point, the pH of a solution in which the solute does not migrate (ionic form), presence of side chains or the conformation of the epitope. Bioavailability is affected by the route of administration, rate of metabolism, lipid solubility and binding proteins. Bioavailability is usually < 100% due to incomplete absorption or first-pass metabolism (degradation or alteration) before reaching the target tissue while in case of intravenously (i.v.) administered drug it is 100%. The measurement of the amount of the drug in the plasma at periodic time intervals indirectly indicates the rate and extent at which the active pharmaceutical ingredient is absorbed from the drug product and becomes available at the site of action. Bioavailability is one of the essential tools in pharmacokinetics, as it must be considered when calculating dosages for non-intravenous routes of administration. It is expressed as either absolute or relative bioavailability (Shargel and Yu, 1999).

### *1.2.1. Absolute bioavailability*

Absolute bioavailability measures the availability of the active drug concentration in systemic circulation after non i.v. administration (i.e., after oral, rectal, transdermal, and subcutaneous). In order to determine absolute bioavailability of a drug, a pharmacokinetic study must be done to obtain a plasma drug concentration vs time plot for the drug after both i.v. and non-intravenous administration. The absolute bioavailability is the dose-corrected area under curve (AUC) non i.v. divided by AUC i.v.

Therefore, a drug given by the i.v. route will have an absolute bioavailability of 1 ($F$=1) while drugs given by other routes usually have an absolute bioavailability of less than one (Shargel and Yu, 1999).

### *1.2.2 Relative bioavailability*

This measures the bioavailability of a certain drug when compared with another formulation of the same drug, usually an established standard, or through administration via a different route. When the standard consists of i.v. administered drug, this is known as absolute bioavailability (Shargel and Yu, 1999).

### *1.2.3. Factors affecting the bioavailability*

Generally, herbal medicines and phytopharmaceutical drugs marketed worldwide are administered orally. The therapeutic efficacy of these drugs is dependent on the oral bioavailability, which in turn, is dependent on drug's physicochemical properties, formulation design and physiological conditions of gastrointestinal tract (Yang et al., 2014).

The absolute bioavailability of a drug, when administered by an extravascular route, is usually less than one (i.e. $F$<1). Various physiological factors affect the availability of drug concentrations prior to their entry into the systemic circulation, as follows:

- Physicochemical properties of the drug (i.e. hydrophobicity, pKa, solubility).
- Type of formulation and drug release pattern (immediate release, excipients used, manufacturing methods, modified release - delayed release, extended release, sustained release, etc.).
- Drug administration in a fed or fasted condition
- Gastric emptying time or rate
- Circadian differences
- Drug metabolism affected by inhibition or induction through CYP450 enzyme
- Drug-drug interaction or herb-drug interaction
    - ✓ Interactions with other drugs (i.e. antacids, alcohol, nicotine)
    - ✓ Interactions with other foods (i.e. grapefruit juice, pomello, cranberry juice)
- Transporters: substrate of an efflux transporter (i.e. P-glycoprotein)
- GI tract: intestinal motility alters the dissolution of the drug and degree of chemical degradation of drug by intestinal microflora.
- Individual variation in metabolic differences
    - ✓ Age: In general, drugs are metabolized more slowly in fetal, neonatal, and geriatric populations
    - ✓ Phenotypic differences, enterohepatic circulation, diet, gender
- Disease condition
    - ✓ Poor liver and renal function

- ✓ Stress, disorders (i.e. achlorhydria, malabsorption syndromes)
- ✓ Previous GI surgery (i.e. bariatric surgery) can also affect the bioavailability of drug or bioactive molecules.

All these factors may vary from patient to patient (inter-individual variation), and indeed in the same patient over time (intra-individual variation) (Shargel and Yu, 1999).

Several phytomedicine and plant extracts despite of their potential health benefits exhibit least pharmacological activity due to their poor lipid solubility and improper size result in poor absorption and bioavailability. Another drawback is their structural instability in biological milieu, premature drug loss through rapid clearance and biotransformation and some plant extract and phytoconstituents are destroyed in gastric fluid during gastric emptying when orally administered (Gunasekaran et al., 2014).

*1.2.3.1. Poor aqueous solubility*

Gupta et al. (2013) have mentioned that about 60–70% of the drug molecules are insufficiently soluble in aqueous media and/or have very low permeability to allow for their adequate and reproducible absorption from the GIT following oral administration. Mostly poor aqueous solubility of a drug associated with poor bioavailability. The contents of GI tract are aqueous and hence a drug having poor aqueous solubility has a low saturation solubility which is typically correlated with a low dissolution velocity, resulting in poor oral bioavailability. About 10% of the present drugs are poorly soluble, about 40% of the drugs in the pipeline possess a poor solubility, and even 60% of drugs coming directly from synthesis have a solubility below 0.1 mg/ml. Out of the research around 40% of lipophilic drug candidates fail to reach the market although exhibiting potential pharmacodynamic activities (Lennemas, 2007). No matter how active or potentially active new chemical entities (NCEs) are against a particular molecular target, if it is not available in a solution form at the site of action, it is not a viable development candidate. As a result, the development of many exciting NCEs has stopped before their potential is realized. Low bioavailability is the most common with oral dosage forms of poorly water-soluble, slowly absorbed drugs (Gupta et al., 2013).

*1.2.3.2. Inappropriate partition coefficient (log p) - poor absorption*

Highly hydrophilic drugs would not be able to permeate through the gastrointestinal mucosa and too lipophilic drug will not dissolve in the aqueous gastrointestinal contents. For optimum absorption, the drug should have sufficient aqueous solubility to dissolve in the gastrointestinal contents and also adequate lipid solubility to facilitate its partitioning into the biological membrane and then into systemic circulation. Drugs having partition coefficient (log P) value in the range of 1 to 3 shows good passive absorption across lipid membranes, and those having log Ps greater than 3 or less than 1 have often poor transport characteristics (Vemulapalli et al., 2007). Lipinski's rule of five has been widely proposed as a qualitative predictive model for the measurement of

absorption of poorly absorbed compounds. In the discovery setting “the rule of 5” predicts that poor absorption or permeation is more likely when there are more than 5 H-bond donors, 10 H-bond acceptors, the molecular weight is greater than 500, and the calculated Log P is greater than 5. The ‘rule of five’ only holds for compounds that are not substrates for active transporters and efflux mechanisms (Lipinski et al., 2001).

*1.2.3.3. Hepatic first-pass metabolism*

Orally administered drugs must pass through the intestinal wall and then through the portal circulation to the liver; both are common sites of first pass metabolism (metabolism of a drug before it reaches systemic circulation). Thus, many drugs may be metabolized before adequate plasma concentrations are reached resulting in poor bioavailability. The enterocyte expresses many of the metabolic enzymes that are expressed in the liver. These include cytochromes P450, UDP-glucuronyltransferases, sulfotransferases, and esterases. The susceptibility of a drug to first-pass metabolism by CYP3A4 has a very high influence on the oral bioavailability, which decreases as the level of first pass metabolism increases (Mukherjee et al., 2011).

CYP450 is a family of haemoproteins, and is the most important Phase-I drug-metabolizing enzyme system, responsible for the metabolism of a variety of xenobiotics including therapeutic drugs and some important endogenous substances. In human hepatic smooth endoplasmic reticulum, the relative abundance of different CYP450 has been optimized as 30% CYP3A4, 13% CYP1A2, 7% CYP2E1, 4% CYP2A6, 2% CYP2D6, 20% CYP2C, and 1% CYP2B6 (Zhou et al., 2003). In humans, the extent of drug metabolism varies with the individual CYP isozymes viz., 50% of drugs are metabolized by CYP3A4, followed by 25% and 20% by CYP2D6 and CYP2C family, respectively (Zhou et al., 2003). These CYP450 iso-enzymes can potentially influence the bioavailability and pharmacokinetics of a broad range of important pharmaceuticals by interfering biotransformation process in liver. The repeated exposure to botanicals along with conventional medicines can lead to decreased bioavailability *in vivo* which leads to therapeutic failure or increased concentrations of phytopharmaceuticals causing serious adverse events (Mukherjee et al., 2011).

*1.2.3.4. Degradation in the GI tract*

Drug substances used as pharmaceuticals or phytopharmaceuticals have diverse molecular structures and are, therefore, prone to many and variable degradation pathways. Particularly protein drugs are highly susceptible to inactivation due to the pH and the enzymes present in gastrointestinal tract.

*1.2.3.4.1. Degradation due to low pH in the stomach*

Most of drug substances are fairly stable at the neutral pH values found in the small intestine (disregarding enzymatic degradation) but can be unstable at low pH values found in the stomach. Knowledge of the stability of a drug in the pH range of 1-2 at 37°C is important in the formulation design of potentially acidlabile drugs. The rapid degradation of drugs under acidic conditions reduces their oral bioavailability. In addition, it may result in inter- and intra-individual variability in the pharmacokinetic profile of the drug. It is essential to know the magnitude of any degradation occurring prior to the absorption of oral doses for unstable compounds under acid conditions (Kosugi et al., 2015). Several studies have been reported about the GIT degradation of ginsenosides (obtained from *Panax* species) in acids, enzymes, intestinal bacteria, and animals (Odani et al., 1983; Stro¨mbom et al., 1985; Karikura et al., 1990; Hasegawa et al., 1996; Akao et al., 1998). From these studies It is confirmed that the protopanaxatriol ginsenosides are hydrolyzed to ginsenoside Rh1 and its hydrated form under mild acidic conditions similar to gastric fluid (Han et al., 1982). Protopanaxadiol ginsenosides are mainly converted to compound-K (C-K1) by intestinal bacteria via stepwise cleavage of the sugar moieties (Hasegawa et al., 1996). However the degradation pathway of ginsenosides in animals has been well pe5rformed *in vivo* and *in vitro*, only very few studies have been reported in humans (Tawab et al., 2003).

*1.2.3.4.2. Chemical degradation of drug in GI tract*

Many phytopharmaceutical and herbal products cannot be administered orally because of their inactivation in GI fluids due to chemical reactions. Possible degradation pathways include hydrolysis, dehydration, isomerization and racemization, elimination, oxidation, photodegradation, and complex interactions with excipients, food and other drugs, thiol/disulfide exchange reactions. A hydrolytic cleavage takes place particularly at low pH of the stomach. Many phytomedicine and plant extract are hydrolyzed in the gastric juice and lead to structural modification hence chemical instability of such type of molecule in stomach invironment (Gunasekaran et al., 2014). Food and other phytomedicine disintegration within the stomach have a major role on the rate and final bioavailability of nutrients within the body. Understanding the link between food material properties and their behaviour during gastric digestion is a key point to the design of novel structures with enhanced functionalities. Upon ingestion, foods undergo a number of physicochemical changes that lead to their disintegration, transport, and absorption into the body. While the result of a complex series of physicochemical processes occurring along the entire gastrointestinal tract, research has evidenced the significant role of gastric digestion on the rate and final bioavailability of nutrients. Depending on the food, when gastric juice penetrates the matrix, a number of structural changes start to occur. By modifying the material properties of the ingested food, these structural changes will modulate its mechanical disintegration when exposed to the peristaltic and grinding activity of the stomach. Only a better understanding of the mechanisms

underlying these processes will allow for a better prediction of the performance of different formulations and structures during digestion. The influence of gastric disintegration and transit time on the absorption and plasma profile of solid drug tables is well established within the pharmaceutical area (Drechsler and Ferrua, 2016).

*1.2.3.4.3. Enzymatic metabolism of drug in GI tract - small intestine*

Metabolism of phytomedicine including polyphenols are conjugated in the small intestine and then in the liver during absorption process. This process mainly includes methylation, sulfation, and glucuronidation. Subsequently, these molecules may be excreted as conjugates in bile, pass through the small intestine and reach the colon. In the other hand, the limited absorption of polyphenols in the ileum allows non-absorbed polyphenols to reach the colon whole, being transformed by the gut microflora enzymes (i.e. esterase, glucosidase, demethylation, dehydroxylation and decarboxylation enzymatic activities) into a wide range of low-molecular-weight phenolic acids. Several studies have shown that polyphenols are transformed by colonic microflora into phenolic acids, such as phenylvaleric, phenylpropionic, phenylacetic, benzoic and hippuric acids. However, the type of metabolic products depends on what phenolic compound is metabolized (Serra et al., 2012). It is generally recognized that intact flavonoid glycosides are hardly absorbed from the small intestine because sugar moieties elevate their hydrophilicity. Flavonoid glycosides from diet are believed to pass through the small intestine, and enter the cecum and colon, where they are hydrolyzed to aglycone by enterobacteria (Bokkenheuser et al., 1987).

Flavonoid aglycone can be absorbed easily into epithelial cells in the large intestine, because its lipophilicity facilitates its passage across phospholipid bilayer of bio-membranes. Thereafter, they enter the circulation and are subject to O-methylation, glucuronidation, and/or sulfation in the liver. A substantial portion of those metabolites may then be excreted in the bile and returns thereby to the intestinal lumen. Once again, they may be hydrolyzed and reabsorbed by intestinal cells or excreted into the feces. Crespy et al. (1999) has been reported a study of *in situ* perfusion in rat small intestine, that rutin was hardly absorbed compared with quercetin aglycone, because rutin was easily digested not in the small intestine but rather in the large intestine, by intestinal microflora. In contrast, Hollman et al. (1995) claimed that intestinal absorption of quercetin glucoside is superior to that of quercetin aglycone, based on an experiment using healthy ileostomy volunteers; they suggested that the glucose transporter (SGLT-1) is responsible for the effective transport of quercetin glucosides from intestinal epithelial cells. However, Walle et al. (2000) demonstrated that quercetin glucosides are completely hydrolyzed in ileostomy patients before intestinal absorption. That is to say, quercetin glucosides are converted to their aglycone form before transport from the intestinal tract. Indeed, recent studies clearly showed the existence of bglucosidase activity in the small intestinal epithelium of rats (Ioku et al., 1998) and human (Day et al., 1998). Day et al. (2000) demonstrated that lactase phlorizin hydrolase (LPH, EC

3.2.1.62), which is bound to intestinal lumen for the hydrolysis of lactose, is also capable of hydrolyzing quercetin glucosides effectively. Morand et al. (2000) demonstrated in rodents that quercetin 3-O-β-glucoside (Q3G) is better absorbed than quercetin aglycone, rutin, or quercetin 3-O-b-rhamnoside. Hollman et al. (2000) showed that quercetin 4-O-β-glucoside (Q4'G) is better absorbed than rutin in humans. On the other hand, Olthof et al. (2000) claimed that the bioavailability of Q3G and Q4'G do not differ in humans. Overall, despite certain discrepancies, it can be concluded that the bioavailability of quercetin glycosides from the diet seems to depend largely on the variety of sugar groups attached to their phenolic group. In addition, glucose-bound glycosides are likely to be much more absorbable than other sugar bound ones. Small intestine is also recognized as the site for metabolic conversion of quercetin and other flavonoids as it possesses enzymatic activity of glucuronidation and sulfation. Modulation of the intestinal absorption and metabolism may be beneficial for regulating the biological effects of dietary quercetin (Murota and Terao, 2003).

*1.2.3.4.4. Drug-herb-food Interaction with CYP450 and intestinal enzymes*

Drug metabolism enzymes are the second line of cellular resistance. This process involves three phases such as Phase I is mediated mainly by CYP450 and epoxide hydrolases (Guengerich et al., 2005). Drug species are metabolized and converted into highly mutagenic aromatic metabolites that can be conjugated by phase II enzymes including glutathione S-transferase (GSTs), UDP-glucuronosyltransferase (UGTs), sulfatransferase (SULTs), and arylamine N-acetyltransferases (NATs) (He et al., 2010). These conjugated metabolites are then effluxed by members of the ABC (ATP-binding cassette) transporters, which can be considered as phase III of drug metabolism (Deeley et al., 2005). Inhibition of the drug metabolism enzymes could become a promising strategy for reversing MDR. Zou et al. evaluated the effects of 25 purified components of commonly used herbal products on the catalytic activity of cytochrome P450 isoforms (Zou et al., 2002). The results showed ginkgolic acids, dihydromethysticin, methysticin, hyperforin and quercetin, etc, significantly inhibited one or more of the human P450 isoforms at concentrations of less than 10 μM. Quercetin has been demonstrated to increase the bioavailability of pioglitazone in rats by inhibiting CYP3A (Umathe et al., 2008). Rosemary extract enhanced antitumor effect of 5-fluorouracil by down regulation of thymidylate synthetase enzyme and TK1 genes, which is essential for the synthesis of thymidine monophosphate (dTMP) and related to 5-fluorouracil resistance (González-Vallinas et al., 2013). Other enzymes including CYP1A, CYP2C9 and UGTs could also be inhibited by herbal ingredients or herbal extracts (Yeung, 2012; Pan et al., 2011; Liu et al., 2012). Drugs that undergo a significant first-pass metabolism with a lower bioavailability ranging from 5% to 30% may be affected to a greater degree by grapefruit juice (Fuhr, 1998). Fong et al. (2012) reported the herb-herb or drug-herb interaction potential of baicalein and other phytomolecules and drugs in *in vitro* and *in situ* models. Baicalein is a bioactive flavone isolated from the root of a traditional Chinese medicinal herb *Scutellaria baicalensis*

Georgi, was found to undergo extensive intestinal Phase II metabolism during its absorption process. Compounds sharing the same metabolic pathways with baicalein or being inhibitors of enzymes UGT and SULT are expected to interfere with the metabolism of baicalein leading to alteration of the absorption of baicalein. These study aims to identify potential intestinal absorption and metabolism interactions between baicalein and four selected compounds, namely acetaminophen, (-)-epicatechin, piperine and curcumin using *in vitro* and *in situ* models. Results demonstrated that the intestinal metabolism of baicalein could be inhibited by all the selected compounds namely acetaminophen, -() -epicatechin, piperine and curcumin among these drug curcumin are being the most potent inhibitor, which could result in subsequent increase of absorption as well as bioavailability of baicalein.

*1.2.3.4.5. Drug efflux pumps like p-glycoprotein*

Drug efflux pumps like P-glycoprotein (P-gp) are also playing a major role in changing the bioavailability and pharmacokinetics of various drugs. Due to selective distribution at the port of drug entry and exit, P-gp has been speculated to play a major physiological role in absorption, distribution and excretion of xenobiotics. Overall P-gp functions are as a biochemical barrier for entry of xenobiotics and as a vacuum cleaner to expel them from the brain, liver, etc. and ultimately from systemic circulation (Manthena et al., 2003). P-gp is one of the most prevalent efflux transporters expressed in a number of cancer cells as well as in several organs such as intestine, liver, kidney and the blood-brain barrier results in reduced drug absorption from the GI tract and enhanced drug elimination into bile and urine (Sharom, 2008).

P-gp plays an important role in limiting the intestinal absorption of its substrates *in vivo* and inhibition of P-gp leads to the improvement of bioavailability of orally administrated drugs and therapeutical agents. For example, ginsenosides have been found to be the main components responsible for ginseng's pharmacological activity. However, the low oral bioavailability of ginsenosides has presented a major barrier to the utilization of those drugs (Joo et al., 2010). Recent work has revealed that the active metabolite of ginsenoside, compound K is a solid substrate of P-gp, and P-gp mediates the efflux of compound K in vitro and in vivo. Using P-gp inhibitor verapamil and cyclosporine A substantially decreased the efflux ratio of compound K in Caco-2 cells. Administration of compound K to P-gp deficiency MDR1a/b$^{-}$/$^{-}$ FVB mice also lead to large enhancement of its absorption and bioavailability (Yang et al., 2012, 2014). Sinomenine (obtained from *Sinomenium acutum*) could significantly improve the bioavailability of paeoniflorin (derived from the root of *Paeonia lactiflora*) in rats. By investigating the intestinal kinetic absorptive characteristics of paeoniflorin as well as the absorptive behavior influenced by co-administration of sinomenine and P-gp inhibitors, Chan et al. suggested that sinomenine in a pattern, which influenced paeoniflorin's absorption, manifested as similar to that of P-gp inhibitors (Chan et al., 2006). In addition, the inhibition of intestinal breast cancer resistance protein (BCRP), which restricts the absorption of

xenobiotics, may also increase the systemic availability of its substrates and various phytochemicals. Natural bioactive compounds such as flavonoids, chalcones, terpenoids, isothiocyanates and nonprenylated rotenoids, are known to inhibit BCRP (Yoshida et al., 2008; Ahmed-Belkacem et al., 2007; Imai et al., 2004).

*1.2.3.4.6. Combined role for P-glycoprotein and CYP3A4 in the gut wall*

Many authors have suggested that gut wall CYP3A4 and P-gp act in an intensive manner to control the absorption of their substrates. This is based on the large overlap of substrates between the two and the proximity of their expression within the gut wall. Thus, it is proposed that P-gp effectively recycles its substrates, thereby allowing CYP3A4 several opportunities to metabolize compounds in the gut. In this way, a small amount of CYP3A4 in the gut wall (relative to the liver content) can exert a profound extraction of the compound. Poor oral bioavailability of a promising anticancer agent andrographolide is due to extensive metabolism and efflux by P-gp. Andrographolide has poor oral bioavailability because of its rapid biotransformation and efflux by P-gp Andrographolide is a substrate for both CYP3A4 and P-gp and which resulting the 2.67% absolute bioavailability (Ye et al., 2011). For example in rats, repeated oral administration of green tea extract (GTE) for one week significantly increased the maximum plasma concentration ($C_{max}$) and area under the time-concentration curve (AUC) of midazolam, which is metabolized extensively by CYP3A, suggesting that catechins in GTE inhibited CYP3A activity in the intestine (Nishikawa et al., 2004).

*1.2.3.4.7. Insufficient time for absorption*

Insufficient time for absorption in the GI tract is a common cause of low bioavailability due to its limited solubility in GI fluids. If the drug is highly ionized and polar in nature that does not dissolve readily or cannot penetrate the epithelial membrane during its residence time in the GI tract, its bioavailability tends to be highly variable as well as low. *Ex vivo* absorption models suggest that ferulic acid (FA) can be absorbed from the stomach and ileum after 25 min incubation of FA in the rat stomach. FA disappeared (>70%) from the stomach and it was recovered in the gastric mucosa, blood, bile and urine that suggesting a fast gastric absorption of FA. Similarly, FA quickly disappeared from the jejunum and to a significantly lesser extent from the ileum when it was perfused in an isolated rat intestine model. Only 0.5-0.8% of ingested FA was found in feces of rats, indicating very efficient absorption rate for FA (Zhao et al., 2008). Lipinski's rule of five has been widely used as a qualitative predictive model for the estimation of absorption of poorly absorbed compounds. The detail about the drug partition coefficient (log-P) was discussed in earlier section (Lipinski et al., 2001).

Medicinal herbal products are composed of different chemical constituents, including flavonoids, alkaloids, glycosides, tannins, xanthonoids, and cinnamates, and possess diverse therapeutic activity. But unfortunately the beneficial roles of potent plant

secondary metabolites are greatly limited due to their poor bioavailability. The solubility of some of these phytoconstituents in GI fluid is low, which leads to poor absorption and hence poor bioavailability. Also, majority of the compounds are present in the food as glycosides, which are known to have poor absorption and low bioavailability. The pharmacokinetic profiles of some phytomolecules are illustrated in Table 1.1.

**Table 1.1. The pharmacokinetics of different phytoconstituents after oral administration (Mean ± SD)**

| Phyto-constituents | Subject | $C_{max}$ (ng/mL) | $T_{max}$ (h) | $T_{1/2el}$ (h) | $C_L$ | Bioavailability (%) | Reference |
|---|---|---|---|---|---|---|---|
| Ferulic acid | Rats | 44.7 ± 8.2[a]<br>1.6 ± 0.3 mg/L[b]<br>8174.55[c] | 1.1 ± 0.65[a]<br>15 min[b]<br>0.03[c] | 5.00 ± 0.78[a]<br>333.2 ± 79.8 min[b]<br>1.77[c] | 46 ± 14[a]<br>0.026 ± 0.001[b]<br>- | - | [a]Zeng et al., 2014; [b]Ge et al., 2015; [c]Li et al., 2011 |
| | Dog | 189.8 ± 12.1 | 0.2 | 2.3 ± 0.7 | 1.9 ± 0.9 | - | Huang et al., 2014 |
| | Human | 2.5 ± 0.5 µM/L[a]; 0.2 µM/L[b] | 24 min[a]; 180 min[b] | 42 min[a]; 325 min[b] | - | 20[b] | Yang et al., 2007[a]; Kern et al., 2003[b], Zhao and Moghadasian, 2008[b] |
| Catechin | Rats | 402.8 ± 65.0[a]<br>86.69 ± 38.65[b] | 1.4 ± 0.3[a]<br>0.15 ± 0.09[b] | 4.5 ± 0.8[a]<br>0.33 ± 0.12[b] | - | - | Huo et al., 2016[a] Zhang et al., 2012[b] |
| | Human | 75.1 ± 8.5 nmol/L | 1.44 ± 0.18 | 4.08 ± 0.38 | - | - | Bell et al., 2000 |
| Genistein | Human | 39 ± 3.7[a]<br>261.84[b] | 6.7 ± 1.1[a]<br>7.00[b] | 10.2 ± 0.9[a]<br>7.96[b] | 37.6 ± 10.9 L/h[a]<br>-- | --<br>-- | [a]Setchell et al., 2005; [b]Anupongsanugool et al., 2005 |
| | Rats | 4876.19 | 2 | -- | -- | 30.75% | Kwon et al., 2007 |
| Betulinic acid | Mice | 4.00 µg/mL | 0.22 | 1.18 | 12.72 | - | Udeani et al., 1999 |
| Quercetin | Human | 86 | 4.9 | 15.1 | -- | -- | Erlund et al., 2000 |
| Rutin | Human | 320 | 7 | 11.8 | -- | -- | Graefe et al., 2001 |
| Andrographolide | Rats | 1620[a]<br>230[b] | 1[a]<br>0.495[b] | 1.7[a]<br>2.37[b] | 7.17 mL/min[a]<br>-- | --<br>2.67%[b] | [a]Suo et al., 2007; [b]Ye et al., 2011 |
| Resveratrol | Human | 1942[a]<br>470 nM[b] | 2.80[a]<br>0.5[b] | 1.06[a]<br>0.82[b] | --<br>-- | --<br>-- | [a]Howells et al., 2011; [b]Amiot et al., 2013 |
| | Dogs | 1700-2600 | 1-2 | 2-4 | 41-58 | -- | Muzzio et al., |

| | | | | | | | |
|---|---|---|---|---|---|---|---|
| | | | | | L/h | | 2012 |
| | Rats | 5900[a]<br>3750[b] | 0.17[a]<br>0.25[b] | 1.16[a]<br>1.97[b] | 74.51 mL/min[a]<br>0.310 L/min[b] | --<br>-- | [a]Mukherjee et al., 2011;<br>[b]Liang et al., 2013 |
| Curcumin | Rats | 500[a]<br>86.55 ± 9.55[b] | 0.75[a]<br>0.60 ± 0.13[b] | 1.45[a]<br>1.21 ± 0.23[b] | 92.26 L/h[a]<br>-- | --<br>-- | [a]Maiti et al., 2007;<br>[b]Zhang et al., 2013 |
| | Rabbits | 230 | 2 | -- | 27.54 ± 3.09 L/h | -- | Arya and Pathak, 2014 |
| Ellagic acid | Human | 3.65 ± 1.71[a]<br>0.06 ±0.01 µmol/L[b] | 1.98 ± 2.87[a]<br>0.98 ± 0.06[b] | 8.41[a]<br>0.71 ±0.09[b] | --<br>-- | --<br>-- | [a]Stoner et al., 2005;<br>[b]Seeram et al., 2004 |
| | Rats | 1750.7 ± 769 | 0.264 ± 0.034 | 5.811 ± 0.93 | -- | -- | Hou et al., 2013 |
| Gallic acid | Human | 1.83 ± 0.16 µmol/L | 1.27 ± 0.20 | 1.19 ± 0.07 | 8.4 ± 2.4 L/h | -- | Shahrzad et al., 2001 |
| | Rats | 175.13 ± 45.2 | 0.2 | 0.57 | -- | -- | Gao et al., 2010 |
| Chlorogenic acid | Rats | 1013.91[a]<br>242[b] | 0.36[a]<br>0.5[b] | 2.54[a]<br>8.55[b] | --<br>-- | --<br>-- | [a]Anupongsanugool et al., 2005<br>[b]Zhou et al., 2013 |
| | Rabbit | 839 | 0.58 | -- | -- | -- | Yang et al., 2004 |

### *1.2.4. Ferulic acid*

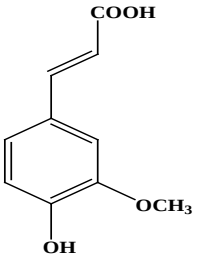


**Ferulic acid (1)**

Ferulic acid (**1**) [FA], (4-hydroxy-3-methoxycinnamic acid) is a dietary antioxidant naturally presents in food plants, especially in the wheat, rice, barley, oats (Alias et al.,. 2009), citrus fruits, tomatoes, a range of vegetables and medicinal herbs (Srinivasan et al., 2007). FA has been proven to afford significant protection to the skin against UV-B-induced oxidative stress in human lymphocytes and erythema (Prasad et al., 2007). The FA has shown to inhibit the expression of cytotoxic and inflammation-associated enzymes, including inducible nitric oxide synthase, caspases and cyclooxygenase-2 (Barone et al., 2009). Staniforth et al. have been reported that FA inhibited the UVB-induced matrix metalloproteinases and attenuates the degradation of collagen fibers, abnormal accumulation of elastic fibers and epidermal hyperplasia through posttranslational mechanisms (Staniforth et al., 2012). Several studies have been demonstrated that FA possesses antiageing (Srinivasan et al., 2006), hepatoprotective (Srinivasan et al., 2005), antiatherogenic (Rukkumani et al., 2004), antimutagenic (Murakami et al., 2002), anti-inflammatory, anticancer, antidiabetic (Barone et al., 2009), neuroprotective and cardioprotective activities (Srinivasan et al., 2007).

Pharmacokinetic profile of FA has been observed after oral administration of Chuanxiong and *Angelica sinensis* extract in rats at dose of 1.176 g/kg (equivalent to 8.82 mg/kg FA). The different pharmacokinetic parameters were detremined by a non-compartment model with $T_{max}$ = 1.1 ± 0.65 h, $C_{max}$ = 44.7 ± 8.2 ng/mL, $C_L$ = 46 ± 14 mL/kg/min, $AUC_{0-t}$ = 165 ± 46 ng h/mL, $T_{1/2}$ = 5.00 ± 0.78 h and MRT = 6.82 ± 0.60 h (Zeng et al., 2014). In another study, FA was orally administered to the rat at dose of 4 mg/kg and pharmacokinetic parameters were calculated by two compartment model with $AUC_{0-\infty}$ = 775.8 ± 59.4 min mg/L, $T_{max}$ = 15 min, $C_{max}$ = 1.6 ± 0.3 mg/L, $C_L$ = 0.026 ± 0.001 L/min/kg, $V_d$ = 12.4 ± 3.3 and $T_{1/2}$ = 333.2 ± 79.8 min (Ge et al., 2015). Similarly, FA pharmacokientics has been performed by Li et al. (2011), FA at 10 mg/kg dose was orally administered to the rat and different parameters were observed. FA was rapidly absorbed with a $T_{max}$ of 0.03 h. The corresponding $C_{max}$ and the $AUC_{0-t}$ were 8174.55 ± 1017.98 ng/mL and 2594.45 ± 237.98 h ng/mL respectively. FA was rapidly absorbed with a low bioavailability after a single oral administration (Li et al., 2011). The pharmacokinetics of FA has also been studied in dog after oral administration of Shao-Fu-Zhu-Yu decoction at a dose of 6.2 g/kg (0.6 mg/kg). Different parameters with $AUC_{0-t}$ = 314.9 ± 123.3 µg h/L, $C_{max}$ = 189.8 ± 12.1, $T_{max}$ = 0.2 h, and $T_{1/2}$ = 2.3 ± 0.7 h have been observed (Huang et al., 2014). In human, pharmacokinetic study of FA has been performed at dose of 4.3 µmol/kg BW after oral administration. $C_{max}$ and $T_{max}$, $T_{1/2}$, $AUC_{0-t}$ were found to be 2.5 ± 0.5 µmol/L, 24 min, 42 min and 114 ± 34 µmol min/L respectively (Yang et al., 2007). *In situ* or *ex vivo* absorption models suggest that FA can be absorbed from the stomach, jejunum and ileum. After a 25-min incubation of FA in the rat stomach, >70% of the FA absorbed from the stomach and it was recovered in the gastric mucosa, blood, bile and urine, resulting a fast gastric absorption of FA. Similarly, FA quickly absorbed from the jejunum and to a significantly lesser extent from the ileum when it was perfused in an isolated rat intestine model. Only 0.5-0.8% of ingested FA was found in feces of rats, indicating very efficient absorption rate for FA (Zhao and Moghadasian, 2008). Metabolic studies have represented that FA can be metabolized *in vivo* into various metabolites such as FA-glucuronide, FA-sulfate, FA-diglucuronide, FA-sulfoglucuronide (FA-diconjugate with sulfate and glucuronide), m-hydroxyphenylpropionic acid, feruloylglycine, dihydroferulic acid, vanillic acid and vanilloylglycine. Conjugated FA including FA-glucuronide, FA-sulfate and FA-sulfoglucuronide are the major metabolites in the plasma and urine of rats. These results suggest that the conjugation reaction with glucuronic acid and sulfate is the main pathway of *in vivo* metabolism of FA.

The metabolism and conjugation of FA takes place in the liver through the activities of mainly two enzyme including sulfotransferases and UDP glucuronosyl transferases. Intestinal mucosa and kidney may also, at least in part, contribute to this metabolism process. FA is mainly eliminated through urine in rats in free and conjugated forms. FA is also eliminated through bile, which accounts for about 4–6% of the oral dose (Zhao and Moghadasian, 2008). The low half-life of FA may suggest its low toxicity profile. The acute oral $LD_{50}$ of FA in female and male F344 rats was 2.1 and 2.4 g/kg, respectively

(Tada et al., 1999). No significant sub-chronic toxicity was found in female and male F344 rats after long-term (13 weeks) intake of of dietary FA at 0.16 g/kg BW per day (Tada et al., 2001). FA undergoes a marked first-pass effect which limits its oral bioavailability. Only a low percentage of unmodified FA (9-20%) was found in the plasma (Bourne and Rice-Evans, 1998).The bioavailability of FA has been addressed in several studies estimated as urinary excretion with variable results: from low to high bioavailability (0.4-98%), in part depending on the food source (Bourne et al., 2000; Karakaya, 2004; Manach et al., 2005). For instance, by consumption of cereal products, particularly bran, FA presented a low bioavailability: 3% in humans (Kern et al., 2003), 2.5-5% in rat (Adam et al., 2002) and even lower, 0.4-0.5%, from corn bran in rat (Zhao et al., 2005). The bioavailability of FA was somewhat higher from other food matrices such as tomato, 11-25% (Bourne and Rice-Evans, 1998) or rye bread, ~28% (Harder et al., 2004), while from beer, FA was highly bioavailable, 19-98% (Bourne et al., 2000).

### *1.2.5. Catechin*

Catechin [CA] (2R,3S)-2-(3,4-dihydroxyphenyl)-3,4-dihydro-1H-chromene-3,5,7-triol) is flavanol and enriched in green tea, coffee and several food products. Mostly (+)-catechin (**2**) is found with its other stereoisomers, (-)-catechin or epicatechin. It has been proven for strong antioxidant property. The other biological activities reported as anticancer, antidiabetic, hepatoprotective, antibacterial, anti-atherosclerotic, antiageing, anti-tyrosinase etc (Manach et al., 2005).

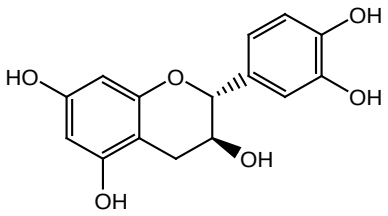


**Catechin (2)**

Pharmacokinetic parameters of catechin (**2**) were analyzed in rat plasma after oral administration of the green tea extract at different doses of 0.4, 1.2 and 2.0 g/kg (~51 mg of catechin). At a 0.4 g/kg dose different pharmacokinetic parameter was observed as, $C_{max}$ = 204.1 ± 32.7 ng/mL, $T_{max}$ = 1.4 ± 0.5 h, $AUC_{0-t}$ = 1214 ± 304.3 ng h/mL and $T_{1/2}$ = 2.9 ± 1.1h. Pharmacokinetic parameters $C_{max}$ = 326.8 ± 49.7 ng/mL, $T_{max}$ = 1.4 ± 0.6 h, $AUC_{0-t}$ = 2786 ± 601.8 ng h/mL and $T_{1/2}$ = 4.8 ± 1.2 h was determined at dose of 1.2 g/kg. At dose of 2.0 g/kg, different parameters such as $C_{max}$ = 402.8 ± 65.0 ng/mL, $T_{max}$ = 1.4 ± 0.3 h, $AUC_{0-t}$ = 3223 ± 649.3 ng h/mL and $T_{1/2}$ = 4.5 ± 0.8 h was calculated (Huo et al., 2016). In another study, pharmacokinetic parameter of catechin was studied in rat after oral administration of *Cynomorium songaricum* extract at dose of 15.25 g/kg (equivalent to 106 mg/kg catechin). $C_{max}$, $T_{max}$, $AUC_{0-t}$, $T_{1/2}$ of catechin in rat plasma were 86.69 ± 38.65 ng/mL, 0.15 ± 0.09 h, 109.7 ± 57.0 ng h/mL and 0.33 ± 0.12 h respectively. It was observed that the catechin was rapidly absorbed in rat plasma after oral administration of *C. songaricum* extracts (Zhang et al., 2012). Bell et al. (2000) investigated the pharmacokinetic study of catechin in human plasma after ingestion of a single serving of reconstituted red wine at dose of 121000 nmol (equivalent to 35 mg or 121 µmol catechin) for 8 h. Red wine was used as dealcoholized red wine reconstituted to its original volume with either water (DRW) or water and ethanol to contain 13%

ethanol (ARW v/v). For ARW, $C_{max}$ (78.3 ± 8.9 nmol/L), $T_{max}$ (1.44 ± 0.24 h), $AUC_{0-t}$ (306 ± 34 nmol·h/L), $T_{1/2}$ (3.17 ± 0.27 h) of catechin was calculated. In case of DRW, $C_{max}$ (75.1 ± 8.5 nmol/L), $T_{max}$ (1.44 ± 0.18 h), $AUC_{0-t}$ (306 ± 29 nmol·h/L), $T_{1/2}$ (4.08 ± 0.38 h) of catechin was estimated (Bell et al., 2000). The partition coefficient (log P) of catechin is ~0.30, demonstrating its hydrophilicity and exhibited poor lipid solubility hence poor bioavailability (Cho et al., 2011). Catechin possesses the extensive first pass (hepatic) metabolism and conjugated with glucuronic acid and sulphate groups. Catechin was also methylated but preferentially in the 3'-position. The exact nature of the major circulating metabolites of epicatechin has been elucidated, i.e., epicatechin-3'-O-glucuronide, 4'-O-methylepicatechin-3'-O-glucuronide, 4'-O-methylepicatechin-5- or 7-O-glucuronide, and the aglycones epicatechin and 4'-O-methylepicatechin. Because of this reason its bioavailability is ~40% (Fung et al., 2013) and half-life is ~1.25 h (Manach et al., 2005; Xie et al., 2011).

### *1.2.6. Genistein*

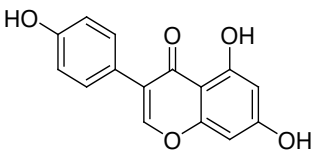


**Genistein (3)**

Genistein (**3**) [4',5,7-trihydroxyisoflavone], an isoflavone present in a number of edible plants, has been reported as a potential therapeutic agent with antiobesity, antidiabetic, anti-cancer, anti-oxidant, anti-inflammatory and anti-osteoporosis effects and proposed as a promising compound for the treatment of metabolic disorders. It is has been also established as a potent hepatoprotective agent in case of liver fibrosis (Behloul and Wu, 2013; Li et al., 2013). Soybean is the main source of isoflavones in the human diet, it contains between 0.6 and 3.8 g isoflavones/kg fresh weight (Cassidy et al., 2000).

Genistein (**3**) [GN] is classified as a poor soluble/permeable drug in the Biopharmaceutical classification system (BCS II) (Motlekar et al., 2006). The pharmacokinetics of GN has been studied in rats and humans (Zhang et al., 199), and demonstrated low bioavailability due first pass effect (Coldham and Sauer, 2000). After oral administration of GN with various doses (4, 20, 40 mg/kg), the bioavailability of GN was 38.58, 24.34 and 30.75%, respectively. The half-life ($t_{1/2}$) was estimated to be 4.53 ± 1.40, 4.41 ± 1.21, 5.25 ± 0.92 h for doses 4, 20, 40 mg/kg respectively. The $T_{max}$, $C_{max}$ and $AUC_{0-\infty}$ of genistein after oral administration of genistein (40 mg/kg), were 2 h, 4876.19 ng/mL, 31269.66 ng h/mL, respectively (Kwon et al., 2007). Further investigation demonstrated that pharmacokinetics of diadzein and GN, after ingestion of soy beverage compared with soy extract capsules in postmenopausal Thai women (Anupongsanugool et al., 2005). They received either 2 soy extract capsules equivalent to genistein (3.90 ± 0.04) and diadzein (11.29 ± 0.17 mg/capsule) or 15 g of soy beverage (genistein and diadzein content 0.62 ± 0.005 and 0.70 ± 0.01 mg/g). The first peak of plasma daidzein concentration was reached ~1 h after ingestion of both preparations, whereas, the second peak attained higher plasma concentrations at 5.92 ± 2.43 h for soy beverage, and 6.25 ± 2.26 h for soy extract capsules. The $C_{max}$ were

96.31 ± 36.18 ng/mL and 96.02 ± 27.71 ng/mL for soy beverage and soy extract capsules, respectively. It also revealed that the elimination $t_{1/2}$ was 7.68 ± 4.14 h for soy beverage and 6.67 ± 1.65 h for soy extract capsules (Anupongsanugool et al., 2005). Especially for this class of substance, solubility enhancement is crucial part of the strategies to improve bioavailability. Even worse once absorbed in human body, GN undergoes rapid degradation and excretion within 24 h (Rusin et al., 2010; Zhou et al., 2008). Poor solubility in aqueous system of GN and daidzein needs a solubility enhancement for pharmaceutical use. There have been several detailed studies on absorption, distribution, metabolism and excretion of GN in rats. Although GN is rapidly absorbed in the small intestine, it has a low bioavailability due to its poor aqueous solubility. GN exists in the systemic circulation after being absorbed as several molecular forms including glucuronide and sulfate conjugates, free GN and protein-bound form. Of these, the primary metabolite of GN is reported to be GN-glucuronide and GN-sulfate, and the metabolism is believed to occur mainly in the liver and epithelial cells of the intestinal wall. It has been reported that following infusion of the duodenum with GN, the major metabolite in portal blood is GN-7-O-glucuronide. Thus, both the liver and intestine seem to contribute to the first pass effect. GN is known to be excreted as GN metabolites such as dihydro-GN, 6'-OH-O-desmethylangolensin, trihydroxybenzene and 3', 4', 5, 7-tetrahydroxyisoflavone through feces and urines (Rusin et al., 2010; Zhou et al., 2008).

### *1.2.7. Betulinic acid*

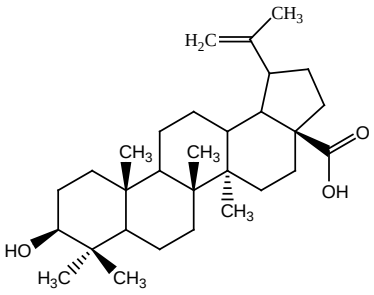


**Betulinic acid (4)**

Betulinic acid (**4**) [BA] (3β-hydroxy-lup-20(29)-en-28-oic acid) is a pentacyclic triterpenoid and widely distributed throughout the plant kingdom (Mukherjee et al., 2010). BA has been proved for its antioxidant, antifibrotic and hepatoprotective activity (Ciesielska et al., 2011; Adesanwo et al., 2013; Yi et al., 2015). BA possess other biological activities including anticancer, antiviral, antimalarial, anti-inflammatory, antimicrobial, anthelmintic, antitumor, anti-HIV, immunemodulatory and antiobesity (Yogeeswari and Sriram, 2005; Subramanyam et al., 2009; Kim et al., 2012; Dash et al., 2015, Melo et al., 2009). BA is a white crystalline solid compound and having poor aqueous solubility. The poor solubility of BA in aqueous systems generated a great deal of interest in investigating several formulation schemes (Cichewicz and Kouzi, 2004). In addition, molecular modeling experiments have predicted that BA may be a substrate for cytochrome P450. Human CYP2C9 exhibits selectivity for substrates containing an ionizable carboxylic acid group or an analogous group lead to biotransformation process (Lewis et al., 1998). The pharmacokinetics of betulinic acid (**4**) is performed the in CD-1 mice. BA is administered at dose of 250 and 500 mg/kg i.p. and the serum concentrations reached peaks ($T_{max}$) at 0.15 and 0.22 h, respectively. $C_{max}$ and AUC was determined as 2.21, 4.00 µg/mL, and 18.40 and 39.90 µg/h/mL for 250 and 500 mg/kg dose. It has been

observed that BA has an elimination half-life of 0.98 and 1.81 h and total clearances of 13.78 and 12.72 L/kg/h at dose of 250 and 500 mg/kg, respectively (Udeani et al., 1999). BA has been associated with several beneficial health effects; however their solubility in the gastrointestinal tract is low and hence its oral bioavailability is limited due to poor absorption and rapid elimination from the body (Garduño et al., 2015).

### *1.2.8. Rutin*

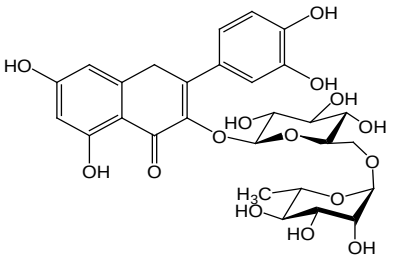

**Rutin (5)**

Rutin (**5**) [3,3',4',5,7-pentahydroxyflavone-3-rutino-quercetin 3-rhamnosylglucoside] is a natural flavones derivative found in abundance in buckwheat but also present in many other plants, including asparagus, citrus fruits and berries. Rutin is classified in class II (poor soluble/permeable) in the BCS (Mauludin et al., 2009). Rutin has significant scavenging properties on oxidizing species such as OH radical, superoxide radical, and peroxyl radical. Furthermore it has been reported for several pharmacological activities including antiallergic, anti-inflammatory and vasoactive, antitumor, antibacterial, antiviral and anti-protozoal properties. Moreover, it has also been reported for hepatoprotective, hypolipidaemic, cardio-protective, neuro-protective cytoprotective, antispasmodic and anticarcinogenic activities (Chat et al., 2011). The disadvantage of the molecule is its poor solubility in aqueous media, being the reason for its poor bioavailability. Therefore it imposes yet some restraints to further pharmaceutical use, especially for oral administration (Miyake et al., 2000). Oral administration is also desired for the application of rutin as nutritional supplement to be taken daily (Mauludin et al., 2009). In the pharmacokinetic study of rutin (**5**) that profound lag-time of several hours has been achieved with $C_{max}$ within ~7 h (Erlund et al., 2000). $C_{max}$ and $AUC_{(0–24)}$ was found linearly with dose dependent manner. After intake of 400 mg rutin [~200 mg quercetin aglycone], mean maximum plasma concentrations were observed 0.32 µg/mL at 7 h, while mean $AUC_{(0–24)}$ was 2.5 µgh/mL. Absorption of the quercetin aglycone was faster than rutin but slower as compared to other glucosides. $T_{max}$ was observed in the range of 1.9 to 4.9 h (Erlund et al., 2000). Mean $AUC_{(0–32)}$ and $C_{max}$ values were similar after intake of comparable doses of free quercetin and rutin (Erlund et al., 2000; Graefe et al., 2001). After oral administration only traces of free quercetin were found in human plasma that means rutin converted into quercetin metabolites such as quercetin 3-O-β-D-glucuronide, quercetin 4'-O-β-glucoside and quercetin 3'-O-sulfate. The $t_{1/2}$ of quercetin was found to be 3.8 h (Morand et al., 2000). Rutin undergoes hepatic first pass metabolism. Rutin was found being hydrolyzed to quercetin in the intestine, then absorbed as quercetin and presented as conjugated metabolites of quercetin in the circulation. Due to this reason its bioavailability is only ~20%. Half-life of rutin is ~11 h (Manach et al., 2005; Yang et al., 2005).

### *1.2.9. Andrographolide*

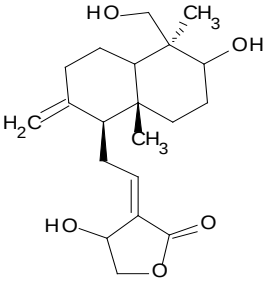

**Andrographolide (6)**

Pharmacokinetic profile of andrographolide (**6**) (AP) has been observed after oral administration of tablets (equivalent to 10 mg/kg) in rats. The different parameters were observed by a one-compartment open model as $T_{max}$ = 59.69 ± 3.61 min, $C_{max}$ = 1.62 ± 0.11 µg/mL, $V_d$ = 1056.90 ± 83.42 mL, $AUC_{0-\infty}$ = 348.75 ± 24.41 µg min/mL (Suo et al., 2007). The absolute bioavailability of AP was found to be 2.67%. AP has poor oral bioavailability because of its rapid biotransformation and efflux by P-gp (Ye et al., 2011).

### *1.2.10. Resveratrol*

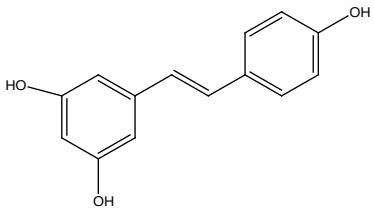

**Resveratrol (7)**

Resveratrol (**7**) [3, 4, 5-trihydroxystilbene] is exhibited low bioavailability in a various pharmacokinetic study (Delmas et al., 2011). The several parameters has been studied after oral administration of resveratrol (~25 mg/70 kg) to healthy male subjects as white wine, white grape juice, or vegetable juice. The $C_{max}$ were achieved after 30 min and concentrations declined rapidly after reaching baseline levels within 4 h due to rapid and extensive metabolism. However, the low plasma levels of free resveratrol attained (<40 nmol/L) (Goldberg et al., 2003). Resveratrol-3-O-sulfate, resveratrol-4′-O-glucuronide and resveratrol-3-O-glucuronide were found as major metabolites of resveratrol (Boocock et al., 2007; Brown et al., 2010).

### *1.2.11. Curcumin*

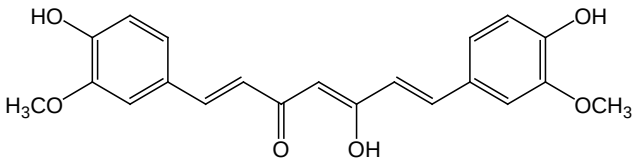

**Curcumin (8)**

Curcumin (**8**), a hydrophobic polyphenol exhibited low bioavailability (Anand et al., 2007) due to extensive metabolism. In pharmacokinetic studies, Holder et al. have been reported that the major biliary metabolites of curcumin were glucuronides of tetrahydrocurcumin and hexahydrocurcumin in rats. A negligible amount of curcumin was observed in blood plasma after oral administration of 1 g/kg, it revealed that curcumin was poorly absorbed from the gut (Holder et al., 1978; Wahlstrom and Blennow, 1978). After oral administration of 400 mg of curcumin to rats, no curcumin was found in blood/plasma, whereas a trace amount (≦5 µg/mL) was found in the portal blood (Ravindranath and Chandrasekhara, 1980). In another study, curcumin was given orally at a dose of 2 g/kg in rats, a maximum serum concentration of 1.35 ± 0.23 µg/mL was observed at time 0.83 h. In humans, the same dose of curcumin resulted in either

undetectable or extremely low (0.006 ± 0.005 µg/mL at 1 h) serum levels (Shoba et al., 1998; Pan et al., 1999). Similarly, in a human clinical trial study, curcumin (3.6 g) produced a plasma level of 11.1 nmol/L after an hour of dosing (Sharma et al., 2004; Marczylo et al., 2007). The absorption and elimination $t_{1/2}$ of orally administered curcumin (2 g/kg) in rats were reported to be 0.31 ± 0.07 and 1.7 ± 0.5 h, respectively (Yang et al., 2007).

*1.2.12. Ellagic acid*

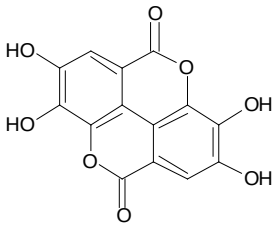

**Ellagic acid (9)**

Ellagic acid (**9**) [EA], is a well known bioactive (polyphenol) compound present in several plants, berries and pomegranate, has received attention due to several health benefits. Photoprotective effects of EA on collagen breakdown and inflammatory responses in UVB irradiated human skin cells and hairless mice have been reported. Ellagic acid attenuated the UVB-induced toxicity of HaCaT keratinocytes and human dermal fibroblasts. EA markedly prevented collagen degradation by blocking matrix metalloproteinase production in UVB exposed fibroblasts (Bae et al., 2010). EA also demonstrates a variety of activities anticarcinogenic anti-bacterial, anti-viral etc. (Hamad et al., 2009). The pharmacokinetics of EA has been determined in healthy volunteers fed with freeze-dried black raspberries 45 g (equivalent to 13.5 mg ellagic acid) for 7 days. After 1 day $C_{max}$, $T_{max}$, AUC and Mean $t_{1/2}$ were found to be 3.65 ±1.71 ng/mL, 1.98 ± 2.87 h, 16.56 ± 7.66 ng.h/mL and 8.41. Similarly 3.25 ± 1.52 ng/mL, 2.00 ± 1.97 h, 17.61 ± 9.15 ng.h/mL and 8.57 h were observed after 7 days (Stoner et al., 2005). In another study, EA was given in 18 human volunteers at a single dose of pomegranate juice 180 mL (~12 mg EA). The $C_{max}$ was 0.06 ± 0.01 µmol/L, and the corresponding AUC [0.17 ± 0.02 (µmol.h).$L^{-}$1] was attained while $T_{max}$ was 0.98 ± 0.06 h. The elimination $t_{1/2}$ was found to be 0.71 ± 0.08 h (Seeram et al., 2004; Murugan et al., 2009).

*1.2.13. Gallic acid*

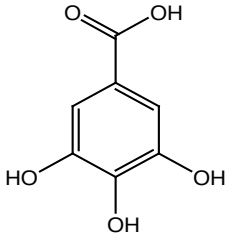

**Gallic acid (10)**

Pharmacokinetics of gallic acid (**10**) [GA; 3,4,5-trihydroxy benzoic acid] has been done through different studies and found low bioavailability (Bhattacharyya et al., 2013). In an experiment, healthy human volunteers have been given 2 *Acidum gallicum* tablets after (25 mg GA each tablet) or 125 mL Assam black tea brew (~50 mg GA).The oral absorption of GA from both sources was fast ($T_{max}$: 1.27 ± 0.20 h for *Acidum gallicum* tablets and 1.39 ± 0.21 h for the tea). But the highest GA concentrations observed in plasma were 1.83 ± 0.16 µmol/L (tablets) and 2.09 ± 0.22 µmol/L (tea). The elimination $t_{1/2}$, elimination rate constant and $C_L$ were found to be 1.19 ± 0.07 h, 0.58 ± 0.03 $h^{-1}$ and 8.4 ± 2.4 $L.h^{-1}$, respectively for the tablets and 1.06 ± 0.06 h, 0.65 ± 0.04 $h^{-1}$ and 8.4 ± 2.0

$L.h^{-1}$ respectively for the tea brew (Gao et al., 2010). In another experiment, the pharmacokinetic profile has been evaluated after oral administration of 50, 100 and 150 mg/kg grape seed extract (equivalent to 91 mg GA/gm) in male Sprague Dawley rats. Absorption of GA was observed to be significantly higher from a single oral dose of 150 mg/kg. AUC and $C_{max}$ were significantly higher. For gallic acid AUC were found to increase by 198% by dose escalation (Ferruzzi et al., 2009).

*1.2.14. Chlorogenic acid*

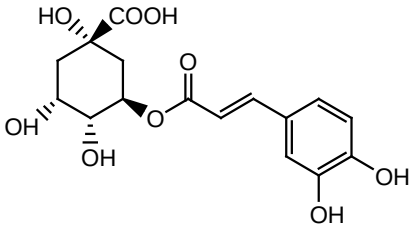


**Chlorogenic acid (11)**

Chlorogenic acid [CGA] (**11**) is an ester formed between caffeic acid and quinic acid (Konishi and Kobayashi, 2004). CGA was hydrolyzed by intestinal microflora into caffeic acid and quinic acid metabolites (Chen et al., 2013). The pharmacokinetic profile of CGA has been determined in rat model after oral administration *Flos lonicerae*. A two-compartment model was selected for calculation of different parameters. At the administered doses of 200, 400 and 600 mg/kg, the absorption half-life ($t_{1/2\ Ka}$) were 10.23, 18.66 and 28.13 min respectively while elimination $t_{1/2}$ were of 231.64, 337.23 and 420.81 min. The $V_d$ at the three doses were 55.26, 35.56, 32.22 L/kg, respectively. The $AUC_{0-\infty}$ was not proportional to the administered dose and found to be nonlinear kinetics (Ren et al., 2007). In another experiments, the plasma levels and pharmacokinetics of CGA has been determined in rabbit after single administration of *Flos lonicerae* extract at a dose of 10 g/kg (~220 mg CGA) body weight (Yang et al., 2004). The plasma CGA level reached a $C_{max}$ of 0.839 ± 0.35 µg/mL at 34.7 ± 1.1 min. A second peak of CGA appeared at 273.4 ± 39.6 min in the plasma with a concentration 0.367 µg/mL. The various pharmacokinetic parameters were found as AUC: 140 ± 65.9 µgmin/mL and $K_{el}$: 0.0130 ± 0.0023 $min^{-1}$ (Qin et al., 2006).

## 1.3. Challenges in developing herbal formulations

Herbal medicine is still a challenge for developing into suitable dosage forms for promotion and development of human health. There are several challenges for developing an appropriate delivery system, due to their limited solubility and permeability through biological membranes, so much so their low therapeutic efficacy and bioavailability. Research is now being concurrently conducted on basic as well as applied fields of herbal medicines, and this has led to the need for research in the delivery system of herbal drugs for maximum concentration as well as bioavailability (Mukherjee et al., 2009).

### *1.3.1. Modification for half-life of herbal drugs*

The biological half-life ($t_{1/2}$) has an immense role in the therapeutic efficacy and potency of drug molecules at the site where it is administered. If drugs have shorter $t_{1/2}$, then they possess low bioavailability when compared to those with higher $t_{1/2}$. The biological membrane permeability of such molecules offers more activity for lipophilic action, hence its chances of availability in the blood/plasma are more in comparison to hydrophilic compounds. However, 40% of the active pharmaceutical ingredients obtained from high-throughput screening are poorly soluble molecules. Lower bioavailability results from poor solubility and incomplete dissolution *in vivo*. This often holds back continuous development and coming into the market of some promising new chemical entities (NCEs), or elicits insufficient therapeutic effects from certain drugs. The increasing numbers of poorly soluble drugs require innovative formulation approaches to acquire a sufficient bioavailability level after oral administration. In other words, the hepatic biotransformation of the drug molecules is related to more renal elimination, which lowers the bioavailability of drugs (Rahman et al., 2013). A lot of research is going on to overcome the problem associated with herbal medicine by applying NDDS.

### *1.3.2. Drug delivery systems to enhance bioavailability of herbal medicine*

A great deal of herbal products for therapeutic application is being acquired through the use of herbs, and information is increasing quickly with greater understanding of molecular mechanisms of diseases. Nevertheless, favorable drug action alone against the disease is insufficient to satisfy the medical community. In addition, avoiding unwanted side effects at the site of action is equally important. The pharmacological activity of any administered drug relies not only on its therapeutic efficacy but also on the bioavailability at the administered site. Several phytopharmaceuticals possess low aqueous solubility, which means poor membrane permeability and therefore low oral bioavailability. Conception and evolution into a suitable pharmaceutical formulation for delivery of certain phytoconstituents is of premier importance. The promotion of novel technologies is providing a large platform for novel delivery systems of herbal medicine to improve the therapeutic activity along with bioavailability of drugs that have poor aqueous solubility. Promising novel approaches are being developed including phytosome/herbosome, liposome, nanostructured lipid carriers (NLCs), NE, polymeric nanoparticles (NPs), dendrimers, micelles, and so on (Mishra et al., 2010). These novel technologies can modulate the pharmacokinetics of existing drugs, and it may be helpful to enhance delivery of herbal medicine to target sites. In this regard, the discussion on some of the delivery systems has made an impact either by enhancing the delivery of the herbal drugs to their target tissues or by increasing their bioavailability by manifold (Aqil et al., 2013).

## 1.4. Techniques for novel drug delivery system for herbal formulation

In the development of novel therapeutics, the ability to devise a suitable pharmaceutical formulation for delivery is of utmost importance. Therefore delivery of the phytomolecules is critical for effective prevention and treatment of diseases. The emergence of new technologies has engendered great interest in developing NDDS to advance both the pharmacological and therapeutic properties of herbal drugs. There is continuous quest for information and technology to overcome the shortcomings associated with herbal medicine for therapeutic effect as well bioavailability enhancement. In this context, the NDDS are pioneering to curb the problems related to herbal drugs, which are systematically represented in Figure 1.1.

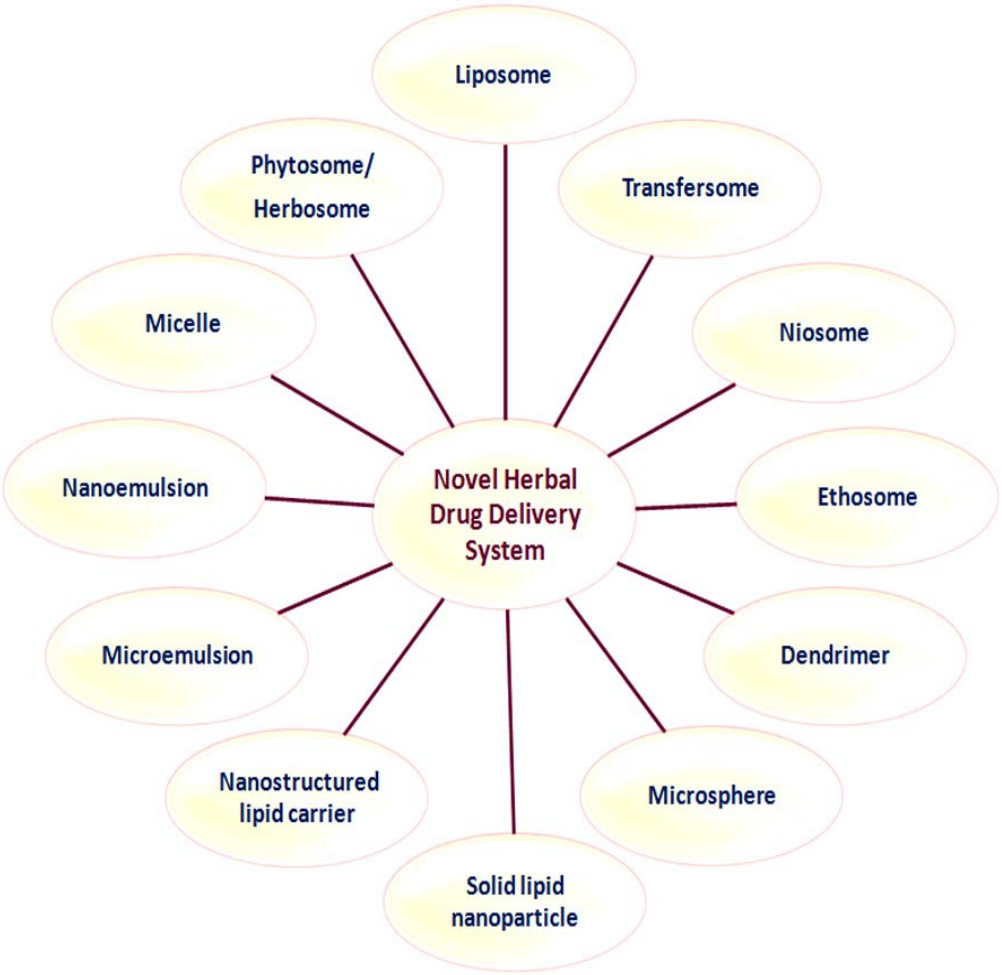


**Figure 1.1. Different novel delivery systems for herbal drugs**

The nano sized novel drug delivery systems of herbal drugs have a potential future for enhancing the activity and overcoming problems associated with plant medicines. The applications of NDDS in herbal medicine are explained through Figure 1.2.

In this section we would discuss some of the delivery methods that have already made an impact either by enhancing the delivery of different herbal products to its target tissue or increasing its bioavailability by many folds (Braithwaite et al., 2014).

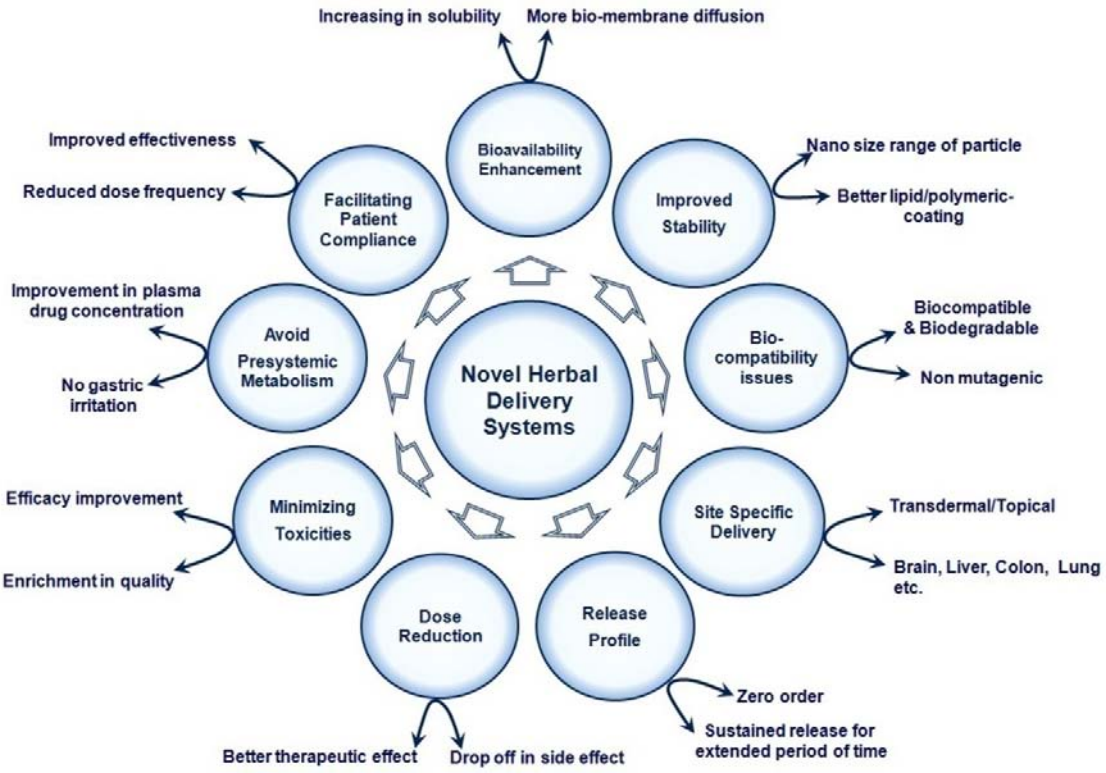


**Figure 1.2. Salient features of novel herbal delivery system**

### *1.4.1. Liposome*

Liposome is a bilayer lipidic vesicular carrier system of phospholipids/cholesterol varies in size ranging from 25 nm to 2.5 nm. The distinct advantages are their ability to encapsulate various materials and their structural versatility. Liposome can encapsulate drugs with a widely varying solubility or lipophilicity, either entrapped in the aqueous core of the phospholipid bilayer or at the bilayer interface. Liposome composed of natural lipids is biodegradable, biologically inactive, non-immunogenic, and possess limited intrinsic toxicity (Aqil et al., 2013). The structure of liposome is described in Figure 1.3. Therefore,

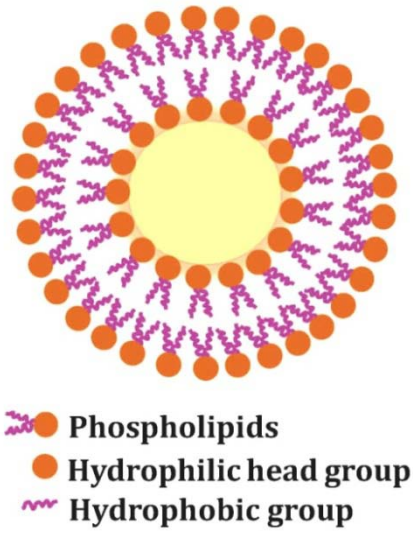


**Figure 1.3. Structure of liposome**

drugs encapsulated in liposome are expected to be transported without rapid degradation and to result in minimum side effect. Liposome is increasingly used with the herbal products to deliver certain drugs for the prevention or treatment of a variety of diseases. Several formulations have been developed and studied in regards to relative stability, pharmacokinetic properties, biodistribution and toxicity. Moreover, liposomes are able to deliver drugs into target site by fusion or endocytosis process. Despite the many advantages of liposomes, including safety and biocompatibility, their main drawback is instability in plasma (Aqil et al., 2013). El-Samaligy et al. prepared silymarin encapsulated hybrid liposomes which shows successful preparation with efficient encapsulation of silymarin. Liposome Herbasec®, one of the liposomal powders marketed with standardized botanical extracts using white and green tea, white hibiscus, guarana and aloe, successfully improved the activities of their herbal ingredients. This is a novel means of delivering drugs in a controlled manner to enhance bioavailability and get the therapeutic effect over a longer period of time (El-Samaligy et al., 2006).

### *1.4.2. Transfersome*

Transfersome are vesicular system consisting of phospholipids as the main ingredient with 10-25% surfactant (such as sodium cholate) and 3-10% ethanol. The surfactants work as “edge activators”, conferring ultra-deformability on the structure of transfersome, which helps them to squeeze through pores in the *stratum corneum* (SC). In comparison to liposome, transfersome can squeeze through SC layers spontaneously at ~ 500 nm pore size while liposome are too large to pass through pore size ≤50 nm (Benson, 2005). Transfersome are also known as elastic vesicles due to its deformability in nature and can pass through intact skin under the influence of hydration gradient, transporting therapeutic agents only when applied under non-occlusive conditions (Bavarsad et al., 2012). The method of preparation of trasfersome is similar to the liposome. The hypothesized mechanism of action of transfersome is described as followings: (i), vesicles act as a drug carrier; intact vesicles enter the SC carrying vesicle bound drug molecules into the skin, (ii) vesicles act as penetration enhancers and enter the SC and then modify the inter-cellular lipid lamellae and consequently facilitate the penetration of unbound drug molecules into and across the SC (Bavarsad et al., 2012). It can be applicable as novel delivery systems for phyto-pharmaceuticals to enhance its permeability as well as bioavailability. Transfersome can penetrate SC and supply the nutrients locally to access its functions resulting maintenance of skin in this context the transfersome of capsaicin has been prepared which exhibited the better topical absorption in comparison to pure capsaicin (Ajazuddin and Saraf, 2010).

### *1.4.3. Niosome*

Niosome is hydrated vesicular systems of nonionic surfactants with phospholipid or cholesterol and deliver drugs to target sites. The lamellar structures of these vasicular

systems are fabricated of amphiphilic molecules and surrounded by an aqueous compartment. Vesicular systems are applicable for both hydrophilic and hydrophobic drug delivery, which is encapsulated in interior hydrophilic compartment and outer lipid layer respectively (Mahale et al., 2012). It is a biodegradable, biocompatible, non toxic, stable over a longer period of time in different conditions, and is capable of encapsulating large quantities of material in a relatively small volume of vesicles. Furthermore, these are versatile carrier systems that can be administered through various routes including i.m., i.v. injection, peroral, ocular, pulmonary, and transdermal (Junyaprasert et al., 2012). The structure of niosome is represented in Figure 1.4. Niosomes are such bilayer lipidic system consisting of nonionic surfactants. Nonionic surfactants used due to their ability to increase solubility of poorly water soluble drugs and therefore enhanced bioavailability. Comparatively to liposome, they have longer shelf life, stability and ability to deliver drugs at target site in a controlled or sustained manner for extended periods. Niosome increased the permeability and fluidity of biological membrane of drug molecules like podophylotoxin, etoposide and methotrexate show enhanced bioavailability by transdermal application (Mahale et al., 2007). Junyaprasert et al (2012) studied the ellagic acid (EA) loaded niosome where the in vitro skin permeation revealed that permeation of EA depends on vesicle size, amount of EA entrapped and the added solubilizers which may act as permeation enhancer. From skin distribution study, the EA-loaded niosome showed more efficiency in the delivery of the EA through human epidermis and dermis than EA solution (Junyaprasert et al., 2012).

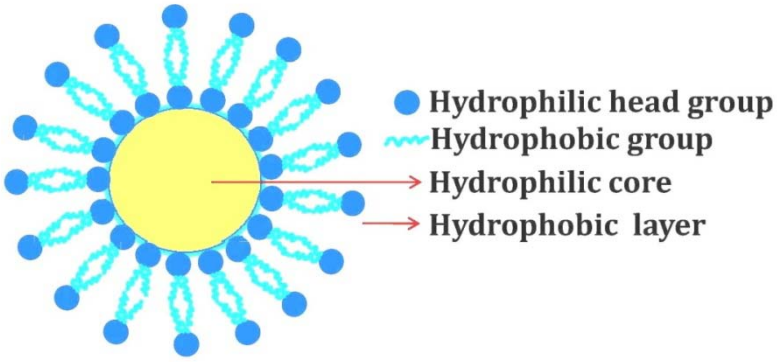


**Figure 1.4. Structure of niosome**

### *1.4.4. Ethosome*

Ethosomes are lipid vesicular systems with alcohol (ethanol) capable of enhancing penetration to the deep tissues of skin and then systemic circulations. It is assumed that the alcohol interacts with ethosomal lipids and SC bilayer lipids, thus allowing the soft, malleable ethosomes to penetrate (Benson, 2005). Recently, ethosomes are promising and novel vesicular systems that have appeared in the fields of the herbal product and drug delivery. This system has interesting characteristic correlated with its ability to permeate intact through the SC due to its high deformability. Indeed, ethosomes are soft, malleable vesicles tailored for enhanced delivery of phytomolecules. It has been reported that the physicochemical features of ethosomes

allow this vesicular carrier to transport drug molecules more efficaciously through the SC into the deeper layers of the skin than conventional liposomes. This is an important aspect in the design of the carriers to be applied topically for delivery of herbal drugs (Paolino et al., 2005). Moreover, it facilitates percutaneous absorption of matrine as an anti-inflammatory herbal agent (Ajazuddin and Saraf, 2010). In addition, ethosomes elicited an increase of the percutaneous permeation of ammonium glycyrrhizinate thereby enhancing the anti-inflammatory activity of this drug in an in vivo model. These results are very encouraging and confirm that ethosomes are a very promising career in the topical administration due to the enhanced delivery of drugs through the skin (Paolino et al., 2005).

### *1.4.5. Dendrimer*

Dendrimers are three dimensional hyperbranched, tree-like polymers having massive potential in drug delivery, targeting, diagnosis and as carriers for DNA/gene delivery. Dendrimers have hydrophilic exteriors and hydrophilic interiors, which are responsible for its unimolecular micellar nature (Jain and Gupta, 2008). Dendrimers have some interesting features because of their globular form and interior cavities. Another feature is the possibility to encapsulate drug molecules in the macromolecule interior. The interactions between drug molecules and poly-amido-amine (PAMAM) dendrimers by covalent conjugation are complexed by van der Waals interactions, or incorporated in the empty spaces within branches. This complexation is important in terms of stability, controlled release, high drug loading and reduced toxicity leads to the higher bioavailability of the drugs. In addition dendrimers can be surface engineered to release the drug at the site specific as targeted drug delivery. This property along with the solubilisation behavior could increase the therapeutic efficacy of drugs (Jain and Gupta, 2008). Abderrezak et al. studied the interaction of several dendrimers of different compositions mPEG-PAMAM (G3), mPEG-PAMAM (G4) and PAMAM (G4) with hydrophilic and hydrophobic drugs cisplatin, resveratrol, genistein and curcumin at physiological conditions. Structural investigation was resulted that cisplatin binds dendrimers in hydrophilic mode via ‘Pt’ cation and polymer terminal $NH_2$ groups, while curcumin, genistein and resveratrol were found in the cavities binding through both hydrophobic and hydrophilic channels (Abderrezak et al., 2012).

### *1.4.6. Microsphere*

Microsphere refers to spherical micro particles with a diameter of 1-1000 µm. Biodegradable polymers are frequently used for development of microsphere matrixes such as polylactic acid (PLA) and copolymer of lactic acid and glycolic acid (PLGA). Beside from them, there is an extensive range of microsphere prepared from albumin, albumin dextran sulfate and fibrinogen. Administration of medication via micro particulate systems is advantageous because microspheres can be ingested or injected; and they can be tailored for desired release profiles and used site-specific

delivery of drugs and in some cases can even provide organ-targeted release. So far a series of phytomedicine such as rutin, camptothecin, zedoary oil, tetrandrine, quercetine and *Cynara scolymus* extract have been successfully exploited through this delivery system. In addition, reports on immune microsphere and magnetic microsphere are also common in recent years. Immune microsphere possesses the immune competence as a result of the antibody and antigen was coated or adsorbed on the polymer microspheres (Ajazuddin and Saraf, 2010).

### *1.4.7. Nanoparticle*

Nanoparticles range in size from 10 to 1000 nm and can be synthesized from lipids, proteins and carbohydrates, as well as several natural and synthetic polymers. For delivery, a drug is dissolved, entrapped, encapsulated or attached to a NPs matrix. Their use to improve the therapeutic index of encapsulated drugs either by protecting them from enzymatic degradation, altering pharmacokinetics, reducing toxicity or providing controlled release over extended periods of time. NPs may enhance the oral bioavailability of poorly soluble drugs and the tissue uptake after parenteral administration, through adherence to the capillary wall. The nanoparticulate systems of herbal medicines have attracted much attention for examples, nanonized curcuminoids (Tiyaboonchai et al., 2007), paclitaxel (Arica et al., 2006) and praziquantel which have a mean particle size of 450, 147.7, and even higher than 200 nm, respectively. Furthermore glycyrrhizic acid, quercetin, berberine and artemisinin have been incorporated in the NPs which found to improve their bioavailability and bioefficacy (Mainardes and Evangelista, 2005).

### *1.4.8. Solid lipid nanoparticles and nanostructured lipid carriers (NLCs)*

Solid lipid nanoparticles (SLNs) are prepared from lipids which are solid at room temperature as well as at body temperature. Different solid lipids are exploited to produce SLNs, such as, tripalmitin, cetyl alcohol, cetyl palmitate, glyceryl monostearate, trimyristin, tristearin, stearic acid etc. There are several advantages of SLN formulations, such as: (i) protection from degradation in the external environment (during storage) and in the gut, (ii) improved bioavailability, (iii) biocompatibility and (iv) easy of scaling up at industrial production level (Das and Chaudhury, 2011). The schematic diagram of SLN is depicted in Figure 1.5. In case of NLCs, spatially very different lipid molecules are mixed to create a lipid particle matrix as imperfect as possible. Generally, solid and liquid lipids are mixed to produce NLCs that are still solid at room temperature as well as at body temperature. Due to many imperfections in NLCs, drug-loading capacity is enhanced and drug expulsion during

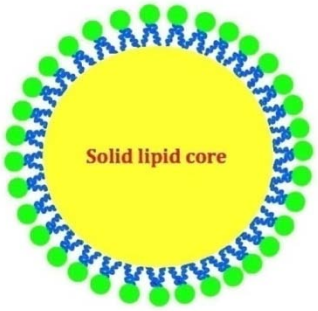


**Figure 1.5. Schematic representation of SLN**

storage is minimized. NLCs have several advantages, such as: (i) NLC dispersions with higher solid content can be produced, (ii) drug-loading capacity is better than SLNs, (iii) drug release profile can be easily modulated, (iv) drug leakage during storage is lower than SLNs, and (v) production of final dosage forms (e.g., tablets, capsules) is feasible (Das and Chaudhury, 2011). These technologies are applied to many herbal compounds. In a pharmacokinetic study in male rats at an oral dose equivalent to 10 mg $kg^{-1}$ demonstrated that α-asarone-loaded SLNs improve oral bioavailability and tissue uptake of the α-asarone compared to pure α-asarone group (Wang et al., 2008). *In vivo* pharmacokinetics following oral administration of curcumin-loaded SLNs (50, 25, 12.5, and 1 mg $kg^{-1}$ dose) and curcumin solution (50 mg $kg^{-1}$) demonstrated significant improvement in oral bioavailability (39, 32, 59, and 155 times at 50, 25, 12.5, and 1 mg $kg^{-1}$ dose, respectively) after administration of SLNs in compare to curcumin solution (Hu et al., 2010). In another pharmacokinetic study with quercetin SLNs in rats following oral administration of quercetin (50 mg $kg^{-1}$) in the form of either SLNs or suspension resulted that the relative bioavailability of quercetin-SLNs to quercetin suspension found to be 571.4%. The Tmax and MRT for quercetin in plasma were delayed. The study suggested that SLNs may be potential carrier systems to enhance the absorption of poorly soluble drugs (Li et al., 2009).

### *1.4.9. Micelles*

Micelles are lipid molecules that set themselves in a spherical form in aqueous solutions. Polymeric micelles range from 10 to 100 nm in size, and they are usually very narrow. They increase the drug solubility, stability hence its bio-membrane permeability and bioavailability through micellar surroundings. Drug release from micelles is governed by various factors, such as micelle stability, the rate of drug diffusion, the partition coefficient and the rate of copolymer biodegradation. Polymeric micelles designed from amphiphilic block copolymers have been found to hold a significant potential as drug delivery vehicles for a variety of anticancer drugs due to unique properties, such as high solubility and low toxicity. They can also lessen the P-glycoprotein efflux effect and, consequently, exerts a different mechanism of action from the entrapped drugs (Mikhail et al., 2009). The high toxicity of potent chemotherapeutic drugs like paclitaxel, doxorubicin and many others limit the therapeutic window in which they can be applied, which can be expanded by using this form of delivery system. Preclinical studies revealed that in colon 26-bearing CDF1 mice, an over 50-times higher AUC obtained, while the maximum plasma concentration ($C_{max}$) in tumors was 3-times higher compared to paclitaxel alone (Hamaguchi et al., 2005). In summary, polymeric micelle systems have become increasingly important in oncology, and so far the evidence

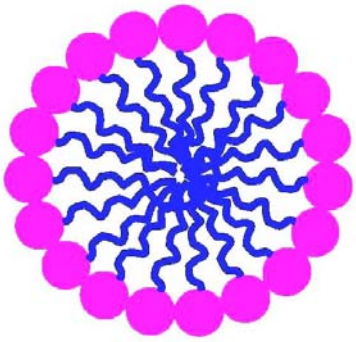

**Figure 1.6. Structure of micelle**

points to an increasing hope for use in cancer therapy. The structure of micelle is shown in Figure 1.6.

### *1.4.10. Phytosome*

Phytosome is a novel technology emerged in 1989. The term “phyto” means plant/herb while “some” means cell-like structure (Kidd, 2009). Phytosome is a technology used as controlled and sustained release delivery system consisting of phospholipid complex system of herbal extract or phytoconstituents with nano size range (<100 nm) of particles (Freag et al., 2013). Phytosomes results from the reaction of a stoichiometric amount (1:1-1:3) of the phospholipid (phosphatidylcholine) with the standardized extract or phyto-constituents in a non polar solvent (Kidd, 2009). It is a patented technology to encapsulate standardized extracts, or phytoconstituents into phospholipids to fabricate molecular complexes for enhancing their permeation and bioavailability, especially for those which have poor aqueous solubility and strong tendency to self-aggregate (Maiti et al., 2006). The schematic illustration of phytosome is shown in Figure 1.7.

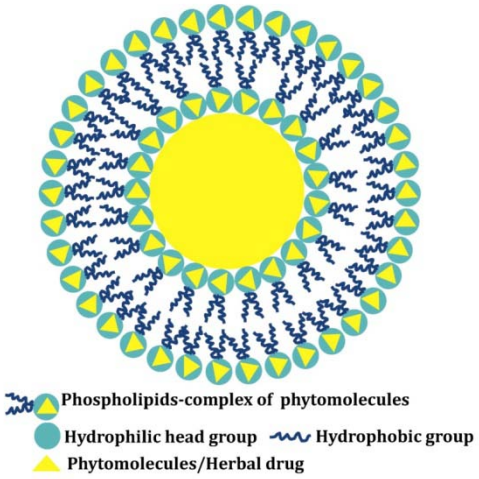


**Figure 1.7. Schematic diagram of phytosome**

The backbone of phytosomal system are only phospholipids (Maiti et al., 2006), several phospholipids such as hydrogenated soy phosphatidylcholine (HSPC), dipalmitoylphosphatidylcholine and distearoylphosphatidylcholine have been employed for this purpose (Maiti et al., 2010). Phospholipid-based delivery systems have been developed to improve the bioavailability of phytoconstituents and the herbal extracts. The phytosome has been successfully applied to many plant extracts (Milk thistle, Ginkgo, Green tea, Boswellia etc.) as well as phytochemicals (silybin, curcumin), with significant results both in animals as well as in human pharmacokinetic studies (Hüsch et al., 2013). Several studies on phytoconstituent-phopholipid complecx has been reported, namely, quercetin (Maiti et al., 2005), curcumin (Maiti et al., 2007), ellagic acid (Murugan et al., 2009), naringenin (Maiti et al., 2006), andrographolide (Maiti et al., 2010), resveratrol (Mukherjee et al., 2011), gallic acid (Bhattacharyya et al., 2013), mangiferin (Bhattacharyya et al., 2014a) and chlorogenic acid (Bhattacharyya et al., 2014b), have been successfully exploited for better therapeutic efficacy as well as bioavailability.

### *1.4.11. Microemulsion and nanoemulsion*

Microemulsions and nanoemulsions are an isotropic mixture of oils, surfactants, and co-solvents/co-surfactants (Harwansh et al., 2011a). Nanoemulsions are thermodynamically stable systems that consist of emulsifier coated oil droplets dispersed within an aqueous medium (Harwansh et al., 2011b). The size of the droplets (o/w and w/o) produced depends on the composition of the system and the homogenization method used. The structure of microemulsions/nanoemulsions is represented in Figure 1.8.

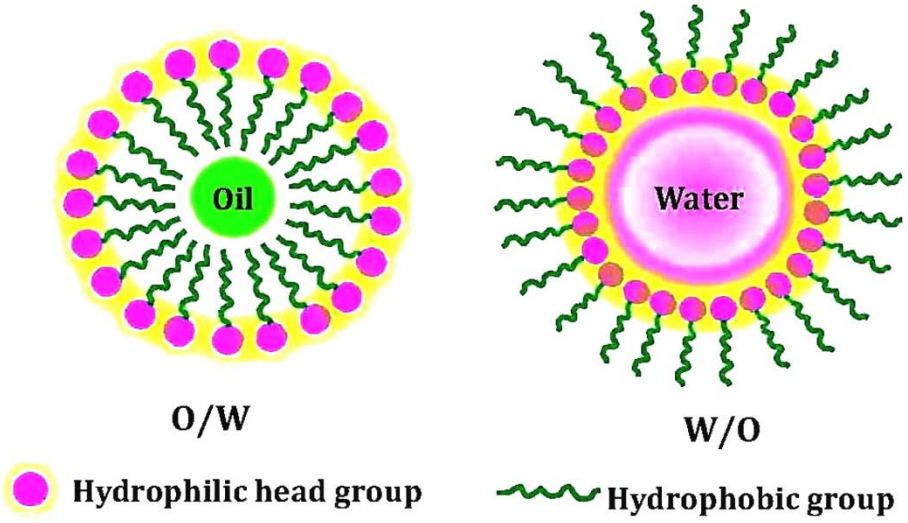


**Figure 1.8. Structure of microemulsion or nanoemulsion**

Nanoemulsions when orally administered quickly disperse in the g.i. fluid through self-emulsifications and form nano droplet size in the range of 20-200 nm with the digestive motility of the stomach and the intestine (Porter et al., 2008). Incorporation of herbal drugs into these systems which strengthen the stability, improve the permeability to the skin and mucous, and produce sustained release effect. So far, herbal drugs, like *Brucea javanica* oil, camptothecin, coixenolide oil and zedoary oil have been explored with these systems. Choudhury et al. developed the nanoemulsions (o/w) to improve the oral bioavailability of paclitaxel. The terminal elimination $t_{1/2}$ was increased in oral nanoemulsion up to 5.79 h as compared to the i.v. formulation ($t_{1/2}$, 1.22 h) thereby indicating a sustained type of the release profile of paclitaxel loaded nanoemulsion. Moreover, the absolute oral bioavailability and sustained release profile of the paclitaxel nanoemulsion evaluated in mouse model is found to improve up to 55.9% (Choudhury et al., 2014).

Choi et al. studied the pharmacokinetic properties of the formulated capsaicin-loaded nanoemulsions. A pharmacokinetic study was carried out using double-layer

nanoemulsions fabricated with alginate and chitosan polymers and triple-layer nanoemulsions fabricated with chitosan/alginate polymers. Capsaicin nanoemulsions and capsaicin control (oleoresin capsicum) were administered to the rat at a dose of 10 mg/kg. A statistically significant difference was found in the area under the curve from time zero to time infinity ($AUC_{inf}$) among formulations ($p<0.01$). In comparison to the control group, the relative bioavailability of formulated nanoemulsions was up to 131.7. The $AUC_{inf}$ increased in a nano-size-dependent manner; as nano size decreased, $AUC_{inf}$ increased. In comparison to the double-layer nanoemulsions, the triple-layer nanoemulsion showed a significantly increased volume of distribution, resulting in the increased clearance and decreased $AUC_{inf}$. It was concluded that the formulated nanoemulsions could significantly enhance the bioavailabilty of capsaicin (Choi et al., 2013).

#### *1.4.11.1. Self-emulsifying, self-micro/nanoemulsifying drug delivery system*

Novel oral self-emulsifying system namely self-emulsifying drug delivery system (SEDDS), self-microemulsifying drug delivery system (SMEDDS) and self-nanoemulsifying drug delivery system (SNEDDS) which is well known for its potential to improve aqueous solubility, dissolution, absorption, therapeutic efficacy, intestinal permeability as well as *in vivo* bioavailability enhancement of poorly soluble drugs (Shakeel et al., 2013). SMEDDS may be defined as an isotropic mixture of oil, surfactant and cosurfactant which could form very fine microemulsions with a droplet size between 5-100 nm upon gentle agitation with an aqueous media such as gastrointestinal (GI) fluids. SNEDDS also composed of oil, surfactant and cosurfactant which form fine nanoemulsions with a droplet size in the rage of 50–300 nm under gentle agitation with GI fluids. However, SEDDS forms milky emulsion upon mild agitation with GI fluids with larger droplet size (few nanometers to several micrometers). All these novel drug delivery systems (SEDDS, SMEDDS and SNEDDS) have great solubilizing potentials and known to enhance solubility, dissolution, intestinal permeability, stability and bioavailability of poorly soluble drugs (Shakeel et al., 2013).

The main characteristic of these types of formulations is to form fine oil-in water (o/w) emulsions upon subsequent dilution in GI fluids, with gastric motility providing the necessary agitation. Fine/nano oil droplets should empty rapidly from the stomach and promote wide distribution of the drug throughout the GIT. Other advantage of the self-emulsified formulations over simple oil solutions is that they provide large interfacial area for partitioning of the drug between oil and water. For drugs subject to dissolution rate limited absorption, self-emulsified formulations may offer an improvement in both the rate and extent of absorption and permeation from the intestinal memdrane. The optimum concentrations of oil, surfactant and co-surfactant necessary to promote self-emulsification are determined by plotting pseudoternary phase diagram, which should also assess the effect of drug loading on the efficiency of self-emulsification (Rahman et al., 2011).

### *1.4.11.2. Advantage of nanoemulsions and SNEDDS as novel drug delivery systems*

The advantages of nanoemulsions as NDDS include:

- ✓ The small size of the droplets offers large interfacial area from which molecules can be quickly released. It improves the solubility, dissolution, absorption and bio-membrane permeation and *in vivo* bioavailability enhancement of poorly soluble drugs.
- ✓ The drug/phytomolecule can be encapsulated into the nanoemulsion matrix so it improves their physical stability.
- ✓ It helps to solubilize lipophilic drug and masks unpleasant taste of some drugs.
- ✓ Various routes like topical/transdermal, oral and intravenous can be used to deliver the product.
- ✓ Nanoemulsions can enhance the stability of chemically unstable compounds by protecting them from UV light and oxidative degradation.
- ✓ Possibilities of controlled drug release and drug targeting, and the incorporation of a great variety of therapeutic actives.
- ✓ The lipids (excipients) are biocompatible, biodegradable and non-mutagenic so nanoemulsion is safe for human health.
- ✓ It offers the site specific and prolonged release delivery of the drugs/phytomolecules.
- ✓ Reductions in the dose thereby minimize associated toxicities and provide better therapeutic effects.
- ✓ In case of topical application, it avoids first-pass metabolisms hence improvement in plasma drug concentrations.
- ✓ Nanoemulsions are suitable for efficient delivery of active ingredients through the skin. The large surface area of the emulsion system allows rapid penetration of actives. It is non-toxic and non-irritant so can be easily applied to skin and mucous membranes.
- ✓ The transparent nature of the system, their fluidity (at reasonable oil concentrations) as well as the absence of any thickeners may give them a pleasant aesthetic character and skin feel.
- ✓ Offers value added drug delivery system for nutraceutical and dietary supplements.
- ✓ Facilitating patient compliance.

### *1.4.11.3. Formulation consideration*

Preliminary studies are performed for selection of oil, which is an important and critical requisite for formulation of nanoemulsions or self-emulsified drug delivery system. Solubility screening of drug is performed in different oils and surfactants for optimum concentration. Prepare a series of such type of formulation containing drug in various oil and surfactant. Then, *in vitro* self-emulsification properties and droplet size analysis of these formulations upon their addition to water under mild agitation conditions is

studied. Pseudoternary phase diagram is plotted for identifying the efficient self-emulsification region (Charman et al., 1992). The application of lipid/oil excipients for formulations is inevitably complicated, and thus has presented challenges to both pharmaceutical and regulatory scientists. Lipid excipients having ablity to solubilize hydrophobic drugs within the dosage form matrix. However, as with dietary lipids, these excipients can also be digested and dispersed in the GIT. Therefore, one of the questions for a lipid-based oral formulation is whether the drug remains in solubilized form in the presence of changing phases of the formulation after it is administered. This is a difficult question, which can be illustrated by a simplified pseudoternary phase diagram for an oily formulation dispersed in water and a surfactant. As shown in Figure 1.9, various possible lipid assemblies/formulations can arise from the interplay of the oil, water and surfactant/co-surfactant ($S_{mix)}$ present in the system (Bummer et al., 2004). These assemblies may include emulsion, micelle, water-in-oil (w/o), oil-in-water (o/w) micro/nanoemulsion and bicontinuous micro/nanoemulsion. The phase of the lipid formulation may be changed as it reaches the GI tract and is subjected to the digestion, dispersion and transport process in the body.

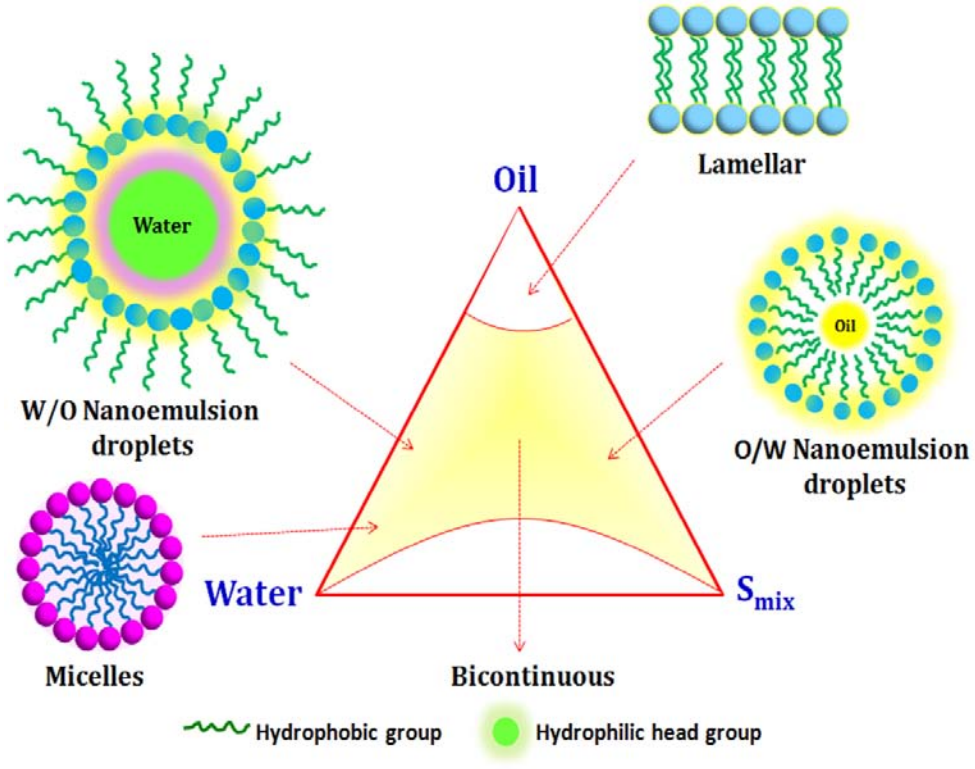


**Figure 1.9. A hypothetical pseudo-ternary phase diagram of an oil, water and surfactant/co-surfactant ($S_{mix}$) system with emphasis on nanoemulsion and emulsion phases**

### *1.4.11.3.1. Oils*

Oil/lipid is a vital ingredient of the nanoemulsion formulation. It can not only solubilize marked amount of lipophilic drugs or facilitate self-emulsification but also enhance the fraction of lipophilic drug transported via intestinal lymphatic system, thereby increasing its absorption from the GIT. In case of topical formulation, it can increase the fraction of lipophilic drug transported via skin, thereby increasing absorption from the skin depending on the molecular nature of the triglyceride. Modified long and medium-chain triglyceride oils, with varying degrees of saturation or hydrolysis, have been used widely for the development of nanoemulsion. Hydrolyzed vegetable oils have been widely used since these excipients form good emulsification systems with a large number of surfactants approved for topical and oral administration and exhibit better drug solubility activities (Constantinides, 1995). Novel semisynthetic medium chain derivatives, which can be defined as amphiphilic compounds with surfactant actions, are gradually and effectively replacing the regular medium chain triglyceride oils (Constantinides, 1995). Solvent capacity for less hydrophobic drugs can be improved by blending triglycerides with other oily excipients, which include mixed monoglycerides and diglycerides. In most cases the drugs are not soluble in hydrocarbon oils. The polarity of the majority of the lipophilic drugs favours their solubilization in small or medium molecular volume oils such as tributyrin, medium chain triglycerides or mono or diglycerides (Lawrence and Rees, 2002).

### *1.4.11.3.2. Surfactant*

Surfactant selection must be able to lower interfacial tension between oil and water interface to a very small concentration to aid dispersion process during the preparation of the nanoemulsion. They should also provide a flexible film that can readily deform around droplets and be of the appropriate lipophillic character to provide the correct curvature at the interfacial region for the desired nanoemulsion formulation. Conventional surfactant molecules comprise a hydrophilic head group region and a hydrophobic tail region, the latter having the larger molecular volume particularly in the case of ionic surfactants. A surfactant is obligatory to provide the essential emulsifying characteristics to micro/nanoemulsion based drug delivery system. Surfactants, being ampiphilic in nature, invariably dissolve (or solubilize) high amounts of hydrophobic drug compounds. The two issues that govern the selection of a surfactant encompass its hydrophilic-lipophilic balance (HLB) and safety. The HLB of a surfactant provides vital information on its potential utility in formulation of nanoemulsion. For attaining high emulsifying performance, the emulsifier involved in formulation of nanoemulsion should have high HLB and high hydrophilicity for immediate formation of o/w droplets and rapid spreading of formulation in the aqueous media such as GI fluids (Constantinides, 1995).

Upon aqueous dispersion, surfactants self-associate into a variety of equilibrium phases, the nature of which stems directly from the interplay of the various intra and

intermolecular forces as well as entropy considerations. The HLB takes into account the relative contribution of hydrophilic and hydrophobic fragments of the surfactant molecule. It is generally accepted that low HLB value (3-8) surfactants are favored for the preparation of w/o micro/nanoemulsions whereas surfactants with high HLBs (8-18) are used for the preparation of o/w micro/nanoemulsion systems (Constantinides, 1995). A list of different oils (lipid ingredients), surfactant and co-surfactant that have been used for preparation of various formulations are given in Table 1.2. Normally the surfactant concentration ranges between 30-60% v/v is preferred in order to form stable formulation. Surfactants used for stabilizing nanoemulsions may be non ionic, zwitterionic, cationic and anionic. There is a relationship between the droplet size and the concentration of the surfactant being used in the formulation. Mean droplet size may increase with increasing concentrations of surfactant (Wakerly et al., 1986; Craig et al., 1995).

#### *1.4.11.3.3. Co-surfactant*

Generally the formulations such as micro/nanoemulsions, self-micro/nanoemulsified drug delivery systems will contain co-surfactants. In most cases, single-chain surfactants alone are unable to reduce the oil/water interfacial tension sufficiently to form an appropriate system (Attwood, 1994; Lawrence, 1994). Co-surfactants are incorporated into the formulation to obtain nanoemulsion systems at low surfactant concentration (Kreilgaard et al., 2000). Short-to medium-chain-length alcohols (C3-C8) are usually used as cosurfactants, which further reduce the oil-water interfacial tension and increase the fluidity of the interface (Tenjarla, 1999). They have the effect of further reducing the interfacial tension, while increasing the fluidity of the interface thereby increasing the entropy of the system. They also increase the mobility of the hydrocarbon tail and allow greater penetration of the oil into this region. Alcohols may also increase the miscibility of the aqueous and oily phases due to its partitioning between these phases. Examples of commonly used cosurfactants are transcutol P, transcutol CG, glycerin, ethyleneglycol, ethanol, isopropyl alcohol, PEG 400, carbitol, and propylene glycol which are given in the Table 1.2. Nanoemulsion area is often used as the measurement criterion for the evaluation of cosurfactants. The larger the size of the nanoemulsion field, the greater the nanoemulsification efficiency of the system (Lawrence, 1994, 1996).

#### *1.4.11.3.4. Surfactant and co-surfactant ($S_{mix}$)*

The surfactant and co-surfactant ($S_{mix}$) ratio is a key factor influencing the phase properties. Attwood et al. showed how size and location of microemulsion is changed on changing the mass ratio of polysorbate 40/sorbitol from 1:1 to 1:3.5 (Attwood et al., 1992). Similar studies using polysorbate 80 and polysorbate 60 have shown a change in the optimum polysorbate/sorbitol mass ratio (i.e., that produce the largest nanoemulsion region) from 1:2.5 for polysorbate 80 to 1:2 for polysorbate 60 to 1:1.5 for

polysorbate 40. Such effects have been attributed to differences in the packing of surfactants and co-surfactants at the oil water interface (Attwood et al., 1989; Kitistis, and Niopas, 1998). In addition, the most important criterion for selection of all the formulation components is that all the excipients should be pharmaceutically acceptable for oral administration or topical application, etc., depending upon the requirement and falling under GRAS category.

**Table 1.2. Example of oils (lipid Ingredients), surfactants and co-surfactants**

| Excipients | Description/main fatty acid (FA) composition | HLB |
|---|---|---|
| **Lipids/Oils** | | |
| Akoline MCM | Caprylic/capric glycerides [MAG and DAG of C8 and C10 with small quantities of TAG] | 5-6 |
| Beeswax | - | |
| Capmul MCM | Caprylic/capric glycerides | 5-6 |
| Caprylic/capric TAG | TAG of C8 and C10 | - |
| Captex 355 | Glycerol caprylate caprate [TAG of C8 and C10] | - |
| Corn oil | - | - |
| Ethyl oleate | Oeic acid ethyl ester | 11 |
| Isopropyl myristate | FA ester [Isopropyl ester of C14 FA-myristic acid] | 11.5 |
| Isostearyl isostearate | - | 7 |
| Labrafac CC* | Caprylic/capric triglyceride [TAG of C8-12 FA] | 1 |
| Labrafac™ lipophile WL1349* | Medium chain triglycerides | 2 |
| Miglyol 812 | Medium-chain TAG | - |
| Oleic acid | - | - |
| Olive oil | - | 7 |
| Peanut oil | - | - |
| Sesame oil | - | - |
| Soyabean oil | Soya oil | 7 |
| Vegetable oil | Long-chain TAG [TAG of C18, C16 and C14 FA] | - |
| Viscoleo | Fractionated coconut oil [TAG of C8-12 FA] | - |

| | | |
|---|---|---|
| **Surfactants** | | |
| Acconon CC-6 | Ethoxylated glycerides | 12.5 |
| Acconon MC-8 | Caprylocaproyl macrogolglycerides (polyoxyglycerides) and C10:0 and some free PEG 400 | 14-15 |
| Brij 35 | Polyoxyethylene lauryl ether | 9.5 |
| Caproyl 90™* | Propylene glycol monocaprylate [C8 FA mono-ester of propylene glycol] | 6 |
| Caproyl™ PGMC* | Propylene glycol caprylate | 5 |
| Captex 350* | Coconut oil transesterified with C8 and C10 fatty acids | - |
| Cremophor EL* | Polyoxy-35-castor oil [Glycerol-PEG ricinoleate, FA ester of PEG] | 12-14 |
| Cremophor RH40* | Polyoxy-40- hydrogenated castor oil [FA ester of glycerol-PEG, FA ester of PEG, free PEG and ethoxylate glycerol] | 14-16 |
| Labrafac™ PG* | Propylene glycol dicaprylocaprate | 2 |
| Labrafil® M 2125CS* | Polyoxyethylated glycerides [Linoleoyl macrogolglycerides] | 4 |
| Labrafil® M1944CS* | Polyoxyethlated oleic glycerides [Oleoyl macrogolglycerides]; Mainly C18:1 mono- and diester of PEG 300 and MAG, DAG and TAG | 4 |
| Labrasol* | Caprylocaproyl macrogol-8-glycerides [FA C8:0/C10:0 mono and diesters of PEG 400 and MAG, DAG and TAG with mainly C8:0 and C10:0 and some free PEG 400] | 14 |
| Lauroglycol™ 90* | Propylene glycol monolaurate [C12 FA mono-ester of propylene glycol] | 5 |
| Lauroglycol™ FCC* | Propylene glycol laurate | 4 |
| Maisine™ 35-1* | Glyceryl monolinoleate [MAG and DAG of C18 and C16 FA with small quantities of TAG] | 4 |
| Plurol isostearique* | Polyglyceryl-6-Isostearate | 10.8 |
| Span 80 | Sorbitan monooleate [Sorbitan (Z)-mono-9-octadecenoate] | 4.3 |
| TPGS | D-alpha Tocopheryl polyethylene glycol 1000 succinate | - |
| Transcutol CG* | Diethyleneglycol monoethyl ether | 4.2 |

| | | |
|---|---|---|
| Transcutol P* | Diethyleneglycol monoethyl ether | 4.2 |
| Tween 20 | Polysorbate 20 [Polyoxyethylene 20-sorbitan monolaurate]; PEG-sorbitan esterified with C12 FA | 16.5 |
| Tween 80 | Polysorbate 80 [Polyoxyethylene 20-sorbitan monooleate]; PEG-sorbitan esterified with 80 C18:1 FA | 15 |
| Tween 85 | Polyxyethylene 20-sorbitan trioleate | 11 |
| **Co-surfactants*** | | |
| Ethanol | Ethyl alcohol | 7.9 |
| Glycerin | - | - |
| Polypylene glycol | - | - |
| PEG-400 | Polyethylene glycol-400 | 15.5 |
| Carbitol | Diglycol monoethyl ether | - |

****Solubilizer, penetration and bioavailability enhancer***

### *1.4.11.4. Preparation methods of nanoemulsions*

Nanoemulsions are non equilibrated formulations. Therefore, for their preparation requires the input of a large amount of either energy or surfactants and in some cases a combination of both. Generally high-energy or low-energy methods can be applied for their formulation (Ravi and Padma, 2011; Mason et al., 2006). High-energy emulsification process is traditional method although it is used for the preparation of nanoemulsion formulation. But low-energy emulsification methods are now gaining attention due to their wide application and benefits as a nanoemulsion formulation and its stability aspects (Anton and Vandamme, 2009). The detail methods of preparation of nanoemulsion are described below.

#### *1.4.11.4.1. Low-energy methods*

Low-energy emulsification methods involve low energy for the preparation of nanoemulsions as the name indicates. The low-energy methods are self-emulsification, phase transition and phase inversion temperature methods (PIT) (Wang et al., 2007). These processes are primarily reliant on inflection of interfacial phenomenon/phase transitions and intrinsic physicochemical properties of the surfactants, co-surfactants and oil to yield nano-sized emulsion droplets. The lower energy method is also known as the condensation method which is based on the phase transitions taking place during the emulsification process (Lamaallam et al., 2005; Solans eta l., 2002). These phase transitions result from changes in the spontaneous curvature of the surfactant and can be achieved (i) at constant composition by altering the spontaneous curvature

of non-ionic surfactants with temperature which is known as Phase Inversion Temperature (PIT) and widely accepted in industry (Izquierdo et al., 2005; Shinoda and Saito, 1968) or (ii) at constant temperature by modifying the composition of the system by the Emulsion Inversion Point (EIP) method (Forgiarini et al., 2001; Pey et al., 2006; Porras et al., 2008). In other words, low energy emulsification method was developed according to the phase behavior and properties of the components, to promote the creation of ultra-small (nano) droplets (Sonneville-Aubrun et al., 2004; Solans et al., 2005). In this method the stored energy of the system is applied for the formation of fine nanoemulsion droplets, so that low-energy method is very interesting. This emulsification process can be made by changing the parameters which would affect the HLB of the system such as temperature, composition, etc. (Sole et al., 2006, 2010). The limitations of these methods are complexity, precise approach and require synthetic surfactants. The most commonly used low-energy emulsification methods are discussed below.

#### *1.4.11.4.1.1. Phase inversion temperature (PIT) method*

PIT method employs temperature-dependent solubility of non-ionic surfactants (polyethoxylated surfactants), to change their affinities for water and oil as a function of the temperature. This function in PIT method makes a basis of nanoemulsion formulation. In this method oil, water and nonionic surfactants are mixed together at room temperature. This mixture normally consists o/w microemulsions coexisting with excess oil, and the surfactant monolayer exhibits positive curvature. Upon heating this o/w microemulsion undergoes phase inversion to w/o emulsion because of polyethoxylated surfactant becomes lipophilic and the surfactant gets completely solubilized in the oily phase. At this stage, the surfactant monolayer has negative curvature (Izquierdo et al., 2005).

At an intermediate temperature (HLB temperature), the non-ionic surfactant has similar affinity for water and oily phase, and this ternary system has extremely low interfacial tension (in the order of $10^{-2}$-$10^{-5}$ $mNm^{-1}$) and spontaneous curvature typically becomes zero (Sole et al., 2006, 2010). At this stage the ternary system involves a mixture of a D-phase bicontinuous microemulsion and lamellar liquid crystalline phases. It has been observed that nanoemulsions with very fine droplet size and polydispersity index (PDI) can be generated by rapid cooling of the single-phase or multi-phase bicontinuous microemulsions maintained at either PIT or a temperature above PIT (Shinoda and Saito, 1968).

Nanoemulsions can also be produced by rapidly diluting the single bicontinuous microemulsions with the aqueous or oil phase (catastrophic phase inversion) to obtain either o/w or w/o nanoemulsion. The characteristics of the nanoemulsion are mainly dependent on the structure of the surfactant at HLB temperature (bicontinuous or lamellar) and also on the ratio of surfactant/oil. Previously, PIT method was believed to

be applicable for formulating o/w nanoemulsions. However, nowadays, the application of this method has been established for formulating w/o nanoemulsions. For preparation of w/o nanoemulsion, it is important to note that the use of lipophilic polyethoxylated surfactants and necessary changes in the typical PIT method are required (Wang et al., 2007).

#### *1.4.11.4.1.2. Solvent displacement method*

The solvent displacement method for spontaneous nanoemulsification has been established from the nano-precipitation method which used for polymeric nanoparticles. In this method, oily phase is dissolved in water-miscible organic solvents, such as acetone, ethanol and ethyl methyl ketone. The organic phase is added into an aqueous phase containing surfactant to produced spontaneous nanoemulsion by rapid diffusion of organic solvent. Then organic solvent is removed from the nanoemulsion by a suitable method such as vacuum evaporation (Pey et al., 2006; Porras et al., 2008; Sonneville-Aubrun et al., 2004; Solans et al., 2005).

#### *1.4.11.4.1.3. Phase inversion composition (PIC) method (self-nanoemulsification method)*

The PIC method produces nanoemulsions at room temperature without use of any organic solvent and heat. Forgiarini et al. observed that kinetically stable nanoemulsions with small droplet size (~50 nm) can be prepared by the stepwise addition of aqueous phase into solution of surfactant in oil phase with mild stirring and at constant temperature. Although the components used in the aforementioned investigation were not of pharmaceutical grade, the investigation opened doors to design pharmaceutically acceptable nanoemulsions using a similar approach. The spontaneous nanoemulsification process has been related to the phase transitions during the emulsification process and involves lamellar liquid crystalline phases or D-type bicontinuous microemulsion during the process (Forgiarini et al., 2001).

### *1.4.11.4.2. High-energy methods*

As name indicates, this method utilizes mechanical devices that employ very high energy to fabricate nanoemulsions with high kinetic energy. This method applies mechanical energy to build intensely disruptive forces which break up the oil-water phases to form nano-sized droplets. Ultrasonicators, microfluidizer and high pressure homogenizers can be used as high-ergy sources for preparation of nanoemulsions (Mason et al., 2006; Graves et al., 2005; Jafari et al., 2007). Droplet size of the nanoemulsion system will depend on the type of instruments used and their operating conditions such as time and temperature along with sample properties and compositions (Quin and Mc Clement, 2011). High-pressure homogenization and ultrasonic emulsification are the most commonly used method for the production of

nanoemulsions. During high-pressure homogenization, the coarse emulsion (>500 µm) is passed through a small orifice at an operating pressure in the range of 500 to 5000 psi. In this process, several forces, such as hydraulic shear, intense turbulence and cavitation, act together to yield nanoemulsions with extremely small droplet size. The resultant product can be re-subjected to high-pressure homogenization until nanoemulsion with desired droplet size and PDI is produced (Mason et al., 2006).

Micro-fluidization is another technique used for preparation of nanoemulsion using a high-pressure positive displacement pump operating at very high pressures, up to 20,000 psi. Macroemulsion is converted into nanoemulsion through the interaction chamber consisting of a series of micro-channels by applying high forces using this pump. In this process the macron size droplets is reduced into fine (nano-sized) droplets (nanoemulsions). Appropriate size of the nanoemulsions with dispersity can be obtained by changing the operating pressure and the number of passes through interaction chambers like high pressure homogenization. Ultrasonic-emulsification method employs a probe that emits ultrasonic waves to reduce the macron size droplets of emulsion by means of cavitation forces. In Ultrasonic-emulsification method, the desired nanoemulsion can be produced by varying the ultrasonic energy input and time (Graves et al., 2005; Jafari et al., 2007). High-energy emulsification technique can be utilized to fabricate both o/w and w/o type nanoemulsions. High-pressure homogenization and micro-fluidization techniques can be used for production of nanoemulsions at laboratory and industrial scale. However, ultrasonic-emulsification is mainly applicable for laboratory purpose. Moreover, high-energy techniques require sophisticated instruments and extensive energy input, which noticeably increases the cost of nanoemulsions manufacture. High energy methods allow for a greater control of particle size and a large choice of composition, which consecutively controls the physical properties like stability, rheology and colour of the emulsion. Although high-energy emulsification technique manufacture nanoemulsions with desired properties as needed by industry. The disadvantage of this methos is that they may not be suitable for thermolabile materials such as retinoids and macromolecules, such as proteins, enzymes and nucleic acids. Additionally, the nano-size (<100 nm) oil droplets can't be yielded alone by high-energy methods (Graves et al., 2005; Jafari et al., 2007; Quin and Mc Clement, 2011).

### *1.4.11.5. Nanoemulsions as a novel vehicle for topical and transdermal delivery*

Topical and transdermal drug delivery systems (TDDS) are alternative and promising approaches for enhancing therapeutic efficacy and bioavailability of low bioavailable drugs through the skin. Topical and TDDS is an attractive route for local and systemic treatment. The drug delivery onto the skin is recognized as an effective means of therapy for skin disorders. It can penetrate deeper into skin and hence give better absorption. These systems have many advantages over the conventional dosage forms. Generally, they are deemed more effective less toxic than conventional

formulations due to the bilayer composition and structure of the skin. In the formulation of topical and TDDS dosage forms, attempts are being made to utilize novel carrier system that ensure adequate localization or penetration of the drug through the skin in order to enhance the local as well as systemic effects by adequate permeability action (Abolmaali et al., 2011). Transdermal or topical application of drug offers the potential advantage of delivering the drug directly to the site of action and acting for an extended period of time. These route eliminates the side effect, increases patient compliance, avoids first-pass metabolism, enhances bioavailability and maintains the plasma drug level for longer periods resulting in improved $t_{1/2}$ (Benson, 2005; Harwansh et al., 2011). The transdermal route has become a most accepted and innovative spotlight for researchers in drug delivery which has been proven in quantitative research with around 40% of the drug moiety being under clinical evaluation and also approved by Food and Drug Administration (FDA). The transdermal product has bright future because of its noteworthy upward trend. The TDDS have been continued to provide good therapeutic benefits to patients around the world (Paudel et al., 2010).

Transdermal delivery allows the permeation of drugs across the skin and overcomes the drawback associated with oral and parenteral route. However, the penetration of drugs across the skin is limited by the barrier function of the enormously organized structure of *stratum corneum* (SC). As protective barrier, the skin occupies about 15% of the total body weight of an adult and has around 2 $m^2$ surface area. The skin is a multilayered organ composed of many tissues such as the epidermis and the dermis as represented in Figure 1.10. Epidermis comprises of keratinocyte (95% of cells) which is the principal cell forms a ‘brick and mortar’ structure of keratin-rich corneocytes (bricks) in an intercellular matrix (mortar) that has been used to conceptualize the barrier property of skin includings melanocytes, langerhans cells and merkel cells (minor components). These cells are involves in the formation of the SC (Candi et al., 2005). The ‘brick and mortar’ cell composed of multiple lipid bilayers of ceramides, free fatty acids, triglycerides, cholesterol and cholesterol esters. These bilayers form regions of semi crystalline gel and liquid crystal domains (Riviere and Papich, 2001). Dermis is a second layer beneath the epidermal layer which is much thicker than the epidermis (usually 1-4 mm). Dermis is mainly associated with the components namely collagen and elastic fibers. In comparison with the epidermis layer, there are much fewer cells and much more fibers in the dermis (Igarashi et al., 2007). Achievement of a therapeutically effective drug concentration is difficult without enhancing their skin permeation profile. There are various techniques have been developed to enhance the drug permeability and transport across the skin. These involve chemical and physical methods, based on two strategies such as enhancing skin permeability and providing driving force acting on the drug. Several technologies have been developed to enhance transdermal delivery of drugs for therapeutic and diagnostic purposes ranging from chemical enhancers to iontophoresis, electroporation, and pressure waves generated by ultrasound effects or the synergistic mixtures of both the mechanism (Ahad et al., 2010). There are so many factors such as species differences, skin age and site, skin

temperature, state of the skin (normal, abraded, or diseased), area of application, contact time, degree of hydration of the skin, pre-treatment of the skin, and physical characteristics of the penetration enhancer which affect the drug permeation through the skin. The main mechanism of drug permeation through the skin is 'diffusion' which is concentration dependent (Prausnitz et al., 2004). Drug molecules penetrate across the skin surface by three potential pathways: intercellular, intracellular (transcellular) and follicular (appendage) route (Benson, 2005; Alexander et al., 2012) as shown in Figure 1.10.

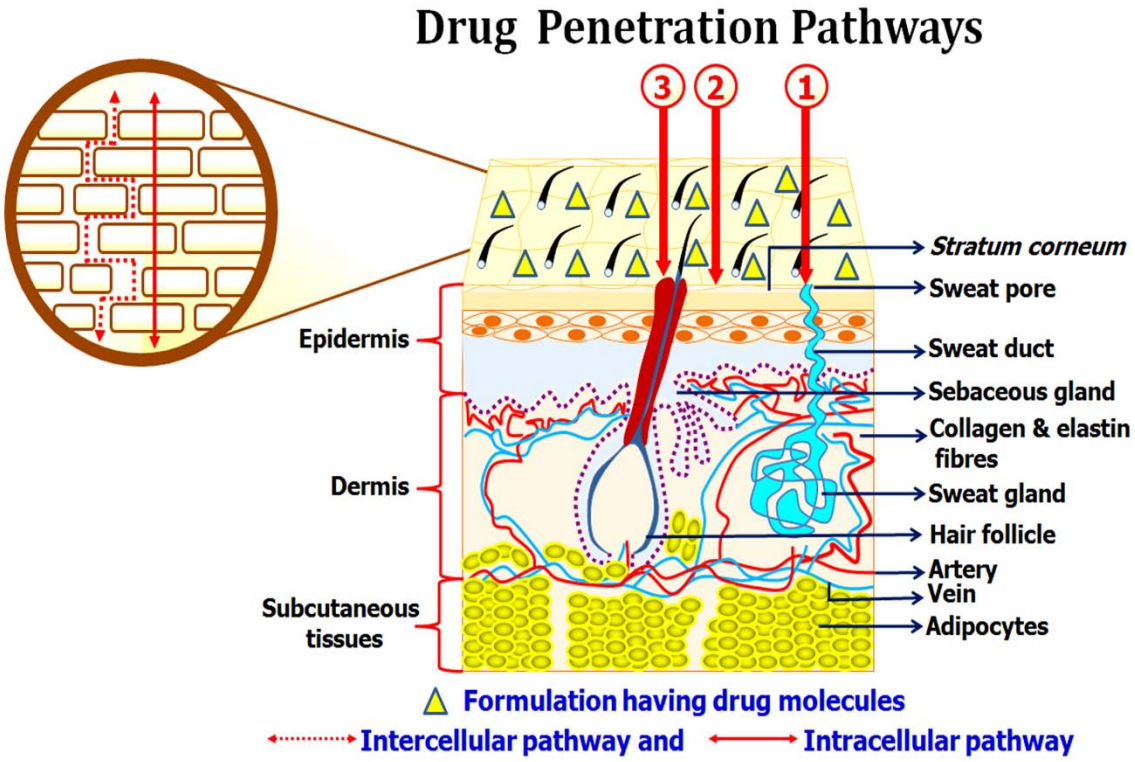


**Figure 1.10. Schematic diagram of skin structure and major routes of drug penetration, (1) via the sweat ducts (intercellular pathway); (2) directly across the *stratum corneum* (intracellular pathway) and (3) through the hair follicles and sebaceous gland (folicullar pathway)**

The skin permeability of catechins from tea extract has been studied by Batchelder et al. and assumed that sufficient amount of catechins were permeated across skin through transdermal route (Batchelder et al., 2004). This result encourages the transdermal routes for catechin delivery. Enhancement of the transdermal delivery of catechins by liposomes has been performed by Fang et al. (2006). Epicatechin was formulated in gel formulation; stability and permeability through human cadaver skin was studied in different gels for topical use (Suppasrivasuseth et al., 2006). Topical application of (-)-epicatechin gallate and caffeine has also been shown to decrease the

number of non-malignant and malignant skin tumours in mice (Lu et al., 2002). Enhanced bioavailability of lacidipine through microemulsion based gel has been achieved after transdermal administration (Gannu et al., 2010). In a different study, enhanced permeability and biological activity of nano-carrier gel of diclofenac diethylamine and curcumin has been achieved by transdermal route (Chaudhary et al., 2014). Recently, Harwansh et al. has reported that ferulic acid loaded nanoemulsion based nanogel showed better skin protection activity against UVA mediated oxidative stress due to its improved permeability and sustained-release profile (Harwansh et al., 2015).

## 1.5. Application of the target based nanotechnology and NDDS with phytopharmaceuticals

Recently the targeted delivery system of phytopharmaceuticals was described by Li et al. (2009), it is summarizing as the theory of targeted agents was postulated earliest by Ehrlichp in 1906. These targeted agents, also known as targeted drug delivery system, refer to the drug carrier that selectively concentrates on the target site through site specific or systemic delivery (Zhan and Zhu, 2008). For a drug to exert its desired effect it needs to be in physical contact with its physiological target, such as a receptor. Site-selective drug delivery ensures that such interactions take place only in the desired anatomical location of the site-selective delivery not every drug is equally suitable for the process. Drugs that are not retained at the site of action for a long enough period of time will not benefit from site specific release. Also, drugs that have the same site for efficacy and toxicity will not improve through site-specific delivery and their effect: side-effect ratio could even get worse. Evidently, drugs that already have an inherently high specificity for reaching and interacting with their targets, for example therapeutic antibodies, do not need to be considered for targeting (Rahman et al., 2013). There are diverse classes of targeted carriers, and the application of each of these has different but interrelated objectives. This variety of classes results in a large number of possible combinations (Grant, 2008). The distinct novel carriers for herbal drug delivery to target site are studied by different researchers and reported for several therapeutic application (Table1.3).

**Table 1.3. Application of the target based NDDS for phytopharmaceuticals**

| Phytopharma-ceuticals | Novel drug delivery approach | Applications | Biological activity | Special features | Route of administration | References |
|---|---|---|---|---|---|---|
| **Ammonium glycyrrhizinate** | Niosomes, ethosome[†] | Increase of the in vitro percutaneous permeation[†] | Useful in the treatment of dermatitis, eczema, psoriasis and antiinflammatory[†] | 350 nm to 100 nm droplet size | Topical | Marianecci et al., 2012; Paolino et al., 2005 |
| **Ampelopsin** | Liposomes | Increased | Anticancer | 62.30% | *In vitro* | He et al., |

| | | | | | | |
|---|---|---|---|---|---|---|
| | | efficiency | | Entrapment efficiency | | 2008 |
| **Artemisinin** | Nanocapsules | Sustained drug release | Anticancer | 90–93% Entrapment efficiency | *In vitro* | Chen et al., 2009 |
| **Berberine** | Nanoparticle[†], nanoemulsion[*] | Sustained drug release[†], Improve residence time and absorption[*] | Anticancer[†,*] | 65.40 ± 0.70% Entrapment efficiency[†], 56.80 nm droplet size[*] | *In vitro*[†], oral[*] | Lin et al., 2007; Sun and Ouyang, 2007 |
| **Breviscapin** | Liposome[†], nanoparticle[*] | Sustained release of breviscapine[†], prolong the half-life and decrease reticuloendothelial system (RES) uptake[*] | Cardiovascular diseases[†,*], cerebrovascular[*] | 87.9 ± 3.1%[†], 93.1%[*] Entrapment efficiency | Intramuscular[†], intravenous[*] | Zhong et al., 2005; Li et al., 2007 |
| **Camptothecin** | Nanoparticle[†], microspheres[†] [†] | Prolonged blood circulation and high accumulation in tumors[†], prolonged-release of camptothecin[††] | Anticancer[†,††] | >80% Entrapment efficiency[†], 10 µm particle size[††] | *In vitro*[†], intraperitoneally and intravenously[††] | Min et al., 2008; Machida et al., 2000 |
| **Capsaicin** | Transferosomes[†], nanoemulsion | Increased skin penetration[†] | Analgesic[†], anticancer, cardiovascular | 150.6 nm droplet size[†] | Topical[†] | Long et al., 2006; Choi et al., 2013 |
| **Catechins** | Liposomes | Increased permeation through skin | Antioxidant and chemopreventive | 93.0 ± 0.1% Entrapment efficiency | Transdermal | Fang et al., 2006 |
| **Chlorogenic acid** | Microemulsion[†], phospholipid complex[††] | Enhancement of skin delivery[†], Sustained delivery of chlorogenic acid[††] | Antioxidant[††], antiinflammatory, anticancer, uses against photoaging, UV (UVA)-protection against oxidative damage[†, ††] | 12.3 ± 4.8 nm Droplet size[†], 91.91 ± 2.3% entrapment efficiency[††], 278.52 ± 18 nm droplet size[††] | Topical[†, ††] | Kitagawa et al., 2011; Bhattacharyya, et al., 2014 |
| **Colchicine** | Liposome[†], transferosome[††] | Enhance skin accumulation, prolong drug release and improve site specificity[†], increased skin penetration[††] | Antigout[†, ††] | 66.3 ± 2.2% Entrapment efficiency[†] | Topical[†], *in vitro*[††] | Godin and Touitou et al., 2004; Singh et al., 2009 |
| **Curcumin** | Liposome[†], phytosome/herbosome[††], nanoemulsions, nanoparticle | Long-circulating with high entrapment efficiency[†], increased antioxidant activity and | Anticancer[†],antioxidant[††], anti-tumour, Antimicrobial, anti-inflammatory | 88.27 ± 2.16% Entrapment efficiency[†], 360 mg/ Kg dose[††] | *In vitro*[†], oral[††] | Maiti et al., 2007; Feng-Lin et al., 2009; Ahmed et al., 2012 |

| | | | | | | |
|---|---|---|---|---|---|---|
| | | increased bioavailability[††] | | | | |
| **Ellagic acid** | Nanoparticle, liposome, niosome[†], phytosome (phospholipid-complex)[*] | Enhanced skin delivery, increased permeability of ellagic acid[†], enhanced bioavailability and sustained release action[*] | Anticancer, antioxidant[†, *], antidiabetic, hepatoprotective[*] | 124-752 nm Droplet size[†], 26.75 ± 0.58%[†], 85.72 ± 2.6%[*]. entrapment efficiency, 1-3 µm particle size[*], 25 & 50 mg/kg dose[*] | *In vitro*[†], oral[*] | Sharma et al., 2007; Madrigal-Carballo et al., 2010; Junyaprasert et al., 2012; Murugan et., 2009 |
| **Gallic acid** | Phospholipid-complex | Enhanced bioavailability and sustained release action | Antioxidant, hepatoprotective, antiinflammatory | 91.95 ± 2.1% entrapment efficiency, 10 µm particle size, 150 mg/kg dose | *In vivo*, oral | Bhattacharyya et al., 2013 |
| **Garlicin** | Liposome[†] | Increase efficiency | Lungs | 90.77 % Entrapment efficiency[†] | - | Sun et al., 2007 |
| ***Ginkgo biloba* extract** | Nanoparticle[†], phytosomes[*] | Improving the cerebral blood flow and metabolism[†], flavonoids of *Ginkgo biloba*-phytosomes stabilize the reactive oxygen species[*] | Brain function activation[†], cardio-protective and antioxidant activity[*], hepatoprotective, | 100 mg and 200 mg/kg dose[*] | Oral [†], subcutaneous[*] | Shimada, 2008; Panda and Naik, 2008 |
| **Ginseng (Ginsenosides)** | Phytosome | Increase absorption | Nutraceutical, immunomodulator | 150 mg dose | Oral | Bhattacharya, 2009 |
| **Glycyrrhetinic acid** | Nanoparticle | ---- | Targeted for liver tumor/cancer | 120.20 ± 2.40 nm particle size | ---- | Zhang et al., 2013 |
| **Glycyrrhizic acid** | Nanoparticle, elastic-liposomes, | Improve the bioavailability | Anti-inflammatory, antihypertensive | 91.76% Entrapment efficiency | - | Hou and Zhou, 2008; Trotta et al., 2002 |
| **Grape seed (Procyanidins)** | Phytosomes | The blood TRAP (Total Radical-trapping Antioxidant Parameter) were significantly elevated over the control | Systemic antioxidant, cardio-protective | 50-100 mg dose | Oral | Bhattacharya, 2009 |
| **Green tea (Epigallocatechin)** | Phytosome[†], nanoemulsion | Increase absorption[†] | Nutraceutical, systemic antioxidant, anticancer[†], hypolipidemics | 50-100 mg dose[†] | Oral[†] | Bhattacharya, 2009; Kim et al., 2012 |

| | | | | | | |
|---|---|---|---|---|---|---|
| **Hawthorn (Flavonoids)** | Phytosome | Increase therapeutic efficacy and absorption | Cardio-protective and antihypertensive | 100 mg dose | Oral | Bhattacharya, 2009 |
| **Hesperetin** | Microemulsion | Enhanced skin permeability, site specific delivery | Skin whitening, antioxidant, anti-inflammatory, UV-protecting | 101.5 - 168.8 nm droplet size, 1.0% (w/w) dose | Topical | Tsai et al., 2010 |
| **Lutein** | Solid lipid nanoparticles (SLN)[†], nanostructured lipid carriers (NLC)[†, #], self-emulsifying phospholipid suspension (SEPS), Enhanced bioavailability[*], retinal accumulation of lutein from SEPS[*], targeted delivery to retina (ocular)[*] | Effective delivery to skin (dermal) [†], enhanced skin permeability, stabilized the formulation against UV-degradation[†], sustained release of lutein delivery[†,#,*] | Antioxidant[†], anti-stress, antiagieng, uses against age-related macular degeneration (AMD) and cataracts[*] | 150-350 nm particle size[†], 1.0% (w/w) dose[†], 134 ± 8 nm[#], 5%, 0.2%, and 0.05% dose[#], 90% entrapment efficiency[#], 10 mg dose[*], 473.13% relative bioavailability (from 500 mg lutein)[*] | Topical[†], *in vitro*[#], *in vivo*[*], oral[*] | Mitri et al., 2011; Liu and Wu, 2010; Shanmugam et al., 2011 |
| **Matrine** | Ethosome | Improved the percutaneous permeation | Antiinflammatory | 110 ± 8 nm droplet size | Topical | Zhaowu et al., 2009 |
| **Naringenin** | Nanoparticle[†], phytosome[††] | Improved the drug release and improved drug solubility[†], prolonged duration of action[††] | Hepatoprotective[†], antioxidant activity[††], antiinflammatory | 100 mg/kg dose[††] | Oral[†,††] | Yen et al., 2009; Maiti et al., 2006 |
| **Oridonin** | Nanoparticle | Sustained release profile, prolonged residence time of drug in live | Targeted for liver (hepatocyte) disease, hepatoprotective | 8 mg /kg, 200.7 ± 2.9 nm particle size and 85% entrapment efficiency | i.v, *in vivo* | Zheng et al., 2012 |
| **Paclitaxel** | Nanoemulsion [†] | sustained release profile, increased bioavailability[†] | Anticancer[†], targeted for breast cancer | Absolute oral bioavailability (55.9%) | *In vitro,* *In vivo* | Choudhury et al., 2014 |
| **Puerarin** | Nanoparticle | Targeted to blood-brain barrier (BBB), used in stroke (cerebral ischemia/reperfusion injury), neuroprotective effect | Cardiovascular and cerebrovascular diseases | 201.2 nm particle size | i.v, *in vivo* | Zhao et al., 2013 |
| **Quercetin** | Liposome[†], | Reduced dose, | Antioxidant[#], | 60%[†] , | Intranasal[†] | Priprem et |

| | | | | | | |
|---|---|---|---|---|---|---|
| | nanoparticle[*], phytosome/herbosome[††], nanostructured lipid carrier (NLC), nanoemulsion, microemulsion[#], solid lipid nanoparticle, | enhance penetration in blood brain barrier[†], increase antioxidant activity and release of the drug 74 times higher[*], exerted better therapeutic efficacy[††], enhanced skin permeability[#] | anticancer[†, *,††], anti-inflammatory, anti-radical, anti-ageing, anti-wrinkle | >99%[*] Entrapment efficiency, 10-100 nm droplet size[#] | , *in vitro*[*], oral[††], topical[#] | al., 2008; Maiti et al., 2005; Chen-yua et al., 2012; Pool al., 2013; Bose et al., 2013 |
| **Resveratrol** | Herbosome[†], Nanoemulsion[††], nanocapsules[††], solid lipid nanoparticles[††], beads[††], microparticules[††], lipospheres[††], liposomes[††] | Improved bioavailability[†, ††], and enhanced cardioprotective efficacy[†], sustained delivery[†], controlled release[††,] pharmacokinetics profile[††] | Antioxidant[†,††],cardioprotective[†], anti-inflammatory[††], anti-tumor[††] | 4 mg/kg dose[†], 5 µm particle size[†], 92.5% entrapment efficiency[†] | Oral[†] , *in vivo*[†] | Mukherjee at al., 2011; Amri et al., 2012; Sessa et al., 2013 |
| **Rutin** | Microcapsules | Targeting into cardiocascular and cerebrovascular region | Cardiovascular, cerebrovascular diseases, antioxidant, antiallergic, anti-inflammatory, antiageing | 165 – 195 µm particle size | *In vitro* | Xiao et al., 2008 |
| **Silibini** | Nanoparticle | High entrapment efficiency and stability | Hepatoprotective | 95.64% Entrapment efficiency | - | Li et al., 2007 |
| **Silybin** | Phytosomes[†], nanoemulsion[*] | Absorption of silybin phytosome from silybin is approximately seven times greater[†], sustained release formulation[*] | Hepatoprotective[*], antioxidant for liver and skin[†] | 120 mg dose[†], 21.20 nm droplet size[*] | Oral[†], intramuscular[*] | Yanyu et al., 2006; Mei et al., 2005 |
| **Silymarin** | Liposome[†], nanoemulsion | Improve bioavailability[†] | Hepatoprotective[†] | 69.22 ± 0.6% Entrapment efficiency[†] | Buccal[†] | El-Samaligy et al., 2006; Parveen et al., 2011 |
| **Taxel** | Nanoparticle | Enhanced bioavailability and sustained drug release | Anticancer | 99.44% Entrapment efficiency | - | Fu et al., 2006 |
| **Tetrandrine** | Nanoparticle | Sustained drug release | Lung | 84% Entrapment efficiency | *In vitro* | Li et al., 2006 |
| **Tretinoin** | Solid lipid nanoparticles, liposome[†], | Enhanced skin delivery[†], sustained drug | Antioxidant, antiagieng, dermatologic | 91-99% Entrapment efficiency[†], 4 | *In vitro*[†], topical[†] | Shah and Patravale, 2007; |

| | | | | | | |
|---|---|---|---|---|---|---|
| | niosome[†] | release[†] | disorders[†] | mg/ml dose[†], 200 nm droplet size[†] | | Manconi, et al., 2002 |
| **Triptolide** | Nanoparticle[†], SLN[††], microemulsion[*] | Enhance the penetration of drugs through the stratum corneum by increased hydration[†], decreasing the toxicity[††], enhance the penetration of drugs through the *stratum corneum* by increased hydration[*] | Anti-inflammatory[†,††,*] rheumatoid arthritis, | <100 nm droplet size [*] | Topical (skin)[†,*] oral[††], | Mei et al., 2005 |
| **Usnea acid** | Liposome | Incrase solubility and localization with prolongedrelease profile | Antimycobacterial | 99.5% Entrapment efficiency | *In vitro* | Lira et al., 2009. |
| **Vincristine** | Transferosomes | Increased entrapment efficiency and skin permeation | Anticancer | 120 nm droplet size | *In vitro* | Zheng et al., 2006 |
| **Wogonin** | Liposome | Sustained release effect | Anticancer | 81.20 ± 4.20% Entrapment efficiency | *In vitro* | Ke et al., 2007 |
| **β-Carotene** | Nanoemulsion[†,*] | Enhanced bioaccessibility and bioavailability[†], increased stability[*], sustained release delivery[†], effective delivery system for gastrointestinal tract (g.i.t.)[†] | Antioxidant[†], anticancer, cardiovascular disease | 140-170 nm particle size[†], 0.5% dose[†], 0.03% (w/w) dose[*], ≈66% bioaccessibility[†,] 9.24 ± 0.16 to 276.77 ± 17.70 nm particle size[*] | *In vitro*[†] | Qian et al., 2012; Silva et al., 2011 |

The advancement of various of disciplines involving molecular biology, cell biology and materials science, the targeted carrier system have gotten rapid development, which has become a thrust areas for research on pharmacy and pharmaceutics field worldwide. Targeted carrier system in the field of modern medicine have been exhaustively studied and applied clinically. Recently, in developed countries like Europe, United States and other developing countries, the related products have been accessible (Lin, 2005). However, the herbal medicine is still in the developing stage. Targeted oriented delivery system of herbal drug, using different carrier's technology makes the effective parts or monomers. After the effective delivery by carriers for extended period of time in the target site, which make the drug concentration on targets higher than that of other normal parts so that the therapeutic efficacy are enhanced and

the dosage related adverse effects are minimized (Zhang, 2006). Unlike the single compounds in modern medicine, effective parts in herbal medicine have relatively complex components, and the targeting preparation of this system of medicine is much more challengeable. For herbal formulation whose molecular mechanisms are mixtures of a variety of substances with different physicochemical properties and their pharmacological concept is unclear to understand the mechanism of action (Wei et al., 2005). In the present scenario, scientist and scholar are selecting single molecules as model drug and using drug carriers of varieties of forms are more profound. The targeted oriented carrier systems can be divided into liposomes, phytosome, NLC, nanoparticles, nanoemulsion, microemulsion, etc. In this system, a carrier for a specific cellular target is conjugated with the drug to form a prodrug which is less toxic than that of the main drug. The carrier offers two main features, one is to minimize the toxicity of the drug to normal cells and the other is to enhance the therapeutic action at the site (Lin et al., 2008). The targeting delivery of herbal drug is achieved mainly by novel carrier system, so researching and profoundly understanding the structural characteristics and mechanism of drug carrier are the basis to achieve clinical approaches (Li et al., 2009; Aqil et al., 2013; Wang et al., 2014). The application of these target based novel and/or nanotechnology drug delivery systems have already been discussed in the earlier section.

## 1.6. Summary and conclusion

Use of phyto-medicines is limited because they are poorly absorbed due to several physico-chemical problems. The goal of novel delivery systems is to enhance permeation and bioavailability of low bioavailable lipophilic plant secondary metabolites by improving its solubility using NDDS. The effectiveness of any herbal medicine is dependent upon delivering an effective level of therapeutically active compounds. Lipid solubility and molecular size are the major rate limiting factors for molecules to cross the biological membrane. The improvement of bioavailability of drugs with such properties presents one of the greatest challenges in drug formulations. Oral lipid based formulations are attracting considerable attention due to their capacitance to increase the solubility, facilitating gastrointestinal absorption and reduce the effect of food on the absorption of low water soluble, lipophilic drug and therefore increasing the bioavailability. Moreover, most of the potential molecules from the herbs are having low bioavailability and pharmacokinetic profile. The half life of phytomolecules plays an important role in the therapeutic effect and availability of drug concentration in blood/plasma. This has resulted in greater dependence on the herbal medicine. With the growth of novel delivery systems, newer formulations of herbal medication can be produced with the intent to change the physical attributes of the phytochemicals which is responsible for its reduced bioavailability. Phospholipid based delivery systems i.e. phytosome, liposome, niosome, transferosome, solid lipid nanoparticle, nanoemulsion etc. are found to be very effective for the delivery of herbal drugs in contrast to conventional delivery systems. This approach may be useful to accomplish the desired

therapeutic effect even at a lower dosage of the same drug and hence with reduced side effects. So a novel attempt in the area of herbal drug delivery system can be successfully exploited to increase the bioavailability as well as pharmacological activity.

## 1.7. Publication

- Pulok K. Mukherjee, Ranjit K. Harwansh, Sauvik Bhattacharyya. Bioavailability of herbal products: approach toward improved pharmacokinetics, in: P.K. Mukherjee (Eds.), Evidence-based validation of herbal medicine, Elsevier, Amsterdam, 2015, pp. 217-245.

# Chapter - 2

## Scope, objective and plan of work

2.1. Scope and rationale of the present study

2.2. Objective of the work

2.3. Frame work of the study

## 2.1. Scope and rationale of the present study

The plant secondary metabolites (flavonoids, alkaloids, terpenoids, glycosides, etc.) have been exploited as medicine in pharmaceutical, medical and food research for their tremendous therapeutic activities. Several phytomolecules are used as therapeutic agents, nutraceuticals and dietary supplements because of their beneficial importances. Flavonoids are a diverse group of polyphenolic compounds present in plants and natural products. Studies have indicated that the flavonoids exhibit antiproliferative activity toward coronary heart disease, lung cancers, and other types of cancers. Polyphenols are abundant micronutrients in our diet, and evidence for their role in the prevention of degenerative diseases is emerging. Flavonoids have also been used in skin rejuvenating creams to heal and moisturize aged and sun burnt skin. Recent interest has increased in the potential protective effects of phenolic compounds against oxidative stress induced diseases (cardiovascular diseases and cancers) caused by reactive oxygen species (ROS) and other free radicals. Though, these molecules exhibit diverse therapeutic effects like antioxidants, anti-inflammatory, hypoglycaemic, hepatoprotective, UV-protective, anticancer and antiobesity effect etc. The efficacy of any plant secondary metabolite depends on effective delivery systems. Apart from various important effects many phytomolecules suffer from poor oral bioavailability due to low aqueous solubility, low permeability, gastrointestinal degradation (instability in G.I. pH) and extensive first-pass metabolism resulted to lower elimination half-life ($t_{1/2}$).
In the last century, attention has been focused on the approaches towards improved bioavailability and pharmacokinetics of herbal drugs through developing a novel drug delivery system (NDDS). The application of NDDS is an important approach towards solving the bioavailability related problems associated with phytomolecules and phytopharmaceuticals. Several novel herbal drug delivery systems specifically liposomes, transfersomes, ethosomes, niosomes, phytosomes, herbosomes dendrimers, micro/nanoparticles, micro/nanoemulsions, micelles, etc. have been successfully employed for the delivery of phyto-pharmaceuticals. The novel formulations have notable advantages compared to conventional formulations like enhancement of solubility and stability, membrane permeability and bioavailability, improved pharmacological activity through sustained release profile and reduced toxicity. The novel systems of herbal medicine have the capability to deliver the drug at a rate directed by the needs of the body for an extended period of time and it should channel the bioactive molecule of herbal products to the site of action. Many bioactive agents intended for oral ingestion (e.g., nutraceuticals and pharmaceuticals) are highly hydrophobic compounds with low water-solubility and poor bioavailability. Many bioactive compounds are highly lipophilic and show a very low solubility in water, which makes the addition to the majority of foods difficult. Furthermore, poor solubility also means lower absorption in the gastrointestinal tract (GIT) and, therefore, limited bioavailability. The application of nanotechnology to food, medical and pharmaceutical industries has received great attention from the scientific community. Driven by the increasing consumers' demand for healthier and safer food products and the need for

edible systems able to encapsulate, protect, and release functional compounds, researchers are currently focusing their efforts in nanotechnology to address issues relevant to food and nutrition.

Nano-emulsification technology is particularly suited for encapsulating phytopharmaceuticals and functional compounds as it prevents their degradation and improves their bioavailability. Nanoemulsion based delivery systems are a particularly convenient means of encapsulating, protecting, and delivering poorly water soluble nutraceuticals and drugs via the oral route for both functional food and pharmaceutical applications. The encapsulation of bioactive compounds in nanoemulsion carrier system enjoys different advantages in comparison with conventional delivery systems which includes (i) stabilization in aqueous systems (such as foodstuffs) of lipophilic bioactive compounds with scarce solubility in water; (ii) protection of bioactive compounds against degradation reactions with food constituents and minimization of the alteration of the food matrix; (iii) control of the release by engineering the dimension and composition of the formulation and (iv) enhancement of cell uptake and bioavailability. In particular, the bioavailability of compounds encapsulated into emulsions is enhanced when emulsion droplets are of nanometric size. Many authors have shown that reducing the particle size to values below cell size (~500 nm) produces higher absorption of the active ingredient and higher particle uptake, by enhancing the mechanisms of passive transport through the intestinal walls.

Nanoemulsions are isotropic mixtures of natural or synthetic oils, solid or liquid surfactants, or alternatively, one or more hydrophilic solvents and co-solvents/co-surfactants. Oil-in-water (o/w) nanoemulsions can be prepared by solubilizing the lipophilic bioactive components within the oil phase and then homogenizing this phase with an aqueous phase containing a water-soluble emulsifier. The size of the droplets produced depends on the composition of the system and the homogenization method used. Nanoemulsions are thermodynamically stable systems that consist of emulsifier coated oil droplets dispersed within an aqueous medium. Upon mild agitation followed by dilution in aqueous media, such as gastrointestinal (GI) fluids, these systems form fine oil-in-water (o/w) nanoemulsions having droplet size in the range of 20-200 nm. After oral administration, nanoemulsions spread readily in the GI tract and the digestive motility of the stomach and the intestine provide the agitation necessary for self-emulsification. Nanoemulsions are characterized by high solvent capacity, fine droplet size and excellent stability. In addition, they can enhance permeation across the intestinal membrane, reduce or eliminate food effect and enhance drug bioavailability.

**Advantages of nano-systems:**

- ✓ Ease of preparation with minimum significant energy contribution
- ✓ The small size of the droplets give large interfacial area from which drug can be quickly released, improving the oral absorption of poorly water soluble drugs

- ✓ They prevent hydrolysis and oxidation of the drug when the drug is in oil phase
- ✓ Improved dose proportionality
- ✓ Reduced fed/fasted variability
- ✓ Reduced inter-and intra subject variability

The goal of NDDS is to enhance the permeability and bioavailability of low bio-available phytopharmaceuticals by improving its solubility using nanoemulsion as a nano-carrier system. The effectiveness of any phytopharmaceuticals is depended upon delivering an effective level of the active compounds. Lipid solubility and molecular size are the major limiting factors for phytomolecules to cross the biological membrane to be absorbed systematically through oral. The improvement of bioavailability of drugs with such properties presents one of the greatest challenges in drug formulations. Nanoencapsulation are attracting considerable attention due to their capacity to increase the solubility, facilitating gastrointestinal absorption and reduce or eliminate the effect of food on the absorption of poorly water soluble, lipophilic drug and thus increasing the bioavailability.

The aim of the study is to prepare nanoemulsions of phytopharmaceuticals using nanoemulsification technique to enhance the bioavailability with an aim to give stable formulation. Generally, nanoemulsions are either administered as liquid dosage forms, encapsulated either in hard or soft gelatin capsules. In case of topical or transdermal application, nanoemulsions are administered in the form of gel after incorporating them into suitable gel matrix. This is an emerging nanotechnology applied to phytopharmaceutical for the enhancement of bioavailability of potent plant secondary metabolites for fulfillment of several therapeutic effects.

## 2.2. Objective of the work

The main objective of this study is to develop nanoemulsions of some therapeutically potent phytopharmaceuticals having low bioavailability profiles. The molecules were selected based on their chemical properties, solubility and bioavailability problems and therapeutic potential. In order to overcome the shortcomings of those molecules, the present study has been undertaken to develop a novel formulation. This includes the preparation, characterization of the nanoemulsions and evaluation of the bioavailability as well as therapeutic efficacy.

The main objectives of the work were based on the following aspects:

- ✓ Selection of potent phytopharmaceuticals having low bioavailability and shorter half-life through literature review.
- ✓ To enhance the solubility and thus bioavailability of the poorly soluble phytomolecules by developing nanoemulsions using nano-emulsification process.
- ✓ Preparation of nanoemulsions of the selected phytopharmaceuticals.

- ✓ Physicochemical characterization of the prepared nanoemulsion and nanoemulsion based nano-gel formulation through UV-spectrophotometry (SpectraMax®), High Performance Thin Layer Chromatography (HPTLC), High Performance Liquid Chromatography (HPLC), Fourier Transform Infrared Spectroscopy (FTIR), Transmission Electron Microscopy (TEM) study and analysis of their pH, conductivity, viscosity, refractive index, rheological behavior characteristics; Droplet size and zeta potential analysis through Zetasizer.
- ✓ Stability study of the formulation.
- ✓ *In vivo* evaluation of therapeutic efficacy.
- ✓ *In vitro* permeability study.
- ✓ *In vivo* bioavailability and pharmacokinetics study.

## 2.3. Framework of the study

In the present study four potent phytomolecules namely ferulic acid, catechin and genistein were selected according to their therapeutic potential and poor bioavailability profiles. Different nanoemulsions of these phytomolecules were prepared, evaluated for their physicochemical characteristics, stability studies, *in vivo* biological activities and *in vivo* pharmacokinetics studies. The detail plan of work is represented in the schematic diagram (Figure 2.1).


**Figure 2.1. Work plan for the study**

# Chapter - 3

## Formulation and evaluation of ferulic acid loaded nanoemulsion for its therapeutic benefit

3.1. Ferulic acid – therapeutic importance and limitation
3.2. Formulation and evaluation of ferulic acid loaded nanoemulsion
3.3. Characterization of nanoemulsion formulations
3.4. Preparation of the gel formulation
3.5. Ex vivo skin permeation study
3.6. Skin irritation study
3.7. Release kinetics of ferulic acid based nanoemulsion and gel formulation
3.8. Efficacy study of the ferulic acid loaded gel formulations as a photoprotective agent against UVA exposure
3.9. In vivo bioavailability study in rats
3.10. Analysis of pharmacokinetic parameters
3.11. Statistical analysis
3.12. Results and discussion
3.13. Conclusion
3.14. Publication

## 3.1. Ferulic acid – therapeutic importance and limitation

Ferulic acid (FA, 4-hydroxy-3-methoxycinnamic acid) is a potent polyphenolic antioxidant compound naturally found in food plants i.e. wheat, rice, barley, oats, citrus fruits, tomatoes, etc. (Alias et al., 2009; Srinivasan et al., 2007). FA has been proven to afford significant protection to the skin against UV-B-induced oxidative stress in human lymphocytes and erythema (Prasad et al., 2007). Staniforth et al. have been reported that FA inhibited the UVB-induced matrix metalloproteinases and attenuates the degradation of collagen fibers, abnormal accumulation of elastic fibers and epidermal hyperplasia through posttranslational mechanisms (Staniforth et al., 2012). FA also possesses antiageing (Srinivasan et al., 2006), hepatoprotective (Srinivasan et al., 2005), antiatherogenic (Rukkumani et al., 2004), antimutagenic (Murakami et al., 2002), anti-inflammatory, anticancer, antidiabetic (Barone et al., 2009), neuroprotective and cardioprotective activities (Srinivasan et al., 2007).

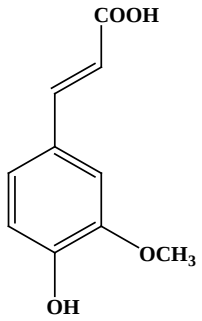


**Ferulic acid**

Pharmacokinetic profile of FA has been studied after oral administration of Chuanxiong and *Angelica sinensis* extract in rats at dose of 1.176 g/kg (equivalent to 8.82 mg/kg FA). The different pharmacokinetic parameters were detremined by a non-compartment model with $T_{max}$ = 1.1 ± 0.65 h, $C_{max}$ = 44.7 ± 8.2 ng/mL, $C_L$ = 46 ± 14 mL/kg/min, $AUC_{0-t}$ = 165 ± 46 ng h/mL, $T_{1/2}$ = 5.00 ± 0.78 h and MRT = 6.82 ± 0.60 h (Zeng et al., 2014). In another study, FA was orally administered to the rat at dose of 4 mg/kg and pharmacokinetic parameters were calculated by two compartment model with $AUC_{0-\infty}$ = 775.8 ± 59.4 min mg/L, $T_{max}$ = 15 min, $C_{max}$ = 1.6 ± 0.3 mg/L, $C_L$ = 0.026 ± 0.001 L/min/kg, $V_d$ = 12.4 ± 3.3 and $T_{1/2}$ = 333.2 ± 79.8 min (Ge et al., 2015). Similarly, FA pharmacokientics has been performed by Li et al. (2011), FA at 10 mg/kg dose was orally administered to the rat and different parameters were observed. FA was rapidly absorbed with a $T_{max}$ of 0.03 h. The corresponding $C_{max}$ and the $AUC_{0-t}$ were 8174.55 ± 1017.98 ng/mL and 2594.45 ± 237.98 h ng/mL respectively. FA was rapidly absorbed with a low bioavailability after a single oral administration (Li et al., 2011). *In situ* or *ex vivo* absorption models suggest that FA can be absorbed from the stomach, jejunum and ileum. After a 25-min incubation of FA in the rat stomach, >70% of the FA absorbed from the stomach and it was recovered in the gastric mucosa, blood, bile and urine, resulting a fast gastric absorption of FA. Similarly, FA quickly absorbed from the

jejunum and to a significantly lesser extent from the ileum when it was perfused in an isolated rat intestine model. Only 0.5-0.8% of ingested FA was found in feces of rats, indicating very efficient absorption rate for FA (Zhao and Moghadasian, 2008). Metabolic studies have represented that FA can be metabolized *in vivo* into various metabolites such as FA-glucuronide, FA-sulfate, FA-diglucuronide, FA-sulfoglucuronide (FA-diconjugate with sulfate and glucuronide), m-hydroxyphenylpropionic acid, feruloylglycine, dihydroferulic acid, vanillic acid and vanilloylglycine. Conjugated FA including FA-glucuronide, FA-sulfate and FA-sulfoglucuronide are the major metabolites in the plasma and urine of rats. These results suggest that the conjugation reaction with glucuronic acid and sulfate is the main pathway of *in vivo* metabolism of FA.

The metabolism and conjugation of FA takes place in the liver through the activities of mainly two enzyme including sulfotransferases and UDP glucuronosyl transferases. Intestinal mucosa and kidney may also, at least in part, contribute to this metabolism process. FA is mainly eliminated through urine in rats in free and conjugated forms. FA undergoes a marked first-pass effect which limits its oral bioavailability. Only a low percentage of unmodified FA (9-20%) was found in the plasma (Bourne and Rice-Evans, 1998). The present study is aimed to develop a ferulic acid loaded nanoemulsion based gel in order to ensure the enhanced permeability as well as bioavailability and maximum antioxidant activity in a sustained manner against UVA induced oxidative stress in rat.

## 3.2. Formulation and evaluation of ferulic acid loaded nanoemulsion

### *3.2.1. Physical and chemical characterization of ferulic acid*

The physico-chemical properties of FA are described as follows:

| | | |
|---|---|---|
| Color | : | White |
| Odor | : | Odorless |
| Taste | : | Characteristic |
| Physical form | : | Crystalline powder |
| Melting point (m. p.) | : | 172°C |
| Solubility | : | Freely soluble in methanol;<br>Soluble in ethanol, DMSO and acetone;<br>Slightly soluble in water |
| Partition coefficient | : | 1.64 ± 0.36 (lipophilic) |
| (log P) | : | ~ 0.37 in water at pH 3; ~ 0.49 at pH 10 |
| $\lambda_{max}$ | : | 321 nm |

### *3.2.2. Chemicals and excipients*

Ferulic acid [assay 99%] was obtained from Sigma-Aldrich Chemicals, Bangalore. Labrafac™ lipophile WL1349 (LLW), labrasol®, plurol oleique®, plurol isostearique®, isostearyl isostearate® (ISIS), lauroglycol™ 90 and transcutol CG® were gift samples from Gattefossé (Saint Priest, Cedex France). Acconon® CC-6 was procured from ABITEC Corporation, Columbus, USA. All other chemicals and reagents used were of analytical grade obtained from Merck, Mumbai. Water was obtained from Milli-Q water purification system (Millipore, MA).

### *3.2.3. RP-HPLC analysis of FA*

#### *3.2.3.1. Chromatographic conditions*

Estimation of FA content in the formulations was analyzed by RP-HPLC (Waters 600, Milford, MA, USA) at a flow rate of 1 mL/min with 15 min run time at 321 nm wavelength at 25 ± 0.5°C using a Spherisorb $C_{18}$ column (250 mm × 4.6 mm, 5 µm; Waters, Ireland) fitted with a $C_{18}$ guard column (10 × 3.0 mm). The samples were injected through 20µL micro-syringe (Hamilton Microliter®; Switzerland).

The standard stock solution was prepared by dissolving the known amount of FA in methanol to get a concentration of 1000 µg/mL. Different aliquots were prepared by subsequent dilution with the same solvent. Samples were stored at 4°C and protected from light before using. In this analysis, mobile phase of acetonitrile and deionized water was used as a proportion of 35:65, 30:70 and 25:75 v/v (1% glacial acetic acid; pH 2.2) which were sonicated for 15 min and degassed prior to use. Before applying all samples were also filtered through 0.45 µm (NYL) syringe filter.

The method was validated in terms of linearity, repeatability, intermediate precision, sensitivity and recovery as per the guideline of International Conference on Harmonization (ICH, 1994). The assay precision was calculated in terms of percentage of the relative standard deviation (% RSD) of determinations. Sensitivity of the system was determined by the limit of detection (LOD) and limit of quantification (LOQ) based on the standard deviation of the response (σ) and the slope (S) of the standard curve using the following equations.

$LOD = 3.3\sigma/S$ and $LOQ = 10\sigma/S$..... Eq. (1)

The recoveries of standard compounds from various samples and formulation at three concentration levels were determined by measuring the percentages of detecting concentrations over additional concentrations. The quantitative analysis was repeated about three times (n = 3) by comparing and interpolating the peak area (response) of the sample with the standard.

### *3.2.4. Solubility study of FA in different excipients*

The solubility of FA in various oils; including labrafac lipophile WL1349, ethyl oleate, IPM, ISIS, oleic acid, olive oil, soybean oil was performed by adding an excess amount of the drug in 1 mL of each of the selected oils and distilled water separately in 2 ml capacity eppendorf tube and mixed using a vortex mixer (Spinix, Tarson, India). Then the mixture tubes were kept at 25 ± 1.0 °C in an isothermal shaker for 72 h to get equilibrium (Shafiq et al., 2007). The equilibrated samples were taken out from the shaker and centrifuged at 13500 rpm (Spinwin MC-02, Tarson, India) for 5 min wherein the supernatant was taken and filtered through a 0.45 µm membrane filter. The concentration of FA was individually analyzed by RP-HPLC method at $\lambda_{max}$ 321 nm.

### *3.2.5. Screening of surfactants and co-surfactants*

Different surfactants (Labrasol, Acconon CC-6, Lauroglycol 90, Span 80, Tween 80 and Brij 35) and cosurfactants (Transcutol CG, PEG 400, Plurol isostearate and Plurol oleaque) were screened for nanoemulsion formulation. Surfactant solution (2.5 mL of 15 wt %) in water was prepared. Initially 5 µL of the selected oil was added with vigorous vortexing until a clear solution was observed. This process was repeated until the opacity of the solution become permanent (Shafiq et al., 2007).

### *3.2.6. Pseudo-ternary phase diagram study*

On the basis of drug excipient solubility studies, oil phase (ISIS), surfactants (labrasol and acconon CC-6), cosurfactants (transcutol CG and plurol isostearique) and Milli-Q water was selected for further study. These were grouped in four different combinations for phase diagram studies (Table 3.1). Surfactant and cosurfactant mixture (Smix) in each group (Table 3.1) were used in different weight ratios (1:0, 1:1, 2:1, 3:1, 1:2, 1:3%, w/w). These Smix ratios were chosen in increasing concentrations of surfactant with respect to cosurfactant and vice versa for the development of various phase diagrams.

**Table 3.1. Oil, surfactant and co-surfactant grouped in different combinations**

| Group | Oil | Surfactant | Co-surfactant |
|---|---|---|---|
| I | ISIS | Labrasol | Transcutol CG |
| II | ISIS | Labrasol | Plurol isostearique |
| III | ISIS | Acconon CC-6 | Transcutol CG |
| IV | ISIS | Acconon CC-6 | Plurol isostearique |

For construction of the phase diagrams, aqueous titration method was adopted where water was added by drop-wise in the mixture of Smix and oil as shown in Figure 3.1. According to transparency and flowability, NE (o/w) phase was recognized. Fourteen various combinations of oil and Smix (1:9, 1:8, 1:7, 1:6, 1:5,1:4, 1:3.5, 1:3, 1:2.5, 1:2,

1:1, 6:4, 7:3, 9:1 w/w) were selected to cover maximum ratios for the study to delineate the boundaries of each phase diagram. Water was added at every 5% interval to find the range of 5-95% of total volume. The physical state of the NE was illustrated in a pseudo three component phase diagram where the three axes denoted oil, aqueous phase and Smix in that order (Choudhury et al., 2014).

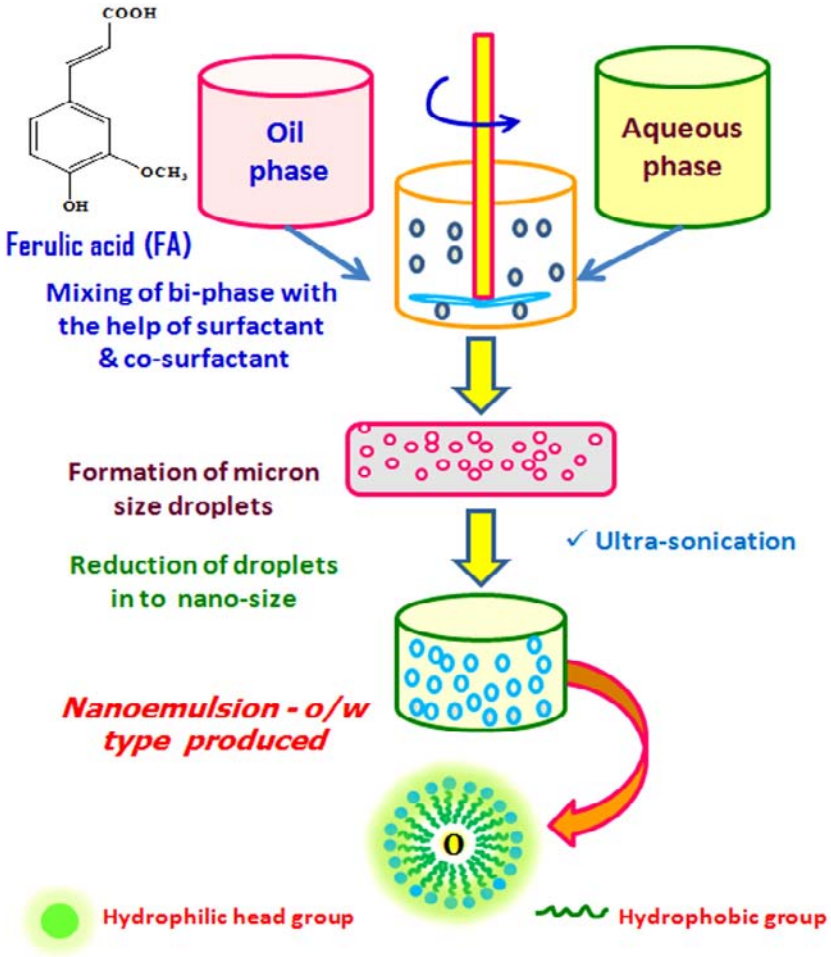


**Figure 3.1. Schematic diagram of preparation for ferulic acid based nanoemulsion**

*3.2.7. Thermodynamic stability study*

Thermodynamic stability of the selected formulations was performed in order to assess the physical stability as per the method described by Choudhury et al. (2014). Evaluation procedure is as follows:

*3.2.7.1. Centrifugation test (Cent.):* The formulations were subjected to centrifugation at 13500 rpm (Spinwin MC-02, Tarson) for 5 min and physically observed for any kind of phase separation. After this test the stable formulations were subjected to the next step.

*3.2.7.2. Heating-cooling cycle (H & C):* In refrigerator, the stable formulations were kept at 4 and 40°C temperature (six cycles each) for 48 h. Those samples which passed this test were further subjected to the freeze thaw stress test.

*3.2.7.3. Freeze-thaw cycle (Freeze Tha.):* The stable formulations after heating and cooling stress were subjected to three freeze-thaw cycles between -20 and 25°C for 48 h of each temperature.

*3.2.8. Selection of formulations from phase diagrams*

Different formulations were selected from a nanoemulsion region of each phase diagram therefore the drug could be dissolved into the oil phase, according to the following criteria.
(a) The amount of oil should be such that it dissolved the single dose of the drug completely depending on the solubility of the drug in the oil. 1 mg of FA will dissolve easily in 1 mL of oil.
(b) To check if there was any effect of drugs on the phase behaviour and nanoemulsion area of the phase diagram.
(c) The minimum amount of the Smix used to that amount of oil was taken.
(d) A little volume (1 mL) of the nanoemulsion formulation was selected for convenience purposes, thus it can be increased or decreased in the proportions as per the need. The system is thermodynamically stable and the scale up of the proportions is easy as the beauty of this system (Shafiq et al., 2007).

*3.2.9. Formulation of ferulic acid nanoemulsions*

FA loaded nanoemulsions were prepared by incorporating 1 mg/mL concentration into selected oil phase at 10, 15, 20, 25, and 30% (w/w) along with respective Smix ratios using spontaneous nano-emulsification method.

**3.3. Characterization of nanoemulsion formulations**

*3.3.1. Electrical conductivity*

The conductivity of the NE was performed by applying electrical current through the formulation to find the formulation type. A measurement in the conductivity meter (Systronic Conductivity meter 306, Systronic Ltd., India) was anticipated for o/w emulsion type (Okur, et al, 2011).

*3.3.2. Percentage transmittance*

Percentage transmittances of the diluted samples of NEs (100 times in water) were analyzed at 450 nm using a spectrophotometer (SpectraMax® M5, USA).

### *3.3.3. Viscosity*

The viscosity of the selected NE was measured by using a Brookfield Viscometer with spindle CPE 41 (Brookfield Engineering Laboratories, Inc., MA). For analysis, 1 mL of the formulation was selected. Prior to the measurement, machine was stabilized for 15 min and the speed of the spindle was adjusted to 10 rpm and a single run was performed at a temperature of 25 ± 0.5°C (Choudhury et al., 2014).

### *3.3.4. pH*

The pH of the NE was measured using a digital pH meter (Orion 3 Star, Thermo Scientific) at 25 ± 0.5°C.

### *3.3.5. Refractive index*

An Abbe refractometer was used for measurement of the refractive index of NE along with placebo (NE without FA) at 25 ± 0.5°C (Choudhury et al., 2014).

### *3.3.6. Drug percentage entrapment efficiency (%EE) and drug loading (%DL)*

%EE and %DL of FA loaded NEs were estimated as per the procedure established by Bu et al. (2014). In brief, content of free FA was separated from FA loaded NE (FA-NE) by the ultrafiltration method (10,000 DA, Millipore) with centrifugation at 13500×g for 5 min. After dissolution and subsequently dilution with methanol, the drug amount in the filtrate and FA-NE formulations were quantified by RP-HPLC method at wavelength 321 nm. The %EE and %DL were calculated according to the following equations.

$$\%\mathrm{EE} = \frac{(\mathrm{Wt}-\mathrm{Wf})}{\mathrm{Wt}} \times 100\% \quad \text{..... Eq. (2a)}$$

$$\%\mathrm{DL} = \frac{(\mathrm{Wt}-\mathrm{Wf})}{\mathrm{Wc}} \times 100\% \quad \text{..... Eq. (2b)}$$

Where, Wt is the total amount of FA in FA-NE, Wf represents the amount of free FA, and Wc refer to the total weight of FA-NE formulation.

### *3.3.7. Droplet size, polydispersity index and zeta potential analysis*

The average droplet size (Z-average) and polydispersity index (PDI) of selected formulations were measured by photon correlation spectroscopy (PCS) using a Malvern Zetasizer (Nano ZS90, Malvern instruments Ltd., UK) with a 50 mV laser. The sensitivity range is 10 nm to 5 μm and the data were shown by computer calculation using the Mie equations of light scattering. The measurements were performed at 25 °C at a fixed angle of 90°. The measurement time was 2 min and each run underwent 12 sub runs. The formulation (0.1 mL) was dispersed into 100 mL of water under gentle

stirring in a glass beaker. Then approx 1 mL aliquot was withdrawn and added into a sample cell for droplet size measurement. Each size value reported was the average of at least three independent measurements. Zeta potential (ξ) measurements were also carried out on the same diluted sample using the same equipment and operating conditions, and the zeta potential values were calculated according to the Smoluchowski equation (Zhao et al., 2010).

*3.3.8. Transmission electron microscopy (TEM) study*

TEM analysis was performed to determine the morphology of FA-NE3. It was performed by using TEM (JEOL JEM 2100, USA) with a working voltage of 200 kV. The diluted and filtered NE sample was placed on 300 mesh size carbon coated copper grid. The filled, copper grid was negatively stained with 2% (w/v) phosphotungstic acid (PTA) for 30 s. Excess of PTA was removed by absorbing on a filter paper and dried overnight at room temperature (25 ± 0.5°C). Photo-micrographs of the sample from the TEM were taken at different magnification.

*3.3.9. UV - spectrophotometry study*

In this assay, The 200 µl of FA (FA equivalent to 0.1 mg/mL) and FA-NE3 (FA equivalent to 0.1 mg/mL) were transferred into 96 well microplate (Quartz) by using micropipette (Eppendorf, Torson). The microplate was scanned at 321 nm at room temperature (25 °C) using spectrophotometer (Multiscan-Go, Thermo Scientific) and the result was recorded. HPLC grade methanol (Merck, Mumbai, India) was used as a blank throughout the study.

*3.3.10. High performance thin layer chromatography (HPTLC) analysis*

The HPTLC (CAMAG, Switzerland) analysis of the FA-NE3 along with standard FA was performed using a solvent system containing toluene: ethyl acetate: formic acid at a ratio of (6: 3: 0.8 v/v/v). The sample was spotted onto the plate through the applicator (Linomat 5). UV densitometry scanning of developed HPTLC plate (Silica gel 60 F254) was done at wavelength 315 nm and data was analyzed by software (WINCATS).

*3.3.11. Fourier transforms infrared (FTIR) study*

FTIR studies were performed to detect any chemical interactions between FA and excipients in the formulation, for followings: (A) pure FA, (B) FA-NE3 and (C) placebo NE (FA-NE3 without FA). The FTIR measurements were done in the range of 4000-450 $cm^{-1}$ using FTIR (Perkin Elmer, USA).

### *3.3.12. Stability study*

The optimized NE formulation (FA-NE3) was subjected to stability studies at long term and accelerated conditions (40 ± 2°C/75 ± 5% RH) as per the ICH guidelines. The formulation was kept in air tight glass vials and assayed periodically at the time interval of 0, 1, 3 and 6 months for any change in appearance, precipitation, clarity, pH, droplet size, zeta potential and drug content. Drug content in the NE was analyzed using RP-HPLC method at 321 nm. Logarithm of percentage of the drug remained to be decomposed was plotted against time in a month to determine the predicted shelf life ($t_{90}$) of the formulation.

## 3.4. Preparation of the gel formulation

The conventional gel of ferulic acid (FA-CG, ~ 0.1 g of FA) was prepared by dispersing the carbopol 940 (1 g) in distilled water up to 100 mL. The dispersion medium was stored in the dark place at room temperature (25°C) for 24 h to swell completely. Other components like PEG 400 – 10 g, propylene glycol (PG) – 10 g, isopropyl alcohol (IPA) – 10 g and triethanolamine (TEA) – 0.5 g were incorporated to obtain a homogeneous dispersion of gel (Harwansh et al., 2011). The NE gel (FA-NG3, ~ 0.1 g of FA) was developed by adding 1 g of an already swollen dispersion system of carbopol 940 into the optimized FA-NE3 to get the homogenous mass.

### *3.4.1. Analysis of rheological property*

The flow behavior of FA-NG3 formulations and the corresponding placebo were evaluated through Anton Paar, Modular Compact Rheometer-MCR 102. A stress/rate with a temperature controller was employed to measure the rheological properties of the formulations. The measurements were performed at a temperature of 25 ± 0.5 °C with a 4°/40 mm cone and plate geometry and gap of 0.100 mm. The steady rheological behaviors of the FA-NG3 and placebo were measured at a controlled rate varying from 0.001 – 100 and 0.0001 – 100 $s^{-1}$ respectively. After being loaded onto the plate, the samples were allowed to rest about 10 minutes prior to measurement.

### *3.4.2. Evaluation of spreadability test*

The spreadability of the FA-NG3 and placebo was evaluated as per the method described by Khurana et al. (2013). Briefly, to assess the spreading properties of the gel formulations (FA-NG3 and placebo), the weighed cellulose acetate filter paper ($W_1$) was placed in the center of the aluminium foil sheet. Several milliliters of the tested formulation were filled into the 5 ml disposable syringe. Then, 20 drops of the formulation were pushed out from the syringe over the defined area in the center of the cellulose acetate filter paper. After 10 min, saturated portion of the filter paper was cut out from the unsaturated portion. The unsaturated portion of the filter paper was

weighed accurately ($W_2$) and % spreadability by weight was calculated using the following equation.

$$\%Spreadability = [(W_1-W_2)/W_1] \times 100 \quad \text{..... Eq. (3)}$$

## 3.5. *Ex vivo* skin permeation study

### *3.5.1. Animals*

Wistar male rats (180-220 g) were selected in this study. Animals were housed in groups (n = 6) at ambient temperature (25 ± 0.5 °C and 45-55% R.H.) and conditions with 12 h light/dark cycles. They had free access to pellet chow (Brook Bond, Lipton India) and water *ad libitum*. The experiment was performed as approved by the Institutional Animal Ethical Committee with the ethical guidelines as provided by the committee (approval number: AEC/PHARM/1501/05/2015) for the purpose of control and supervision of experiment on animals (CPCSEA), India.

### *3.5.2. Preparation of the skin*

The abdominal rat skin was used after removing the hairs using a soft hair removing lotion. The rats were anesthetized under diethyl ether and sacrificed by cervical dislocation after that full thickness abdominal skin was excised. Any adhered subcutaneous tissue on the visceral side of skin was removed surgically, wiped with isopropyl alcohol to remove adhered fat and washed with phosphate buffer saline (PBS, pH 7.4). The skin was then carefully checked through a magnifying glass to ensure about any surface irregularity, such as tiny holes or crevices.

### *3.5.3. Procedure of evaluation*

Hairless abdominal skin was mounted in the *Franz diffusion* cell with the *stratum corneum* side faced towards the donor compartment and the dermal side towards the receptor compartment with an effective diffusion surface area of 1.766 $cm^2$. The receptor compartment was filled with phosphate buffer saline (PBS - pH 7.4). The diffusion cell was maintained at 37 ± 0.5°C with constant stirring. FA-NE1-5, FA-NG3 and FA-CG (1 mL equivalent to 0.1 g of FA) were evenly spread over the skin in donor compartment and sealed with paraffin film to provide occlusive conditions. 200 μL sample of the receptor medium was withdrawn at predetermined time intervals over a period of 24 h, and an equivalent volume of fresh PBS was replenished to maintain the sink conditions. All experiments were performed in triplicate. All samples were filtered, suitably diluted and analyzed by RP-HPLC.

## 3.6. Skin irritation study

The skin irritation study was performed using dorsal side of hairless rats (n = 6). The gel formulations (~500 mg) of FA-CG, FA-NG3 and placebo-NG (without FA) were applied. The animals were observed and evaluated for any sign of erythema, oedema and erosion for a period of 7 days.

## 3.7. Release kinetics of ferulic acid based nanoemulsion and gel formulation

To assess the drug release kinetics of data the different formulations obtained from *in vitro* drug release study were fitted with the following mathematical model (Dash et al., 2010).

### *3.7.1. Zero-order equation*

The z*ero-order* equation assumes that the cumulative amount of drug release is directly related to time. The equation is as follows:

$C = K_0 t$ ……..Eq. (4)

Where, '$K_0$' = zero order rate constant expressed in unit concentration/time, 't' = time in hour. A graph between concentration and time would yield a straight line with a slope equal to $K_0$ and intercept the origin of the axes.

### *3.7.2. First-order equation*

The release behavior of first-order equation is expressed as log cumulative percentage of drug remained Vs time. The equation is as follows:

$Log\ C = Log\ C_0 - kt/2.303$ ……Eq. (5)

Where, $C$ = Concentration of un-dissolved drug at t time, $C_0$ = Drug concentration at $t$ = 0, $k$ = Corresponding release rate constant.

### *3.7.3. Higuchi square root law*

The Higuchi release model indicates the cumulative percentage of drug release Vs square root of time. The equation is as follows:

$Q = k\sqrt{t}$ ……Eq. (6)

Where, $Q$ = The amount of drug dissolved at time $t$. $K$ = Constant reflecting the design variables of the system. Hence, drug release rate is proportional to the reciprocal of the square root of time.

### *3.7.4. Korsmeyer-Peppas equation*

Korsmeyer *et al* established a simple, semi-empirical model relating exponentially the drug release to the elapsed time. The equation is as follows:

$Q/Q_0 = Kt^n$ ……Eq. (7)

Where, $Q/Q_0$ = The fraction of drug released at time '*t'. 'k'* = Constant comprising the structural geometric characteristics. '*n'* = The diffusion exponent that depends on the release mechanism. If $n \leq 0.5$, the release mechanism follows a *Fickian diffusion*, and if $0.5<n<1$, the release follows a *non-Fickian diffusion* or anomalous transport (Korsmeyer et al., 1983).

The drug release follows zero-order kinetics and case II transport if n = 1. But in case n > 1, then the release mechanism is super case II transport. This model is used in the carrier mediated dosage form when the release mechanism is unknown or more than one release phenomena is present in the preparation.

## 3.8. Efficacy study of the ferulic acid loaded gel formulations as a photoprotective agent against UVA exposure

Photo-damage of skin is the most occurring dermatological problems worldwide (Mukherjee et al., 2011). A majority of UVB is absorbed through the epidermis of the skin, but UVA reaches the dermal layer and also the circulating blood, tissues and produces reactive oxygen species (ROS) (Bhattacharyya et al., 2014; Butnariu and Giuchici, 2011). ROS can influence lipid peroxidation in membranes (Afaq and Mukhtar, 2006) which leads to melanoma, dermatitis, ageing, inflammations and other severe skin problems (Couteau et al., 2007). Endogenous antioxidant capability of the skin is a major determinant in its response to oxidative stress-mediated damage involving reduced level of antioxidant enzymes, including glutathione (Campanini et al., 2013), superoxide dismutase, catalase, glutathione peroxidase and increased levels of thiobarbituric acid reactive substances (Saija et al., 2000). The various consequences of UV radiations on the skin are described in Figure 3.2.

### *3.8.1. UVA exposure to rats*

The UV protective effect of the FA loaded gel formulations were evaluated based upon the method established by Bhattacharyya et al. (2014). In brief, UV lamp (TL 100W, Philips, India) was served as UVA source which emitted radiations in the range between 315-400 nm with an output peak at 370 nm. UV lamp was equipped with the UVX digital UV intensity meter (Cole-Parmer, India) for measurement of incident light intensity which was found to be 508.3 $nW/cm^2$.

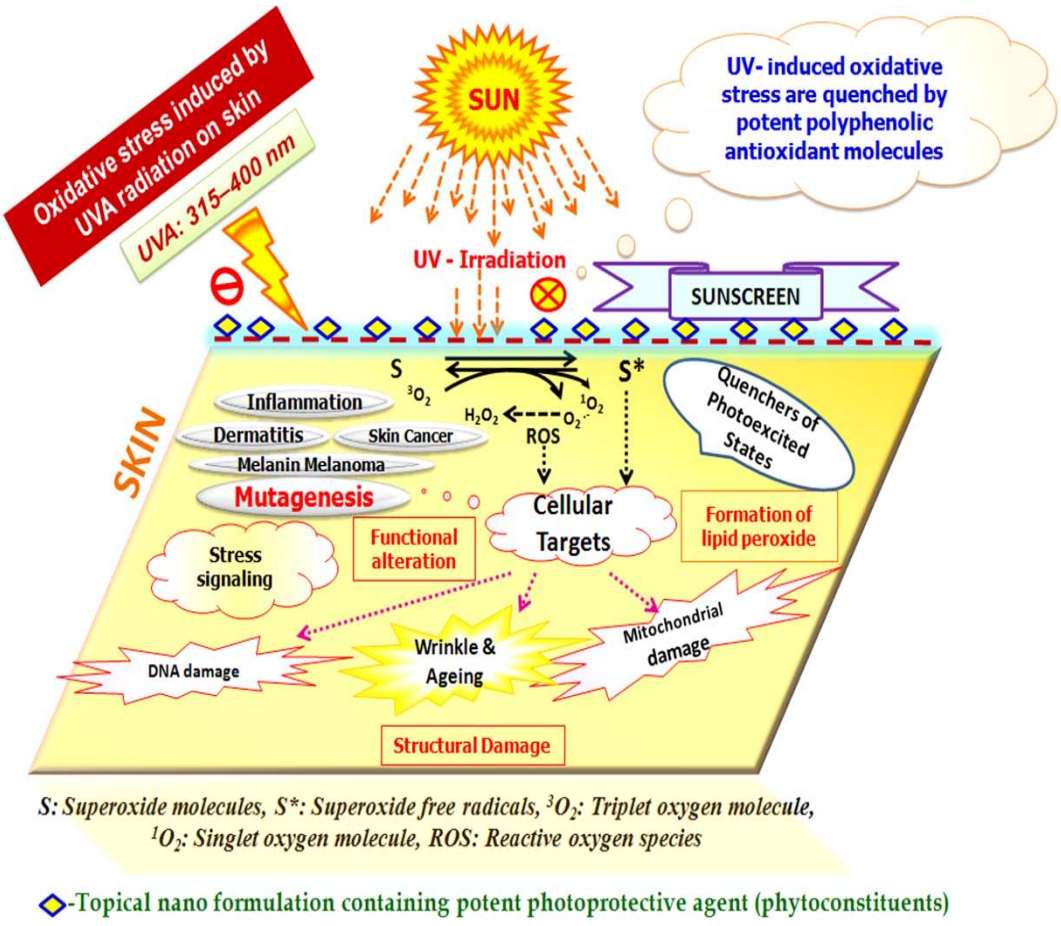


**Figure 3.2. Consequences of UV radiations on the skin**

The distance between the UV lamps and dorsal rat skin was 40 cm. A distinguished area of about 2×3 $cm^2$ on the dorsal skin of the rat was shaved using a soft hair-removing lotion. The rats were observed for 48 h to exclude rats showing abnormal hair growth or a reaction to the depilatory preparation. A soft hair-removing lotion was favored over a shaving blade to minimize free radical production due to trauma from the blade. For each subject, the minimally erythemogenic dose (MED) [138 $mJ/cm^2$, obtained by exposure for approximately 4.30 min from a distance of approximately 40 cm] was determined preliminarily and a UVA irradiation dose (610 $mJ/cm^2$) for 20 min corresponding to the 4.42 times of the MED was used throughout the study.

*3.8.2. Animal grouping and application of gel formulations*

The rats were divided into 7 groups, each containing six animals (n = 6). A thin and uniform layer of gel formulation (500 mg ≈ 5 mg of FA) was applied to the demarcated shaved area on the dorsal skin of the rats. Group I (control, untreated UV radiation) and Group II (UV irradiated) were treated with placebo formulation. Group III was applied

for FA conventional gel (FA-CG1 equivalent to 0.1% FA). Group IV was applied to FA-NE3 loaded nano gel (FA-NG1 equivalent to 0.1% FA). Group V was applied to FA conventional gel (FA-CG2 equivalent to 0.1% FA). Group VI was applied to FA-NE3 loaded nano gel (FA-NG2 equivalent to 0.1% FA). Group VII was applied to NG (NE3 loaded nano gel containing 0.1% NE3 without FA). Exposure of UVA radiation was done to UVA irradiated, FA-CG1, FA-NG1 and NG groups immediately after topical application while to FA-CG2 and FA-NG2 groups after 4 h of topical application for seven days.

On the eighth day, all the animals were anesthetized using diethyl ether and sacrificed by cervical dislocation. The UVA treated portion of cutaneous (epidermis and dermis) tissues was quickly dissected, washed with ice-cold saline and the homogenate were prepared in 0.1 M PBS (pH 7.4) and centrifuged at 13500 rpm for 5 min (Spinwin MC-02, Tarson, India). Then the supernatant was collected and stored at -20 °C for further use.

*3.8.3. Estimation of antioxidant biochemical marker enzymes in cutaneous tissue*

*3.8.3.1. Glutathione peroxidase (GPX)*

The GPX level was estimated according to the method proposed by Paglia and Valentine (1967). Briefly, the reaction mixture composed of 400 μL 0.25 M potassium phosphate buffer (pH 7.0), 200 μL supernatant, 100 μL reduced glutathione (10 mM), 100 μL nicotinamide adenine di-nucleotide phosphate reduced (2.5 mM) and 100 μL glutathione reductase (6 U/mL). Reaction was initiated by incorporating 100 μL hydrogen peroxide (12 mM) as a starting agent and absorbance recorded spectrophotometrically at 340 nm at 1 min intervals for 5 min using SpectraMax® M5. Data were expressed as units/mg of protein.

*3.8.3.2. Superoxide dismutase (SOD)*

The level of SOD was determined as per the procedure suggested by Kakkar et al. (1984). The assay mixture included 0.1 mL of supernatant, 1.2 mL of sodium pyrophosphate buffer (pH 8.3; 0.052 M), 0.1 mL of phenazine methosulphate (186 μm), 0.3 mL of nitro blue tetrazolium (300 μM) and 0.2 mL of reduced nicotinamide adenine di-nucleotide (750 μM). Then the reaction was started by incorporation of reduced nicotinamide adenine di-nucleotide and incubated at 30 °C for 90 s. Finally, the reaction was arrested by adding 0.1 mL of stopping reagent (glacial acetic acid). The reaction mixture was agitated vigorously with 4.0 mL of n-butanol. The color intensity of the chromogen in the butanol layer was measured spectrophotometrically at 560 nm (SpectraMax® M5, USA).

*3.8.3.3. Catalase (CAT)*

Antioxidant level of CAT was estimated using the method of Beers and Seizer (1952). In brief, 0.1 mL of supernatant was added to the cuvette containing 1.9 mL of 50 mM phosphate buffer (pH 7.0). Reaction was started by the addition of 1.0 mL of freshly prepared 30 mM hydrogen peroxide. The rate of decomposition of hydrogen peroxide was noted spectrophotometrically at 240 nm (SpectraMax® M5, USA).

*3.8.3.4. Thiobarbituric acid reactive substances (TBARS)*

TBARS was calculated according to the procedure of Ohkawa et al. (1979). Assay procedure in concise, acetic acid 1.5 mL (20%; pH 3.5), 1.5 mL of thiobarbituric acid (0.8%) and 0.2 mL of sodium dodecyl sulfate (8.1%) were added to 0.1 mL of supernatant and heated at 100 °C for 1 h. The mixture was cooled at room temperature and 5 mL of n-butanol-pyridine (15:1) mixture, 1 mL of distilled water was added with vigorous shaking. The mixture was centrifuged at 1200 × g for 10 min, the organic layer was separated and absorbance was recorded at 532 nm through spectrophotometer (SpectraMax® M5, USA).

*3.8.3.5. Estimation of total protein*

Estimation of total protein was performed as a procedure described by Lowry et al. (1951). Briefly, 0.01 mL of tissue homogenate (2.5%) was diluted to 1.2 mL and mixed with 6 mL of solution-A (1 mL copper sulphate (1%) + 1 mL sodium potassium tartarate (2%) + 98 mL 2% sodium carbonate in 0. 1 N sodium hydroxide). The mixture was incubated at room temperature for 10 min and 0.3 mL of solution-B (phosphomolybdate-phosphotungstate reagent) was added, mixed thoroughly and stored at room temperature for 30 min. Absorbance was measured as optical density at 750 nm using SpectraMax® M5. Data were expressed as units/mg of protein.

## 3.9. *In vivo* bioavailability study in rats

The bioavailability of FA (500 mg of FA-NG3 equivalent to 5 mg of FA) was studied after transdermal administration of FA-NG3 compared with an oral suspension of pure FA. The oral suspension was prepared by mixing 5 mg of FA in 5 mL of water containing 0.5% (w/v) of sodium carboxymethyl cellulose (CMC). The animals were allowed free access to food and water, until the night prior to dosing and were fasted for 10 h. Latin square cross over design was followed; the animals were divided into two groups (n = 6). In group I, oral suspension (5 mg /5 mL) was administered through a feeding tube followed by rinsing with 10 mL of purified water and FA-NG3 (~5 mg FA) was administered to group II in phase I. In phase II *vice versa* was followed and conducted after 15 days of the washout period. The uniform layer of FA-NG3 was applied over a surface area of 1.766 $cm^2$ and covered with a water impermeable membrane and

further fixed with the help of adhesive membrane. Blood samples (2.5 mL) were taken from retro-orbital plexus of rats at pre-determined intervals of 0.0, 0.5, 1, 2, 4, 8 and 12 h; 0.0, 1, 2, 4, 6, 8, 12, 18, 24, 36 and 48 h respectively, after administration of FA-oral suspension and nano-gel (FA-NG3). All blood samples were allowed to clot and centrifuged at 13500 rpm for 10 min (Spinwin MC-02, Tarson, India). Plasma was separated and kept at -20°C prior to analysis. The FA contents in the samples were analyzed through RP-HPLC method at 321 nm.

## 3.10. Analysis of pharmacokinetic parameters

Several pharmacokinetic parameters of ferulic acid was studied after administration of FA-NG3 and FA-oral suspension for each rat with the help of a computer designed program, Phoenix WinNonlin® 6.4 (Certara, USA). Non-compartmental model was used to calculate the pharmacokinetic parameters. Maximum concentration ($C_{max}$) and time to reach maximum concentration ($T_{max}$) are the values obtained directly from plasma concentration Vs time curve. Area under the concentration–time curve ($AUC_{0-t}$), area under the concentration-time curve until infinite observation ($AUC_{0-t\infty}$), area under the moment curve ($AUMC_{0-t}$), mean residence time ($MRT_{0-t}$) and mean residence time to the infinite observation ($MRT_{0-t\infty}$) were calculated. The relative bioavailability (%*F*) was estimated as a ratio of the plasma $AUC_{0-t}$ of the FA-NG3 and FA-oral suspension.

## 3.11. Statistical analysis

The data were statistically analyzed by one-way analysis of variance (ANOVA) followed by Dunnet's post hoc test using Graph Pad Prism software-5.0 (San Diego, CA, USA). The differences between means were considered to be significant when the $P < 0.05$.

## 3.12. Results and discussion

### *3.12.1. Method validation of RP-HPLC-PDA*

The optimum separation of FA was achieved by using the mobile phase at ratio of 30:70 v/v (1% glacial acetic acid; pH 2.2) at a flow rate of 1 mL/min at 25 ± 0.5°C under the isocratic conditions. The $R_t$ of FA was found to be 8.083 ± 0.01 min. A good linear precision relationship between the concentrations (200-1000 ng/mL) and peak areas was obtained as the correlation coefficient ($r^2$) of 0.9992 ± 0.01. Intra-assay precision was performed at four different concentrations and measured the %RSD. The %RSD of both instrumental precision and intra-assay precision was estimated to be <1.00. The precision to the method was optimized by calculating intra-day and inter-day repeatability at four subsequent concentrations ranging from 250-1000 ng/mL. The RSD values in all tested groups were found less than 3%, which was significant. The LOD and LOQ of were estimated to be 0.023 and 0.072 ng/mL, relatively, which indicated that the proposed method can be used for detection and quantification of FA.

The recovery rates of FA from low, middle and high concentrations were 100.07, 100.01 and 100% respectively.

*3.12.2. Solubility studies of FA in various oils*

The solubility of FA was performed in various oils and maximum solubility of FA in ISIS was found to be 2.60 ± 0.04 mg/mL while in water; it was 0.09 ± 0.14 mg/mL (Figure 3.3). Therefore, ISIS was selected as oil phase for the development of the formulations.

*3.12.3. Pseudo-ternary phase diagram study*

The individual pseudo-ternary phase diagrams were plotted to get the maximum o/w NE regions for each group. Results have been shown in the Table 3.2-3.5 and Figure 3.4-3.7 (A-E). Among the four groups, the maximum widespread region and stability of NE were found for the group II (Table 3.3). NE region was found to be very less at Smix 1:0 [Figure 3.5A]. After addition of cosurfactant along with a surfactant in equal proportion Smix (1:1) [Figure 3.5B], a stable and flowable NE region was obtained. In Smix ratio of 2:1, 3:1 and 1:2 [Figure 3.5C, 3.5D and 3.5E], the lower NE regions were found in comparison with Smix ratio (1:1). Therefore, Smix (1:1) was further selected for the development of various formulations.

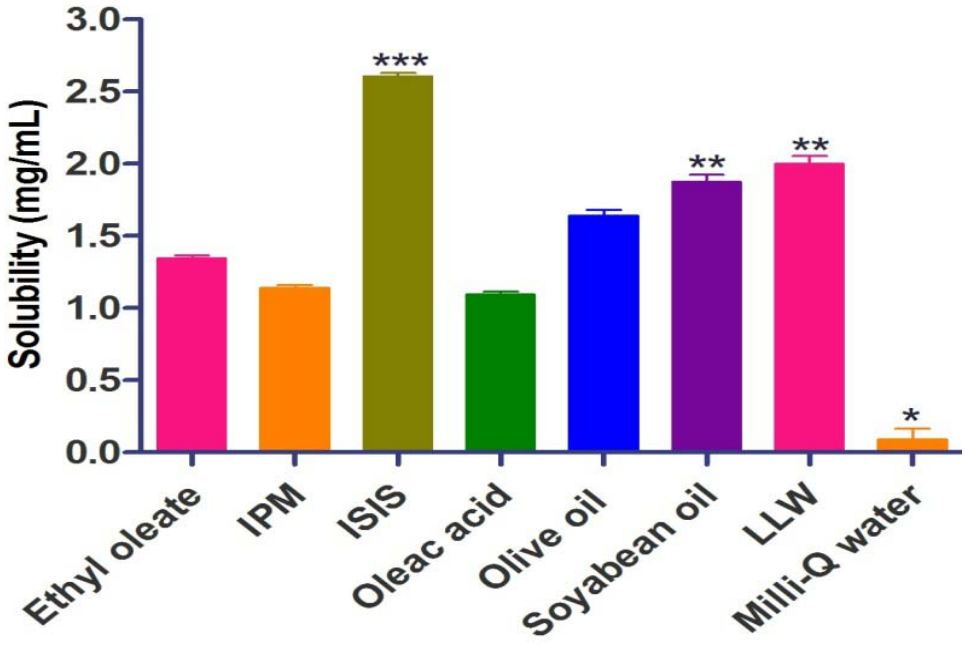


**Figure 3.3. Solubility studies of FA in several excipients. Values were mean ± SEM (n = 6). $^{*}P$ &$^{**}P < 0.05$, $^{***}P < 0.01$**

**Table 3.2. Thermodynamic stability studies of various formulations selected from group I at a 5% w/w increasing amount of oil**

| Smix ratio (S:Cos) | Amount of excipients in formulations (% w/w) | | | Observations based on the preparation and thermodynamic stability studies | | |
|---|---|---|---|---|---|---|
| | Oil | Milli-Q water | Smix | H & C | Cent. | Freeze Tha. |
| 1:0 | 10 | 39 | 51 | × | √ | √ |
| | 15 | 29 | 56 | √ | × | √ |
| | 20 | 40 | 40 | √ | √ | √ |
| 1:1 | 10 | 40 | 50 | √ | √ | √ |
| | 15 | 30 | 55 | √ | √ | √ |
| | 20 | 35 | 45 | √ | √ | √ |
| | 25 | 30 | 45 | √ | √ | √ |
| 2:1 | 10 | 48 | 42 | √ | × | √ |
| | 15 | 45 | 40 | √ | √ | × |
| | 20 | 22 | 58 | × | √ | √ |
| 3:1 | 10 | 45 | 45 | √ | × | √ |
| | 15 | 50 | 35 | √ | × | × |
| | 20 | 25 | 55 | √ | √ | √ |
| 1:2 | 10 | 35 | 55 | √ | × | √ |
| | 15 | 45 | 40 | √ | √ | × |

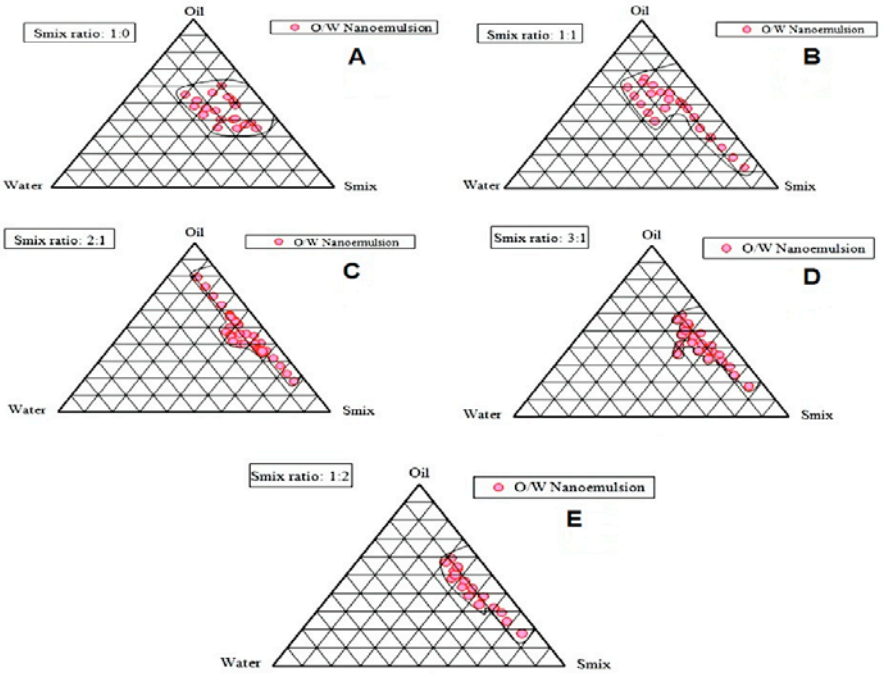


**Figure 3.4 (A-E). Pseudo-ternary phase diagrams of group I, indicating o/w nanoemulsion region at different Smix ratios**

**Table 3.3. Thermodynamic stability studies of group II formulations at increasing amount of oil (5% w/w)**

| Smix ratio (S:Cos) | Amount of excipients in formulations (% w/w) | | | Observations based on the preparation and thermodynamic stability studies | | |
|---|---|---|---|---|---|---|
| | Oil | Milli-Q water | Smix | H & C | Cent. | Freeze Tha. |
| 1:0 | 10 | 45 | 45 | √ | √ | √ |
| | 15 | 40 | 45 | √ | √ | √ |
| | 20 | 25 | 55 | √ | √ | √ |
| | 25 | 30 | 45 | √ | √ | √ |
| 1:1 | 10 | 35 | 55 | √ | √ | √ |
| | 15 | 20 | 65 | √ | √ | √ |
| | 20 | 30 | 50 | √ | √ | √ |
| | 25 | 30 | 45 | √ | √ | √ |
| 2:1 | 10 | 40 | 50 | √ | √ | √ |
| | 15 | 35 | 50 | √ | √ | √ |
| | 20 | 65 | 15 | √ | √ | √ |
| | 25 | 20 | 55 | √ | √ | √ |
| | 30 | 26 | 44 | √ | √ | √ |
| 3:1 | 10 | 30 | 60 | √ | √ | √ |
| | 15 | 10 | 75 | √ | √ | √ |
| | 20 | 25 | 55 | √ | √ | √ |
| | 25 | 40 | 35 | √ | √ | √ |
| 1:2 | 10 | 40 | 50 | √ | √ | √ |
| | 15 | 45 | 40 | √ | √ | √ |
| | 20 | 37 | 43 | √ | √ | √ |
| | 25 | 28 | 47 | √ | √ | √ |
| | 30 | 45 | 25 | √ | √ | √ |

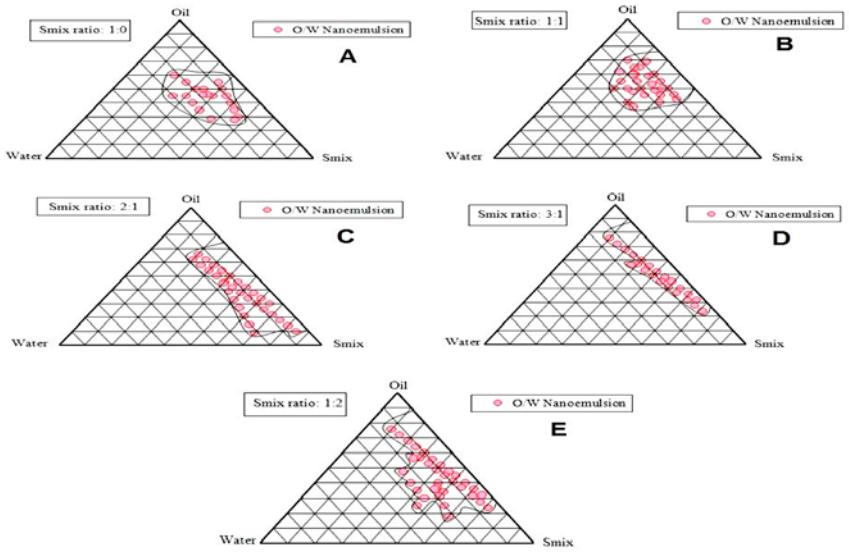


**Figure 3.5 (A-E). Studies of pseudo-ternary phase diagrams for group II at various Smix**

**Table 3.4. Evaluation of thermodynamic stability test for group II formulations**

| Smix ratio (S:Cos) | Amount of excipients in formulations (% w/w) | | | Observations based on the preparation and thermodynamic stability studies | | |
|---|---|---|---|---|---|---|
| | Oil | Milli-Q water | Smix | H & C | Cent. | Freeze Tha. |
| 1:0 | 10 | 50 | 40 | √ | √ | √ |
| | 15 | 38 | 47 | √ | × | √ |
| 1:1 | 10 | 25 | 65 | √ | √ | √ |
| | 15 | 35 | 50 | √ | √ | √ |
| | 20 | 40 | 40 | √ | × | √ |
| | 25 | 28 | 47 | √ | √ | √ |
| 2:1 | 10 | 42 | 48 | √ | × | √ |
| | 15 | 31 | 44 | √ | √ | √ |
| | 20 | 41 | 39 | × | × | √ |
| | 25 | 22 | 53 | √ | √ | √ |
| 3:1 | 15 | 45 | 40 | √ | × | √ |
| | 20 | 30 | 50 | √ | √ | × |
| 1:2 | 15 | 34 | 51 | √ | √ | √ |
| | 20 | 17 | 63 | √ | √ | × |
| | 25 | 36 | 39 | × | √ | √ |

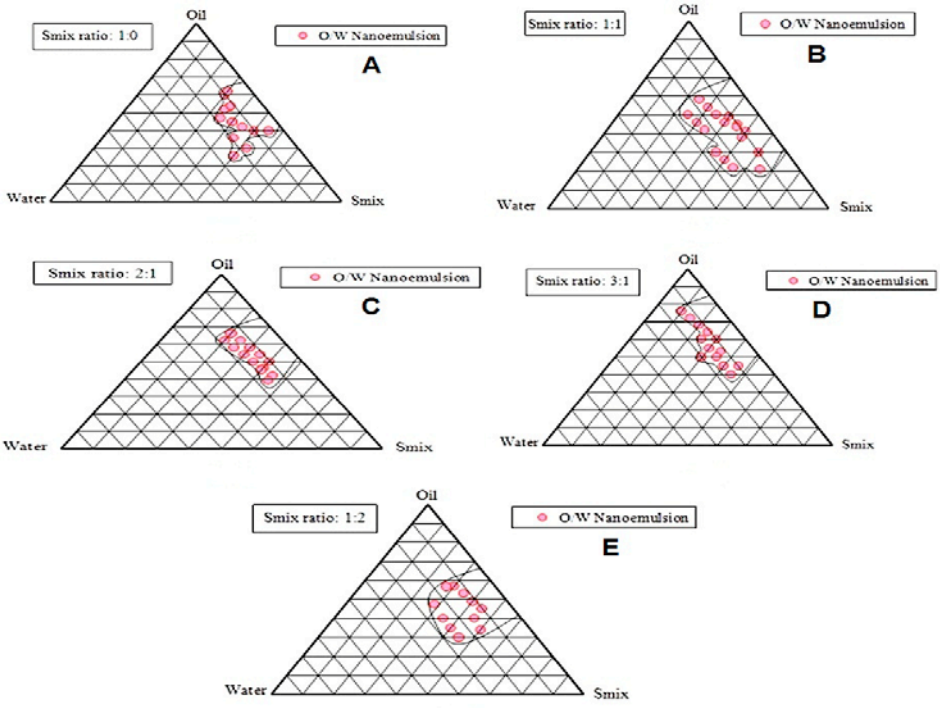


**Figure 3.6 (A-E). Construction of pseudo-ternary phase diagrams for group III formulations at different Smix ratios**

**Table 3.5. Investigation of thermodynamic stability test for group IV formulations**

| Smix ratio (S:Cos) | Amount of excipients in formulations (% w/w) | | | Observations based on the preparation and thermodynamic stability studies | | |
|---|---|---|---|---|---|---|
| | Oil | Milli-Q water | Smix | H & C | Cent. | Freeze Tha. |
| 1:0 | 10 | 38 | 52 | × | √ | √ |
| | 15 | 44 | 41 | √ | × | √ |
| | 20 | 41 | 39 | √ | √ | √ |
| 1:1 | 10 | 42 | 48 | √ | √ | √ |
| | 15 | 40 | 45 | √ | √ | √ |
| | 20 | 36 | 44 | √ | √ | √ |
| | 25 | 30 | 55 | √ | √ | √ |
| 2:1 | 10 | 35 | 55 | √ | √ | √ |
| | 15 | 35 | 50 | √ | √ | × |
| | 20 | 40 | 50 | √ | × | √ |
| | 25 | 30 | 45 | √ | √ | √ |
| 3:1 | 15 | 30 | 55 | √ | × | √ |
| | 20 | 40 | 40 | √ | √ | × |
| | 25 | 45 | 30 | × | × | √ |
| 1:2 | 10 | 40 | 50 | √ | √ | √ |
| | 15 | 45 | 40 | √ | √ | × |
| | 20 | 45 | 35 | √ | × | √ |
| | 25 | 40 | 35 | √ | √ | √ |

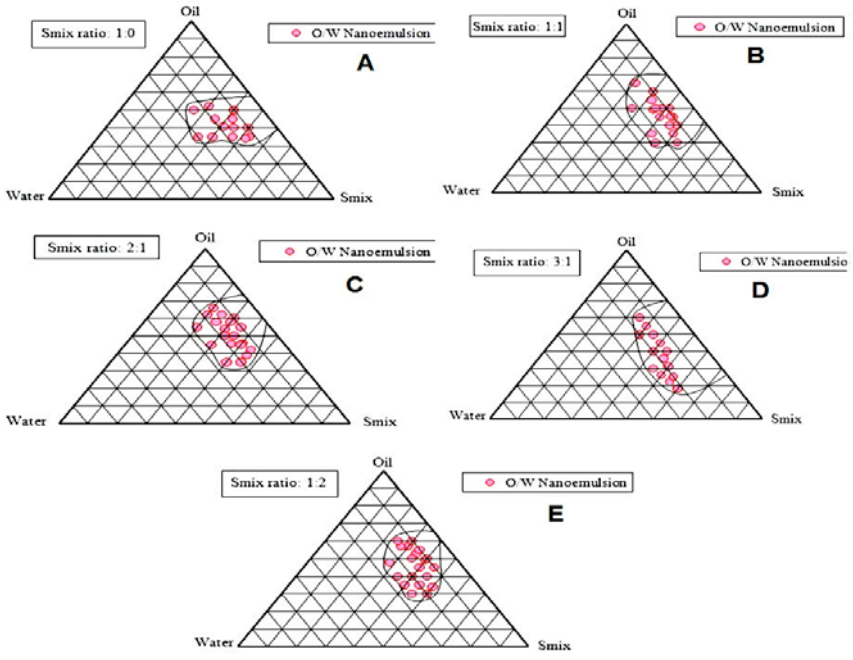


**Figure 3.7 (A-E). Pseudo-ternary phase diagram studies for group IV formulations at Smix ratios (1:0-1:2)**

### *3.12.4. Thermodynamic stability study*

The selected formulations were subjected to different thermodynamic stability by using heating-cooling cycle, centrifugation and freeze thaw cycle stress tests. There was no obvious event seen during these tests, although some formulations were unstable as represented in Table 3.2-3.5.

### *3.12.5. Selection of formulations from phase diagrams and development of FA nanoemulsions*

From pseudo-ternary phase diagrams [Figure 3.5 (A-E)] it is revealed that oil could be solubilized up to 25% (w/w). Thus from each phase diagram, a different concentrations of oil was selected within the range of 10 - 30% so that maximum formulations could be selected to cover the NE area on the phase diagram (Table 3.3). For each portion of oil selected, only those preparations with minimal concentration of Smix were studied. No event was observed about the phase behavior and the NE region of phase diagrams after inclusion of FA (1 mg) in the formulations, which was likely as the formation of stable NE. Composition of optimized FA loaded nanoemulsion has been explained in Table 3.6.

**Table 3.6. Composition of optimized nanoemulsion formulations selected from group II**

| NE Code | Smix (S:Cos) | Ingredients in nanoemulsion formulation (% w/w) | | | | Oil:Smix ratio |
|---|---|---|---|---|---|---|
| | | Oil | Water | S | Cos | |
| FA-NE1 | 1:1 | 10 | 35 | 27.5 | 27.5 | 1:5.5 |
| FA-NE2 | 2:1 | 15 | 35 | 33.33 | 16.67 | 1:3.3 |
| FA-NE3 | 1:1 | 20 | 30 | 25 | 25 | 1:2.5 |
| FA-NE4 | 1:2 | 25 | 28 | 15.67 | 31.33 | 1:1.8 |
| FA-NE5 | 2:1 | 30 | 26 | 29.33 | 14.67 | 1.47 |

*Where, 'S' = Surfactant, 'Cos'= Co-surfactant.*

Surfactants, labrasol (HLB = 14) and acconon CC-6 (HLB = 12.5) and cosurfactants, transcutol CG (HLB = 4.2) and plurol isostearique (HLB = 10.8) could work better along with its Smix (Warisnoicharoen et al., 2000; Kommuru et al., 2001). The formation of free energy during nano-emulsification mainly depends on the concentration of the surfactant used that lowers the surface tension at the oil-water interface and resulting in the thermodynamically stable system (Lawrence and Rees, 2000; Craig et al., 1995). High amount of surfactant may lead to untoward effect to the skin (Shakeel and Ramadan, 2010). Therefore, the minimum amount of Smix (1:1) was optimized for formulation (FA-NE3).

### *3.12.6. Characterization of developed nanoemulsion*

Developed NEs were characterized by measuring different parameters, including electrical conductivity, percentage transmittance, viscosity, pH, refractive index, drug entrapment efficiency and drug loading, droplet size, PDI and zeta potential. The PDI reflects the uniformity of particle diameter and can be used to depict the size distribution of nanoemulsion population. The PDI value provides a measure of the narrowness of the particle size distribution, with values ≤ 0.1 indicating a very narrow distribution (Saberi et al., 2013). The observed results have been shown in Table 3.7. Homogeneous droplet size distribution was studied in the formulation with the help of diversity in the intensity of light scattering by the oil droplets which expressed as PDI. The uniformity of the droplet size in the formulation was indicated by the PDI value. PDI values of all formulations were found to be low, indicating uniformity of droplet size within each formulation. The lowest PDI value for FA-NE3 indicated that the system was homogenous.

Suitable droplet size (102.3 ± 1.14 nm) and zeta potential (-35.2 ± 0.41 mV) was found for the FA-NE3 as shown in Figure 3.8. Zeta potential (ξ) is an important parameter to check the stability of the formulation. It is very well known that the zeta potential indicates the degree of repulsion between adjacent charged droplets in a colloidal dispersion such as NE, which is related to the stability of the formulation. Usually, -30 mV or +30 mV should be considered as high zeta potential value (Bali et al., 2011). The zeta potential of the FA-NE1-3 was negatively charged, and found within the range of -35.2 ± 0.41 to -63.4 ± 0.85 mV as shown in Table 3.7. This was due to the smallest droplet size of the formulations.

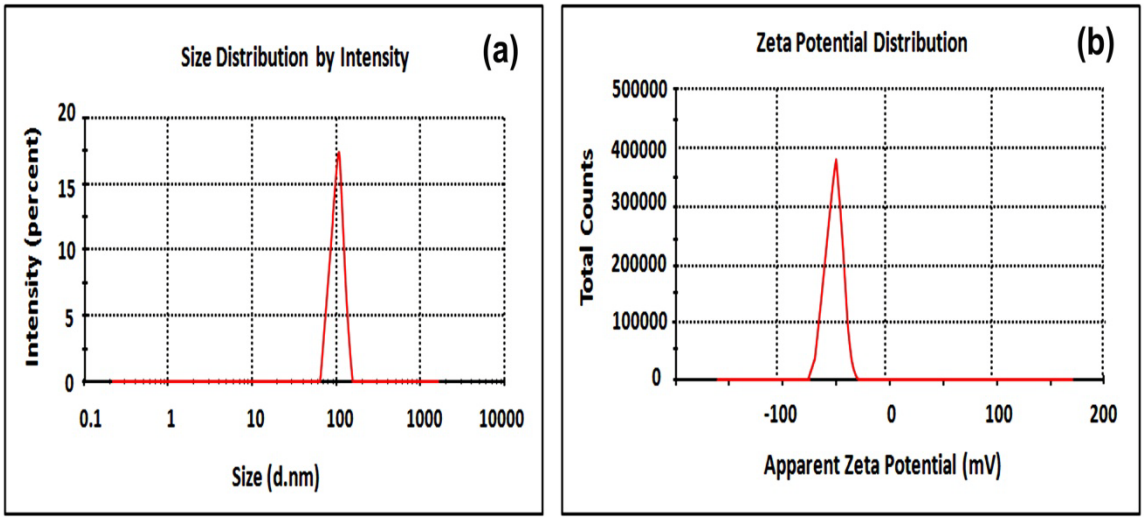


**Figure 3.8. Droplet size (a) and zeta potential (b) study of optimized formulation, FA-NE3**

The high negative charge of the optimized NE is probably influenced by the anionic groups of the fatty acids, and glycols present in the oil and Smix. The nano size range of droplets with higher zeta potential in the formulation is generally attributed to prevent coalescence between droplets. Thus ξ sustains the homogeneity as well as the stability to the system (Bali et al., 2011). Therefore, it can be concluded that there were least chances of coagulation or flocculation of the system in the biological environment and during its storage condition.

### *3.12.7. TEM and UV - spectrum analysis*

The morphology and surface structure of the optimized FA-NE3 has been shown in Figure 3.9A where the droplets appeared as dark spot due to the dispersed oil droplets. The size of droplet was similar to that obtained by Zetasizer.

UV spectrum showed that FA was present in the formulation (FA-NE3), when scanned at 321 nm wavelength as like as the pure FA (321 nm). Detail has been shown in Figure 3.9B.

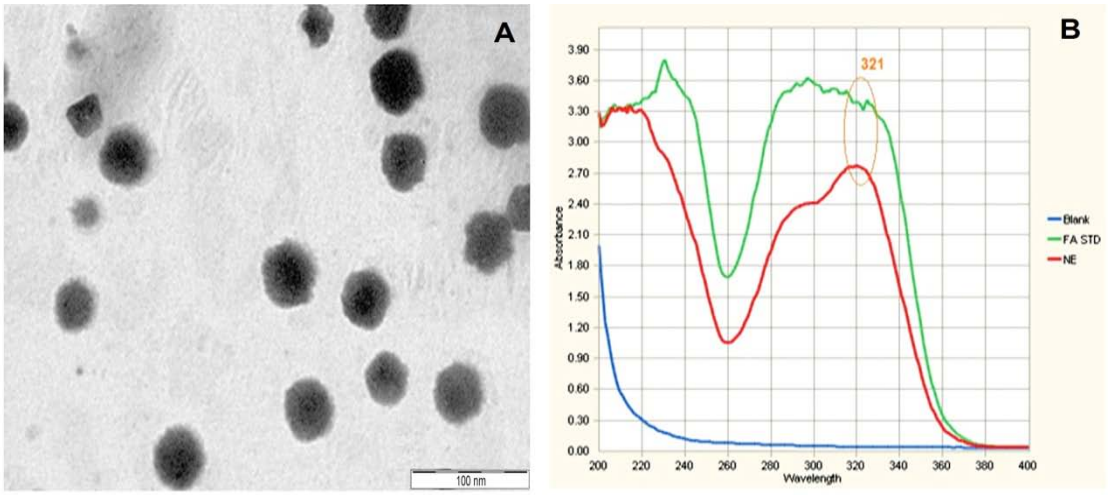


**Figure 3.9. Transmission electron microscope photograph (A) and UV spectra (B) of FA-NE3 nanoemulsion**

### *3.12.8. HPTLC analysis*

The optimized solvent system [toluene-ethyl acetate-formic acid at a ratio of (6: 3: 0.8, v/v/v)] produced a sharp and well-defined symmetrical peak with $R_f$ in 0.38 for FA, when the chamber was saturated with the mobile phase for 30 min at room temperature

(25$^{o}$C). HPTLC chromatogram of standard FA and the FA-NE3 showed the $R_f$ value of 0.38 and 0.39 respectively (Figure 3.10 and 3.11). The result indicated that the FA was quite compatible with their excipient, which was used for development of NE.

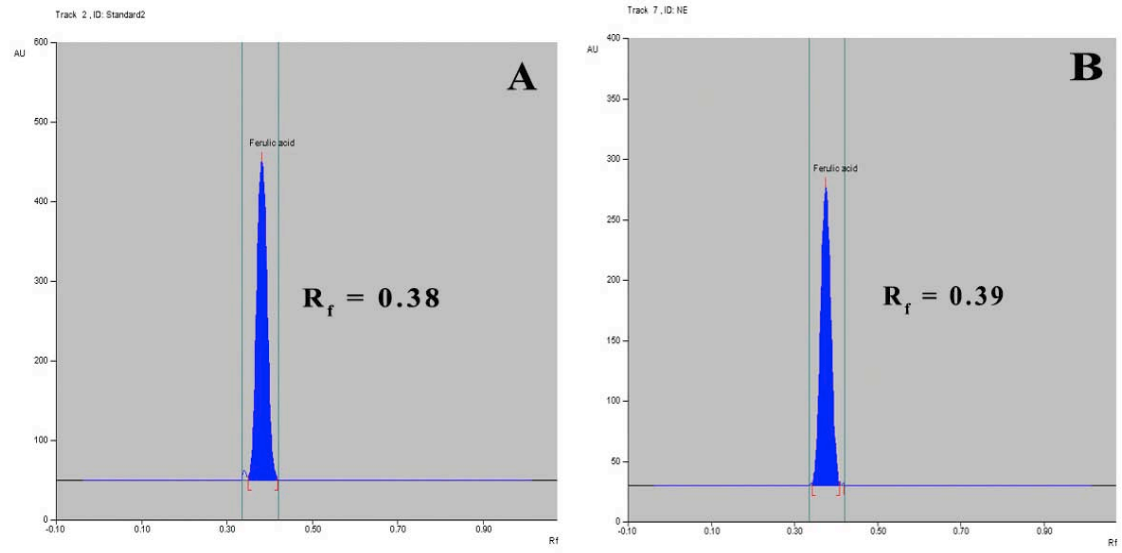


**Figure 3.10. HPTLC chromatogram of standard FA (A) and FA-NE3 formulation (B)**

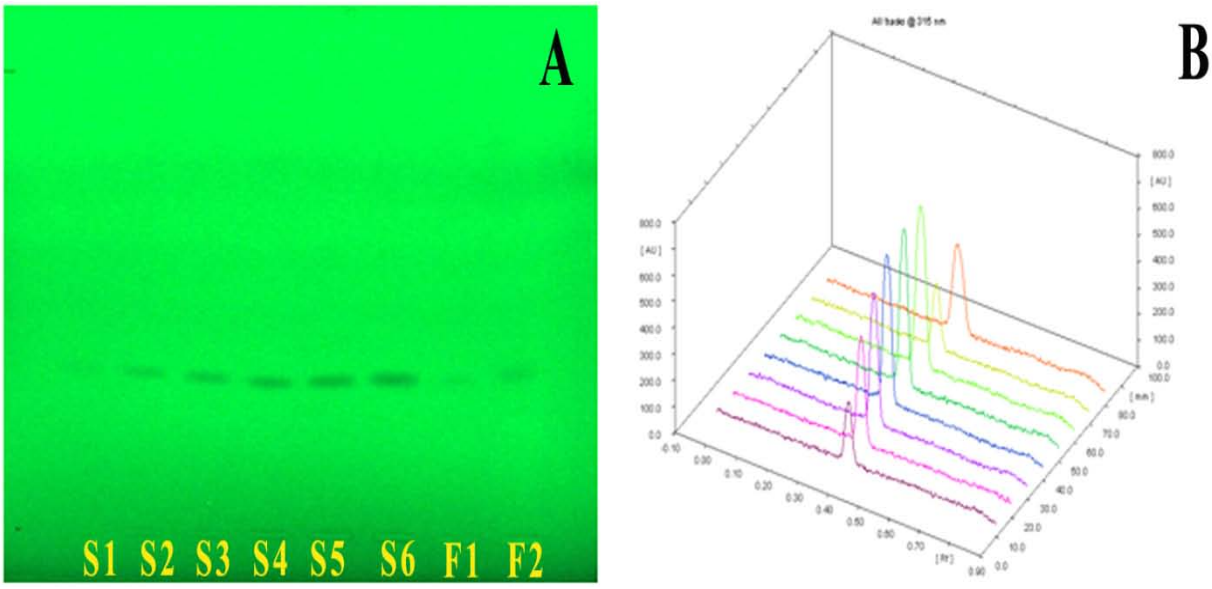


**Figure 3.11. HPTLC plate (A) and 3D-chromatogram (B) of standard ferulic acid and FA-NE3 formulation at 315 nm [S1-6 = Standard ferulic acid and F1-2 = FA-NE3 formulation]**

**Table 3.7. Characterization of various nanoemulsions**

| NE code | pH | Viscosity (cP) | Cond. (ms/cm) | P.T. | R.I. | (%EE) | (%DL) | Z-average (nm) | PDI | Z.P. (mV) |
|---|---|---|---|---|---|---|---|---|---|---|
| FA-NE1 | 6.92 ± 0.06 | 8.42 ± 0.02 | 0.67 ± 0.34 | 80.89 ± 0.12 | 1.416 ± 0.16 | 90.89 ± 0.21 | 0.91 ± 0.04 | 185.8 ± 1.38 | 0.612 ± 0.01 | -63.4 ± 0.85 |
| FA-NE2 | 6.96 ± 0.04 | 7.65 ± 0.02 | 0.60 ± 0.21 | 67.80 ± 1.23 | 1.429 ± 0.38 | 92.78 ± 0.18 | 0.93 ± 0.05 | 158.5 ± 1.19 | 0.508 ± 0.04 | -58.8 ± 0.65 |
| FA-NE3 | 6.98 ± 0.02 | 5.36 ± 0.03 | 0.56 ± 0.10 | 99.21 ± 0.89 | 1.401 ± 0.18 | 98.88 ± 0.12 | 1.03 ± 0.02 | 102.3 ± 1.14 | 0.158 ± 0.02 | -35.2 ± 0.41 |
| FA-NE4 | 6.97 ± 0.03 | 6.11 ± 0.01 | 0.70 ± 0.48 | 78.34 ± 1.78 | 1.408 ± 0.21 | 95.68 ± 0.15 | 0.96 ± 0.06 | 138.4 ± 1.01 | 0.189 ± 0.01 | -47.1 ± 0.48 |
| FA-NE5 | 7.04 ± 0.02 | 7.87 ± 0.01 | 0.63 ± 0.57 | 75.88 ± 2.10 | 1.420 ± 0.44 | 93.87 ± 0.25 | 0.94 ± 0.03 | 154.6 ± 1.12 | 0.234 ± 0.06 | -48.2 ± 0.52 |

Cond.: Conductivity; P.T.: Percentage transmittance; R. I.: Refractive index; %EE: Percentage entrapment efficiency; %DL: Percentage drug loading; PDI: Polydispersity index; Z.P.: Zeta potential. Value was represented as (Mean ± SD) (n = 3).

### *3.12.9. FTIR study*

The chemical interactions amongst the excipients and FA were confirmed further in order to understand the compatibility of FA-NE3 formulation (Figure 3.12), for pure FA (curve A), FA-NE3 (curve B) and placebo (curve C). The characteristic sharp peak of FA was found at 3436.6 $cm^{-1}$ (carboxylic acid O-H stretching), 1690.7 $cm^{-1}$ (carboxylic acid C=O stretching), 1276.6 $cm^{-1}$ (carboxylic acid C-O stretching); 1517 and 1620.1 $cm^{-1}$ (aromatic C=C) which confirm the skeleton of FA. These peaks were found with slight variation even after the nano-formulations, thus indicating the absence of chemical interactions between FA and the excipients. This confirmed that FA was compatible with other excipients used in formulations.

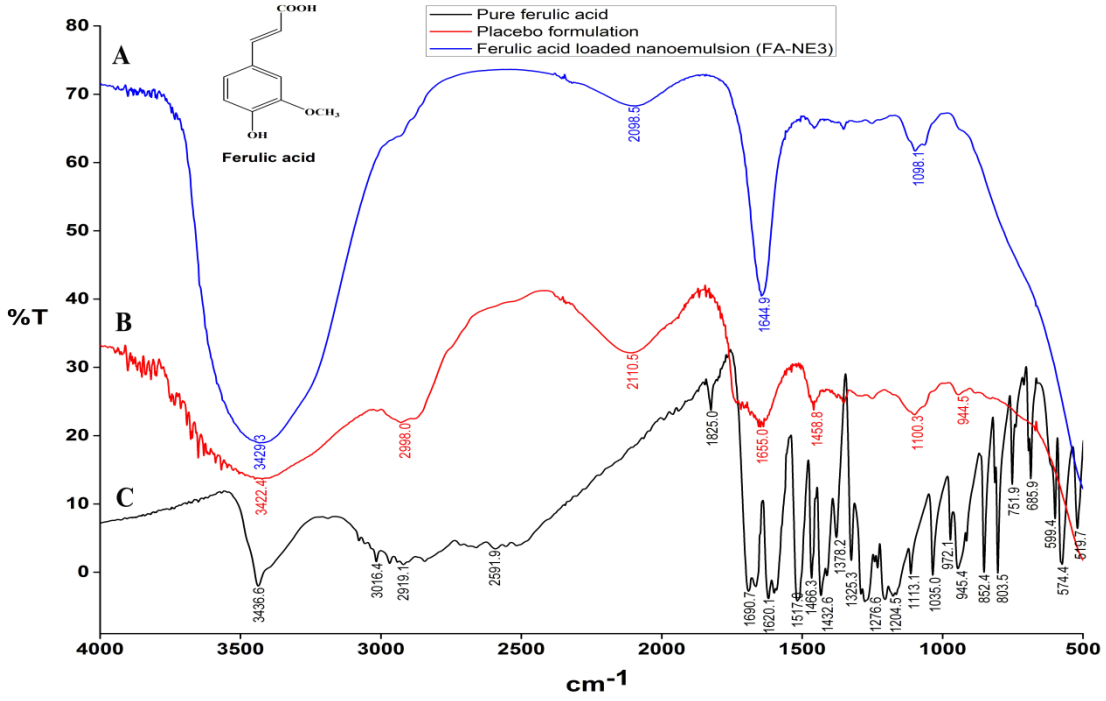


**Figure 3.12. FTIR spectrum of ferulic loaded formulation, FA-NE3 (A), placebo formulation (B) and pure ferulic acid (C)**

### *3.12.10. Stability study*

The FA-NE3 when subjected to stability study based on ICH guidelines, there was no substantial alteration observed with its droplet size, zeta potential and pH at 40°C (Table 3.8). A first order degradation of FA content in the FA-NE3 was found to be 3.41% at the remainder of 6 months at 40°C. First order degradation kinetics at 40°C was graphically represented in Figure 3.13.

From the stability studies, it can be anticipated that the FA-NE3 was stable at 40°C for longer periods. Shelf-life ($t_{90}$) of the formulation was estimated to be 2.06 years.

**Table 3.8. Degradation study of optimized ferulic acid loaded NE formulation, FA-NE3**

| Time (month) | Temper-ature (°C) | Droplet size (nm) | Zeta potential (mV) | pH | % Drug remained | Log % drug remained |
|---|---|---|---|---|---|---|
| 0 | 40 ± 2 (75 ± 5% RH) | 105 ± 0.14 | -35 ± 0.21 | 6.96 ± 0.13 | 100 | 2 |
| 1 | | 106 ± 2.07 | -35 ± 0.57 | 6.98 ± 0.21 | 99.54 | 1.9979 |
| 3 | | 104 ± 1.10 | -34 ± 1.08 | 6.92 ± 2.04 | 98.40 | 1.9928 |
| 6 | | 106 ± 1.04 | -34 ± 1.11 | 6.95 ± 1.00 | 96.59 | 1.9849 |

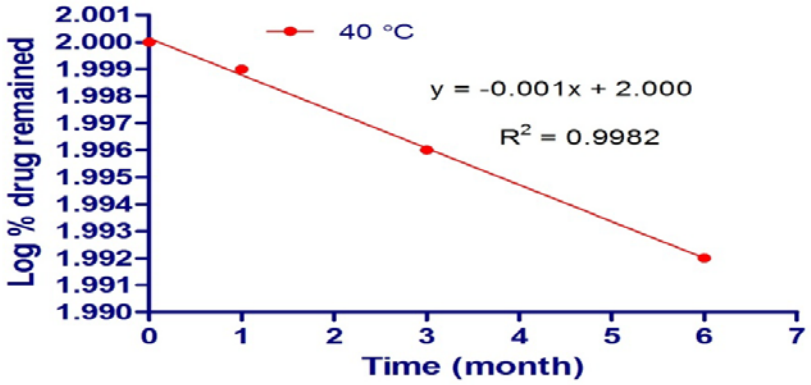


**Figure 3.13. First order degradation kinetics of ferulic acid from FA-NE-3 at 40°C**

*3.12.11. Rheological studies*

The viscosity of the placebo and FA-NG3 were found in the range of 600 to 0.68 and 3,790 to 1.83 Pa.s respectively and represented in Figure 3.14. In the rheological study of gel, FA-NG3 expressed high viscosity as compared to placebo, which may be due to the drug integrated into the gel matrix and leads to increase in viscosity. Thus the nano-gel may be suitable for topical administration. The FA-NG3 exhibited non-Newtonian shear thinning phenomenon when viscosity decreases with the rate of shear stress. Carbopol-940 was used as a gelling agent and results in improved skin permeability (Lala and Awari, 2014).

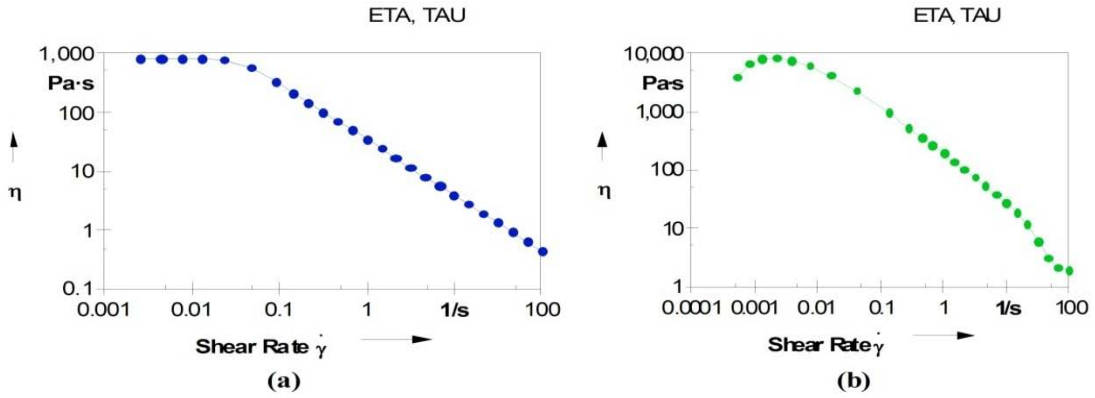


**Figure 3.14. Rheological behavior of placebo (a), FA-NG3 (b) where, η = viscosity (Pa.s), γ = shear rate (1/s)**

*3.12.12. Spreadability test*

The placebo and FA-NG3 were found to exhibit good spreadability (63.18 ± 1.08 and 65.86 ± 0.82% w/w respectively) that would assure the practicability to skin administration. There was no significant difference ($P < 0.05$) between the spreadability of placebo and FA-NG3 formulations.

*3.12.13. Skin permeation studies*

The percentage cumulative permeation of FA from different FA-NE1-5, FA-NG3 and FA-CG were studied through rat skin [Figure 3.15 (A & B)]. The cumulative permeation of FA-NE3 for 24 h was significantly higher (91.33%) than that of other formulations; this may be due to low viscosity, nano droplet size and appropriate pH of FA-NE3, when compared with FA-NE1, FA-NE2, FA-NE4 and FA-NE5. Further, the comparative studies between FA-CG, FA-NE3 and FA-NG3 were performed. In case of FA-NG3, nano-gel formulation exhibited better permeation profile (96.95%) in comparison with FA-CG conventional gel (61%) at 24h. A significant difference was observed with percentage cumulative permeation profile of FA from FA-NG3 and FA-CG; this could be due to the average size of internal phase droplets (o/w), which were significantly smaller in NEs.

Flux *Jss* (µg/h/cm$^2$) and permeability *Kp* (cm/h) of FA from various formulations across the skin has been shown in Table 3.9 and Figure 3.15 (C). Maximum flux and permeability of FA were achieved with FA-NG3 compared to others. The result stated that *Jss*, lag time and *Kp* were estimated to be 2.319 ± 0.19 µg/h/cm$^2$, 0.256 h and 0.519 ± 0.09 cm/h respectively. FA-NG3 nano gel showed enhanced drug permeability across the skin, which may be due to quick diffusion of water from the formulation to the skin membrane and easy drug release (Yilmaz and Borchert, 2006). In the oil phase, ISIS was selected as an effective penetration enhancer.

The Smix (labrasol/plurol isostearique) in the NE based gel may reduce the diffusion barrier of the *stratum corneum* by acting as permeation enhancers.

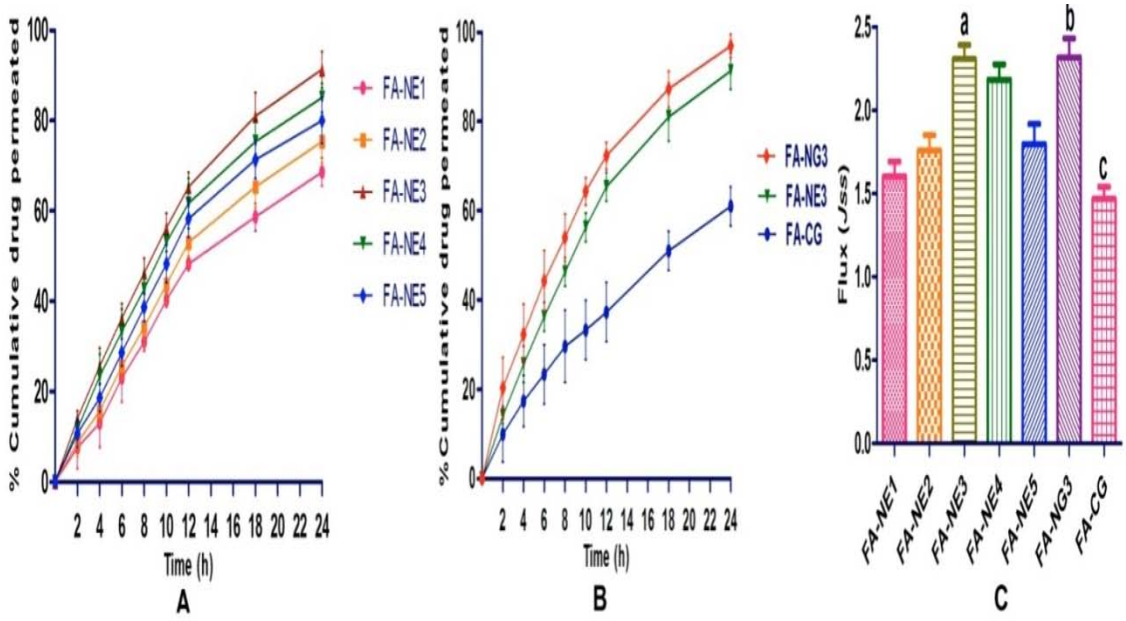


**Figure 3.15. Permeation study of ferulic acid from various nanoemulsions (A) FA-NE (1-5), (B) FA-CG, FA-NE3 and FA-NG3 through rat skin and (C) steady state flux of various formulations across rat skin [Values were mean ± SEM (n = 6), $^{c}P < 0.05$, $^{a, b}P < 0.01$]**

**Table 3.9. Transdermal steady state flux and permeability coefficient of formulations across rat skin**

| Formulation | Steady state flux *Jss* (μg $cm^{-2}$ $h^{-1}$) Mean ± SD | Lag time (h) | Permeation coefficient *Kp* (×$10^{-3}$ cm $h^{-1}$) Mean ± SD |
|---|---|---|---|
| FA-NE1 | 1.603 ± 0.153 | 0.336 | 0.367 ± 0.047 |
| FA-NE2 | 1.759 ± 0.159 | 0.307 | 0.393 ± 0.025 |
| FA-NE3 | 2.308 ± 0.148 | 0.262 | 0.490 ± 0.063 |
| FA-NE4 | 2.183 ± 0.161 | 0.278 | 0.455 ± 0.072 |
| FA-NE5 | 1.797 ± 0.207 | 0.290 | 0.406 ± 0.015 |
| FA-NG3 | 2.319 ± 0.196 | 0.256 | 0.519 ± 0.099 |
| FA-CG | 1.467 ± 0.128 | 0.408 | 0.298 ± 0.020 |

### *3.12.14. Skin irritation study*

There were no substantial clinical signs of irritation, erythema or oedema observed throughout the study period. These results indicated that the nano-gel formulation of FA (FA-NG3) was non-irritant and safe for topical application.

### *3.12.15. Release kinetics of ferulic acid based nanoemulsion and gel formulation*

Drug release model of FA-NE1-5, FA-CG and FA-NG3 was fitted with Zero order, First order, Higuchi's model, Korsmeyer - Peppas model. This demonstrated that the higher coefficient of correlation ($r^2$) was found to be 0.996 for FA-NG3. Assuming highest $r^2$, the best fit was shown by zero-order drug release for nano gel formulation. The optimized FA-NG3 formulation was suitable for non-*Fickian* pattern ($0.5 < Kp < 1$) of drug release through diffusion and matrix erosion. Details of drug release kinetics have been shown in Table 3.10.

**Table 3.10. Model fitting of accumulated release data of different formulations**

| Formulations | Zero order | | First order | | Higuchi model | | Korsmeyer-Peppas model | |
|---|---|---|---|---|---|---|---|---|
| | $r^2$ | $k$ | $r^2$ | $k$ | $r^2$ | $k$ | $r^2$ | $n$ |
| FA-NE1 | 0.992 | 4.91 | 0.993 | 2.00 | 0.943 | -9.76 | 0.926 | 0.29 |
| FA-NE2 | 0.995 | 5.38 | 0.995 | 2.01 | 0.947 | -10.36 | 0.914 | 0.32 |
| FA-NE3 | 0.999 | 6.85 | 0.990 | 2.04 | 0.972 | -8.84 | 0.852 | 0.45 |
| FA-NE4 | 0.998 | 6.50 | 0.998 | 2.02 | 0.967 | -8.88 | 0.871 | 0.41 |
| FA-NE5 | 0.996 | 6.03 | 0.993 | 2.01 | 0.954 | -9.85 | 0.890 | 0.37 |
| FA-NG3 | 0.996 | 7.69 | 0.966 | 2.08 | 0.986 | -5.19 | 0.797 | 0.53 |
| FA-CG | 0.995 | 3.74 | 0.996 | 1.98 | 0.974 | -5.68 | 0.872 | 0.37 |

### *3.12.16. The consequence of UVA exposure on the skin antioxidant biochemical marker enzymes*

The antioxidant enzyme levels in the UVA irradiated rat skin was reduced significantly in comparison to the control group (without UVA exposure) ($P < 0.01$). The levels of skin antioxidant enzymes (GPX, SOD and CAT) were significantly higher in case of the groups pre-treated with FA-CG1and FA-NG1, than UVA irradiated group ($P < 0.01$) [Figure 3.16 (A-C)]. The group pre-treated with NG did not produce any effect on the

skin antioxidant enzymes as compared to the UVA irradiated group, which may be due to the placebo NG [Figure 3.16 (A-C)]. Significant increase in the level of SOD, GPX and CAT was observed with FA-NG2 group (***$P < 0.01$) comparing to FA-CG2 group (**$P < 0.05$), after 4 h of UVA irradiation and treatment with FA loaded nano-gel and FA conventional gel respectively as shown in Figure 3.16 (A-C).

The raised level of TBARS was significantly reduced with FA-CG1, FA-NG1 and FA-NG2 treated groups compared to the UVA irradiated group (***$P < 0.01$). FA-CG2 group reduced the TBARS to the minimum extent compared to FA-NG2 (**$P < 0.05$), after 4 h of UVA irradiation [Figure 3.16 (D)]. This may be due to less permeability of FA conventional gel. FA-NG2 showed the better therapeutic effect because of its enhanced permeability than the conventional gel. Thus, FA encapsulated nano-gel formulations could enhance UV protective activity of the skin for longer periods rather than conventional topical formulations.

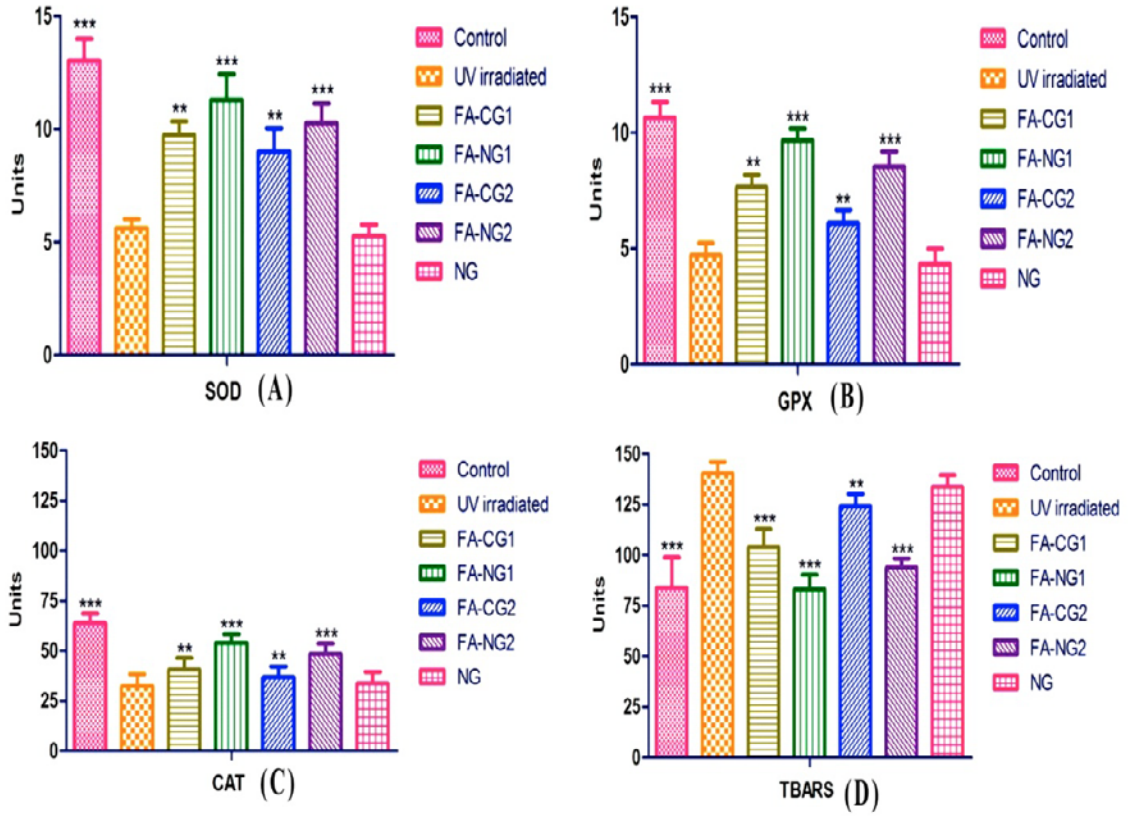


**Figure 3.16. Effect of FA loaded different gel formulations on (A) SOD, (B) GPX, (C) CAT and (D) TBARS levels in rat skin [Values were mean ± SEM (n = 6), **$P < 0.05$, ***$P < 0.01$]**

The topical or transdermal drug delivery route can avoid hepatic first-pass metabolism resulting in the possible prolongation of the $t_{1/2}$ and a sufficient concentration in the systemic circulation (Zhang et al., 2010).

FA loaded nano-gel exhibited better UVA protection activity even after 4 h of application to the skin surface due to its improved permeability and sustained-release profile compared to conventional gel.

*3.12.17. In vivo bioavailability study*

The bioavailability study of ferulic acid was performed after administration of its oral suspension and FA-NG3. Results have been represented in Figure 3.17 and Table 3.11. FA has been well released and permeated from FA-NG3 as compared to the oral suspension for longer periods (48 h). Statistically significant $C_{max}$, $T_{max,}$ MRT and AUC profiles were observed with FA-oral suspension and FA-NG3 ($P < 0.05$). The $C_{max}$ of FA was found to be 80.98 ± 6.93 and 96.21 ± 5.49 $ngmL^{-1}$ after administration of oral suspension and FA-NG3 respectively. The $T_{max}$ and MRT were higher for transdermal nano-gel than the oral administration ($P < 0.05$).

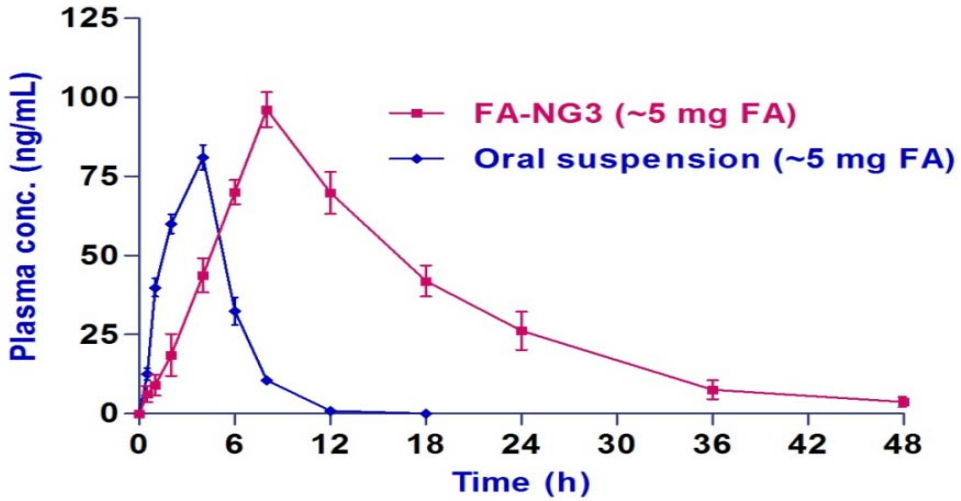


**Figure 3.17. Plasma concentration profiles of ferulic acid in rats, after administration of oral suspension (~5 mg of FA) and FA-NG3 (~5 mg of FA), values were mean ± SD (n = 6)**

For transdermal route, *stratum corneum* acts as a permeation barrier and thereby the sustained-release activity of FA was found with FA-NG3 in comparison to orally administered suspension is an immediate release dosage form. The mean value of $AUC_{0-t}$ by transdermal route was 3.96 times higher than that of oral route, and the difference was found to be statistically significant ($P < 0.05$). This indicated enhanced bioavailability of FA from the transdermal nano-gel. This could be due to avoidance of first-pass hepatic metabolism by transdermal route. The reported oral bioavailability of FA was 9% because of hepatic first-pass metabolism. In the current investigation, the relative bioavailability ($F$) of FA by transdermal route was found to be 396.26.

Thus, FA loaded nano-gel could provide an effective strategy for the management of skin damage by extreme exposure of the UV radiations.

**Table 3.11. Pharmacokinetic parameters of ferulic acid in rats after administration of oral suspension and FA-NG3, values represented are mean ± SD (n = 6)**

| Pharmacokinetic parameter | Oral suspension (≈5 mg of FA) | FA-NG3 (≈5 mg of FA) |
|---|---|---|
| $C_{max}$ ($ngmL^{-1}$)[a] | 80.98 ± 6.93 | 96.21 ± 5.49 |
| $T_{max}$ (h)[b] | 4.26 ± 0.27 | 8.30 ± 0.41 |
| $AUC_{0-t}$ ($nghmL^{-1}$)[c] | 369.24 ± 43.54 | 1463.13 ± 133.17 |
| $AUC_{0-t\infty}$ ($nghmL^{-1}$)[d] | 369.34 ± 43.51 | 1508.47 ± 156.82 |
| $AUMC_{0-t}$ ($nghmL^{-1}$)[e] | 1483.45 ± 188.83 | 22112.30 ± 3358.36 |
| $AUMC_{0-t\infty}$ ($nghmL^{-1}$)[f] | 1485.58 ± 188.34 | 24857.92 ± 4976.19 |
| $MRT_{0-t}$ (h)[g] | 4.01 ± 0.03 | 15.05 ± 1.00 |
| $MRT_{0-t\infty}$ (h)[h] | 4.02 ± 0.03 | 16.37 ± 1.68 |
| ($t_{1/2}$el) (h)[i] | 1.29 ± 0.12 | 8.05 ± 1.34 |
| Kel ($h^{-1}$)[j] | 0.5375 ± 0.04 | 0.08613 ± 0.01 |
| Cl ($Lh^{-1}$) [k] | 0.01365 ± 0.001 | 0.00334 ± 0.0003 |
| Vd (L)[l] | 0.02563 ± 0.004 | 0.03902 ± 0.0031 |
| %*F*[m] | - | 396.26 |

[a]Peak of maximum concentration; [b]Time of peak concentration; [c]Area under the concentration-time curve until last observation; [d]Area under the concentration-time curve until infinite observation; [e]Area under moment curve computed to the last observation; [f]Area under moment curve computed to the infinite observation; [g]Mean residence time to the last observation; [h]Mean residence time to the infinite observation; [i]Elimination half life; [j]Elimination rate constant; [k]Clearance; [l]Volume of distribution; [m]Relative bioavailability of ferulic acid.

## 3.13. Conclusion

A topical nano-gel of ferulic acid was developed, which showed sustained-release effect against UVA exposure in skin. The optimized gel formulation showed improved drug permeability as well as bioavailability and enhanced UV protection activity, which might be due to the potent antioxidant activity of FA in opposition to oxidative stress mediated by UVA. It significantly elevates the level of the antioxidant markers and arrested the unwanted effects generated by ultraviolet radiation. This phenomenon attributed towards the encapsulated FA in NE having a nano size range of droplets provided large surface area, which possess superior skin penetration potential when compared with its conventional gel. The enhanced relative bioavailability of ferulic acid (396.26%) was

obtained with nano-gel formulation after its transdermal administration for extended periods. The nanoemulsion based FA nano-gel was found to be stable, safe and effective for topical application against UV. Therefore, the FA nano-gel formulation could be explored further as a promising nano-carrier for skin delivery.

## 3.14. Publication

- Ranjit K. Harwansh, Pulok K. Mukherjee, Shiv Bahadur, Rajarshi Biswas. Enhanced permeability of ferulic acid loaded nanoemulsion based gel through skin against UVA mediated oxidative stress. Life Sciences, Elsevier, 2015, 141, 202-211, doi: 10.1016/j.lfs.2015.10.001 (Impact Factor: 2.70).

# Chapter - 4

## Catechin loaded nanoemulsion - formulation and its evaluation

4.1. Therapeutic importance of catechin
4.2. Preparation and evaluation of catechin based nanoemulsion formulations
4.3. Characterization of catechin encapsulated nanoemulsions
4.4. Development and evaluation of catechin based gel formulations
4.5. Evaluation of skin permeation studies of different formulations
4.6. Skin irritation studies of various gel formulations
4.7. Kinetic studies of several formulations
4.8. Evaluation of photoprotection potential of catechin loaded gel formulations against UVA irradiation
4.9. Investigation of bioavailability of catechin in rats
4.10. Estimation of several pharmacokinetic parameters
4.11. Statistical analysis of data
4.12. Results and discussion
4.13. Conclusion
4.14. Publication

## 4.1. Therapeutic importance of catechin

Catechin (CA) is a flavanol type polyphenolic antioxidant molecule which is present in green tea, red wine, coffee, apple, chocolate and several nutritional and functional food products (Pomponio et al., 2003; Dube et al., 2010). CA possesses potent antioxidant potential and is capable of scavenging free reactive oxygen radicals by virtue of its reducing properties arising from the multiple hydroxyl groups attached to the aromatic rings (Li et al., 2012). CA has been proven to afford significant photoprotection to the skin against UV-mediated oxidative stress (Levin and Maibach, 2002), photo-damage, basal cell carcinoma, melanoma and sunburn (Fang et al., 2007). Several research reports suggested that CA has shown to exhibit cytostatic properties and induce apoptosis in many tumor cells (Al-Hazzani et al., 2011). It inhibits the expression of inflammation-associated enzymes, matrix metalloproteinases (MMPs) and restores levels of cutaneous antioxidant enzymes (Pinnell, 2003).

Other different activities of CA have been reported including antiaging (Cooper et al., 2005), antidiabetic (Shoji and Nakashima, 2006), neuroprotective (Ramassamy, 2006), anti-obesity, antibacterial, hypolipidemic (Li et al., 2012), anti-HIV (Wu et al., 2012) and anti-inflammatory (Chatterjee et al., 2012). Despite their exciting array of therapeutic effects, CA has a short (1.25 h) half-life ($t_{1/2}$) (Manach et al., 2005) and less than 5% oral bioavailability because of their extensive first-pass hepatic metabolism and elimination (Chen et al., 2011). Poor oral bioavailability of CA is also associated with its digestive instability and poor intestinal uptake (Tang et al., 2013).

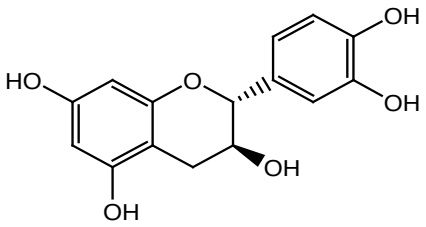


**Catechin**

Pharmacokinetic study of catechin was evaluated in rat plasma after oral administration of the green tea extract at doses of 0.4, 1.2 and 2.0 g/kg (~51 mg of catechin). At a 0.4 g/kg dose different pharmacokinetic parameter was observed as, $C_{max}$ = 204.1 ± 32.7 ng/mL, $T_{max}$ = 1.4 ± 0.5 h, $AUC_{0-t}$ = 1214 ± 304.3 ng h/mL and $T_{1/2}$ = 2.9 ± 1.1h. Pharmacokinetic parameters $C_{max}$ = 326.8 ± 49.7 ng/mL, $T_{max}$ = 1.4 ± 0.6 h, $AUC_{0-t}$ = 2786 ± 601.8 ng h/mL and $T_{1/2}$ = 4.8 ± 1.2 h was determined at dose of 1.2 g/kg. At dose of 2.0 g/kg, different parameters such as $C_{max}$ = 402.8 ± 65.0 ng/mL, $T_{max}$ = 1.4 ± 0.3 h, $AUC_{0-t}$ = 3223 ± 649.3 ng h/mL and $T_{1/2}$ = 4.5 ± 0.8 h was calculated (Huo et al., 2016). Pharmacokinetic parameters of catechin were also studied in human plasma

after ingestion of a single serving of reconstituted red wine at dose of 121000 nmol (equivalent to 35 mg or 121 µmol catechin) for 8 h (Bell et al., 2000).

Catechin is highly hydrophilic (log P ~0.30) compound exhibited poor lipid solubility hence poor bioavailability (Cho et al., 2011). Catechin undergoes the extensive hepatic metabolism and eliminated. It conjugated with glucuronic acid and sulphate groups. Catechin was also methylated but preferentially in the 3'-position. The exact nature of the major circulating metabolites of epicatechin has been elucidated, i.e., epicatechin-3'-O-glucuronide, 4'-O-methylepicatechin-3'-O-glucuronide, 4'-O-methylepicatechin-5- or 7-O-glucuronide, and the aglycones epicatechin and 4'-O-methylepicatechin. Because of this reason its bioavailability is ~40% (Fung et al., 2013) and half-life is ~1.25 h (Manach et al., 2005; Xie et al., 2011). The present study was aimed to develop a CA loaded nanoemulsion based nano-gel for the protection of skin against ultraviolet radiation (UV) induced photo-damage and to ensure its enhanced skin permeability as well as bioavailability through transdermal route.

## 4.2. Preparation and evaluation of catechin based nanoemulsion formulations

### *4.2.1. Physico-chemical properties of catechin*

The physico-chemical properties of CA are described as follows:

| | | |
|---|---|---|
| Color | : | Yellowish white |
| Odor | : | Odorless |
| Taste | : | Astringent and bitter |
| Physical form | : | Powder |
| Melting point (m. p.) | : | 114°C |
| Solubility | : | Freely soluble in methanol;<br>Freely soluble (methanol), soluble (ethanol, DMSO) and sparingly soluble in water and phosphate buffer pH 7.4 |
| Partition coefficient | : | ~ 0.30 in Milli-Q water (hydrophilic) |
| (log P) | : | ~ 0.38 in phosphate buffer pH 7.4 |
| $\lambda_{max}$ | : | 280 nm |

### *4.2.2. Chemicals and excipients*

(+) Catechin (assay 98%) was purchased from Sigma-Aldrich Chemicals, St. Louis, MO. Labrafac™ lipophile WL1349 (LLW), labrasol®, plurol oleique®, plurol isostearique®, isostearyl isostearate® (ISIS), lauroglycol™ 90 and transcutol CG® were provided as gift samples from Gattefossé (Saint Priest, France). Acconon® CC-6 was

supplied from ABITEC Corporation, Columbus, USA. All other chemicals and reagents used were of analytical grade and procured from Merck, Mumbai. Purified water was obtained from Milli-Q water purification system (Millipore, MA).

### *4.2.3. RP-HPLC analysis of CA*

#### *4.2.3.1. Chromatographic conditions*

RP-HPLC method was used to estimate the CA content in the excipients and their formulations. The HPLC system (Waters 600, Milford, MA, USA) equipped with the injection valve (rheodyne-7725i) with 20 µL sample loop, vacuum degasser, quaternary pump and photodiode array detector (PDA) was used for this analysis. The data were analyzed by Empower$^{TM}$-2 software. Chromatographic separation of the sample was done at a 1 mL/min flow rate, 280 nm wavelengths and 15 min run time at controlled temperature (25 ± 0.5°C). The sample was eluted through a Spherisorb $C_{18}$ column (250 mm × 4.6 mm, 5 µm; Waters, Ireland) attached to a $C_{18}$ guard column (10 × 3.0 mm).

The samples were injected into the valve by microsyringe (20 µL) [Hamilton Microliter®; Switzerland]. The stock solution was prepared by dissolving the weighed amount of CA in methanol to get 1000 µg/mL concentration in each case. Aliquots were prepared by dilution of the stock using the same solvent and kept in the refrigerator at 2 to 8°C for further uses. To obtain good resolution different mobile system composed of methanol and water at the ratio of 65: 35, 70: 30, 75: 25 v/v (1% glacial acetic acid; pH 2.5) were used in isocratic mode. Prior to use, the mobile system was sonicated for 15 min and degassed. Before analysis, all samples were properly filtered through the syringe filter (0.45 µm; NYL).

The method validation of CA was performed in terms of linearity, repeatability, intermediate precision, sensitivity and recovery according to the recommended guideline of International Conference on Harmonization (ICH). The assay's precision was analyzed in terms of % relative standard deviation (%RSD) of determinations. Sensitivity was determined by estimation of the limit of detection (LOD) and limit of quantification (LOQ) based on the standard deviation of the response (σ) and the slope (S) of the standard curve by using the following equations: LOD = 3.3σ/S and LOQ = 10σ/S.

The % recoveries of CA from quality control (QC) samples and formulations at three different concentrations were analyzed by calculating the % of detecting concentrations over additional concentrations. The quantitative analysis was repeated for three times (n = 3) by comparing and interpolating the QC sample peak area with the standard CA area.

### *4.2.4. Solubility study of CA in various oil components*

Screening of CA in different oil phase [LLW, ethyl oleate (EO), isopropyl myristate (IPM), isostearyl isostearate (ISIS), oleic acid (OA), olive oil (OL), soybean oil (SBO), liquid paraffin oil (LPO), sesame oil (SO) and eucalyptus oil (ELO)] was studied by dissolving an excess amount of the CA in 1 mL of each of the selected oils in Eppendorf tube (2 mL capacity) and mixed by a vortex mixer (Spinix, Tarson, India). Different mixture tubes were agitated in an isothermal shaker for 72 h at 25 ± 1.0°C to reach equilibrium (Shafiq et al., 2007). The equilibrated samples were removed and centrifuged at 13500 rpm for 5 min using Spinwin MC-02, Tarson, India. The supernatant was taken and filtered through a 0.45 μm membrane filter. The CA concentration was analyzed from each sample through RP-HPLC method at 280 nm wavelength.

### *4.2.5. Screening of surfactants and co-surfactants*

The surfactants like labrasol, acconon CC-6, lauroglycol 90, span 80, tween 80 and brij 35 and cosurfactants e.g. transcutol CG, PEG 400, plurol isostearate and plurol oleaque were screened for development of NEs. Surfactant solution (2.5 mL of 15 wt %) was prepared. Initially, 5 μL of the selected the oil was added into surfactant solution with vigorous vortexing until a clear solution was seen. Different excipients like EO, span 80 and transcutol CG were selected as oil phase, surfactant and cosurfactant respectively for development of the formulation (Shafiq et al., 2007).

### *4.2.6. Construction of ternary phase diagram*

The oil phase (EO), surfactants (span 80), cosurfactants (transcutol CG) and aqueous system (Milli-Q) were selected for the construction of pseudo-ternary phase diagrams. Surfactant and cosurfactant mixture ($S_{mix}$) were used in different ratios (1:0, 1:1, 2:1, 3:1, 1:2, 1:3 w/w). This $S_{mix}$ ratio was prepared in increasing amount of surfactant with respect to cosurfactant and vice versa. For the construction of phase diagram, water was added drop-wise to the mixture of $S_{mix}$ and oil by aqueous titration method. NE (w/o) region was developed based on the observation of its transparency and flowability. Various combinations of oil and $S_{mix}$ [1:9, 1:8, 1:7, 1:6, 1:5, 1:4, 1:3.5, 1:3, 1:2.5, 1:2, 1:1, 6:4, 7:3 and 9:1 w/w] were chosen to cover maximum ratios to delineate the boundaries of each phase diagram. The aqueous system was added at every 5% interval to obtain the range of 5-95% of total volume. Physical states of the formulations were observed through the pseudo-ternary phase diagrams where triangle apexes represented by the oil, $S_{mix}$ and aqueous phase respectively (Choudhury et al., 2014). Preparation techniques of the CA based nanoemulsions are represented through schematic diagram as shown in Figure 4.1.

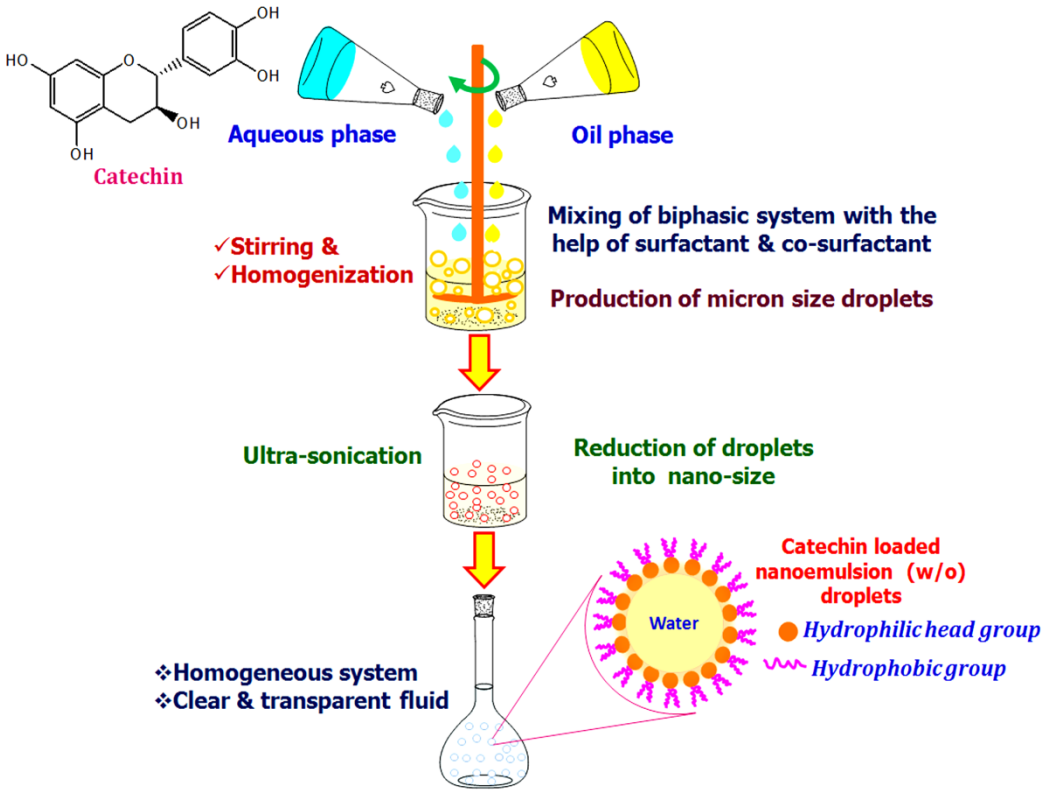


**Figure 4.1. Schematic presentation of preparation of catechin loaded nanoemulsion**

*4.2.7. Study of thermodynamic stability*

Thermodynamic stability of the NE was performed in order to assess the physical stability as per the procedure described by Choudhury et al. (2014). Briefly, centrifugation (Cent.), heating-cooling cycle (H & C) and freeze-thaw cycle (Freeze Tha.) tests were evaluated to find out suitable formulations. Detailed procedure has been described in the section 3.2.7.

*4.2.8. Selection of formulations from phase diagrams*

Different formulations were selected from a nanoemulsion region of each phase diagram thus the drug could be dissolved into the oil phase. Detailed procedure has been described in the section 3.2.8.

*4.2.9. Preparation of CA loaded NE formulations*

CA based NEs were prepared by incorporating 1 mg/mL amount into optimized oil phase at 10, 15, 20, 25 and 30% with respective $S_{mix}$ ratio using spontaneous nano-emulsification method.

## 4.3. Characterization of catechin encapsulated nanoemulsions

### *4.3.1. Analysis of conductivity*

The conductivity of the NE was measured by applying an electrical potential through the conductometer (Systronic Conductivity meter 306, Systronic Ltd., India) to find the type of formulation.

### *4.3.2. %Transmittance evaluation*

%Transmittance of the diluted sample of NE (100 times in water) was recorded at 450 nm using a spectrophotometer (SpectraMax® M5, USA).

### *4.3.3. Viscosity measurement*

The viscosity of NE was measured at 25 ± 0.5°C by using a Brookfield viscometer with spindle CPE 41 (Brookfield Engineering Laboratories, Inc., MA). Detailed procedure has been given in the section 3.3.3.

### *4.3.4. pH*

The pH of NE was analyzed through a digital pH meter (Orion 3 Star, Thermo Scientific, India) at controlled temperature (25 ± 0.5°C).

### *4.3.5. Analysis of refractive index*

Refractive index (R.I.) of the NE along with placebo (NE without CA) was analyzed through an Abbe refractometer at 25 ± 0.5°C.

### *4.3.6. Study of drug entrapment efficiency (%EE) and drug loading (%DL)*

%EE and %DL of CA loaded NEs were carried out according to the method established by Bu et al. (2014). Briefly, free CA content was separated from CA loaded NE (CA-NE) by ultrafiltration method (10,000 Da, Millipore) with centrifugation at 13500×g for 5 min. CA content was analyzed by using RP-HPLC method at 280 nm. Detailed methodology has been given in the section 3.3.6.

### *4.3.7. Droplet size, polydispersity index and zeta potential analysis*

The droplet size (Z-average), polydispersity indexes (PDI) and zeta potential of diluted NEs were determined by Zetasizer (Nano ZS90, Malvern instruments Ltd., UK) with a 50 mV laser. Analysis was carried out at working condition of 25 ± 0.5°C. Detailed methodology has been given in the section 3.3.7.

### *4.3.8. Analysis of TEM*

Morphology and surface structure of optimized CA-NE4 was analyzed by using TEM (JEOL JEM 2100, USA) with a working voltage of 200 kV. The diluted and filtered NE sample was carefully placed on carbon-coated copper grid (300 mesh size). Filled copper grid was negatively stained with phosphotungstic acid [PTA 2% (w/v)] for 30 s. Extra PTA was removed by absorbing on a filter paper and dried overnight at room temperature (25 ± 0.5°C). Photomicrograph of the sample was taken at different magnification.

### *4.3.9. UV - spectrum analysis*

Diluted sample of CA-NE4, placebo and pure CA were scanned together at 280 nm at 25 ± 0.5°C through a spectrophotometer (Multiskan-Go, Thermo Scientific, USA) and the spectrum was recorded. 96-well microplate (Quartz) was used for this study. Detailed methodology has been mentioned in the section 3.3.9.

### *4.3.10. HPTLC analysis*

The chromatographic study of the CA-NE4 and pure CA was performed through HPTLC (CAMAG, Switzerland) using a solvent system of toluene: ethyl acetate: formic acid in a ratio of (7:5:1 v/v/v). The sample was applied onto the HPTLC plate (Silica gel 60 F254) through the Linomat-5 applicator. UV-densitometry scanning of developed HPTLC plate was carried out at $\lambda_{max}$ 280 nm and data acquisition was made by software (WINCATS).

### *4.3.11. FTIR study*

FTIR study was performed for assessment of drug-excipient compatibility in the formulation. FTIR spectrum of the pure CA (A), placebo-NE4 (B) and CA-NE4 (C) were analyzed in the range of 4000-450 $cm^{-1}$ by using FTIR (Perkin Elmer, USA).

### *4.3.12. Evaluation of stability study*

Accelerated stability study of the optimized CA-NE4 was performed at 40 ± 2°C /75 ± 5% RH according to recommended ICH guidelines. The formulation was packed in an air-tight glass vial and kept in a stability chamber for 0, 30, 60 and 90 days. Formulation was observed periodically for any change in its droplet size, zeta potential, drug content, appearance, precipitation, clarity and pH. Drug content was analyzed by using RP-HPLC method at 280 nm. Logarithm of percentage of the drug remained to be decomposed was plotted against time (days) to estimate shelf-life ($t_{90}$) of the CA-NE4.

## 4.4. Development and evaluation of catechin based gel formulations

CA based gel formulation was prepared as per method reported by the Harwansh et al. (2015). In brief, catechin conventional gel (CA-CG, equivalent to 0.1 g of CA) was prepared with carbopol gel base and other ingredients. Nanoemulsion, CA-NE4-based nano-gel (CA-NG4, equivalent to 0.1 g of CA) and placebo-NG4 (nano-gel without CA) was developed. The detailed preparation procedure has been discussed in earlier section 3.4.

### *4.4.1. Rheological studies*

The flow behaviors of CA-NG4 and placebo-NG4 formulations were studied through a rheometer (Anton Paar, Modular Compact Rheometer-MCR 102). Detailed methodology has been provided in the section 3.4.1.

### *4.4.2. Spreadability test*

The spreadability of gel formulations CA-NG4 and placebo-NG4 were tested according to the procedure reported by Khurana et al. (2013). Detailed methodology has been provided in the section 3.4.2.

## 4.5. Evaluation of skin permeation studies of different formulations

*Ex vivo* skin permeation profile of the CA-NE1-5, CA-NG4 and CA-CG (500 mg ≈ 5 mg of CA) were studied. Detailed evaluation procedure has been described in earlier section 3.5.3.

## 4.6. Skin irritation studies of various gel formulations

The skin irritation study of CA-CG, CA-NG4 and placebo-NG4 was evaluated as method described in the section 3.6.

## 4.7. Kinetic studies of several formulations

Drug release kinetic study of data of the different formulations obtained from skin permeation study were calculated after fitted with Zero-order equation, First-order equation, Higuchi square root law and Korsmeyer-Peppas equation. Detailed methodology has been given in the section 3.7.

## 4.8. Evaluation of photoprotection potential of catechin loaded gel formulations against UVA irradiation

### *4.8.1. UVA treatment to rats*

Detailed methodology has been mentioned in the section 3.8.1.

### *4.8.2. Animal grouping and application of gel formulations*

The rats were divided into 5 groups (n = 6). Thin and uniform layers of gel formulations (500 mg equivalent to 5 mg of CA) were applied on the dorsal surface of the rat's skin. Group I was control (untreated UV irradiation) and Group II was irradiated with UVA. Group (III-V) were treated with CA-CG, CA-NG4 and placebo-NG4 respectively. All the animals of group II-V (except group I) was exposed to UVA radiation immediately after application of the different gel formulations for seven days.

On the eighth day, all the animals were anesthetized and sacrificed as per the protocols of CPCSEA. The UVA treated portion of cutaneous (epidermis and dermis) tissues were dissected and quickly put in ice-cold saline solution. The homogenate of skin tissue was prepared in 0.1 M PBS (pH 7.4) and centrifuged at 13500 rpm for 5 min (Spinwin MC-02, Tarson, India). Then the supernatant was collected and stored at -20°C for further use.

### *4.8.3. Estimation of antioxidant biochemical marker enzymes in cutaneous tissue*

The glutathione peroxidase (GPX) level was estimated according to the method proposed by Paglia and Valentine (1967) and the level of superoxide dismutase (SOD) was determined based on the procedure suggested by Kakkar et al. (1984). Antioxidant level of catalase (CAT) was estimated using the method of Beers and Seizer (1952) and thiobarbituric acid reactive substances (TBARS) was calculated according to the procedure of Ohkawa et al. (1979). Estimation of total protein was performed in a procedure described by Lowry et al. (1951). Data were expressed as units/mg of protein. All the enzyme estimations were performed by using a spectrophotometer (SpectraMax® M5, USA). Detailed procedure has been given in the section 3.8.3.

## 4.9. Investigation of bioavailability of catechin in rats

The bioavailability of CA (500 mg of CA-NG4 equivalent to 5 mg CA) was studied after transdermal administration of CA-NG4 compared with an oral suspension of pure CA. The oral suspension was prepared by mixing 5 mg of CA in 5 mL of water containing 0.5% (w/v) of sodium carboxymethyl cellulose (CMC). The animals were allowed free access to food and water, until the night prior to dosing they fasted for 10 h. Latin square crossover design was followed; the animals were divided into two groups (n =

6). In group I, oral suspension (5 mg /5 mL) was administered through a feeding tube followed by rinsing with 10 mL of purified water and group II was applied with CA-NG4 (~5 mg CA) in phase I. In phase II vice versa was followed and conducted after 15 days of the washout period. The uniform layer of CA-NG4 was applied over a surface area of 1.766 $cm^2$ and covered with a water impermeable membrane and further fixed with the help of adhesive membrane. 2.5 mL of blood samples were withdrawn from retro-orbital plexus of rats after administration of CA oral suspension and CA-NG4 at pre-determined intervals of time 0.0, 0.5, 1, 2, 4, 8 and 12 h; 0.0, 1, 2, 4, 6, 8, 12, 18, 24, 36, 48 and 72 h respectively. All blood samples were allowed to clot and centrifuged at 13500 rpm for 10 min (Spinwin MC-02, Tarson, India). Plasma was separated and kept at -20°C prior to analysis. The CA contents in the samples were estimated by RP-HPLC method at 280 nm.

## 4.10. Estimation of several pharmacokinetic parameters

The pharmacokinetic parameters of CA were determined with the help of a computer designed program, Phoenix WinNonlin® 6.4 (Certara, USA) after administration of CA-NG4 and CA-oral suspension to each rat. The non-compartmental model was used for calculating the pharmacokinetic parameters. Maximum concentration ($C_{max}$) and time to reach maximum concentration ($T_{max}$) are the values obtained directly from plasma concentration Vs time curve. Area under the concentration–time curve ($AUC_{0-t}$), area under the concentration-time curve until infinite observation ($AUC_{0-t\infty}$), mean residence time ($MRT_{0-t}$), mean residence time to the infinite observation ($MRT_{0-t\infty}$) and elimination half-life ($t_{1/2}$el), elimination rate constant (Kel), clearance (Cl), and volume of distribution (Vd) were determined. The relative bioavailability (*F*) of CA was calculated as a ratio of the plasma $AUC_{0-t}$ of the CA-NG4 and CA-oral suspension.

## 4.11. Statistical analysis of data

Statistical comparisons of data were made by one-way ANOVA followed by Dunnet's multiple comparison tests by using Graph Pad Prism software-5.0 (San Diego, CA, USA). All the data were expressed as mean ± standard deviation (SD) except estimation of antioxidant enzyme levels in rat skin where data are expressed as mean ± standard error of means (SEM). The differences between means were considered to be significant at the $P < 0.05$.

## 4.12. Results and discussion

### *4.12.1. RP-HPLC-PDA method validation of CA*

The RP-HPLC chromatographic separation of CA was carried out with the mobile phase in a ratio of 65:35 v/v (1% glacial acetic acid; pH 2.5) at a flow rate of 1 mL/min at 25 ± 0.5°C under the isocratic conditions. The retention time (Rt) of CA was found to be 9.45

± 0.02 min. A good linear precision relationship between the concentrations (20-100 μg/mL) and peak areas were obtained for the correlation coefficient ($r^2$) of 0.9993 ± 0.001. Intra-assay precision was performed at four different concentrations, and the %RSD of both instrumental precision and intra-assay precision were estimated to be <2.00. The precision of the method was optimized by calculating intra-day and inter-day repeatability at four subsequent concentrations ranging from 10-25 μg/mL. The RSD values in all tested groups were found to be <3%, which was significant. The LOD and LOQ were estimated to be 0.042 and 0.129 μg/mL respectively, which indicated that the proposed method can be used for detection and quantification of CA. The recovery rates of CA after spiking the additional standard drug concentrations at the different level (low: 20 μg/mL, middle: 30 μg/mL and high: 40 μg/mL) to the previously analyzed QC samples were estimated to be 19.94 ± 0.15 (99.70%), 29.94 ± 0.07 (99.80%) and 39.81 ± 0.12 μg/ml (99.52%) respectively.

*4.12.2. Solubility studies of CA in various oils*

The solubility studies of CA were carried out in the different oil phase and maximum solubility of CA was found to be 2.68 ± 0.29 mg/mL in EO (Figure 4.2). Therefore, EO was selected as an oil phase for the development of the formulations.

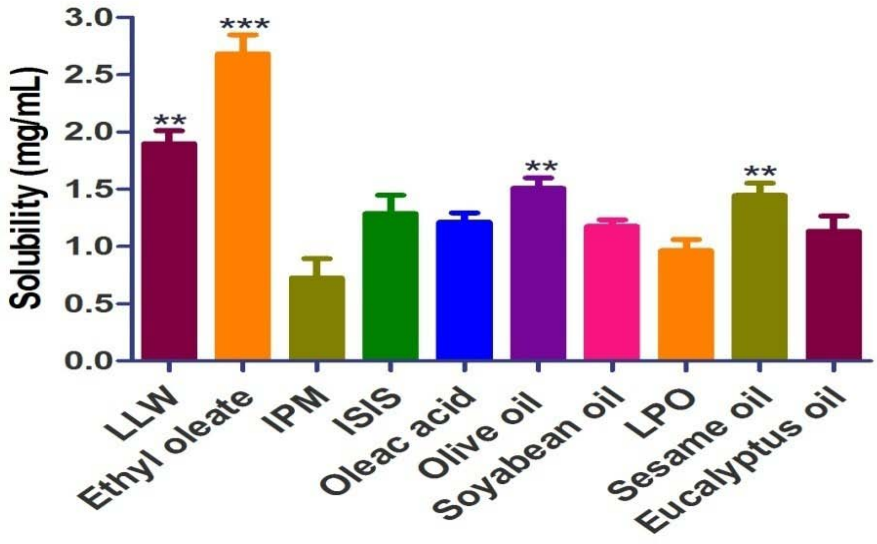


**Figure 4.2. Solubility profile of CA in different excipients**
**[Values were mean ± SEM (n = 6) $^{**}P < 0.05$, $^{***}P < 0.01$]**

*4.12.3. Pseudo-ternary phase diagram study*

The pseudo-ternary phase diagram was plotted to get the maximum water in oil (w/o) NE regions, which consists of EO, span 80, transcutol CG and aqueous system.

This formulation was appropriate due to its widespread NE (w/o) region. Individual phase diagrams were plotted and observed for each $S_{mix}$ (1:0-1:2) as shown in Figure 4.3 (A-E) and Table 4.1. In Figure 4.3A, a small area was found at $S_{mix}$ (1:0) without cosurfactant but the w/o NE region was too preliminary towards aqueous and $S_{mix}$ rich apex. After addition of cosurfactant along with a surfactant in equal proportion $S_{mix}$ (1:1), a stable and flowable NE region was obtained which, was optimized for selection of various formulations from this region as depicted in a Figure 4.3B. In this area, the oil was solubilized up to 30% along with 30% (w/w) $S_{mix}$ respectively. The surfactant amount was increased to double at the $S_{mix}$ ratio (2:1) NE area was smaller with the $S_{mix}$ ratio (1:1) [Figure 4.3C]. NE region was narrowed at a $S_{mix}$ ratio (3:1) in comparison with $S_{mix}$ (1:1) [Figure 4.3D]. A gel area was also observed at higher concentration of surfactant which was unfavorable for development of NE. When cosurfactant was increased at $S_{mix}$ (1:2) [Figure 4.3E], oil was solubilized up to 15% (w/w). A little NEs region was obtained in comparison to $S_{mix}$ (1:1).

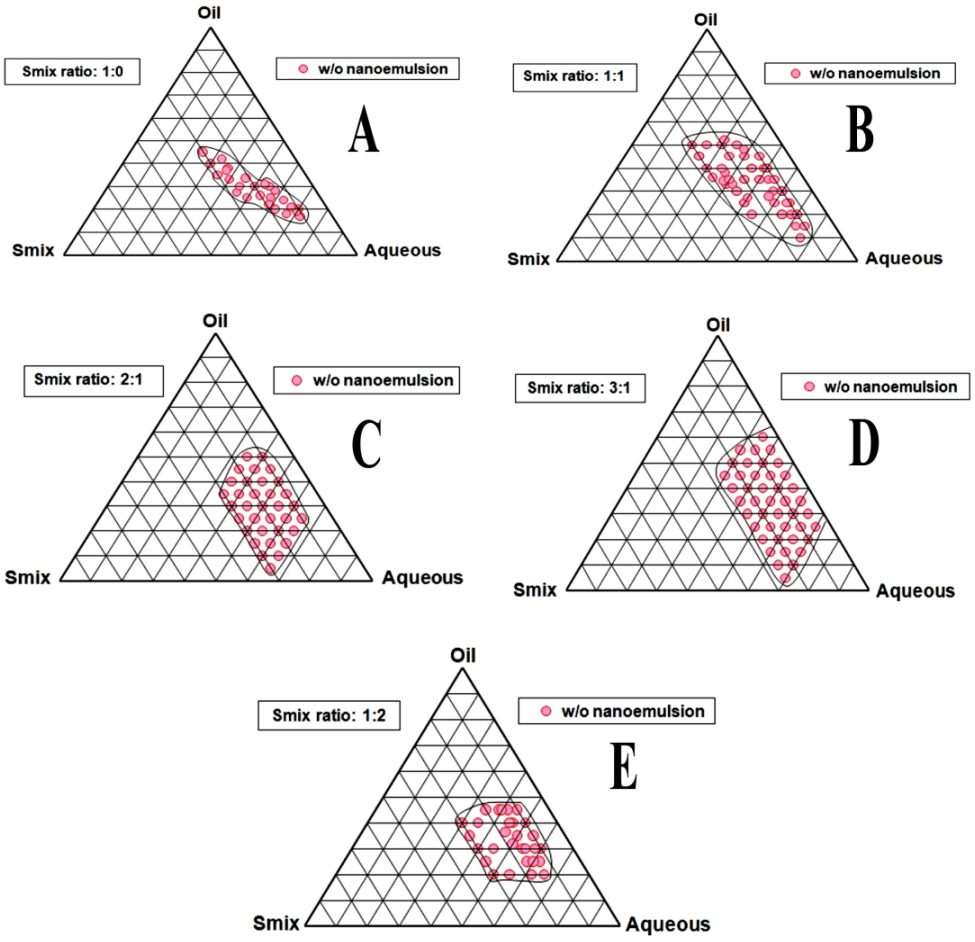


**Figure 4.3 (A-E). Construction of pseudo-ternary phase diagram for CA based formulations at $S_{mix}$ (1:0-1:2)**

### *4.12.4. Thermodynamic stability study*

The formulations were subjected to heating-cooling cycle, centrifugation and freeze-thaw cycle stress tests to assess their thermodynamic stability. No obvious consequence was observed during the test. However, some formulations were unstable as represented in Table 4.1.

**Table 4.1. Analysis of thermodynamic tests of formulations**

| $S_{mix}$ ratio (S:Cos) | Amount of excipients in formulations (% w/w) | | | Observations based on the preparation and thermodynamic stability studies | | |
|---|---|---|---|---|---|---|
| | Oil | Milli-Q water | $S_{mix}$ | [a]H & C | [b]Cent. | [c]Freeze Tha. |
| 1:0 | 10 | 18 | 72 | √ | × | √ |
| | 15 | 22 | 63 | √ | √ | √ |
| | 20 | 20 | 60 | √ | √ | × |
| | 25 | 25 | 50 | √ | √ | √ |
| | 30 | 35 | 35 | √ | √ | √ |
| 1:1 | 10 | 17 | 73 | √ | √ | √ |
| | 15 | 23 | 62 | √ | √ | √ |
| | 20 | 32 | 48 | √ | √ | √ |
| | 25 | 38 | 37 | √ | √ | √ |
| | 30 | 40 | 30 | √ | √ | √ |
| 2:1 | 10 | 21 | 69 | √ | √ | √ |
| | 15 | 23 | 62 | √ | √ | √ |
| | 20 | 27 | 53 | √ | √ | √ |
| | 25 | 33 | 42 | √ | √ | √ |
| | 30 | 40 | 30 | √ | √ | √ |
| 3:1 | 10 | 23 | 67 | √ | √ | √ |
| | 15 | 29 | 56 | √ | √ | √ |
| | 20 | 34 | 46 | √ | √ | √ |
| | 25 | 38 | 37 | √ | √ | √ |
| | 30 | 43 | 27 | √ | √ | √ |
| 1:2 | 10 | 17 | 73 | √ | √ | √ |
| | 15 | 25 | 60 | √ | √ | √ |
| | 20 | 34 | 46 | √ | √ | √ |
| | 25 | 42 | 33 | √ | √ | √ |
| | 30 | 35 | 35 | √ | √ | √ |

[a]Heating and cooling cycle (H & C); [b]Centrifugation (Cent.); [c]Freeze-thaw cycle (Freeze Tha.)

*4.12.5. Selection of formulations from phase diagrams and development of CA loaded nanoemulsions*

From each phase diagram, a different amount of oil were selected between the ranges of 10 - 30% (w/w) so that maximum formulations could be selected, covering the maximum NEs region. The amount of oil was selected at a low amount of $S_{mix}$ from each phase diagram. The favorable event was observed in the NE region of phase diagram after incorporation of CA (1 mg). Compositions of CA encapsulated nanoemulsions have been explained in Table 4.2.

**Table 4.2. Compositions of CA based different nanoemulsion formulations**

| NE Code | $S_{mix}$ | Ingredients in nanoemulsion formulation (% w/w) | | | | Oil:$S_{mix}$ Ratio |
|---|---|---|---|---|---|---|
| | | Oil | Water | S | Cos | |
| CA-NE1 | 1:1 | 10 | 17 | 36.5 | 36.5 | 1:7.3 |
| CA-NE2 | 2:1 | 20 | 27 | 35.32 | 17.66 | 1:2.6 |
| CA-NE3 | 3:1 | 15 | 29 | 42 | 14 | 1:3.7 |
| CA-NE4 | 1:1 | 15 | 23 | 31 | 31 | 1:4.1 |
| CA-NE5 | 1:2 | 15 | 25 | 20 | 40 | 1:4 |

*Where, 'S' = Surfactant, 'Cos'= Co-surfactant.*

For the development of nanoemulsion (w/o), span 80 (HLB = 4.3) and transcutol CG (HLB = 4.2) was chosen as surfactant and cosurfactant respectively, and that could work better in a $S_{mix}$ ratio. Nanoemulsions (w/o) were prepared through self nano-emulsification process and resulting into the thermodynamically stable system (Craig et al., 1995). A Formulation containing the higher amount of surfactant may lead to unwanted effect to the skin (Shakeel and Ramadan, 2010). Thus, the lower amount of $S_{mix}$ (1:1) was selected for development of optimized formulation, CA-NE4.

*4.12.6. Characterization of developed nanoemulsion*

Different NEs were characterized by using different parameters including droplet size, zeta potential (Figure 4.4), conductivity, %transmittance, viscosity, pH, R.I., %EE and %DL. The results have been shown in Table 4.3. Uniform droplets may enhance the drug solubility and stability in the formulation. The uniformity of the droplet size was indicated by polydispersity index (PDI) value. The low PDI value (0.120) has been observed for the optimized formulation that indicating uniformity of droplet size. The best droplet's uniformity was concerned with CA-NE4, and the formulation was a homogenous system.

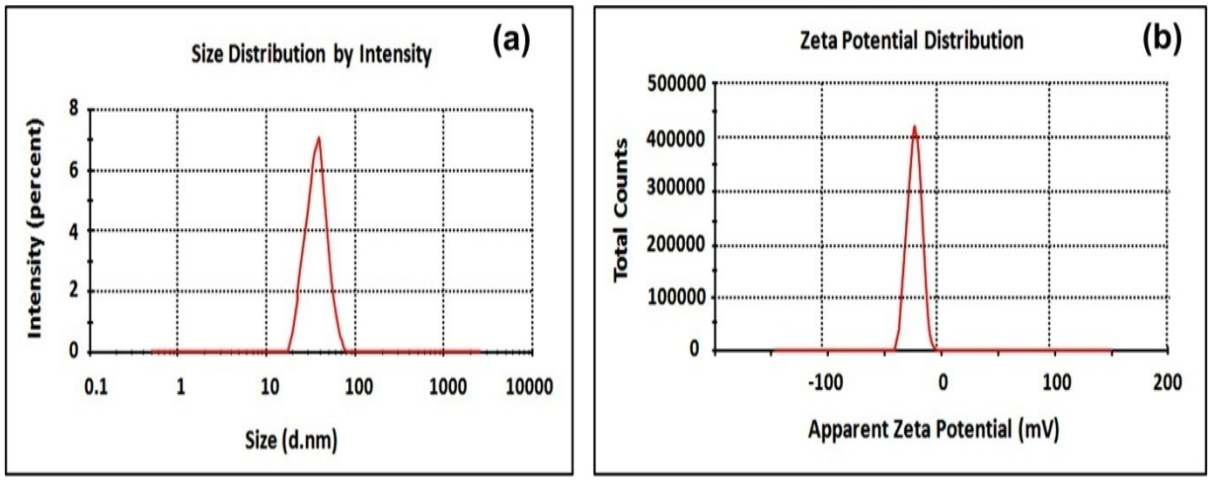


**Figure 4.4. Droplet size (a) and zeta potential (b) analysis of CA-NE4**

Appropriate nano droplet (98.6 nm) and zeta potential (-27.3 mV) were obtained with CA-NE4. Zeta potential plays an important role in the stability of the formulation. It is very well known that the zeta potential indicated by the degree of repulsion between adjacent charged droplets in a dispersion system such as nanoemulsion, which deals with the stability of the system. Generally, -30 mV or +30 mV is considered as high zeta potential value (Bali et al., 2011). The high negative charge of CA-NE4 is probably influenced by the anionic groups of the fatty acids present in the oil and $S_{mix}$. The nano size range of droplets with a higher zeta potential of CA-NE4 is generally attributed to preventing coalescence between droplets. Thus, zeta potential sustains the homogeneity as well as the stability to the system.

*4.12.7. TEM and UV - spectrum analysis*

The TEM morphology of the optimized CA-NE4 has been shown in Figure 4.5A. The surface of the droplet was observed as a dark spot in a photograph, which may be due to the dispersed oil droplets. Droplet size produced by TEM was quite similar to that obtained by Zetasizer.

UV spectrum showed that CA was present in the formulation (CA-NE4), when scanned at 280 nm wavelength as like as the pure CA (280 nm). The peak of UV spectra (CA-NE4) has been very slightly shifted due to drug entrapment with NE matrix. Detail has been graphically shown in Figure 4.5B.

*4.12.8. HPTLC analysis*

HPTLC chromatogram produced a sharp and well-defined symmetrical peak when the chamber was saturated with the mobile phase for 30 min at a controlled temperature (25 ± 0.5 $^{\circ}$C). HPTLC chromatogram of pure CA (A) and CA-NE4 (B) confirmed the $R_f$

value of 0.20 and 0.21 respectively (Figure 4.6 and 4.7). The result stated that the CA found quite compatible with their excipient, which was used for NE formulation.

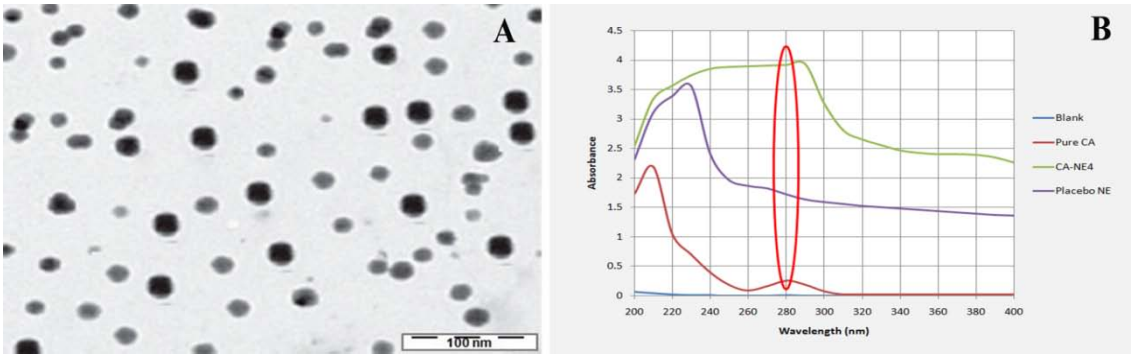


**Figure 4.5. TEM photograph (A) and UV spectra (B) analysis of CA-NE4 formulation**

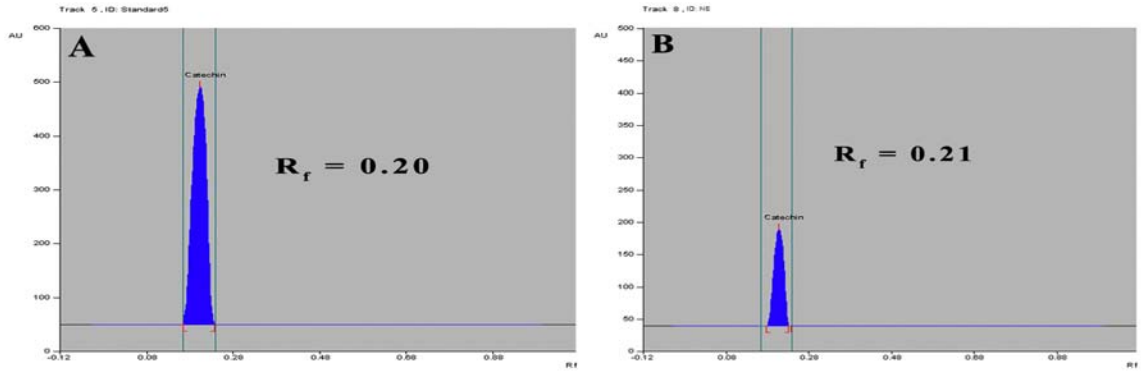


**Figure 4.6. HPTLC chromatogram of pure CA (A) and catechin loaded nanoemulsion, CA-NE4 (B)**

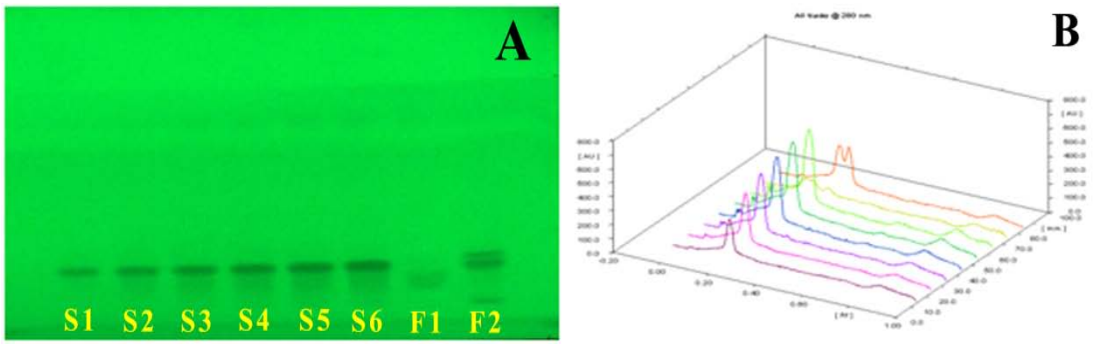


**Figure 4.7. HPTLC plate (A) and 3D-chromatogram (B) of pure CA and CA-NE4 formulation at 280 nm [S1-6 = Standard catechin and 'F1-2' = CA-NE4 formulation]**

**Table 4.3. Characterization of catechin loaded different nanoemulsions**

| NE code | Z-average (nm) | PDI | Z.P. (mV) | pH | Visco. (cP) | Cond. (ms/cm) | P.T. | R.I. | (%EE) | (%DL) |
|---|---|---|---|---|---|---|---|---|---|---|
| CA-NE1 | 181.8 ± 1.12 | 0.231 ± 0.16 | -43.6 ± 0.90 | 6.85 ± 0.04 | 12.34 ± 0.05 | 21.58 ± 1.20 | 88.78 ± 0.82 | 1.436 ± 0.02 | 97.72 ± 0.11 | 1.01 ± 0.02 |
| CA-NE2 | 253.7 ± 1.10 | 0.305 ± 0.14 | -52.5 ± 0.95 | 6.89 ± 0.02 | 15.89 ± 0.12 | 22.99 ± 1.15 | 82.74 ± 1.12 | 1.443 ± 0.03 | 95.73 ± 0.16 | 0.98 ± 0.01 |
| CA-NE3 | 382.7 ± 1.08 | 0.430 ± 0.07 | -39.5 ± 0.73 | 6.83 ± 0.03 | 17.24 ± 0.03 | 24.89 ± 1.52 | 81.31 ± 1.56 | 1.484 ± 0.08 | 93.61 ± 0.33 | 0.93 ± 0.03 |
| CA-NE4 | 98.6 ± 1.05 | 0.120 ± 0.03 | -27.3 ± 0.20 | 6.80 ± 0.01 | 10.18 ± 0.01 | 19.59 ± 0.70 | 99.88 ± 1.09 | 1.421 ± 0.01 | 99.02 ± 0.13 | 1.12 ± 0.02 |
| CA-NE5 | 314.7 ± 1.15 | 0.187 ± 0.09 | -24.5 ± 0.35 | 7.34 ± 0.10 | 18.56 ± 0.04 | 27.56 ± 1.25 | 79.98 ± 1.21 | 1.450 ± 0.04 | 94.37 ± 0.46 | 0.96 ± 0.01 |

PDI: Polydispersity index; Z.P.: Zeta potential; Visco.: Viscosity; Cond.: Conductivity; P.T.: Percentage transmittance; R. I.: Refractive index; %EE: Percentage entrapment efficiency; %DL: Percentage drug loading. Values were Mean ± SD (n = 3).

### *4.12.9. FTIR study*

The chemical compatibility of catechin with the excipients was analyzed by FTIR study which was used in the formulation (CA-NE4). Details of FTIR spectrum have been shown in Figure 4.8 (A-C). The wave numbers of FTIR spectra of pure catechin at 965.3, 1020.1, 1144.1, 1285.0,1474.4, 1514.5 and 1610.5 $cm^{-1}$ were assigned to C-H alkenes, -C-O alcohols, -OH aromatic, C-O alcohols, C-H alkanes, C=C aromatic ring and C=C alkenes respectively. Stretching of O-H was found at 3412.0 $cm^{-1}$. In case of CA-NE4 formulation, the wave numbers at 965.3, 1020.1, 1285.0, 1474.4, 1610.5 $cm^{-1}$ and 3412.0 $cm^{-1}$ were shifted to 947.0, 1115.6, 1249.6, 1455.9, 1702.2 and 3454.8 respectively. Other wave numbers at 1364.9 and 1864.2 were also shifted to 1351.7 and 2088.1 $cm^{-1}$ respectively. It may be due to the coordination bonding of several -OH groups of parent ring with the water content of the nanoemulsion (w/o). This result confirms that CA was pretty compatible with their excipients used in the formulations.

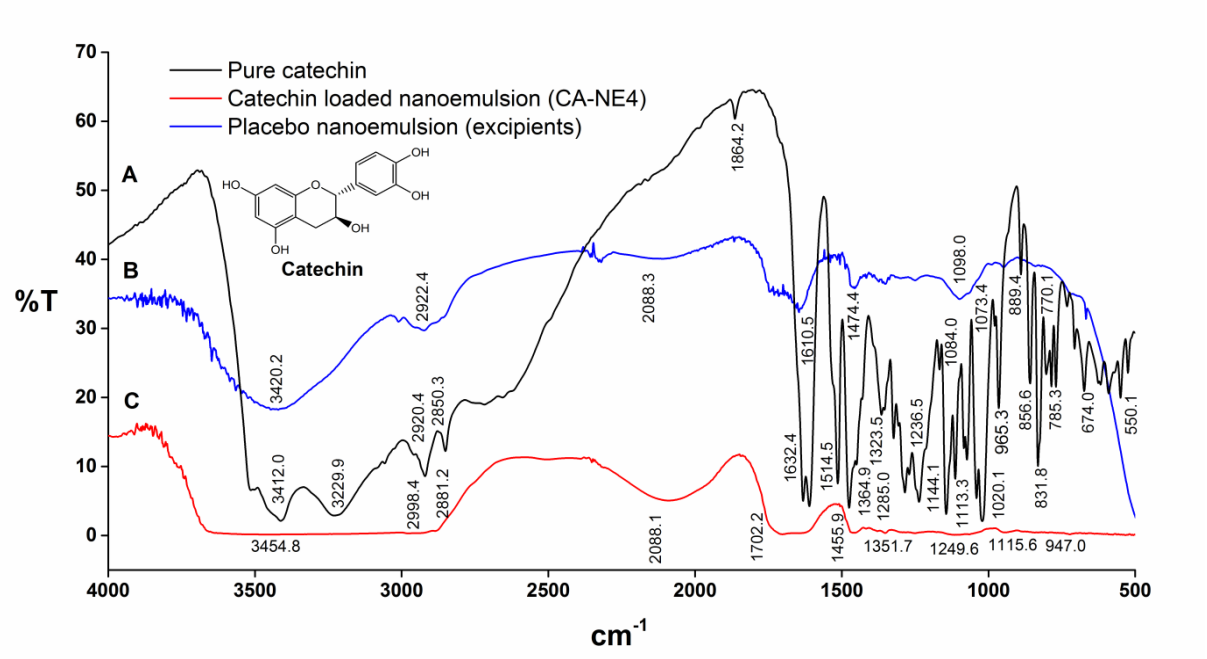


**Figure 4.8. FTIR spectrum of pure CA (A), placebo nanoemulsion (B) and CA-NE4 (C)**

### *4.12.10. Stability study*

The optimized CA-NE4 was evaluated during the period of 0, 30, 60 and 90 days at 40°C. No changes were observed in the droplet size, zeta potential and pH of the CAT-NE4 formulation and results have been shown in Table 4.4. A first order degradation of CA content in the formulation was found to be 0.71% for the remainder of 90 days at 40°C (Figure 4.9). From the results, it can be concluded that the CA-NE4 was stable at 40°C. Shelf-life ($t_{90}$) of CA based nano-gel was found to be 3.23 years.

**Table 4.4. Degradation study of optimized CA-NE4 formulation**

| Time (days) | Temper -ature (°C) | Droplet size (nm) | Zeta potential (mV) | pH | % Drug remained | Log % drug remained |
|---|---|---|---|---|---|---|
| 0 | 40 ± 2 (75 ± 5% RH) | 99.01 ± 1.12 | -27.8 ± 1.14 | 6.87 ± 1.41 | 100 | 2 |
| 30 | | 99.76 ± 2.32 | -28.5 ± 1.67 | 6.79 ± 2.21 | 99.71 | 1.9988 |
| 60 | | 100.08 ± 1.56 | -30.63 ± 2.24 | 6.85 ± 1.18 | 99.48 | 1.9978 |
| 90 | | 108.89 ± 1.85 | -31.67 ± 1.89 | 6.90 ± 2.78 | 99.29 | 1.9969 |

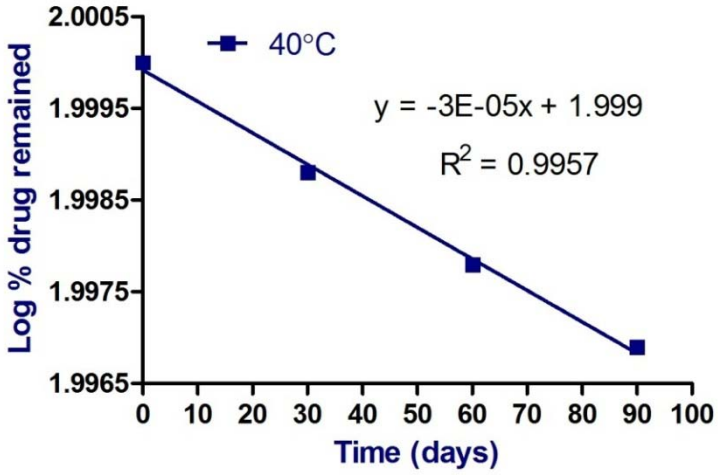


**Figure 4.9. First order degradation kinetics of CA from CA-NE-4 at 40°C**

*4.12.11. Rheological studies*

The viscosities were calculated in a range of 37.1 - 0.123 and 46.1 - 0.0784 Pa.s for placebo-NG4 and CA-NG4 formulation respectively. Higher viscosity attributed to the CA-NG4 was due to the drug which integrated into the gel matrix and leads to close proximity hence viscosity increased. The CA-NG4 showed non-Newtonian shear thinning and viscosity decreases with the rate of shear stress. Thus, the nano-gel formulation may be suitable for skin administration. Details have been shown in Figure 4.10. In the rheological behavior of gel formulation, CA-NG4 showed high viscosity than the placebo due to drug integration into the gel matrix of carbopol 940. Therefore, the catechin based nano-gel may be suitable for transdermal administration. The CA-NG4 has expressed non-Newtonian shear thinning property. Its viscosity decreases with the rate of shear stress. Carbopol-940 was used as a viscosity modifier resulting in improved membrane permeability (Lala and Awari, 2014).

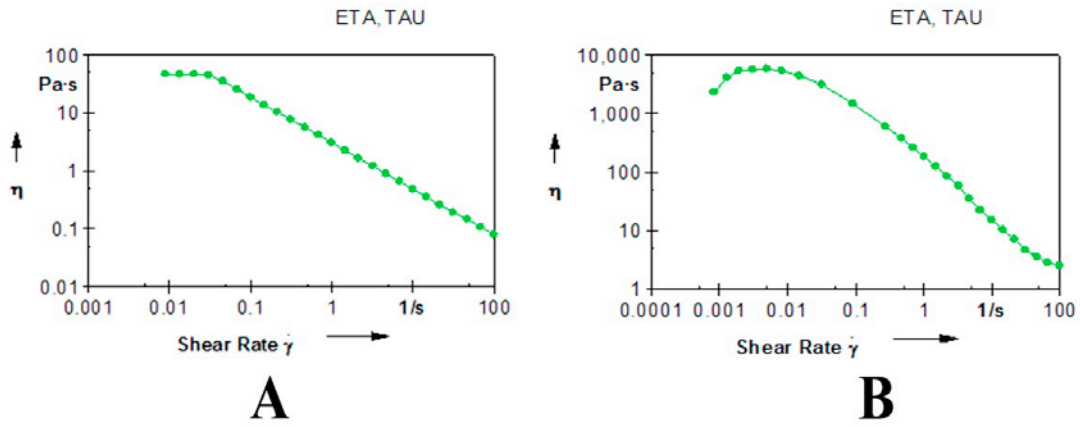


**Figure 4.10. Rheogram of placebo-NG4 (A) and CA-NG4 (B) where, η = viscosity (Pa.s), γ = shear rate (1/s)**

*4.12.12. Spreadability test*

The placebo-NG4 (58.43 ± 0.85% w/w) and CA-NG4 (59.87 ± 0.59% w/w) showed good spreadability that would assure practicability to the skin administration. No significant difference ($P < 0.05$) between the spreadability of placebo-NG4 and CA-NG4 were observed in this study.

*4.12.13. Skin permeation profiles*

%Cumulative skin permeation profile of CA from different CA-NE1-5, CA-NG4 and CA-CG were studied as shown in Figure 4.11 (A & B). The best release profile (93.76%) has been exhibited by the CA-NE4 compared to other formulation for 24 h. CA-NG4 and CA-CG showed skin permeability of 96.62 and 53.01% respectively for 24 h. CA-NG4 demonstrated better drug permeability, which may be due to enhanced solubility, low viscosity, nano-droplet size, favorable zeta potential and an appropriate pH comparatively to others. While a significant difference between skin permeation profile of CA-CG and CA-NG4 was observed. This may be due to the poor permeability of conventional formulation because of its non-uniform droplet size distribution and low solubility.

The transdermal flux [*Jss* (μg/h/cm$^2$)] and permeability coefficient [*Kp* (cm/h)] of CA from different formulations across the skin have been explained in Figure 4.11 (C) and Table 4.5. Significantly maximum flux (2.25 ± 0.11 μg/h/cm$^2$) and permeability (0.450 ± 0.05 cm/h) of CA were achieved with CA-NG4 ($^{***}P < 0.01$) compared to other formulations. The lag time was found to be 0.25 h for CA-NG4.

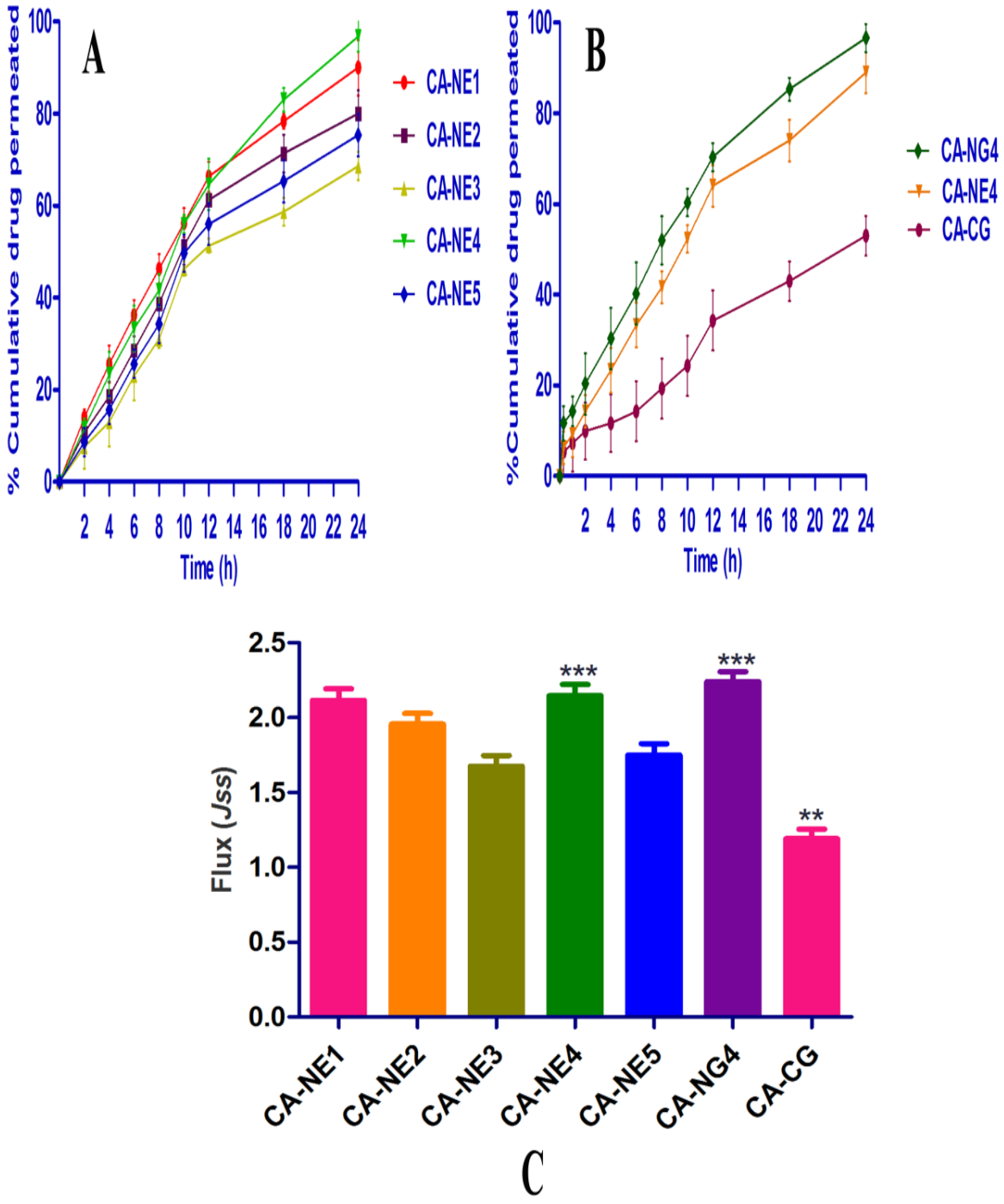


**Figure 4.11. Transdermal skin permeation profiles of CA from different nanoemulsions (A) CA-NE (1-5), (B) CA-CG, CA-NE4 and CA-NG4 through rat skin and (C) steady state flux of different formulations across rat skin**
**[Values were mean ± SD (n = 3), $^{**}P < 0.05$, $^{***}P < 0.01$ when compared to the conventional group]**

**Table 4.5. Transdermal steady state flux and permeability coefficient of CA nano formulations across rat skin, Mean ± SD**

| Formulation | Steady state flux *Jss* (μg $cm^{-2}$ $h^{-1}$) | Lag time (h) | Permeation coefficient *Kp* (×$10^{-3}$ cm $h^{-1}$) |
|---|---|---|---|
| CAT-NE1 | 2.11 ± 0. 130 | 0.26 | 0.422 ± 0.004 |
| CAT-NE2 | 1.96 ± 0.125 | 0.28 | 0.392 ± 0.002 |
| CAT-NE3 | 1.69 ± 0.121 | 0.33 | 0.338 ± 0.004 |
| CAT-NE4 | 2.14 ± 0.130 | 0.26 | 0.424 ± 0.005 |
| CAT-NE5 | 1.85 ± 0.132 | 0.30 | 0.370 ± 0.005 |
| CAT-CG | 1.21 ± 0.115 | 0.46 | 0.242 ± 0.003 |
| CAT-NG4 | 2.25 ± 0.111 | 0.25 | 0.450 ± 0.050 |

Nano-gel has been showed enhanced drug permeability across the rat skin after transdermal application, which may be due to diffusion of water content from the formulation and improved drug release. Transcutol CG could also play a role in the drug permeation by reducing the diffusion barrier of the *stratum corneum*, which is known as permeation enhancers.

*4.12.14. Study of skin irritation*

There were no substantial clinical signs of irritation, erythema or oedema observed throughout the study period. These results indicated that the gel formulation of CA (CA-NG4) was non-irritant and safe for skin application.

*4.12.15. Release kinetics of CA based various formulations*

Permeation profiles of CA-CG and CA-NG4 were fitted with Zero-order, First-order, Higuchi's model, Korsmeyer-Peppas model. The best release pattern of CA-CG ($r^2$ = 0.937) and CA-NG4 ($r^2$ = 0.992) was achieved with Korsmeyer-Peppas model. The CA-NG4 showed a non-Fickian pattern (0.5 < *Kp* < 1) of drug release by diffusion and matrix erosion. Details of drug release kinetics have been shown in Table 4.6.

*4.12.16. Efficacy evaluation of gel formulations against UVA exposure*

In group II (UVA irradiated), the antioxidant enzyme level of rat skin was elevated significantly compared to the control group (untreated UV irradiation) ($^{***}P$ < 0.01) [Figure 4.12 (A & B)]. In test groups (III and IV), the levels of cutaneous antioxidant enzymes (SOD, GPX and CAT) were significantly increased when treated with CA-CG and CA-NG4 respectively compared to UVA irradiated group. The placebo-NG4 group did not produce any significant effect on the skin antioxidant system in comparison to group II, which may be due to placebo-NG (nano-gel formulation without catechin).

The high level of TBARS has been significantly improved with CA-CG and CA-NG4 treated groups compared to the UVA irradiated group. Details have been explained in Figure 4.12 (A & B).

**Table 4.6. Release kinetics of data of CA based formulations**

| Formulations | Zero order | | First order | | Higuchi model | | Korsmeyer-Peppas model | |
|---|---|---|---|---|---|---|---|---|
| | $r^2$ | *k* | $r^2$ | *k* | $r^2$ | *k* | $r^2$ | *n* |
| CAT-NE1 | 0.934 | 11.10 | 0.991 | 2.03 | 0.972 | - 8.21 | 0.848 | 0.46 |
| CAT-NE2 | 0.928 | 7.45 | 0.978 | 2.02 | 0.942 | - 10.32 | 0.893 | 0.38 |
| CAT-NE3 | 0.923 | 5.30 | 0.970 | 2.00 | 0.929 | - 9.53 | 0.923 | 0.29 |
| CAT-NE4 | 0.966 | 7.27 | 0.928 | 2.14 | 0.955 | - 12.48 | 0.886 | 0.40 |
| CAT-NE5 | 0.930 | 6.12 | 0.982 | 2.01 | 0.938 | - 10.13 | 0.912 | 0.33 |
| CAT-NG4 | 0.946 | 12.88 | 0.952 | 2.05 | 0.984 | - 4.59 | 0.992 | 1.11 |
| CAT-CG | 0.979 | 3.65 | 0.982 | 1.99 | 0.924 | - 4.50 | 0.937 | 0.68 |

The CA-CG group showed less cutaneous protection efficacy than the CA-NG4 due to less availability of CA to the blood circulation and associated tissue. CA-NG4 showed enhanced photoprotective potential because of its improved permeability than its conventional gel. Thus, CA loaded transdermal nano-gel formulations could enhance UV protective activity for longer periods than the conventional dosage form.

*In vivo* antioxidant potential of catechin based transdermal nano-gel formulations were found significantly against UVA exposure except placebo formulation. CA-NG4 exhibited better UV protective activity after its transdermal administration. This activity may be due to its improved permeability and sustained-release profile compared to conventional gel. This result indicated that the use of catechin in transdermal nano-gel formulation might increase its penetration or absorption capacity inside the skin layers and that the presence of a higher concentration may be responsible for better sun protection. Transdermal route can avoid first-pass metabolism and resulting in the possible prolongation of drug action due to sufficient drug concentration in the systemic circulation (Zhang et al., 2010).

*4.12.17. Bioavailability study of CA*

The bioavailability study of CA was performed after administration of its oral suspension and CA-NG4. Results have been represented in Figure 4.13 and Table 4.7. CA has been well released and permeated from CA-NG4 as compared to the oral suspension for longer periods (72 h). Statistically significant $C_{max}$, $T_{max,}$ MRT and AUC profiles were observed with oral suspension and CA-NG4 ($P < 0.05$). The $C_{max}$ of CA was found to be 87.52 ± 8.56 and 93.79 ± 6.19 $ngmL^{-1}$ after administration of oral suspension and CA-

NG4 respectively. The $AUC_{0\text{-}t\infty}$ (2653.99 ± 515.02 nghmL$^{-1}$), $T_{max}$ (12.05 ± 0.02 h) and $MRT_{0\text{-}t\infty}$ (35.98 ± 10.34 h) were higher for CA-NG4 comparatively to the oral suspension ($P < 0.05$).

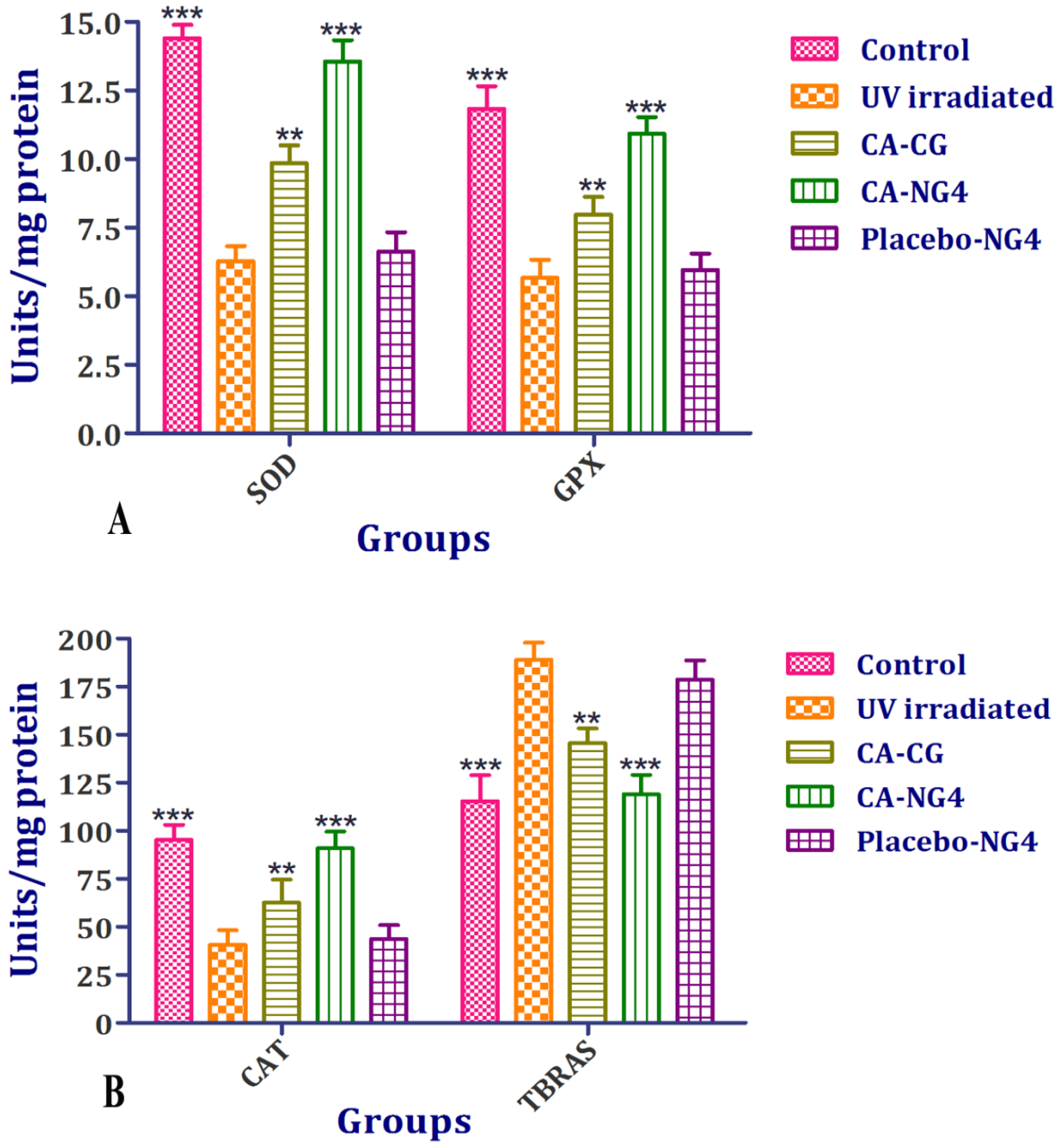


**Figure 4.12. Effect of transdermal gel formulations of CA on different cutaneous antioxidant enzyme levels (A) SOD and GPX, (B) CAT and TBARS**
**[Values are mean ± SEM (n = 6), $^{**}P < 0.05$, $^{***}P < 0.01$ when compared to the control and UVA irradiated group]**

The $t_{1/2}$el of CA was increased when it was in the nano-gel (24.75 ± 13.60 h) form and eventually the Kel (0.028 ± 0.02 $h^{-1}$) and Cl (0.0021 ± 0.04 $Lh^{-1}$) of the molecule in nano-gel form were also lowered. The mean value of $AUC_{0-t}$ by transdermal route was 8.94 times higher than that of oral route, and the difference was found to be statistically significant ($P < 0.05$). This could be due to avoidance of first-pass hepatic metabolism by the transdermal route.

The reported oral bioavailability of CA was 5% because of hepatic first-pass metabolism (Chen et al., 2011). In the current investigation, the relative bioavailability (*F*) of CA (CA-NG4) by transdermal route was found to be 894.73. This indicated enhanced bioavailability of CA (nano-gel) through transdermal route. This may be due to that the CA-NG4 releases drug in a sustained manner for extended periods (72 h). For transdermal route, *stratum corneum* acts as a permeation barrier and thereby the sustained-release activity of CA was found with CA-NG4 in comparison to orally administered suspension is an immediate release dosage form. Therefore, CA based nano-gel could provide an effective treatment for the management of skin damage mediated by the UV exposure.

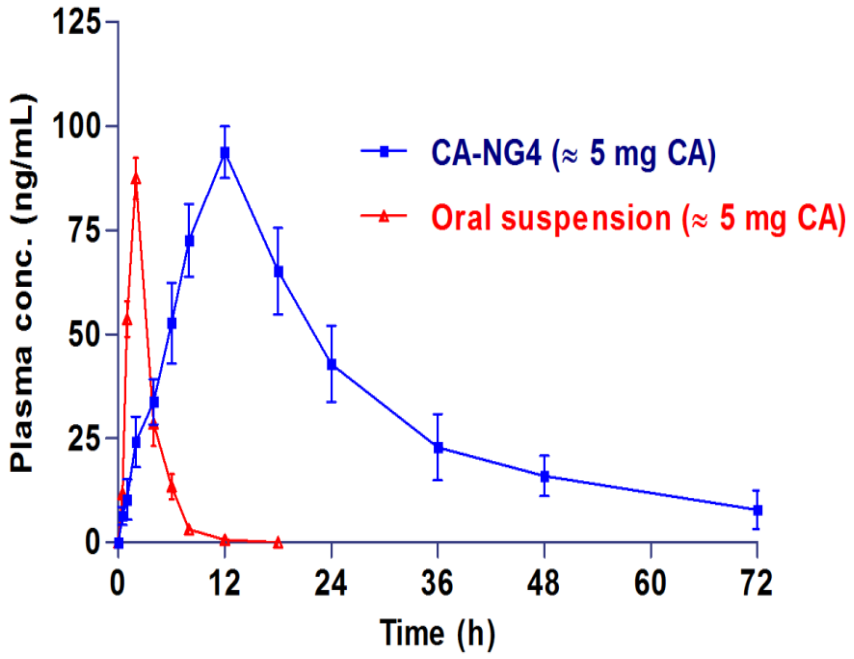


**Figure 4.13. Plasma concentration profiles of CA in rats, after administration of oral suspension (~ 5 mg of CA) and CA-NG4 (~ 5 mg of CA) [Values were mean ± SD (n = 6)]**

**Table 4.7. Analysis of pharmacokinetic parameters of CA in rats**

| Pharmacokinetic parameter | Oral suspension mean ± SD (n = 6) | CAT-NG4 mean ± SD (n = 6) |
|---|---|---|
| $C_{max}$ ($ngmL^{-1}$)[a] | 87.52 ± 8.56 | 93.79 ± 6.19 |
| $T_{max}$ (h)[b] | 2.02 ± 0.01 | 12.05 ± 0.02 |
| $AUC_{0-t}$ ($nghmL^{-1}$)[c] | 256.70 ± 37.16 | 2296.78 ± 293.39 |
| $AUC_{0-t\infty}$ ($nghmL^{-1}$)[d] | 256.86 ± 37.14 | 2653.99 ± 515.02 |
| $AUMC_{0-t}$ ($nghmL^{-1}$)[e] | 798.37 ±149.89 | 55236.97 ± 11746.28 |
| $AUMC_{0-t\infty}$ ($nghmL^{-1}$)[f] | 801.68 ± 148.67 | 98386.54 ± 45652.13 |
| $MRT_{0-t}$ (h)[g] | 3.10 ± 0.27 | 23.88 ± 2.03 |
| $MRT_{0-t\infty}$ (h)[h] | 3.11 ± 0.26 | 35.98 ± 10.34 |
| ($t_{1/2}$el) (h)[i] | 1.71 ± 0.24 | 24.75 ± 13.60 |
| Kel ($h^{-1}$)[j] | 0.405 ± 0.06 | 0.028 ± 0.02 |
| Cl ($Lh^{-1}$)[k] | 0.019 ± 0.02 | 0.0021 ± 0.04 |
| Vd (L)[l] | 0.047 ± 0.01 | 0.0745 ± 0.03 |
| %*F*[m] | 894.73 | |

[a]Peak of maximum concentration; [b]Time of peak concentration; [c]Area under the concentration-time curve until last observation; [d]Area under the concentration-time curve until infinite observation; [e]Area under moment curve computed to the last observation; [f]Area under moment curve computed to the infinite observation; [g]Mean residence time to the last observation; [h]Mean residence time to the infinite observation; [i]Elimination half life; [j]Elimination rate constant; [k]Clearance; [l]Volume of distribution; [m]Relative bioavailability of catechin.

## 4.13. Conclusion

Excessive UV exposure interferes with the cellular defense system of human skin and causes oxidative stress. ROS as a result of UV irradiation may oxidize and damage cellular lipids, proteins and DNA. This leads to the destruction of skin structures and results in hindrance of regular function of the cutaneous antioxidant defense system of skin. The enhanced relative bioavailability of catechin (894.73%) was achieved with nano-gel formulation after its transdermal application for 72 h. The nano-gel increased antioxidant potential of catechin against UVA-induced oxidative stress in a sustained manner. Nano-gel formulation of catechin was developed with nanoemulsion that could be useful as an effective strategy for photoprotection against UVA-induced oxidative stress. The CA-NG4 formulation was found to be stable, safe and effective for transdermal delivery. Thus, nanoemulsion based gel formulation of catechin may be a promising nanocarrier for skin delivery.

## 4.14. Publication

- Ranjit K Harwansh, Pulok K Mukherjee, Amit Kar, Shiv Bahadur, Naif Abdullah Al-Dhabi, V. Duraipandiyan. Enhancement of photoprotection potential of catechin loaded nanoemulsion gel against UVA induced oxidative stress. Journal of Photochemistry and Photobiology B: Biology, Elsevier, 2016, 160, 318-329, doi: 10.1016/j.jphotobiol.2016.03.026 (Impact Factor: 2.96).

# Chapter - 5

## Development and evaluation of genistein loaded nanoemulsion for its therapeutic benefits

5.1. Therapeutic benefits and limitations of genistein
5.2. Development and evaluation of genistein loaded nanoemulsions
5.3. Characterization of genistein based nanoemulsion formulations
5.4. Formulation and investigation of the genistein loaded gel formulations
5.5. Skin permeation study of various formulations
5.6. Evaluation of skin irritation study
5.7. Analysis of release kinetics of genistein based different formulations
5.8. Investigation of antioxidant potential of genistein loaded gel formulations against UVA mediated oxidative stress
5.9. In vivo bioavailability study of pure genistein and its nano-gel in rats
5.10. Analysis of pharmacokinetics for pure genistein and its nano-gel formulation
5.11. Analysis of statistical test
5.12. Results and discussion
5.13. Conclusion
5.14. Publication

## 5.1. Therapeutic benefits and limitations of genistein

Genistein (GN) [4',5,7-trihydroxyisoflavone; 5,7-dihydroxy-3-(4-hydroxyphenyl)-4H-1-benzopyran-4-one] is mainly found in dietary and food plants. GN is a phytoestrogen, which belongs to the isoflavone class of flavonoids, naturally occurring in soybean seeds (Manach et al., 2004; Ososki and Kennelly, 2003). GN is a potent tyrosinase enzyme inhibitor and helpful in ultraviolet radiation (UV) induced oxidative stress mediated skin damage. GN has been used as a photo-protective agent and it down-regulates UVB induced signal transduction cascades in carcinogenesis and proves photo-protective effect in SKH-1 murine skin and in human reconstituted skin. GN protects the human skin against UVB induced photoaging and photodamage (Wang et al., 2010). GN has been proven for their other potential therapeutic benefits like antioxidant, anti-inflammatory, hepatoprotective, antiobesity, antidiabetic, anti-cancer and anti-osteoporosis. It is proposed as a potent phytopharmaceutical for the treatment of metabolic disorders (Behloul and Wu, 2013; Li et al., 2013). Soybean is the main source of isoflavones in the human diet, it contains between 0.6 to 3.8 g isoflavones/kg fresh weights (Cassidy et al., 2000).

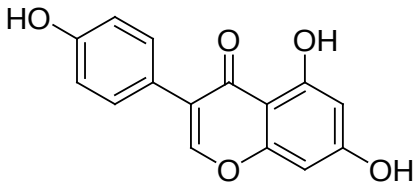


**Genistein**

GN is BCS II molecule suffer from poor solubility as well as low bioavailability due to its rapid absorption and clearance from the small intestine and liver (Motlekar et al., 2006). There have been several detailed studies on absorption, distribution, metabolism and excretion of GN in rats and humans. Pharmacokinetics of GN has been studied in rats and humans (Zhang et al., 199), and demonstrated low bioavailability due to first pass effect (Coldham and Sauer, 2000). After oral administration of GN with various doses (4, 20, 40 mg/kg), the bioavailability of GN was reported as 38.58, 24.34 and 30.75%, respectively. The half-life ($t_{1/2}$) was estimated to be 4.53 ± 1.40, 4.41 ± 1.21, 5.25 ± 0.92 h for doses 4, 20, 40 mg/kg respectively. The $T_{max}$, $C_{max}$ and $AUC_{0-\infty}$ of genistein after oral administration of genistein (40 mg/kg), were 2 h, 4876.19 ng/mL, 31269.66 ng h/mL, respectively (Kwon et al., 2007).

Poor aqueous solubility of GN offers a novel formulation for bioavailability enhancement and better therapeutic benefits. GN exists in the systemic circulation after being absorbed as several molecular forms including glucuronide and sulfate conjugates, free GN and protein-bound form. Because of these, the primary metabolite of GN is reported to be GN-glucuronide and GN-sulfate, and the metabolism is believed to occur mainly in

the liver and epithelial cells of the intestinal wall. It has been reported that following infusion of the duodenum with GN, the major metabolite in portal blood is GN-7-O-glucuronide. Thus, both the liver and intestine seem to contribute to the first pass effect. GN is known to be excreted as GN metabolites such as dihydro-GN, 6'-OH-O-desmethylangolensin, trihydroxybenzene and 3', 4', 5, 7-tetrahydroxyisoflavone through feces and urines (Rusin et al., 2010; Zhou et al., 2008). The aim of the current study is to enhance its solubility by using a nanoemulsion like carrier system and develop a GN loaded nanoemulsion based nano-gel for the photoprotection of skin against UV mediated oxidative stress, and also to ensure its enhanced skin permeability as well as bioavailability through transdermal route.

## 5.2. Development and evaluation of genistein loaded nanoemulsions

### *5.2.1. Evaluation of physico-chemical characteristics of genistein*

Physico-chemical features of GN are as follows:

| | | |
|---|---|---|
| Color | : | Crystalline white |
| Odor | : | Odorless |
| Taste | : | Characteristic |
| Physical form | : | Powder |
| Melting point (m. p.) | : | 298°C |
| Solubility | : | Soluble in DMSO, chloroform, methanol, ethanol, acetone; Insoluble in water |
| Partition coefficient (log P) | : | 2.96 ± 1.40 (lipophilic) |
| $\lambda_{max}$ | : | 260 nm |

### *5.2.2. Chemicals and excipients*

Genistein (assay ≥98%) was procured from Sigma-Aldrich Chemicals, St. Louis, MO. Labrafac™ lipophile WL1349 (LLW), labrasol®, plurol oleique®, plurol isostearique®, isostearyl isostearate® (ISIS), lauroglycol™ 90 and transcutol CG® were used as a gift sample from Gattefossé (Saint Priest, France). Acconon® CC-6 was obtained from ABITEC Corporation, Columbus, USA. All other chemicals and reagents were of analytical grade and purchased from Merck, Mumbai. Milli-Q water was prepared from Millipore, MA purification system.

### *5.2.3. Analysis of GN through RP-HPLC method*

#### *5.2.3.1. Chromatographic conditions*

Analysis of GN content in the excipients and their formulations was estimated by using RP-HPLC method. HPLC system (Waters 600, Milford, MA, USA) equipped with the injection valve (rheodyne-7725i) with 20 µL sample loop, vacuum degasser, quaternary pump and photodiode array detector (PDA) was used for this study. The data were analyzed by Empower$^{TM}$-2 software. Chromatographic separation of the sample was performed at a 1 mL/min flow rate, 260 nm wavelengths and 15 min run time at optimized temperature (25 ± 0.5°C). The sample was eluted through a Spherisorb $C_{18}$ column (250 mm × 4.6 mm, 5 µm; Waters, Ireland) fitted with a $C_{18}$ guard column (10 × 3.0 mm).

The samples were injected into the valve by using 20 µL microsyringe [Hamilton Microliter®; Switzerland]. The standard GN stock solution was prepared by dissolving the weighed quantity in methanol to obtain concentration (1000 µg/mL) in each case. Different aliquots were prepared by dilution of the stock using the same solvent and stored in the refrigerator at 2 to 8°C for further uses. To get optimum resolution different mobile system of methanol and water at the ratio of 65: 35, 70: 30, 75: 25 v/v (1% glacial acetic acid; pH 2.5) were used in isocratic mode. The freshly prepared mobile system was sonicated for 15 min and degassed before analysis. Prior to analysis, all the samples were filtered properly by using syringe filter (0.45 µm; NYL). The detailed procedure of method validation has been provided in the section 3.2.3.

### *5.2.4. Screening of GN solubility in excipients*

Solubility study of GN was studied in different excipients including isopropyl myristate (IPM), oleic acid (OA), LLW, eucalyptus oil (ELO), ethyl oleate (EO), olive oil (OL), sesame oil (SO), liquid paraffin oil (LPO), soybean oil (SBO), isostearyl isostearate (ISIS), and Milli-Q water. Analysis was performed by dissolving an excess amount of the GN in 1 mL of each of the selected excipients in Eppendorf tube (2 mL capacity) and mixed properly by a vortex mixer (Spinix, Tarson, India). The mixture tubes of different excipients were agitated in an isothermal shaker for 72 h at 25 ± 1.0°C to reach equilibrium (Shafiq et al., 2007). The equilibrated samples were centrifuged at 13500 rpm for 5 min by using Spinwin MC-02, Tarson, India. The supernatant was separated and filtered through a 0.45 µm membrane filter. The GN content was analyzed from each sample by RP-HPLC method at 260 nm wavelength.

### *5.2.5. Selection of surfactants and co-surfactants*

Various kind of surfactants (labrasol, acconon CC-6, lauroglycol 90, span 80, tween 80 and brij 35) and cosurfactants (transcutol CG, PEG 400, plurol isostearate and plurol

oleaque) were screened for development of NEs. Surfactant solution (2.5 mL of 15%, w/w) was prepared for this study (Shafiq et al., 2007). Initially, 5 μL of the selected oil was added into surfactant solution with vigorous vortexing until a clear solution was observed. Different excipients like LLW, labrasol and PEG 400 were selected as oil phase, surfactant and co-surfactant respectively for further development of the NE formulations.

*5.2.6. Design and development of pseudo-ternary phase diagram*

LLW, labrasol, PEG 400 and purified water were chosen for the construction of pseudo-ternary phase diagrams. Surfactant and co-surfactant mixture ($S_{mix}$) were used in different ratios (1:0, 1:1, 2:1, 3:1, 1:2, 1:3%, w/w). The $S_{mix}$ ratio was prepared in increasing amount of surfactant with respect to cosurfactant and vice versa. For the phase diagram study, water was incorporated drop-wise into the mixture of $S_{mix}$ and oil by aqueous titration method. Oil-in-water (o/w) NE region was developed based on the observation of its transparency and flow ability. Different combinations of oil and $S_{mix}$ [1:9, 1:8, 1:7, 1:6, 1:5, 1:4, 1:3.5, 1:3, 1:2.5, 1:2, 1:1, 6:4, 7:3 and 9:1 w/w] were selected to cover the maximum ratios to delineate the boundaries of each phase diagram. The water was added at every 5% interval to attain the range of 5-95% of total volume. Physical states of the formulations were observed through the pseudo-ternary phase diagram. Triangle apexes in phase diagrams were represented by the oil, $S_{mix}$ and aqueous phase respectively (Choudhury et al., 2014). Schematic representation of preparation techniques of GN based NEs are as shown in Figure 5.1.

*5.2.7. Evaluation of thermodynamic stability test*

Thermodynamic stability study of the NEs was tested in order to assess the physical stability according to the procedure described by Choudhury et al. (2014). Briefly, centrifugation (Cent.), heating-cooling cycle (H & C) and freeze-thaw cycle (Freeze Tha.) tests were performed to find out suitable formulations. Detailed procedure has been described in the section 3.2.7.

*5.2.8. Optimization of formulations from pseudo-ternary phase diagrams*

Different formulations were chosen from a nanoemulsion region of each phase diagram so the maximum amount of drug could be dissolved into the oil phase. Detailed procedure has been described in the section 3.2.8.

*5.2.9. Fabrication of GN loaded NEs*

GN based NEs were prepared by adding 1 mg/mL amount into optimized oil phase at $S_{mix}$ of 10, 15, 20, 25 and 30% using spontaneous nano-emulsification method.

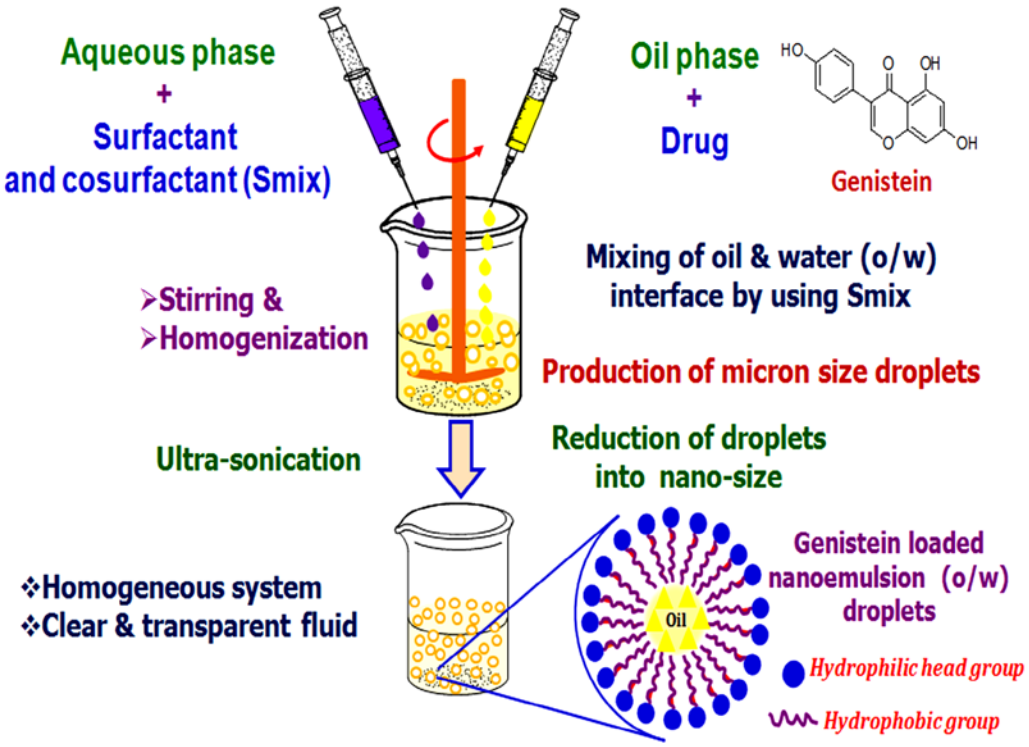


**Figure 5.1. Schematic preparation techniques of GN encapsulated nanoemulsion formulation**

## 5.3. Characterization of genistein based nanoemulsion formulations

### *5.3.1. Measurement of conductivity*

Detailed description has been provided in the section 3.3.1.

### *5.3.2. Evaluation of percentage transmittance (P.T.)*

Detailed method has been mentioned in the section 3.3.2.

### *5.3.3. Analysis of viscosity*

Detailed procedure has been given in the section 3.3.3.

### *5.3.4. Analysis of pH*

Detailed description of pH analysis has been shown in the section 3.3.4.

### *5.3.5. Measurement refractive index (R.I.)*

Detailed method of R.I. measurement has been discussed in the section 3.3.5.

### *5.3.6. Evaluation of entrapment efficiency and drug loading*

Entrapment efficiency (%EE) and drug loading (%DL) of GN loaded NEs were calculated according to the method established by Bu et al. (2014). In Brief, free GN content was separated from GN loaded NE (GN-NE) by ultrafiltration method (10,000 Da, Millipore) with centrifugation at 13500 × g for 5 min. GN content was estimated by using RP-HPLC method at 260 nm. Detailed procedure has been given in the section 3.3.6.

### *5.3.7. Droplet size, polydispersity index and zeta potential analysis*

Detailed methodology has been given in the section 3.3.7.

### *5.3.8. TEM analysis*

Detailed methodology has been given in the section 3.3.8.

### *5.3.9. Study of UV - spectrum*

Pure GN, placebo and diluted sample of GN-NE2 were scanned together at 260 nm at 25 ± 0.5°C through a spectrophotometer (Multiskan-Go, Thermo Scientific, USA) and the spectrum was recorded. 96-well microplate (Quartz) was used for this study. Detailed methodology has been mentioned in the section 3.3.9.

### *5.3.10. Study of HPTLC*

HPTLC analysis of the GN-NE2 and pure GN was performed through HPTLC system (CAMAG, Switzerland) using a solvent system of toluene: ethyl acetate: formic acid in a ratio of (7:3:0.5 v/v/v). The sample was spotted onto the HPTLC plate (Silica gel 60 F254) through the Linomat-v applicator. HPTLC plate was scanned at λmax 260 nm through UV-densitometry scanner and data acquisition was made by WINCATS software.

### *5.3.11. FTIR - spectrum analysis*

FTIR - spectrum analysis was performed for assessment of drug-excipient compatibility in the formulation. FTIR spectrum of the pure GN (a) and GN-NE2 (b) was analyzed in the range of 4000-500 $cm^{-1}$ by using FTIR (Perkin Elmer, USA).

*5.3.12. Analysis of accelerated stability study*

The stability study of the optimized GN-NE2 was performed at accelerated condition of 40 ± 2°C /75 ± 5% RH according to guideline of ICH. Drug content was estimated by using RP-HPLC method at 260 nm. Detailed methodology has been given in the section 3.3.12.

## 5.4. Formulation and investigation of the genistein loaded gel formulations

Formulation of GN based gel was developed as per method reported by Harwansh et al. (2015). Briefly, the conventional gel of genistein (GN-CG ≈ 0.1 g of GN) was developed with gel (carbopol 940) base and other excipients. The nanoemulsion (GN-NE2) based nano-gel (GN-NG2, ≈ 0.1 g of GN) and placebo-NG2 (nano-gel without GN) formulation was prepared. The detailed methodology has been described in earlier section 3.4.

*5.4.1. Study of rheological behavior*

The flow behaviors of GN-NG2 and placebo-NG2 formulations were determined through a rheometer (Anton Paar, Modular Compact Rheometer-MCR 102). Detailed methodology has been described in the section 3.4.1.

*5.4.2. Testing of spreadability*

The spreadability of gel formulations (GN-NG2 and placebo-NG2) were tested according to the procedure reported by Khurana et al. (2013). Detailed procedure has been provided in the section 3.4.2.

## 5.5. Skin permeation study of various formulations

Skin permeation study of the different formulations i.e. GN-NE1-4, GN-NG2 and GN-CG (500 mg equivalent to 20 mg of GN) were evaluated. Detailed methodology has been provided in the section 3.5.3.

## 5.6. Evaluation of skin irritation study

Evaluation of skin irritation studies of formulations like GN-NG2 and GN-CG and placebo-NG4 has been performed according to method described in the earlier section 3.6.

## 5.7. Analysis of release kinetics of genistein based different formulations

Drug release kinetic study of *in vitro* drug release data of the different formulations were calculated and fitted with Zero-order equation, First-order equation, Higuchi square root law and Korsmeyer-Peppas equation. Detailed procedure has been mentioned in the section 3.7.

## 5.8. Investigation of antioxidant potential of genistein loaded gel formulations against UVA mediated oxidative stress

### *5.8.1. UVA treatment to rats*

Detailed methodology has been given in the section 3.8.1.

### *5.8.2. Grouping and application of gel formulations to rats*

The rats were divided into 5 groups (n = 6). Thin and uniform layers of gel formulations (500 mg ≈20 mg of GN) were applied on the dorsal surface of the rat's skin. Group I was control (untreated UV irradiation) and Group II was irradiated with UVA. Group (III-V) were treated with GN-CG, GN-NG2 and placebo-NG2 respectively. All the animals of group II-V (except group I) was irradiated with UVA immediately after application of the gel formulations for seven days. Detailed methodology has been given in the section 4.8.2.

### *5.8.3. Estimation of cutaneuos antioxidant enzyme levels*

The cutaneuos antioxidant level of glutathione peroxidase (GPX) was estimated according to the method proposed by Paglia and Valentine (1967) and superoxide dismutase (SOD) level was determined based on the procedure suggested by Kakkar et al. (1984). The level of catalase (CAT) was estimated using the method of Beers and Seizer (1952) and thiobarbituric acid reactive substances (TBARS) was calculated according to the procedure of Ohkawa et al. (1979). Total protein was estimation as procedure described by Lowry et al. (1951). Data were expressed as units/mg of protein. All the enzyme estimations were performed by using a spectrophotometer (SpectraMax® M5, USA). Detailed procedure has been described in the section 3.8.3.

## 5.9. *In vivo* bioavailability study of pure genistein and its nano-gel in rats

Bioavailability of GN (500 mg of GN-NG2 ≈20 mg GN) was evaluated after transdermal application of GN-NG2 compared with oral suspension of pure GN. The pure GN (20 mg) oral suspension was prepared in purified water with 0.5% (w/v) of sodium CMC. The animals were allowed free access to food and water, until the night prior to dosing they fasted for 10 h. For this study Latin square crossover was designed; the animals

were divided into two groups (n = 6). In group I, oral suspension (20 mg GN) was administered through a feeding tube followed by rinsing with 10 mL of purified water and group II was applied with GN-NG2 (~20 mg GN) in phase I. In phase II vice versa was followed and conducted after 15 days of the washout period. The GN-NG2 was applied uniformly over a surface area of 1.766 $cm^2$ and covered with a water impermeable membrane and fixed with the help of adhesive membrane. Blood samples (2.5 mL) were withdrawn from retro-orbital plexus of rats after administration of GN orally and GN-NG2 transdermally at pre-determined intervals of time 0.0, 0.5, 1, 2, 4, 8 and 12 h; 0.0, 1, 2, 4, 6, 8, 12, 18 and 24 h respectively. Plasma from blood samples were separated and kept at -20°C prior to analysis. Analysis of GN contents in the sample was determined by RP-HPLC method.

## 5.10. Analysis of pharmacokinetics of pure genistein and its nano-gel formulation

The pharmacokinetic parameters of GN were determined with the help of a computer designed program, Phoenix WinNonlin® 6.4 (Certara, USA) after administration of GN-NG2 and pure GN-oral suspension to each rats. Detailed procedure has been described in the section 3.10.

## 5.11. Analysis of statistical test

Statistical analysis was made by one-way ANOVA followed by Dunnet's multiple comparison tests by using Graph Pad Prism software-5.0 (San Diego, CA, USA). Data were expressed as mean ± SD except measurement of cellular antioxidant enzyme levels and pharmacokinetic parameters in rats where data were expressed as mean ± SEM. The differences between means were considered to be significant at value ($P$ < 0.05).

## 5.12. Results and discussion

### *5.12.1. RP-HPLC method validation of GN*

The RP-HPLC analysis of GN was performed with the mobile phase in a ratio of 70:30 v/v (1% glacial acetic acid; pH 2.5) at a flow rate of 1 mL/min at controlled temperature of 25 ± 0.5°C under the isocratic mode. The retention time ($R_t$) of GN was found to be 6.547 ± 0.02 min. A good linear precision relationship between the concentrations (100-1000 ng/mL) and peak areas were obtained with the correlation coefficient ($r^2$) of 0.9998 ± 0.01. Intra-assay precision was performed at four different concentrations, and the %RSD of both instrumental precision and intra-assay precision were estimated to be <0.001. The precision of the method was optimized by performing intra-day and inter-day repeatability at four subsequent concentrations ranging from 250-1000 ng/mL. The RSD values in all tested groups were found to be <1%, which was significant. The LOD and LOQ were estimated to be 0.0080 and 0.0242 ng/mL respectively, which indicated

that the proposed method can be applied for detection and quantification of GN. The recovery rates of GN after spiking the additional standard drug concentrations at the different level (low: 300 ng/mL, middle: 600 ng/mL and high: 900 ng/mL) to the previously analyzed QC samples were estimated to be 300.21 ± 34.80 (100.07%), 600.98 ± 24.51 (100.16%) and 900.06 ± 20.52 μg/ml (100.00%) respectively.

*5.12.2. Solubility profile of GN in oil system*

Solubility studies of GN were performed in the different excipients and maximum solubility of GN was found to be 4.11 ± 0.22 mg/mL in LLW (Figure 5.2). Hence, LLW was selected as an oil phase for the development of the formulations.

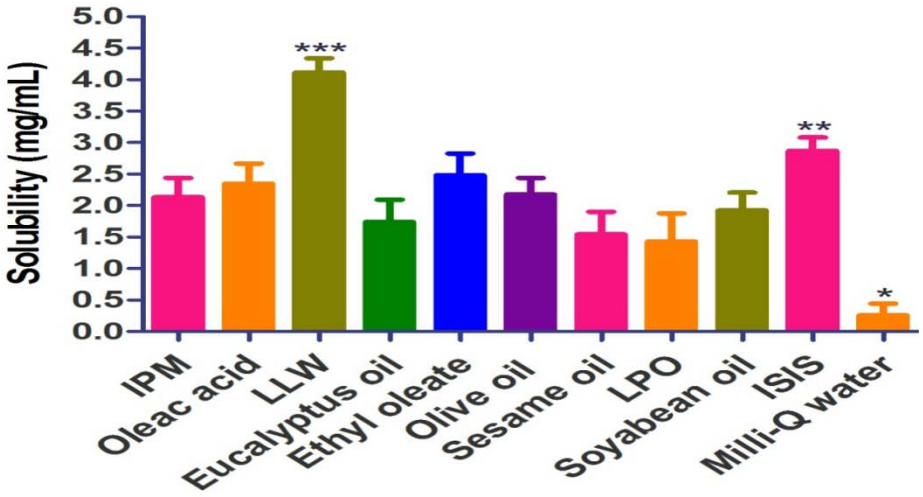


**Figure 5.2. Solubility studies of GN in several excipients**
**[Values were mean ± SEM (n = 6) $^{*}P$ & $^{**}P < 0.05$, $^{***}P < 0.01$]**

*5.12.3. Phase diagram study*

The pseudo-ternary phase diagram was constructed to find the maximum oil in water (o/w) NE regions, which consists of LLW, labrasol, PEG 400 and aqueous system. This formulation was appropriate due to its widespread NE (w/o) region. Individual phase diagrams were plotted and observed for each $S_{mix}$ (1:0-4:1) as shown in Figure 5.3 (a-g) and Table 5.1.

In Figure 5.3a, a small area of o/w NE region was achieved at $S_{mix}$ (1:0) without using co-surfactant. It was too preliminary towards aqueous and $S_{mix}$ rich apex. After addition of cosurfactant along with a surfactant in equal proportion $S_{mix}$ (1:1), a stable and flowable NE region was obtained which, was optimized for selection of formulations from this region as shown in a Figure 5.3b. In this area, oil was solubilized up to 30% along with 35% (w/w) $S_{mix}$ respectively.

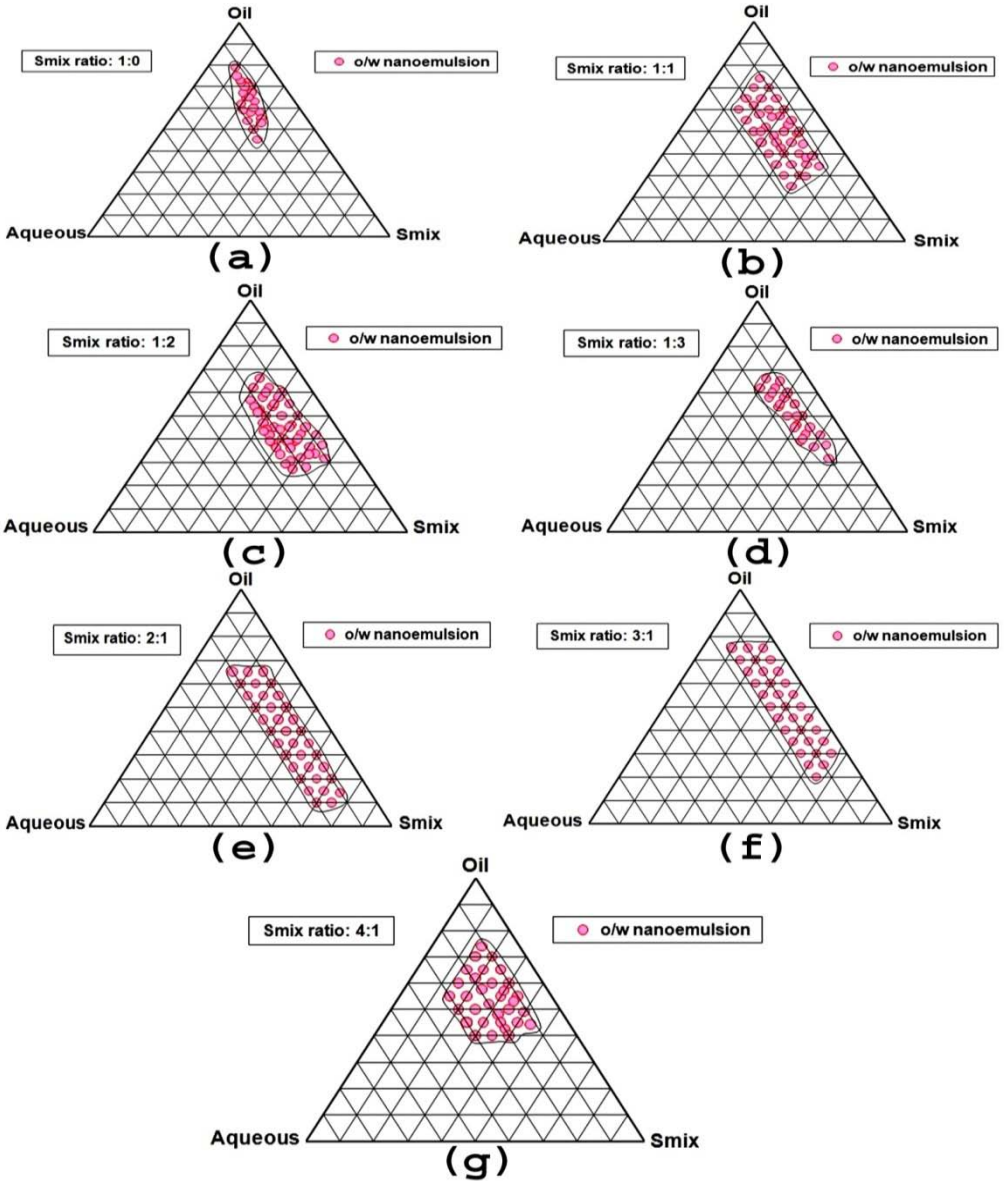


**Figure 5.3. Ternary phase diagrams indicating NEs (o/w) region at different $S_{mix}$ 1:0 (a), $S_{mix}$ 1:1 (b), $S_{mix}$ 1:2 (c), $S_{mix}$ 1:3 (d), $S_{mix}$ 2:1 (e), $S_{mix}$ 3:1 (f) and $S_{mix}$ 4:1 (g)**

The co-surfactant concentration was increased to double at the $S_{mix}$ ratio (1:2); o/w NE area was good as compared with others [Figure 5.3c]. When cosurfactant concentration was increased to triple at the $S_{mix}$ ratio (1:3); o/w NE area was not found suitable due to too preliminary NE region as compare with $S_{mix}$ ratio (1:2) [Figure 5.3d]. The surfactant amount was increased to double and triple at the $S_{mix}$ ratio (2:1 and 3:1) where NE area was wide and appropriate [Figure 5.3e&f]. NE region was narrowed at a $S_{mix}$ ratio (4:1) in comparison with $S_{mix}$ (1:1) [Figure 5.3g] and gel area was also observed at higher concentration of surfactant which was unfavorable for development of NE.

**Table 5.1. Evaluation of thermodynamic stability of different formulations (5% w/w increasing amount of oil)**

| $S_{mix}$ ratio (S:Cos) | Amount of excipients in formulations (% w/w) | | | Observations based on the preparation and thermodynamic stability studies | | |
|---|---|---|---|---|---|---|
| | Oil | Milli-Q water | $S_{mix}$ | H & C[a] | Cent.[b] | Freeze Tha.[c] |
| 1:0 | 10 | 15 | 75 | √ | × | √ |
| | 15 | 25 | 60 | √ | √ | × |
| | 20 | 30 | 50 | √ | × | √ |
| | 25 | 28 | 47 | √ | × | √ |
| 1:1 | 10 | 25 | 65 | √ | √ | √ |
| | 15 | 35 | 50 | √ | √ | √ |
| | 20 | 28 | 52 | √ | √ | √ |
| | 25 | 30 | 45 | √ | √ | √ |
| | 30 | 35 | 35 | √ | √ | √ |
| 1:2 | 10 | 30 | 60 | √ | √ | √ |
| | 15 | 30 | 55 | √ | √ | √ |
| | 20 | 35 | 45 | √ | √ | √ |
| | 25 | 38 | 37 | √ | √ | √ |
| | 30 | 28 | 42 | √ | √ | √ |
| 1:3 | 10 | 35 | 55 | √ | √ | √ |
| | 15 | 40 | 45 | √ | √ | √ |
| | 20 | 25 | 55 | √ | √ | √ |
| 2:1 | 10 | 20 | 70 | √ | √ | √ |
| | 15 | 28 | 47 | √ | √ | √ |
| | 20 | 36 | 44 | √ | √ | √ |
| | 25 | 40 | 35 | √ | √ | √ |
| | 30 | 30 | 40 | √ | √ | √ |
| 3:1 | 10 | 18 | 72 | √ | √ | √ |
| | 15 | 33 | 52 | √ | √ | √ |
| | 20 | 37 | 43 | √ | √ | √ |
| 4:1 | 10 | 22 | 68 | √ | √ | √ |
| | 15 | 20 | 65 | √ | √ | √ |
| | 20 | 32 | 48 | √ | √ | √ |
| | 25 | 36 | 39 | √ | √ | √ |
| | 30 | 40 | 30 | √ | √ | √ |

[a]Heating and cooling cycle (H & C); [b]Centrifugation (Cent.); [c]Freeze-thaw cycle (Freeze Tha.)

*5.12.4. Thermodynamic stability study*

The formulations were tested for heating-cooling cycle, centrifugation and freeze-thaw cycle stress no obvious consequence was seen during the test. However, some formulations were unstable as represented in Table 5.1.

### *5.12.5. Selection of formulations from phase diagrams and development of GN loaded nanoemulsions*

From each phase diagram, different amount of oil were selected in the range of 10 - 30% (w/w) so that maximum NEs region could be selected. The amount of oil was selected at a low amount of $S_{mix}$ from each phase diagram. The favorable event was observed in the NE region of phase diagram after incorporation of GN (1 mg/mL). Compositions of GN loaded NEs have been described in Table 5.2.

**Table 5.2. Compositions of GN encapsulated nanoemulsion formulations**

| NE Code | $S_{mix}$ (S:Cos) | Ingredients in nanoemulsions (% w/w) | | | | Oil:$S_{mix}$ Ratio |
|---|---|---|---|---|---|---|
| | | Oil | Water | S | Cos | |
| GN-NE1 | 1:1 | 10 | 25 | 32.5 | 32.5 | 1:6.5 |
| GN-NE2 | 1:2 | 15 | 30 | 18.34 | 36.66 | 1:3.6 |
| GN-NE3 | 2:1 | 20 | 36 | 29.34 | 14.66 | 1:2.2 |
| GN-NE4 | 3:1 | 15 | 33 | 39 | 13 | 1:3.4 |

*Where, 'S' = Surfactant, 'Cos'= Co-surfactant.*

For the development of nanoemulsion (o/w), labrasol (HLB = 14) and PEG 400 (HLB = 15.5) has been selected as surfactant and cosurfactant respectively and that could work better in a $S_{mix}$ ratio. Nanoemulsions (o/w) were fabricated through self nano-emulsification process which resulted into the thermodynamically stable system. Formulation containing the higher amount of surfactant may lead to undesirable effect to the skin. Thus, the lower amount of $S_{mix}$ was selected for development of optimized formulation.

### *5.12.6. Characterization of developed nanoemulsion*

Different NE1-4 were characterized through different parameters like droplet size, zeta potential (Figure 5.4), conductivity, %transmittance, viscosity, pH, R.I., %EE and %DL. The results have been shown in Table 5.3. Uniform droplets could enhance the drug solubility and stability in the formulation. The uniformity of the droplet size was indicated by PDI value. The low PDI value (0.218 ± 0.03) has been observed for the optimized formulation (GN-NE2) thus indicating uniformity of droplet size.

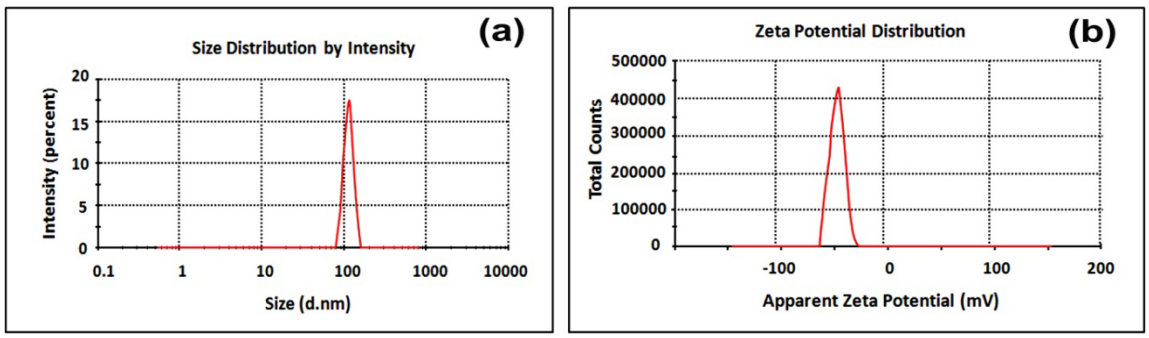


**Figure 5.4. Analysis of droplet size (a) and zeta potential (b) of optimized formulation, GN-NE2**

Suitable nano droplet size (110.2 ± 1.13 nm) and zeta potential (-33.1 ± 0.05 mV) were achieved with GN-NE2. Zeta potential plays an important role in the stability of the formulation. Favorable zeta potential was obtained which sustained the stability of the system. The high negative charge is probably influenced by the anionic groups of the fatty acids present in the oil and $S_{mix}$ of the formulation.

*5.12.7. TEM and UV - spectrum analysis*

TEM photomicrograph of the optimized formulation, GN-NE2 has been depicted in Figure 5.5 (a). The surface of the droplet was seen as a dark spot in a photograph, which may be due to the dispersed oil droplets. Droplet size measured through TEM was quite similar to that obtained by Zetasizer.

UV spectrum showed that GN was encapsulated in the GN-NE2 formulation, when scanned at 260 nm wavelength as like as the pure GN. The peak of UV spectra of GN-NE2 has been very slightly shifted due to drug entrapment with NE matrix. Detail has been graphically represented in Figure 5.5 (b).

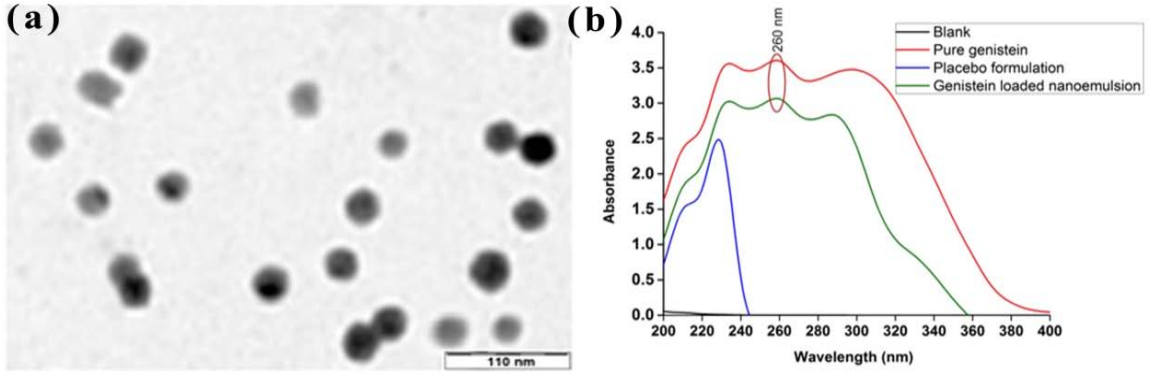


**Figure 5.5. TEM photograph (a) and UV spectrum of pure GN, placebo formulation and GN-NE2 formulation (b)**

**Table 5.3. Characterization of genistein loaded different nanoemulsions**

| NE code | (%EE) | (%DL) | Z-average (nm) | PDI | Z.P. (mV) | pH | Viscosity (cP) | Cond. (ms/cm) | P.T. | R.I. |
|---|---|---|---|---|---|---|---|---|---|---|
| GN-NE1 | 88.95 ± 0.45 | 0.89 ± 0.01 | 220.8 ± 1.45 | 0.305 ± 0.06 | -53.2 ± 0.31 | 6.88 ± 0.23 | 10.32 ± 0.12 | 0.78 ± 0.11 | 82.86 ± 0.23 | 1.313 ± 0.21 |
| GN-NE2 | 99.92 ± 0.10 | 1.01 ± 0.03 | 110.2 ± 1.13 | 0.218 ± 0.03 | -33.1 ± 0.05 | 7.04 ± 0.12 | 9.85 ± 0.78 | 0.52 ± 0.76 | 98.95 ± 0.83 | 1.306 ± 0.12 |
| GN-NE3 | 90.67 ± 0.21 | 0.91 ± 0.04 | 232.4 ± 1.09 | 0.364 ± 0.01 | -45.5 ± 0.21 | 7.15 ± 0.24 | 12.39 ± 0.27 | 0.67 ± 0.58 | 89.26 ± 0.19 | 1.321 ± 0.68 |
| GN-NE4 | 92.77 ± 0.34 | 0.93 ± 0.08 | 216.8 ± 1.15 | 0.295 ± 0.07 | -39.3 ± 0.08 | 6.90 ± 0.18 | 14.19 ± 0.51 | 0.72 ± 0.19 | 86.78 ± 0.95 | 1.356 ± 0.84 |

%EE: Percentage entrapment efficiency; %DL: Percentage drug loading; PDI: Polydispersity index; Z.P.: Zeta potential; Visco.: Viscosity; Cond.: Conductivity; P.T.: Percentage transmittance; R. I.: Refractive index. Values were Mean ± SD (n = 3).

### *5.12.8. HPTLC study*

HPTLC analysis produced a sharp and well-defined symmetrical chromatogram peak when the chamber was saturated with the mobile phase for 30 min at a 25 ± 0.5 °C temperature. HPTLC chromatogram of pure GN (a) and GN-NE2 (b) confirmed the $R_f$ value of 0.44 and 0.45 at 254 nm respectively as shown in Figure 5.6 and 5.7. The result stated that the GN was encapsulated in the NE and found quite compatible with their excipient, which was used for NE development.

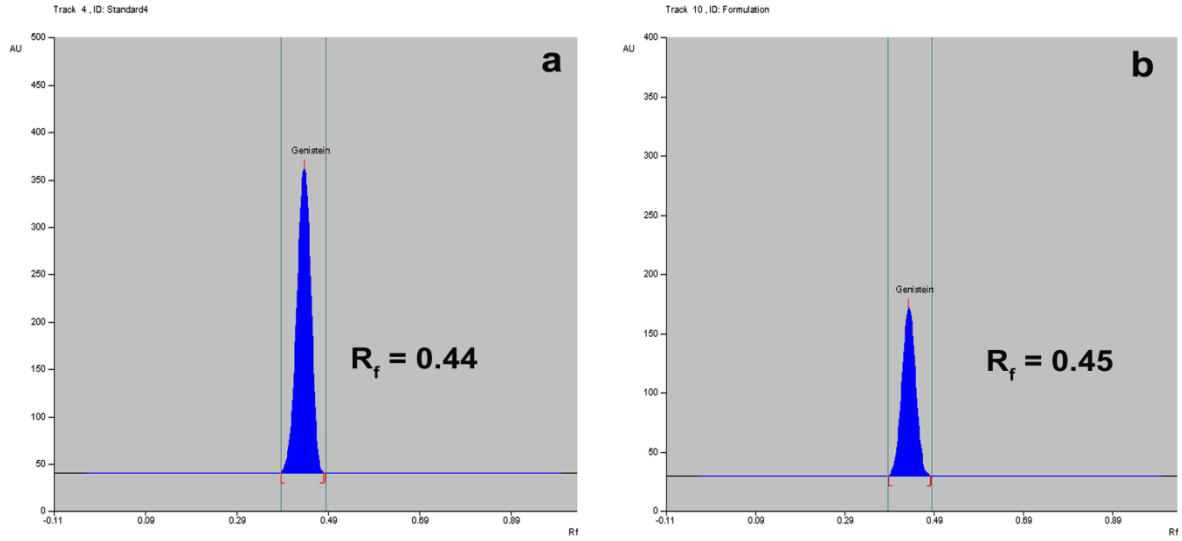


**Figure 5.6. HPTLC chromatogram of pure GN (a) and GN loaded nanoemulsion, GN-NE2 (b)**

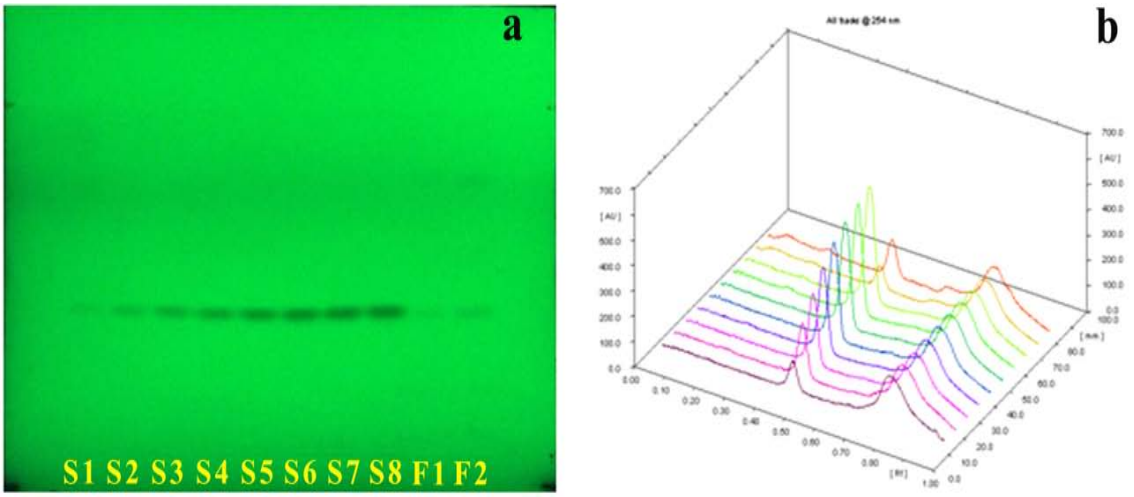


**Figure 5.7. HPTLC plate (a) and 3D-chromatogram (b) of pure GN and GN-NE2 formulation at 254 nm (S1-8 = Standard GN and F1-2 = GN-NE2 formulation)**

### *5.12.9. FTIR - spectrum analysis*

The chemical compatibility of GN with the excipients was analyzed by FTIR which was used in the GN-NE2 formulation. Details of FTIR spectrum have been shown in Figure 5.8 (a, b). The wave numbers of FTIR spectra of pure GN (a) at 910.40, 1043.49, 1145.71, 1205.51,1425.40, 1566.20 and 1614.41 $cm^{-1}$ were corresponded to C-H alkenes, -C-O alcohols, -OH aromatic, C-O alcohols, C-H alkanes, C=C aromatic ring and C=C alkenes respectively. Stretching of O-H (phenolic) was found at 3414.0 $cm^{-1}$. In case of GN-NE2 (b) formulation, the wave numbers at 910.40, 1145.71, 1205.51, 1425.40, 1566.20 and 1614.41 and 3414.00 $cm^{-1}$ were slightly shifted to 912.32, 1172.72, 1232.51, 1502.54, 1562.34 and 3136.25 $cm^{-1}$ respectively. Other wave numbers at 1815.01, 2104.33, 2951.08, 3035.95 and 3981.07 $cm^{-1}$ were also slightly shifted to 1710.85, 2129.41, 2964.59, 3078.39 and 3977.21 $cm^{-1}$ respectively. It may be due to the coordination bonding of several -OH groups of parent ring with the water content of the nanoemulsion (o/w). This result affirms that GN was pretty compatible with their excipients used in the formulations.

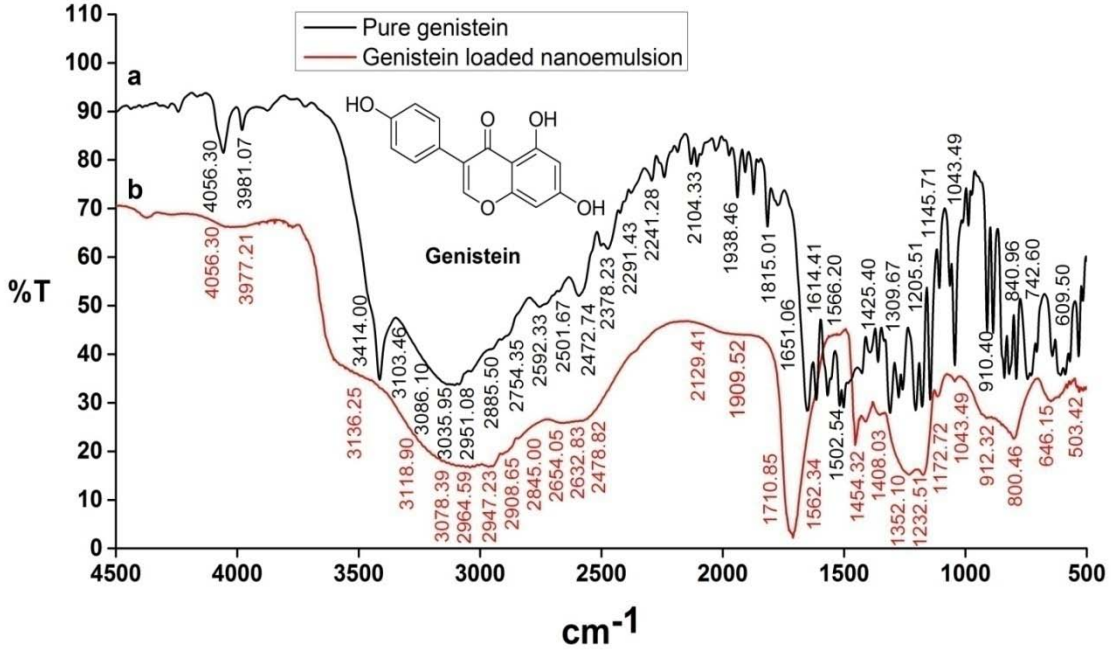


**Figure 5.8. FTIR spectrum of pure GN (a) and GN-NE2 (b)**

### *5.12.10. Analysis of stability test*

Stability of optimized formulation, GN-NE2 was evaluated during the period of 0, 30, 60 and 90 days at 40°C. No apparent changes were observed in the droplet size, zeta potential and pH of the GN-NE2 formulation and results have been explained in Table 5.4. A first order degradation of GN content in the GN-NE2 was found to be 1.22% at

the remainder of 90 days as shown in Figure 5.9. Results, confirms that the GN-NE2 was stable at 40°C for longer periods. Shelf life ($t_{90}$) of GN based nano-gel was found to be 2.98 years.

**Table 5.4. Stability test of optimized GN-NE2 formulation**

| Time (days) | Tempe -rature (°C) | Droplet size (nm) | Zeta potential (mV) | pH | % Drug remained | Log % drug remained |
|---|---|---|---|---|---|---|
| 0 | 40 ± 2 (75 ± 5% RH) | 110.07 ± 1.04 | -33.3 ± 0.21 | 7.07 ± 0.11 | 100.00 | 2.00 |
| 30 | | 110.05 ± 0.12 | -32.9 ± 0.12 | 6.65 ± 1.15 | 99.62 | 1.9983 |
| 60 | | 109.88 ± 1.25 | -32.6 ± 0.38 | 6.78 ± 1.10 | 99.23 | 1.9966 |
| 90 | | 108.97 ± 2.09 | -32.7 ± 1.02 | 6.85 ± 1.08 | 98.78 | 1.9946 |

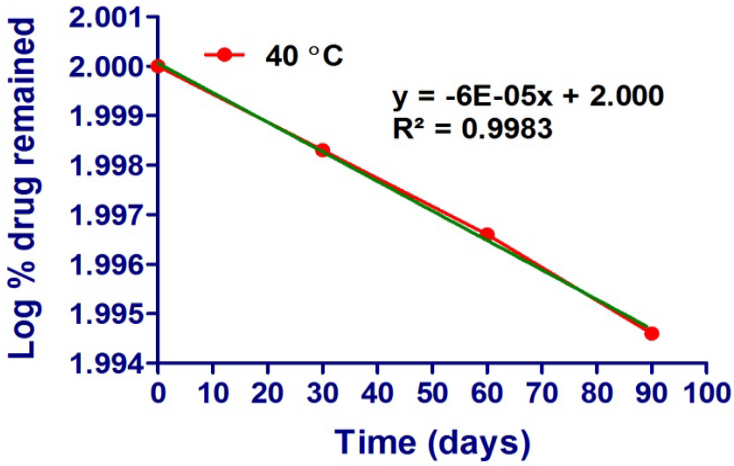


**Figure 5.9. Degradation kinetics of GN from GN-NE2 at 40°C**

*5.12.11. Rheological behavior studies*

The viscosities were observed for placebo-NG2 and GN-NG2 formulation in the range of 20 to 0.0268 and 1910 to 3.14 Pa.s respectively. Higher viscosity was attributed for GN-NG2 due to the drug which integrated into the gel matrix of carbopol 940 and leads to close proximity therefore viscosity was increased. The GN-NG2 showed non-Newtonian shear thinning behavior and viscosity decreases with the rate of shear stress. Thus, the nano-gel formulation may be suitable for transdermal (skin) application. Details have been shown in Figure 5.10.

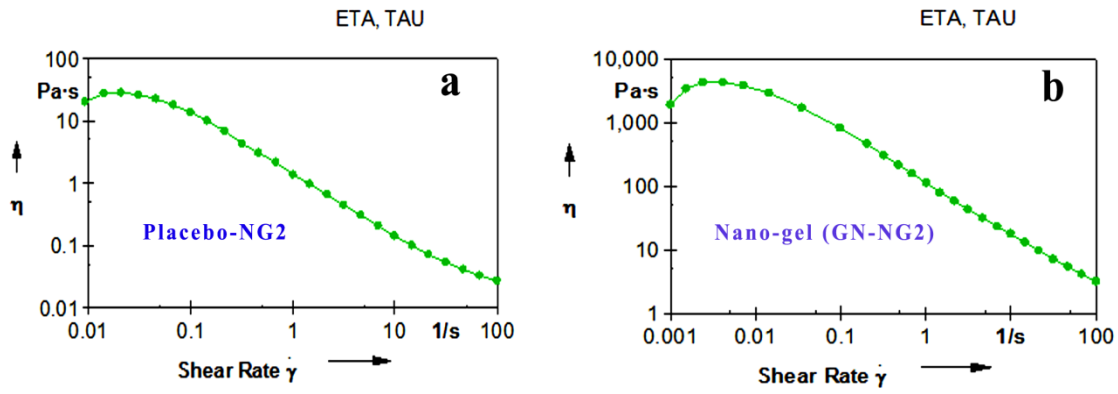


**Figure 5.10. Rheogram of placebo-NG2 (a) and GN-NG2 (b) where, η = viscosity (Pa.s), γ = shear rate (1/s)**

Carbopol-940 was used as a gelling agent and viscosity modifier resulting in enhanced membrane permeability through the skin (Lala and Awari, 2014).

*5.12.12. Testing of spreadability*

The semi-solid placebo-NG2 and GN-NG2 formulation exhibited good spreadability at 60.67 ± 0.21 and 62.98 ± 0.15% w/w respectively that would assure the practicability to skin administration. No significant difference ($P < 0.05$) between the spreadability of placebo-NG2 and GN-NG2 were seen in this study.

*5.12.13. Skin permeability profiles*

The % cumulative skin permeability of GN from different GN-NE1-4, GN-NG2 and GN-CG were studied as shown in Figure 5.11 (a & b). The best release profile (93.81 ± 3.33%) was achieved with the GN-NE2 as compared with other formulation for 24 h. Skin permeability of GN-NG2 and GN-CG was found to be 95.99 ± 2.70 and 56.57 ± 1.86% respectively for 24 h. GN-NG2 showed better skin permeability, which may be due to enhanced solubility, nano-droplet size, favorable zeta potential and an appropriate pH comparatively to others. However a significant difference between skin permeation profile of GN-CG and GN-NG2 was observed. This may be due to the poor permeability of conventional gel because of its distribution of non-uniform droplet size and low solubility. Conventional gel contains no nano-carrier system to increase the solubility hence low permeability was achieved.

The transdermal flux [*Jss* (µg/h/cm$^2$)] and permeability coefficient [*Kp* (cm/h)] of GN from different formulations across to the skin have been explained through Figure 5.11 (c) and Table 5.5. The maximum steady flux (2.322 ± 0.42 µg/h/cm$^2$) and permeability (0.0994 ± 0.03 cm/h) were significantly achieved with GN-NG2 ($^{a,b}P < 0.01$) when compared with other formulations. The lag time was found to be 0. 0.27 h for GN-NG2.

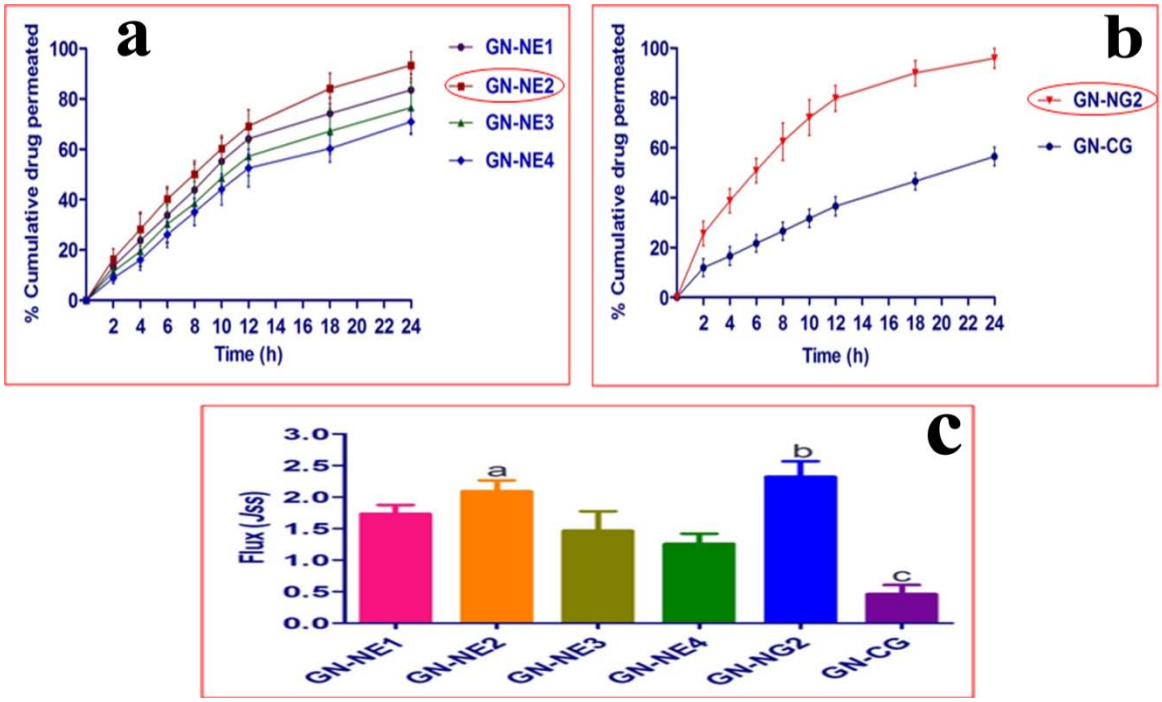


**Figure 5.11. Skin permeability profiles of GN from different nanoemulsions (a) GN-NE1-4, (b) GN-CG and GN-NG2 through rat skin and (c) steady state flux of different formulations across rat skin**
**[Values were mean ± SEM (n = 3), $^{a,b}P < 0.01$, $^{c}P < 0.05$ when compared to the conventional group]**

**Table 5.5. Transdermal steady state flux and permeability coefficient of formulations across rat skin, Mean ± SEM**

| Formulation | Steady state flux *Jss* (µg $cm^{-2}$ $h^{-1}$) | Lag time (h) | Permeation coefficient Kp (×$10^{-3}$ cm $h^{-1}$) |
|---|---|---|---|
| GN-NE1 | 1.734 ± 0.24 | 0.2857 | 0.0867 ± 0.02 |
| GN-NE2 | 2.091 ± 0.30 | 0.2593 | 0.1045 ± 0.01 |
| GN-NE3 | 1.463 ± 0.53 | 0.3097 | 0.0731 ± 0.05 |
| GN-NE4 | 1.250 ± 0.27 | 0.3316 | 0.0625 ± 0.04 |
| GN-NG2 | 2.322 ± 0.42 | 0.2664 | 0.0994 ± 0.03 |
| GN-CG | 0.459 ± 0.25 | 0.4495 | 0.0229 ± 0.07 |

Nano-gel showed enhanced drug skin permeability after transdermal application, which may be due to diffusion of aqueous content from the formulation and increased drug release. Labrasol and PEG 400 are also acting as permeation enhancer which could

play a role in the drug permeability by reducing the diffusion barrier of the *stratum corneum*.

*5.12.14. Study of skin irritation*

There were no serious clinical signs of irritation, erythema or oedema observed throughout the study. These results indicated that the GN based nano-gel formulation was non-irritant and safe for skin application.

*5.12.15. Release kinetics of GN based nanoemulsion and gel formulation*

Skin permeation data of GN-CG and GN-NG2 were fitted with Zero-order, First-order, Higuchi's model, Korsmeyer-Peppas model. The best release pattern of GN-CG ($r^2$ = 0.937) and GN-NG2 ($r^2$ = 0.992) was achieved with Korsmeyer-Peppas model. The GN-NG2 showed a non-Fickian pattern (0.5 < *Kp* < 1) of drug release by diffusion and matrix erosion. Details of drug release kinetics of GN loaded different formulations have been shown in Table 5.6.

**Table 5.6. Drug release kinetic profiles of GN loaded different formulations**

| Formulations | Zero order | | First order | | Higuchi's model | | Korsmeyer-Peppas model | |
|---|---|---|---|---|---|---|---|---|
| | $r^2$ | *k* | $r^2$ | *k* | $r^2$ | *k* | $r^2$ | *n* |
| GN-NE1 | 0.919 | 10.89 | 0.993 | 2.002 | 0.966 | - 7.483 | 0.852 | 0.443 |
| GN-NE2 | 0.926 | 13.12 | 0.990 | 2.049 | 0.977 | - 7.257 | 0.828 | 0.491 |
| GN-NE3 | 0.932 | 8.67 | 0.991 | 1.997 | 0.963 | - 7.877 | 0.873 | 0.401 |
| GN-NE4 | 0.936 | 6.71 | 0.986 | 1.997 | 0.953 | - 8.437 | 0.902 | 0.343 |
| GN-NG2 | 0.845 | 22.27 | 0.997 | 2.013 | 0.979 | - 0.146 | 0.748 | 0.605 |
| GN-CG | 0.965 | 6.82 | 0.995 | 1.982 | 0.978 | - 4.267 | 0.840 | 0.408 |

*5.12.16. Efficacy evaluation of GN based gel formulations against UVA exposure*

In group II (UVA irradiated), the level of antioxidant enzyme was decreased significantly when compared with control group (untreated UV irradiation) [Figure 5.12 (a, b)]. In test groups (III and IV), the levels of cutaneous antioxidant enzyme systems like SOD, GPX and CAT have been significantly improved when treated with GN-CG ($^{c}P$ < 0.05) and GN-NG2 ($^{a,b}P$ < 0.01) respectively as compared with UVA irradiated group. The placebo-NG2 group could not produce any significant effect on the skin antioxidant system in comparison with group II, which may be due to placebo-gel (nano-gel formulation without GN loaded).

The higher level of TBARS was also been significantly decreased with nano-gel formulation as compared to the UVA irradiated group ($^{a,b}P < 0.01$). Details have been explained in Figure 5.12 (a, b).

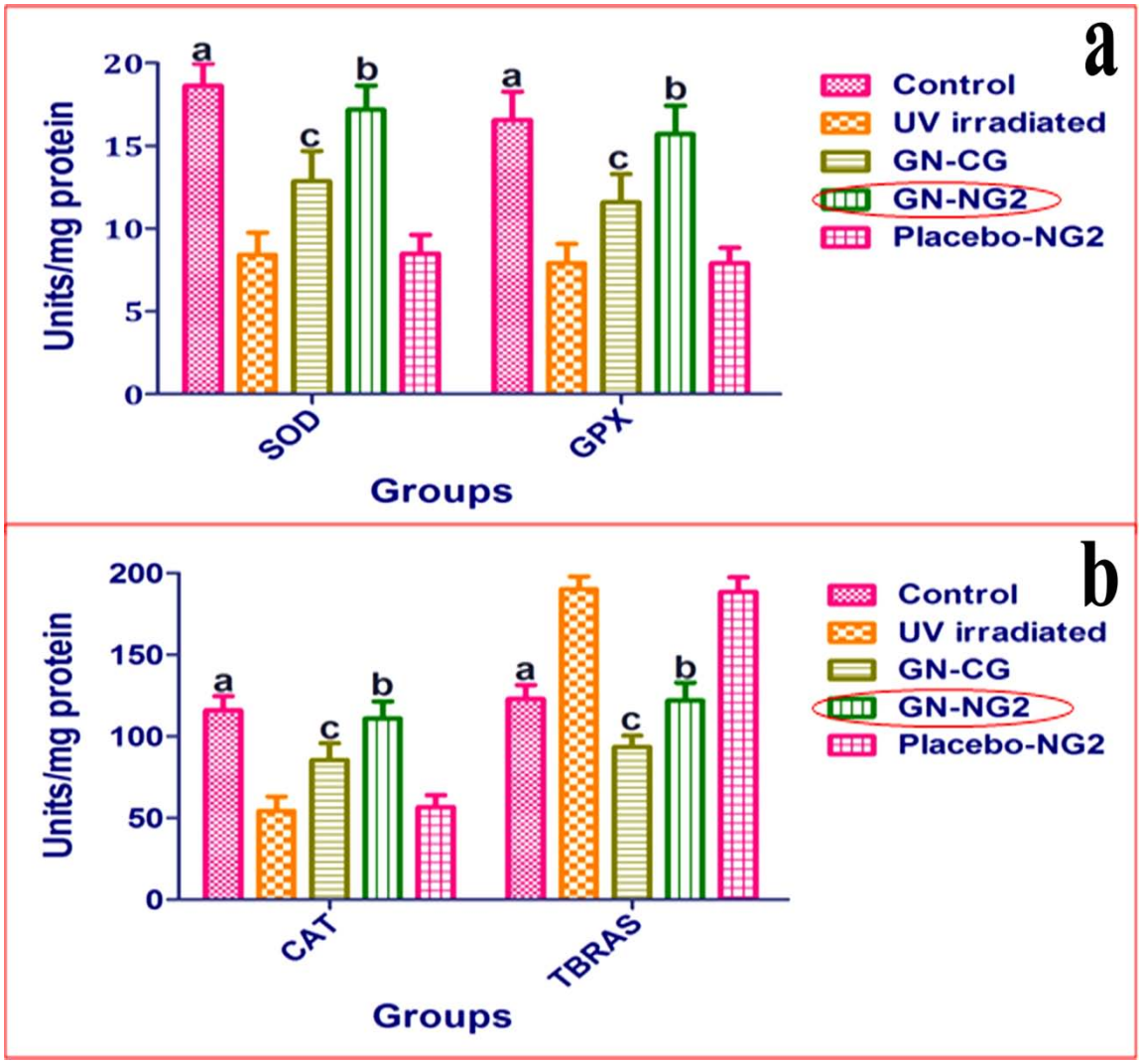


**Figure 5.12. Cutaneous antioxidant enzyme levels (a) SOD and GPX, (b) CAT and TBARS after transdermal application of GN based gel formulations**
**[Values are mean ± SEM (n = 6), $^{a,b}P < 0.01$, $^{c}P < 0.05$ when compared to the control and UVA irradiated group]**

The GN-CG group showed less cutaneous protection potential than the GN-NG2 due to less availability of GN to the systemic circulation and associated tissue. Nano-gel showed enhanced photoprotective potential because of its improved permeability than its conventional gel. Thus, GN loaded transdermal nano-gel formulations could enhance UV protective activity for longer periods than the conventional gel.

*In vivo* antioxidant potential of nano-gel formulations were found significant against UVA exposure except placebo gel formulation. Nano-gel exhibited better UV protective and sun-screening activity after its transdermal administration. This activity may be due to its improved permeability and sustained-release profile. Result demonstrated that the use of genistein in transdermal nano-gel formulation might increase its penetration or absorption capacity inside the skin layers and that the availability of a sufficient drug concentration may be responsible for better sun/photo-protection. Transdermal route can avoid hepatic first-pass metabolism and resulting in the prolongation of duration drug action (Zhang et al., 2010).

### *5.12.17. In vivo bioavailability of GN*

The bioavailability of GN was studied after administration of its oral suspension (20 mg GN) and GN-NG2 (~20 mg GN). Results have been represented in Figure 5.13 and Table 5.7. GN has been well released and permeated from GN-NG2 in comparison with oral suspension for extended periods (24 h). Statistically significant $C_{max}$, $T_{max,}$ MRT and AUC profiles were observed with oral suspension and GN-NG2 ($P < 0.05$). The $C_{max}$ of GN was found to be 57.48 ± 4.42 and 95.06 ± 4.09 $ngmL^{-1}$ for oral suspension and GN-NG2 respectively. The $AUC_{0-t\infty}$ (911.55 ± 69.11 $nghmL^{-1}$), $T_{max}$ (6.53 ± 0.19 h) and $MRT_{0-t\infty}$ (8.52 ± 0.38 h) were higher for GN-NG2 comparatively to the pure GN-oral suspension ($P < 0.05$). The $t_{1/2}$el of GN was increased with nano-gel (3.81 ± 0.25 h) while the Kel (0.18150 ± 0.01 $h^{-1}$) and Cl (0.02259 ± 0.02 $Lh^{-1}$) were also lowered. The mean value of $AUC_{0-t}$ by transdermal route was 3.52 times higher than oral route, and the difference was found to be statistically significant ($P < 0.05$). This could be due to avoidance of hepatic first-pass metabolism by the transdermal route.

Reported oral bioavailability of GN (20 mg/kg) was ~24% because of its extreme hepatic first-pass metabolism (Kwon et al., 2007). In the present study, relative bioavailability (*F*) of GN was found to be 352.58 by transdermal route. This indicates enhanced bioavailability of nano-gel through transdermal route and avoidance of hepatic first-pass metabolism. This may be also due to that the nano-gel releases drug in a sustained manner for 24 h periods. For transdermal route, *stratum corneum* acts as a permeation barrier and thereby the sustained-release activity was produced with nano-gel in comparison with orally administered suspension which is an immediate release dosage form. Therefore, GN based nano-gel could provide an effective approach for the treatment and management of skin damage caused by intemperate exposure of the UV radiations.

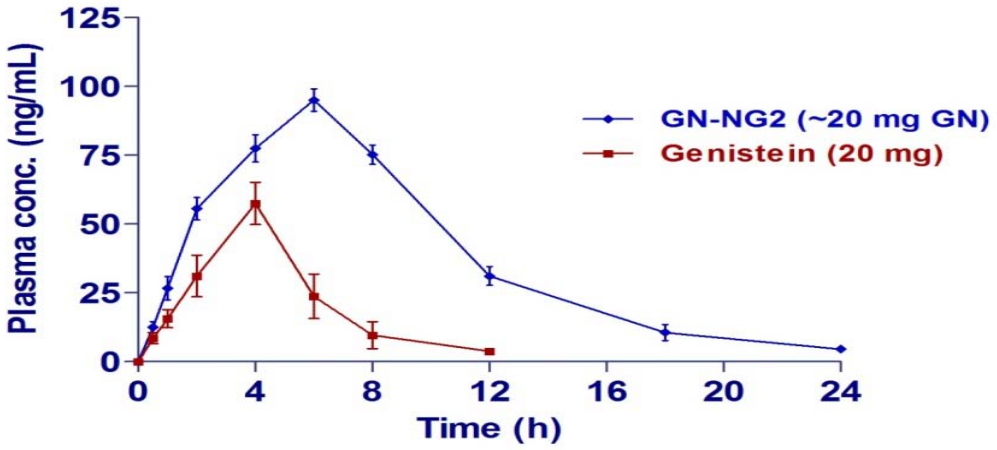


**Figure 5.13. Plasma profiles of GN in rats after administration of pure GN and GN-NG2 [Values were mean ± SEM (n = 6)]**

**Table 5.7. Pharmacokinetic profiles of GN in rats after administration of pure GN oral suspension and GN-NG2 [Values represented were mean ± SEM (n = 6)]**

| Pharmacokinetic parameter | Oral suspension (20 mg of GN) | GN-NG2 (~ 20 mg of GN) |
|---|---|---|
| $C_{max}$ ($ngmL^{-1}$)[a] | 57.48 ± 4.42 | 95.06 ± 4.09 |
| $T_{max}$ (h)[b] | 4.34 ± 0.12 | 6.53 ± 0.19 |
| $AUC_{0-t}$ ($nghmL^{-1}$)[c] | 251.06 ± 8.81 | 885.20 ± 63.27 |
| $AUC_{0-t\infty}$ ($nghmL^{-1}$)[d] | 266.81 ± 5.09 | 911.55 ± 69.11 |
| $AUMC_{0-t}$ ($nghmL^{-1}$)[e] | 1151.94 ± 75.16 | 7023.65 ± 723.43 |
| $AUMC_{0-t\infty}$ ($nghmL^{-1}$)[f] | 1414.43 ± 64.79 | 7810.07 ± 915.70 |
| $MRT_{0-t}$ (h)[g] | 4.58 ± 0.14 | 7.90 ± 0.25 |
| $MRT_{0-t\infty}$ (h)[h] | 5.31 ± 0.22 | 8.52 ± 0.38 |
| ($t_{1/2}$el) (h)[i] | 2.53 ± 0.68 | 3.81 ± 0.25 |
| Kel ($h^{-1}$)[j] | 0.27419 ± 0.06 | 0.18150 ± 0.01 |
| Cl ($Lh^{-1}$)[k] | 0.07967 ± 0.01 | 0.02259 ± 0.02 |
| Vd (L)[l] | 0.29056 ± 0.07 | 0.12446 ± 0.04 |
| %*F*[m] | - | 352.58 |

[a]Peak of maximum concentration; [b]Time of peak concentration; [c]Area under the concentration-time curve until last observation; [d]Area under the concentration-time curve until infinite observation; [e]Area under moment curve computed to the last observation; [f]Area under moment curve computed to the infinite observation; [g]Mean residence time to the last observation; [h]Mean residence time to the infinite observation; [i]Elimination half life; [j]Elimination rate constant; [k]Clearance; [l]Volume of distribution; [m]Relative bioavailability of genistein.

## 5.13. Conclusion

Intense UV irradiation interacts with the cutaneous antioxidant system and intervenes to oxidative stress. ROS generated as an intermediate product of UV irradiation may oxidize and damage the cellular lipids, proteins and DNA. This intermediated product leads to the alteration of skin structures and results in obstruction of normal function of the cellular antioxidant system of skin. The improved antioxidant potential was achieved with nano-gel formulation which may be due to enhanced relative bioavailability of genistein (352.58%). Nano-gel released the GN content in a sustained manner for longer periods. The GN-NG2 was found to be stable, safe and effective for topical application. Genistein nano-gel of was developed with nanoemulsion that could be promising as a useful strategy for sun or photoprotection against UVA-mediated oxidative stress.

## 5.14. Publication

- Ranjit K Harwansh, Pulok K Mukherjee, Sayan Biswas. Nanoemulsion based nano-gel of genistien enhancing UVA protection efficacy and bioavailability by improving its pharmacokinetics through transdermal route. Journal of Pharmaceutical and Biomedical Analysis, Elsevier, 2016, Impact Factor: 2.82 (Communicated).

# Chapter - 6

## Summary and conclusion

6.1. Summary

6.2. Conclusion

## 6.1. Summary

The phytopharmaceuticals and plant derived drugs are being used as therapeutic agents, nutraceuticals and dietary supplements because of their several health benefits. Phytomolecules have been explored for their vast pharmacological activities such as antioxidants, anticancer, antiviral, hepatoprotective, anti-inflammatory, antidiabetic, antiobesity, UV-protective etc. The efficacy of bioactive molecules depends on effective delivery systems. Mostly phytomolecules are suffering from low aqueous solubility, low permeability, less half-life hence poor bioavailability which may due to gastro intestinal degradation and extensive hepatic first-pass metabolism. To overcome these limitations of therapeutic efficacy and bioavailability of important phytomolecules, developing novel drug delivery systems (NDDS) are pioneering in the phytopharmaceuticals with better therapeutic potential are the main objective. NDDS is particularly suited for encapsulating the phytopharmaceuticals into carriers as it prevents their degradation and improves their stability as well as bioavailability. Nanoemulsion is a nanocarrier system suitable for encapsulating, protecting, and delivering poorly soluble phytopharmaceuticals and drugs at the target sites. This novel delivery system offers different advantages in comparison with conventional delivery systems such as stabilization of molecules in aqueous environment of stomach and foodstuffs with scarce solubility in aqueous environment. Goal of the present work is to enhance the permeability and bioavailability of low bioavailable phytopharmaceuitcals by improving its solubility through nanoemulsion as a carrier system. Drug delivery systems are one of the significant aspects for efficacy of the phytomolecules. Solubility and molecular size are the major rate limiting factors for molecules to cross the biological membrane and systemic absorption.

Nanoemulsions are isotropic and thermodynamically stable systems of oils, surfactants/co-surfactants and aqueous system. NEs can be produced in the form of fine droplets of o/w and w/o systems. Generally NEs are preparing by spontaneous nanoemulsification process. This method is very convenient and easy for developing phytomolecule encapsulated NEs. The aim of the study was to prepare NEs of some potent phytomolecules using nanoemulsification technique to enhance the bioavailability with stable formulation. Lipid or oil based nanoemulsion formulations are attracting considerable attention due to their capacity to increase the drug solubility, facilitating gastrointestinal absorption and reduce or eliminate the effect of food on the absorption of molecules and thus increasing their permeability as well as bioavailability. In most of cases NEs are either administered as liquid dosage forms, encapsulated either in hard or soft gelatin capsules. For transdermal application, NEs are administered in the form of gel after incorporating them into suitable gel matrix. This is an evolving delivery system of phytopharmaceutical for better biological activity as well as bioavailability.

The work performed in this thesis highlights on several aspects of development of novel drug delivery system with potent phytomolecules. Most of these phytomolecules which have therapeutic activities but less half-life and so they have metabolized and excreted from the body early. In this context the main purpose of this work was to increase the bioavailability of the molecules through development of some value added formulation of NDDS with several carriers. We have chosen ferulic acid, catechin and genistein as the biologically active phytopharmaceuticals which have less half-life and low bioavailability but have very important therapeutic potential. In order to combat the limitations of these molecules, the present study has been undertaken to develop a novel formulation. These include the preparation, characterization and evaluation of the nanoemulsions to ensure the enhanced bioavailability as well as therapeutic efficacy. Different nanoemulsions of these phytomolecules were prepared and evaluated for their physicochemical characteristics, stability studies, *in vivo* biological activities and pharmacokinetics studies. The detailed studies of these three phytomolecules have been described in the respective chapters of this thesis.

Chapter 1 of this thesis dealt with the several aspects on pharmacokinetics and bioavailability enhancement techniques and NDDS approaches of the phytopharmaceuticals. The therapeutic potential of most of the phytomolecules is restricted due to their low solubility and low bioavailability apart from their diverse health benefits. The pharmacokinetic profiles of phytomolecules are mainly depends on the various factors such as log P value, pH, absorption, distribution, metabolism, elimination etc. Pharmacokinetics and bioavailability related different aspects of important phytopharmaceuticals/phytomolecules have been described in chapter 1 of this thesis. The various formulation approaches and strategies for improving therapeutic efficacy and bioavailability of plant based bio-active molecules have been discussed in this chapter.

The development of novel drug delivery system of phytopharmaceuticals is pioneering for increasing their pharmacological activity and bioavailability which are associated with poor solubility. Several novel herbal dosage forms and delivery systems of therapeutically important phytoconstituents are being continuously exploited and explored for finding better therapeutic effect. Several aspects of the development of NDDS for phytomolecules with the special emphasis on nanoemulsion as a carrier system have been discussed in chapter 1 of this thesis. A book chapter “Bioavailability of herbal products: approach toward improved pharmacokinetics”, has been published in: P.K. Mukherjee (Eds.), Evidence-based validation of herbal medicine, Elsevier, Amsterdam, 2015, pp. 217-245.

Chapter 2 of the thesis highlights on the scope, objective and plan of work of the study to develop the nanoemulsions of some therapeutically potent phytomolecules such as ferulic acid, catechin and genistein which have less half-life, poor permeation/absorption and early elimination profile thereby poor bioavailability.

Chapter 3 described the development, characterization, pharmacological evaluation and bioavailability study of ferulic acid based different nanoemulsions and their nano-gel formulations. Ferulic acid (FA) is a potent polyphenolic antioxidant compound naturally found in food plants i.e. wheat, rice, barley, oats, citrus fruits, tomatoes, etc. (Alias et al., 2009). FA has been proven to afford significant protection to the skin against UV-B-induced oxidative stress in human lymphocytes and erythema (Prasad et al., 2007). Staniforth et al. have been reported that FA inhibited the UVB-induced matrix metalloproteinases and attenuates the degradation of collagen fibers, abnormal accumulation of elastic fibers and epidermal hyperplasia through posttranslational mechanisms (Staniforth et al., 2012). Other pharmacological activities of FA are reported as antiaging, hepatoprotective, antiatherogenic, antimutagenic, anti-inflammatory, anticancer, antidiabetic, neuroprotective and cardioprotective (Staniforth et al., 2012; Prasad et al., 2007). These activities are restricted due to its poor bioavailability and early clearance and elimination from the body.

Therefore it is utmost important that FA should be incorporated in some novel delivery system which can increase the concentration of FA and maintain its minimum effective level in blood for a longer period of time to enhance its therapeutic efficacy. Nanoemulsion of FA was developed with several excipients like oil, surfactant, co-surfactant and aqueous system by spontaneous nanoemulsification method. Solubility studies of FA in different excipients were analyzed and found to be maximum soluble in isostearyl isostearate (ISIS) as oil phase. Developed FA loaded NEs were characterized by measuring different parameters, including electrical conductivity, % transmittance, viscosity, pH, refractive index, drug entrapment efficiency (%EE), drug loading (%DL), droplet size, PDI and zeta potential. The favorable conditions were observed for FA-NEs. The drug-excipients compatibility of FA encapsulated NEs in comparison with pure FA were evaluated through UV-spectrophotometry, HPTLC, FTIR analysis and it was observed that FA was quite compatible with the excipients used for development of formulations. The shape and surface morphology of the optimized formulations, FA-NE3 was evaluated through TEM analysis and it was observed that the droplets appeared as dark spot due to dispersed oil droplets. The size of droplet (~100 nm) was similar to that obtained by Zetasizer. Also the accelerated stability of the optimized formulation was studied and found stable for longer periods. The different FA-NE1-5, FA-CG and FA-NE3 based nano-gel (FA-NG) was evaluated for *ex vivo* skin permeation studies through rat's skin. Skin permeability studies were resulted that the nano-gel formulation significantly ($P < 0.01$) released the drug for extended period of time in a sustained manner in comparison with its conventional gel. The UV-protection efficacy of various gel formulations were evaluated on the rats skin against UVA mediated oxidative stress. Among the different gel formulations, nano-gel exhibited better antioxidant activity by improving the cutaneous antioxidant enzyme levels of skin against UVA mediated oxidative stress. It may be due to its enhanced permeability profile (96.95%) for extended periods. Skin irritation study of nano-gel was also evaluated along with its placebo gel.

There were no substantial clinical signs of irritation, erythema or oedema observed throughout the study period. These results indicated that the nano-gel formulation of FA (FA-NG3) was non-irritant and safe for topical application.

*In vivo* bioavailability study of ferulic acid was performed in rats after administration of its oral suspension (5 mg FA) and FA-NG3 (equivalent to 5 mg FA). Result stated that FA has been well released and permeated from FA-NG3 as compared to the oral suspension for longer periods (48 h). The $C_{max}$ of FA was found to be 80.98 ± 6.93 and 96.21 ± 5.49 $ngmL^{-1}$ after administration of oral suspension and FA-NG3 respectively. The $T_{max}$ and MRT were higher for transdermal nano-gel than the oral administration ($P < 0.05$). The mean value of $AUC_{0-t}$ by transdermal route was 3.96 times higher than that of oral route, and the difference was found to be statistically significant ($P < 0.05$). This indicated enhanced bioavailability of FA from the transdermal nano-gel. This could be due to avoidance of first-pass hepatic metabolism by transdermal route. The reported oral bioavailability of FA was 9% because of hepatic first-pass metabolism. In the current investigation, the relative bioavailability (*F*) of FA by transdermal route was found to be 396.26. Thus, FA loaded nano-gel could provide an effective strategy for the management of skin damage by extreme exposure of the UV radiations. Thus a thorough study of FA based NEs have been done and reported in this chapter. A research paper entitled “Enhanced permeability of ferulic acid loaded nanoemulsion based gel through skin against UVA mediated oxidative stress” has been published in *Life Sciences*, Elsevier, 2015, 141, 202-211, doi: 10.1016/j.lfs.2015.10.001.

Formulation, characterization, pharmacological evaluation and bioavailability studies of catechin based nanoemulsions and their nano-gel formulation have been described in chapter 4. Catechin (CA) is a flavanol type polyphenolic antioxidant molecule which is present in green tea, red wine, coffee, apple, chocolate and several nutritional and functional food products (Pomponio et al., 2003; Dube et al., 2010). CA possesses potent antioxidant potential and is capable of scavenging free reactive oxygen radicals by virtue of its reducing properties arising from the multiple hydroxyl groups attached to the aromatic rings. CA has been proven to afford significant photoprotection to the skin against UV-mediated oxidative stress (Levin and Maibach, 2002), photo-damage, basal cell carcinoma, melanoma and sunburn (Fang et al., 2007). It inhibits the expression of inflammation-associated enzymes, matrix metalloproteinases (MMPs) and restores levels of cutaneous antioxidant enzymes (Pinnell, 2003). Other different activities of CA have been reported including antiaging, antidiabetic, neuroprotective, anti-obesity, antibacterial, hypolipidemic, anti-HIV and anti-inflammatory. Despite their exciting array of therapeutic effects, CA has a short (1.25 h) half-life ($t_{1/2}$) (Manach et al., 2005) and less than 5% oral bioavailability because of their extensive first-pass hepatic metabolism and elimination (Chen et al., 2011). Poor oral bioavailability of CA is also associated with its digestive instability and poor intestinal uptake (Tang et al., 2013).

Thus, to enhance the bioavailability of CA is necessary for fulfillment of the optimum therapeutic efficacy. It should be made by encapsulating in suitable carrier system which can increase the solubility of CA and thereby the bioavailability for an extended periods in a sustained manner. CA loaded different nanoemulsions are prepared with several excipients by using spontaneous nanoemulsification process. CA solubility was performed in different oil components and optimum solubility was observed in ethyl oleate (EO). CA loaded different NEs were characterized by measuring different parameters, including electrical conductivity, % transmittance, viscosity, pH, refractive index, %EE, %DL, droplet size, PDI and zeta potential. The favorable conditions were observed for CA-NEs. The drug-excipients compatibility of CA loaded NEs along with pure CA were evaluated through UV-spectrophotometry, HPTLC, FTIR analysis and it was observed that CA was quite compatible with the excipients. The TEM morphology of the optimized formulations (CA-NE4) was evaluated and it was observed that the surface of the droplet was observed as a dark spot in a photograph, which may be due to the dispersed oil droplets. Droplet size (100 nm) produced by TEM was quite similar to that obtained by Zetasizer. The accelerated stability of the optimized formulation was also studied and found stable at 40ºC for longer periods. Shelf life ($t_{90}$) of CA based nano-gel was found to be 3.23 years. Skin permeation studies of different formulations (CA-NE1-5, CA-CG and CA-NE4 based nano-gel (CA-NG4) were evaluated through rat's skin. From result it can be revealed that the nano-gel formulation significantly ($P$ < 0.01) released the drug for 24 h in a sustained manner in comparison with its conventional gel. *In vivo* UV-protection efficacy of CA based different gel formulations were studied on the rat's skin against UVA induced oxidative stress. Nano-gel of CA showed enhanced photoprotection activity by improving the cutaneous antioxidant enzyme levels of skin against UVA induced oxidative stress. This may be due to its enhanced permeability profile (96.62%) for longer periods. Evaluation of skin irritation study of CA nano-gel was also performed along with its placebo gel. There were no substantial clinical signs of irritation, erythema or oedema observed throughout the study period. These results indicated that the nano-gel was non-irritant and can be safe for skin application.

The bioavailability study of CA was performed after administration of its oral suspension (5 mg CA) and CA-NG4 (≈5 mg CA). CA has been well released and permeated from CA-NG4 as compared to the oral suspension for longer periods (72 h). Statistically significant $C_{max}$, $T_{max,}$ MRT and AUC profiles were observed with oral suspension and CA-NG4 ($P$ < 0.05). The $C_{max}$ of CA was found to be 87.52 ± 8.56 and 93.79 ± 6.19 $ngmL^{-1}$ after administration of oral suspension and CA-NG4 respectively. The $AUC_{0\text{-}t\infty}$ (2653.99 ± 515.02 $nghmL^{-1}$), $T_{max}$ (12.05 ± 0.02 h) and $MRT_{0\text{-}t\infty}$ (35.98 ± 10.34 h) were higher for CA-NG4 comparatively to the oral suspension ($P$ < 0.05). The $t_{1/2}$el of CA was increased when it was in the nano-gel (24.75 ± 13.60 h) form and eventually the Kel (0.028 ± 0.02 $h^{-1}$) and Cl (0.0021 ± 0.04 $Lh^{-1}$) of the molecule in nano-gel form were also lowered.

The mean value of $AUC_{0-t}$ by transdermal route was 8.94 times higher than that of oral route, and the difference was found to be statistically significant ($P < 0.05$). This could be due to avoidance of first-pass hepatic metabolism by the transdermal route. The reported oral bioavailability of CA was 5% because of hepatic first-pass metabolism (Chen et al., 2011). In the current investigation, the relative bioavailability (*F*) of CA (CA-NG4) by transdermal route was found to be 894.73. This indicated enhanced bioavailability of CA nano-gel through transdermal route. This may be due to that the CA-NG4 releases drug in a sustained manner for extended periods (72 h). For transdermal route, *stratum corneum* acts as a permeation barrier and thereby the sustained-release activity of CA was found with CA-NG4 in comparison to orally administered suspension is an immediate release dosage form. Therefore, CA based nano-gel could provide an effective treatment for the management of skin damage mediated by the UV exposure. The study explained in this chapter thus provided an approach and strategy to overcome the limitation of the phytomolecule related to its poor bioavailability and to enhance its therapeutic efficacy. A research paper entitled "Enhancement of photoprotection potential of catechin loaded nanoemulsion gel against UVA induced oxidative stress" has been published in *Journal of Photochemistry and Photobiology B: Biology,* Elsevier, 2016, 160, 318-329, doi: 10.1016/j.jphotobiol. 2016.03.026.

Chapter 5 described the formulation & development, characterization, evaluation of therapeutic efficacy and bioavailability study of genistein-nanoemulsions and their nano-gel formulation. Genistein (GN) is occurred manly in dietary and food plants. GN is a phytoestrogen, which belongs to the isoflavone class of flavonoids, naturally occurring in soybean seeds. Soybean is the main source of isoflavones in the human diet, it contains between 0.6 and 3.8 g isoflavones/kg fresh weight (Manach et al., 2004; Cassidy et al., 2000). GN is a potent tyrosinase enzyme inhibitor. GN has been used as a sunscreening and photoprotective agent against UV induced oxidative stress leading to skin damage (Wang et al., 2010). GN has been proven for their other potential therapeutic benefits like antioxidant, anti-inflammatory, hepatoprotective, antiobesity, antidiabetic, anti-cancer and anti-osteoporosis. It is proposed as a potent phytopharmaceuticals for the treatment of metabolic disorders. GN belongs to BCS II molecule which has poor solubility and low bioavailability due to its rapid absorption and clearance from the small intestine and liver. Several studies reported on absorption, distribution, metabolism and excretion of GN in rats and humans. Pharmacokinetics of GN has been studied in rats and humans and demonstrated low bioavailability due first pass effect (Coldham and Sauer, 2000).

Hence, it is necessary to formulate novel drug delivery system of GN which can increase the solubility by using nanocarrier system which can enhance their efficacy and bioavailability by improving permeation profiles in a sustained manner. In this context nanoemulsion of GN was developed with several excipients like oil, water and Smix through spontaneous nanoemulsification method. Solubility of GN in different

excipients were performed and found to be maximum solubility in labrafac™ lipophile WL1349 (LLW), as an oil phase. GN loaded NEs were characterized by measuring different parameters like electrical conductivity, % transmittance, viscosity, pH, refractive index, %EE, %DL, droplet size, PDI and zeta potential. The favorable conditions were observed for GN-NE2. The drug-excipients compatibility of GN encapsulated NEs were analyzed through UV-spectrophotometry, HPTLC, FTIR in comparison with pure GN and it was observed that GN was pretty compatible with the excipients used for NEs formulation. TEM was performed to analyze the shape and surface morphology of the optimized formulations, GN-NE2 and it was observed that the droplets seen as dark spot in photograph which may be due to the dispersed oil droplets. Droplet size (~110 nm) measured through TEM was quite similar to that obtained by Zetasizer. An accelerated stability of the optimized formulation was studied and found stable for longer periods at 40ºC. *Ex vivo* skin permeation of GN-NE1-4, GN-CG and GN-NE2 based nano-gel (GN-NG2) was studied through rat's skin. Result demonstrated that the nano-gel formulation significantly ($P < 0.01$) released the drug in a sustained manner in comparison with its conventional gel for extended period of time (24 h). Photoprotection efficacy of various gel formulations were evaluated on the rats skin against UVA mediated oxidative stress. Nano-gel of GN exhibited better antioxidant activity among the different gel formulations by improving the cutaneous antioxidant enzyme levels of skin against UVA mediated oxidative stress. This may be due to its enhanced permeability profile (95.99 ± 2.70%) for longer periods. Skin irritation of nano-gel was also studied along with its placebo gel. There were no serious clinical signs of irritation, erythema or oedema observed throughout the study periods. These results indicated that the GN based nano-gel formulation was found to be non-irritant and safe for skin application.

The bioavailability of GN was studied after administration of its oral suspension (20 mg GN) and GN-NG2 (≈20 mg GN). GN has been well released and permeated from GN-NG2 in comparison with oral suspension for extended periods (24 h). Statistically significant $C_{max}$, $T_{max,}$ MRT and AUC profiles were observed with oral suspension and GN-NG2 ($P < 0.05$). The $C_{max}$ of GN was found to be 57.48 ± 4.42 and 95.06 ± 4.09 $ngmL^{-1}$ for oral suspension and GN-NG2 respectively. The $AUC_{0\text{-}t\infty}$ (911.55 ± 69.11 $nghmL^{-1}$), $T_{max}$ (6.53 ± 0.19 h) and $MRT_{0\text{-}t\infty}$ (8.52 ± 0.38 h) were higher for GN-NG2 comparatively to the pure GN-oral suspension ($P < 0.05$). The $t_{1/2}$el of GN was increased with nano-gel (3.81 ± 0.25 h) while the Kel (0.18150 ± 0.01 $h^{-1}$) and Cl (0.02259 ± 0.02 $Lh^{-1}$) were also lowered. The mean value of $AUC_{0\text{-}t}$ by transdermal route was 3.52 times higher than oral route, and the difference was found to be statistically significant ($P < 0.05$). This could be due to avoidance of hepatic first-pass metabolism by the transdermal route. The reported oral bioavailability of GN (20 mg/kg) was ~24% because of its extreme hepatic first-pass metabolism (Kwon et al., 2007). In the present study, relative bioavailability ($F$) of GN was found to be 352.58 by transdermal route. This indicates enhanced bioavailability of nano-gel through transdermal route due to avoidance of hepatic first-pass metabolism.

This may be also due to that the nano-gel releases molecule in a sustained manner for 24 h. For transdermal route, *stratum corneum* acts as a permeation barrier and thereby the sustained-release was produced with nano-gel in comparison with orally administered suspension which is an immediate release dosage form. Therefore, GN based nano-gel could provide an effective approach for the treatment and management of skin damage caused by intemperate exposure of the UV radiations. Thus the study showed that development of genistein-nanoemulsion can overcome the limitation of the molecule related to low bioavailability and enhanced the therapeutic efficacy of the molecule. Based on this work, a research paper entitled “Nanoemulsion based nano-gel of genistein enhancing UVA protection efficacy and bioavailability by improving its pharmacokinetics through transdermal route” has been communicated in *Journal of Pharmaceutical and Biomedical Analysis*, Elsevier.

## 6.2. Conclusion

Nanoemulsions are isotropic and thermodynamically stable systems of oils, surfactants/co-surfactants and water. The pseudo-ternary phase diagrams were constructed to optimize the different nanoemulsion formulations. Phytomolecule loaded several nanoemulsions have been successfully developed with appropriate ratio of oil, aqueous and Smix system through spontaneous nanoemulsification method. This method was very effective and convenient for producing phytomolecule encapsulated formulations which used to give better therapeutic efficacy.

In this context this present work was undertaken to develop nanoemulsions of ferulic acid, catechin and genistein. Ferulic acid is a cinnamic acid derivative potent antioxidant naturally occurring in several functional food products/plants such as wheat, rice, barley, oats, citrus fruits, tomatoes, etc. It has been proven for photoprotection potential to the skin against UVB induced oxidative stress. Ferilic acid also exhibits several other therapeutic effects including anticancer, neuroprotective, cardioprotective, antidiabetic, antiaging, hepatoprotective and anti-inflammatory. Apart from these several biological effects, its therapeutic efficacy is limited due to short half-life and low bioavailability due to rapid clearance and elimination from the body. Catechin is a flavanol type polyphenolic molecule present in green tea, red wine, coffee, apple, chocolate and other medicinal plants. Catechin possesses potent antioxidant effect by scavenging free ROS and has been proven to afford significant photoprotection to the skin against UV mediated oxidative stress and from other problems i.e. photo-damage, melanoma and sunburn. Catechin is well known for its other therapeutic activities like anticancer, anti-HIV, antiobesity, antiaging, antidiabetic, neuroprotective, antibacterial, hypolipidemic and anti-inflammatory. Despite of several therapeutic effects, its efficacy is limited due to its short half-life (1.25 h) and less oral bioavailability (5%) because of their digestive instability, poor intestinal uptake, extensive first-pass metabolism and elimination. Genistein is an isoflavone naturally present in food plants and dietary sources. In the human diet, soybean is the rich source of this molecule.

It is a phytoestrogen and potent tyrosinase enzyme inhibitor. Genistein is famous for its sunscreening and photoprotective properties against UV mediated several consequences. There are other several therapeutic effects of genistein like antioxidant, anti-inflammatory, hepatoprotective, antiobesity, antidiabetic, anti-cancer and anti-osteoporosis have been explored. Genistein suffers from its low aqueous solubility and poor bioavailability due to its rapid absorption and clearance from the small intestine and liver. These bioactive phytomolecules have been found to possess several health benefits but their therapeutic efficacy are limited due to short half-life, poor solubility and low oral bioavailability due to rapid clearance and excretion rates. Through advancement of nanotechnology, it is possible to fabricate these phytopharmaceuticals with several nanocarrier systems which used to enhance efficacy at the target sites.

Intemperate exposure of UV radiations interacts with the cutaneous antioxidant defense system of the skin and produces ROS as an oxidative intermediate product. These ROS may change the regular function of the cellular lipids, proteins and DNA through peroxidation process. These changes leads to the structural damage of skin and results in obstruction of normal level of the cutaneous antioxidant enzyme systems. In this regard a ferulic acid loaded nanoemulsion was successfully developed with suitable excipients. Topical nano-gel of ferulic acid was developed to combat these problems. Ferulic acid nano-gel showed improved photoprotection and sustained-release effect against UVA exposure in skin. The optimized gel formulation showed improved drug permeability as well as bioavailability and enhanced UV protection activity, which might be due to the potent antioxidant activity of FA in opposition to oxidative stress mediated by UVA. It significantly elevates the level of the antioxidant markers and arrested the unwanted effects generated by ultraviolet radiation. This phenomenon attributed towards the encapsulated FA in NE having a nano size range of droplets provided large surface area, which possess superior skin penetration potential when compared with its conventional gel. The enhanced relative bioavailability of ferulic acid (396.26%) was obtained with nano-gel formulation after its transdermal administration for extended periods. The nanoemulsion based FA nano-gel was found to be stable, safe and effective for topical application against UV. The enhanced relative bioavailability of catechin (894.73%) was achieved with nano-gel formulation after its transdermal application for 72 h. The nano-gel increased antioxidant potential of catechin against UVA-induced oxidative stress in a sustained manner. The CA-NG4 formulation was found to be stable, safe and effective for transdermal delivery. Thus, nanoemulsion based gel formulation of catechin may be a promising nanocarrier for skin delivery. The enhanced relative bioavailability of genistein (352.58%) was obtained with nano-gel formulation. The nano-gel significantly improved antioxidant potential of genistein by enhancing their skin permeability against UVA-induced oxidative stress in a sustained manner. The GN-NG2 was found to be stable, safe and effective for transdermal delivery. Thus, nanoemulsion based gel formulation of genistein may be a novel approach for skin delivery. Result concluded that the nano-gel formulation of ferulic

acid, catechin and genistein was developed with nanoemulsion that could be promising as a useful strategy for sun or photoprotection against UVA-induced oxidative stress.

As a promising nanocarrier to increase the solubility of phytoconstituents and stability of the formulations so to enhances the therapeutic efficacy and bioavailability of phytomolecules. This work was performed to enhance the availability of these potent phytoconstituents at the sites. In this respects these nano-delivery system was made based on the idea of exploitation and exploration where the leads from the phytopharmaceuticals were exploited for their opportunities to make value added delivery as a nanocarrier. It was observed that these formulations were therapeutically more bioavailable than their isolated components and showed better therapeutic efficacy. Thus this work highlights on the aspects of developing nanoemulsions with potent plant secondary metabolites which may be useful in further for development of novel drug delivery system with phytopharmaceuticals.

# Chapter – 7

# References

Abderrezak, A., Bourassa, P., Mandeville, J.S., Sedaghat-Herati, R., Tajmir-Riahi, H.A., 2012. Dendrimers bind antioxidant polyphenols and cisplatin drug. PLoS ONE 7, 1-12.

Abolmaali, S.S., Tamaddon, A.M., Farvadi, F.S., Daneshamuz, S., Moghimi, H., 2011. Pharmaceutical nanoemulsions and their potential topical and transdermal applications. Iran. J. Pharm. Sci. 7, 139-150.

Adam, A., Crespy, V., Levrat-Verny, M.A., Leenhardt, F., Leuillet, M., Demigne, C., Re´me´sy, C., 2002. The bioavailability of ferulic acid is governed primarily by the food matrix rather than its metabolism in intestine and liver in rats. J. Nutr. 132, 1962-1968.

Adesanwo, J.K., Makinde, O.O., Obafemi, C.A., 2013. Phytochemical analysis and antioxidant activity of methanol extract and betulinic acid isolated from the roots of *Tetracera potatoria*. J. Pharm. Res. 6, 903-907.

Afaq, F., Mukhtar, H., 2006. Botanical antioxidants in the prevention of photocarcinogenesis and photoaging. Exp. Dermatol. 15, 678-684.

Ahad, M.A.A., Kohli, K., Sultana, Y., Mujeeb, M., Ali, A., 2010. Transdermal drug delivery: the inherent challenges and technological advancements. Asian J. Pharm. Sci. 5, 276-288.

Ahmed, K., Li, Y., McClements, D.J., Xiao, H., 2012. Nanoemulsion- and emulsion-based delivery systems for curcumin: encapsulation and release properties. Food Chem. 132, 799-807.

Ahmed-Belkacem, A., Macalou, S., Borrelli, F., Capasso, R., Fattorusso, E., Taglialatela-Scafati. O., Di Pietro A., 2007. Nonprenylated rotenoids, a new class of potent breast cancer resistance protein inhibitors. J. Med. Chem. 50, 1933-8.

Ajazuddin, Saraf, S., 2010. Applications of novel drug delivery system for herbal formulations. Fitoterapia 81, 680-689.

Akao, T., Kanaoka, M., Kobashi, K., 1998. Appearance of compound K, a major metabolite of ginsenoside Rb1 by intestinal bacteria, in rat plasma after oral administration-measurement of compound K by enzyme immunoassay. Biol. Pharm. Bull. 21, 245-249.

Alexander, A., Dwivedi, S., Ajazuddin, Giri, T.K., Saraf, S., Saraf, S., Tripathi, D.K., 2012. Approaches for breaking the barriers of drug permeation through transdermal drug delivery. J. Control Release 164, 26-40.

Al-Hazzani, A.A., Alshatwi, A.A., 2011. Catechin hydrate inhibits proliferation and mediates apoptosis of SiHa human cervical cancer cells. Food Chem. Toxicol. 49, 3281-3286.

Amiot, M.J., Romier, B., Dao, T.M., Fanciullino, R., Ciccolini, J., Burcelin, R., Pechere, L., Emond, C., Savouret, J.F., Seree, E., 2013. Optimization of trans-Resveratrol bioavailability for human therapy. Biochimie 95, 1233-1238.

Amri, A., Chaumeil, J.C., Sfar, S., Charrueau, C., 2012. Administration of resveratrol: What formulation solutions to bioavailability limitations? J. Control Release 158, 182-193.

Anand, P., Kunnumakkara, A.B., Newman, R.A., Aggarwal, B.B., 2007. Bioavailability of curcumin: problems and promises. Mol. Pharmaceutics 4, 807-818.

Anton, N., Vandamme, T., 2009. The universality of low-energy nano-emulsification. Int. J. Pharm. 377, 142-147.

Anupongsanugool, E., Teekachunhatean, S., Rojanasthien, N., Pongsatha, S., Sangdee, C., 2005. Pharmacokinetics of isoflavones, daidzein and genistein, after ingestion of soy beverage compared with soy extract capsules in postmenopausal Thai women. BMC Clin. Pharmacol. 3, 5-2.

Aqil, F., Munagala, R., Jeyabalan, J., Vadhanam, M.V., 2013. Bioavailability of phytochemicals and its enhancement by drug delivery Systems. Cancer Lett. 334, 133-141.

Arica, Y.B., Benoit, J.P., Lamprecht, A., 2006. Paclitaxel-loaded lipid nanoparticles. Drug Dev. Ind. Pharm. 32, 1089-1094.

Arya, P., Pathak, K., 2014. Assessing the viability of microsponges as gastro retentive drug delivery system of curcumin: optimization and pharmacokinetics. Int. J. Pharm. 460, 1-12.

Attwood, D., 1994. Microemulsions. In Colloidal drug Delivery Systems. Kreuter J., (Ed.), Marcel Dekker, New York, pp. 31-71.

Attwood, D., Ktistis, G., McCormick, Y., Story, M.J., 1989. Solubilization of indomethacin by polysorbate 80 in mixed water-sorbitol solvents. J. Pharm. Pharmacol. 41, 83-6.

Attwood, D., Mallon, C., Taylor, C.J., 1992. Phase studies of oil-in-water phospholipid microemulsions. Int. J. Pharm. 84, R5-R8.

Bae, J.Y., Choi, J.S., Kang, S.W., Lee, Y.J., Park, J., Kang, Y.H., 2010. Dietary compound ellagic acid alleviates skin wrinkle and inflammation induced by UV-B irradiation. Exp. Dermatol. 19, e182–e190.

Bali, V., Ali, M., Ali, J., 2011. Nanocarrier for the enhanced bioavailability of a cardiovascular agent: in vitro, pharmacodynamic, pharmacokinetic and stability assessment. Int. J. Pharm. 403, 46-56.

Barone, E., Calabrese, V., Mancuso, C., 2009. Ferulic acid and its therapeutic potential as a hormetin for age-related diseases. Biogerontol. 10, 97-108.

Batchelder, R.J., Calder, R.J., Tomas, C.P., Heard, C.M., 2004. In vitro transdermal delivery of the major catechins and caffeine from extract of *Camellia sinensis.* Int. J. Pharm. 283, 45-51.

Bavarsad, N., Bazzaz, B.S.F., Khamesipour, A., Jaafari, M.R., 2012. Colloidal, in vitro and in vivo anti-leishmanial properties of transfersomes containing paromomycin sulfate in susceptible BALB/c mice. Acta Trop. 124, 33-41.

Beers, R.F., Seizer, I.W., 1952. A spectrophotometric method for measuring breakdown of hydrogen peroxide by catalase, J. Biol. Chem. 115, 130-140.

Bell, J.R.C., Donovan, J.L., Wong, R., Waterhouse, A.L., German, J.B., Walzem, R.L., Kasim-Karakas, S.E., 2000. (+)-Catechin in human plasma after ingestion of a single serving of reconstituted red wine. Am. J. Clin. Nutr. 71, 103-8.

Benson, H.A.E., 2005. Transdermal drug delivery: penetration enhancement techniques. Curr. Drug Deliv. 2, 23-33.

Bhattacharya, S., 2009. Phytosomes: emerging strategy in delivery of herbal drugs and nutraceuticals. Pharma times 41, 9-12.

Bhattacharyya, S., Ahammed, S.M., Saha, B.P., Mukherjee, P.K., 2013. The gallic acid-phospholipid complex improved the antioxidant potential of gallic acid by enhancing its bioavailability. AAPS PharmSciTech 14, 1025-1033.

Bhattacharyya, S., Ahmmed, S.M., Saha, B.P., Mukherjee, P.K., 2014. Soya phospholipid complex of mangiferin enhances its hepatoprotectivity by improving its bioavailability and pharmacokinetics. J. Sci. Food. Agric. 94, 1380-8.

Bhattacharyya, S., Majhi, S., Saha, B.P., Mukherjee, P.K., 2014. Chlorogenic acid-phospholipid complex improve protection against UVA induced oxidative stress. J. Photochem. Photobiol. B 130, 293-298.

Bokkenheuser, V.D., Shackleton, C.H.L., Winter, J., 1987. Hydrolysis of dietary flavonoid glycosides by strains of intestinal Bacteroides from humans. J. Biochem. J. 248, 953-956.

Boocock, D.J., Faust, G.E., Patel, K.R., Schinas, A.M., Brown, V.A., Ducharme, M.P., Booth, T.D., Crowell, J.A., Perloff, M., Gescher, A.J., Steward, W.P., Brenner, D.E., 2007. Phase I dose escalation pharmacokinetic study in healthy volunteers of resveratrol, a potential cancer chemopreventive agent. Cancer Epidemiol. Biomarkers Prev. 16, 1246-1252.

Bose, S., Du, Y., Takhistov, P., Michniak-Kohn, B., 2013. Formulation optimization and topical delivery of quercetin from solid lipid based nanosystems. Int. J. Pharm. 441, 56-66.

Bourne, L., Paganga, G., Baxter, D., Hughes, P., Rice-Evans, C., 2000. Absorption of ferulic acid from low-alcohol beer. Free Radical Res. 32, 273–280.

Bourne, L.C., Rice-Evans, C., 1998. Bioavailability of ferulic acid. Biochem. Biophys. Res. Commun. 253, 222–227.

Braithwaite, M.C., Tyagi, C., Tomar, L.K., Kumar, P., Choonara, Y.E., Pillay, V., 2014. Nutraceutical-based therapeutics and formulation strategies augmenting their efficiency to complement modern medicine: an overview. J. Funct. Foods 68, 2-99.

Brown, V.A., Patel, K.R., Viskaduraki, M., Crowell, J.A., Perloff, M., Booth, T.D., Vasilinin, G., Sen, A., Schinas, A.M., Piccirilli, G., Brown, K., Steward, W.P., Gescher, A.J., Brenner, D.E., 2010. Repeat dose study of the cancer chemopreventive agent resveratrol in healthy volunteers: safety, pharmacokinetics, and effect on the insulin-like growth factor axis. Cancer Res. 70, 9003-9011.

Bu, H., He, X., Zhang, Z., Yin, Q., Yu, H., Li, Y., 2014. A TPGS-incorporating nanoemulsion of paclitaxel circumvents drug resistance in breast cancer. Int. J. Pharm. 471, 206-213.

Bummer, P.M., 2004. Physical chemical considerations of lipid-based oral drug delivery-solid lipid nanoparticles. Crit. Rev. Ther. Drug carr. Syst. 21, 1-19.

Butnariu, M.V., Giuchici, C.V., 2011. The use of some nanoemulsions based on aqueous propolis and lycopene extract in the skin's protective mechanisms against UVA radiation. J. Nanobiotechnol. 9, 1-9.

Campanini, M.Z., Pinho-Ribeiro, F.A., Ivan, A.L.M., Ferreira, V.S., Vilela, F.M.P., Vicentini, F.T.M.C., Martinez, R.M., Zarpelon, A.C., Fonseca, M.J.V., Faria, T.J., Baracat, M.M., Verri, W.A., Georgetti, S.R., Casagrande, R., 2013. Efficacy of topical formulations containing *Pimenta pseudocaryophyllus* extract against UVB-induced oxidative stress and inflammation in hairless mice. J. Photochem. Photobiol. B 127, 153.

Candi, E., Schmidt, R., Melino, G., 2005. The cornified envelope: a model of cell death in the skin. Nat. Rev. Mol. Cell Biol. 6, 328-340.

Chan, K., Liu, Z.Q., Jiang, Z.H., Zhou, H., Wong, Y.F., Xu, H.X., Liu L., 2006. The effects of sinomenine on intestinal absorption of paeoniflorin by the everted rat gut sac model. J Ethnopharmacol. 103, 425-32.

Charman, S.A., Charman, W.N., Rogge, M.C., Wilson, T.D., Dukto, F.J., Pouton, C.W., 1992. Self-emulsifying drug delivery systems: Formulation and biopharmaceutic evaluation of an investigational lipophilic compound. Pharm. Res. 9, 87-93.

Chat, O.A., Najar, M.H., Mir, M.A., Rather, G.M., Dar, A.A., 2011. Effects of surfactant micelles on solubilization and DPPH radical scavenging activity of rutin. J. Colloid Interface Sci. 355, 140-149.

Chatterjee, P., Chandra, S., Dey, P., Bhattacharya, S., 2012. Evaluation of anti-inflammatory effects of green tea and black tea: a comparative in vitro study. J. Adv. Pharm. Technol. Res. 3, 136-138.

Chaudhary, H., Kohli, K., Kumar, V., 2014. A novel nano-carrier transdermal gel against inflammation. Int. J. Pharm. 465, 175-186.

Chen, C.H., Hsieh, M.F., Ho, Y.N., Huang, C.M., Lee, J.S., Yang, C.Y, Chang, Y., 2011. Enhancement of catechin skin permeation via a newly fabricated mPEG-PCL-graft-2-hydroxycellulose membrane. J. Membr. Sci. 371, 134-140.

Chen, W.C., Liou, S.S., Tzeng, T.F., Lee, S.L., Liu, I.M., 2013. Effect of topical application of chlorogenic acid on excision wound healing in rats. Planta Med. 79, 616-621.

Chen-yua, G., Chun-fen, Y., Qi-lu, L., Qi, T., Yan-wei, X., Wei-na, L., Guang-xi, Z., 2012. Development of a quercetin-loaded nanostructured lipid carrier formulation for topical delivery. Int. J. Pharm. 430, 292-298.

Cho, H.K., Kim, H.H., Seo, D.H., Jung, J.H., Park, J.H., Baek, N.I., Kim, M.J., Yoo, S.H., Cha, J., Kim, Y.R., Park, C.S., 2011. Biosynthesis of (+)-catechin glycosides using recombinant amylosucrase from *Deinococcus geothermalis* DSM 11300. Enzyme Microb. Technol. 49, 246-253.

Choi, A.Y., Kim, C.T., Park, H.Y., Kim, H.O., Lee, N.R., Lee, K.E., Gwak, H.S., 2013. Pharmacokinetic characteristics of capsaicin-loaded nanoemulsions fabricated with alginate and chitosan. J. Agric. Food Chem. 61, 2096-2102.

Choudhury, H., Gorain, B., Karmakar, S., Biswas, E., Dey, G., Barik, R., Mandal, M., Pal, T.K., 2014. Improvement of cellular uptake, in vitro antitumor activity and sustained release profile with increased bioavailability from a nanoemulsion platform. Int. J. Pharm. 460, 131-143.

Cichewicz, R.H., Kouzi, S.A., 2004. Chemistry, biological activity, and chemotherapeutic potential of betulinic acid for the prevention and treatment of cancer and HIV infection. Med. Res. Rev. 24, 90-114.

Ciesielska, A.S., Plewka, K., Daniluk, J., Szerszen, M.K., 2011. Betulin and betulinic acid attenuate ethanol-induced liver stellate cell activation by inhibiting reactive oxygen species (ROS), cytokine (TNF-α, TGF-β) production and by influencing intracellular signaling. Toxicology 280, 152-163.

Coldham, N.G., Sauer, M.J., 2000. Pharmacokinetics of [14C]genistein in the rat: gender-related differences, potential mechanisms of biological action, and implications for human health. Toxicol. Appl. Pharmacol. 164, 206-215.

Constantinides, P.P., 1995. Lipid microemulsions for improving drug dissolution and oral absorption: Physical and biopharmaceutical aspects. Pharm. Res. 12, 1561-1572.

Cooper, R., Morr´e, D.J., Morr´e, D.M., 2005. Medicinal benefits of green tea: Part I. Review of noncancer health benefits. J. Altern. Complement. Med. 11, 521-528.

Couteau, C., Faure, A., Fortin, J., Paparis, E., Coiffard, L.J.M., 2007. Study of the photostability of 18 sunscreens in creams by measuring the SPF in vitro. J. Pharm. Biomed. Anal. 44, 270-273.

Craig, D.Q.M., Barker, S.A., Banning, D., Booth, S.W., 1995. An investigation into the mechanisms of self-emulsification using particle size analysis and low frequency dielectric spectroscopy. Int. J. Pharm. 114, 103-110.

Crespy, V., Morand, C., Manach, C., Besson, C., Demigne, C., Remesy, C., 1999. Part of quercetin absorbed in the small intestine is conjugated and further secreted in the intestinal lumen. Am. J. Physiol. 277, G120-G126.

Das, S., Chaudhury, A., 2011. Recent advances in lipid nanoparticle formulations with solid matrix for oral drug delivery. AAPS PharmSciTech 12, 62-76.

Dash, S., Murthy, P.N., Nath, L., Chowdhury, P., 2010. Kinetic modeling on drug release from controlled drug delivery systems. Acta Pol. Pharm.67, 217-223.

Dash, S.K., Chattopadhyay, S., Dash, S.S., Tripathy, S., Das, B., Mahapatra, S.K., Bag, B.G., Karmakar, P., Roy, S., 2015. Self assembled nano fibers of betulinic acid: a selective inducer for ROS/TNF-alpha pathway mediated leukemic cell death. Bioorg. Chem. 63, 85-100.

Day, A.J., Canada, F.J., Diaz, J.C., Kroon, P.A., Mclauchlan, R., Faulds, C.B., Plumb, G.W., Morgan, M.R.A., Williamson, G., 2000. Dietary flavonoid and isoflavone glycosides are hydrolysed by the lactase site of lactase phlorizin hydrolase. FEBS Lett. 436, 166-170.

Day, A.J., DuPont, M.S., Ridley, S., Rhodes, M., Rhodes, M.J.C., Morgan, M.R.A., Williamson, G., 1998. Deglycosylation of flavonoid and isoflavonoid glycosides by human small intestine and liver beta-glucosidase activity. FEBS Lett. 436, 71-75.

Deeley, R.G., Westlake, C., Cole, S.P., 2006. Transmembrane transport of endo and xenobiotics by mammalian ATP-binding cassette multidrug resistance proteins. Physiol. Rev. 86, 849-99.

Delmas, D., Aires, V., Limagne, E., Dutartre, P., Mazué, F., Ghiringhelli, F., Latruffe, N., 2011. Transport, stability, and biological activity of resveratrol. Ann. N. Y. Acad. Sci. 1215, 48-59.

Drechsler, K.C., Ferrua, M.J., 2016. Modelling the breakdown mechanics of solid foods during gastric digestion. Food Res. Int. http://dx.doi.org/10.1016/j.foodres.2016.02.019.

Dube, A., Ng, K., Nicolazzo, J.A., Larson, I., 2010. Effective use of reducing agents and nanoparticle encapsulation in stabilizing catechins in alkaline solution. Food Chem. 122, 662-667.

El-Samaligy, M.S., Afifi, N.N., Mahmoud, E.A., 2006. Evaluation of hybrid liposomes-encapsulated silymarin regarding physical stability and in vivo performance. Int. J. Pharm. 319, 121-129.

Erlund, I., Kosonen, T., Alfthan, G., Maenpaa, J., Perttunen, K., Kenraali, J., Parantainen, J., Aro, A., 2000. Pharmacokinetics of quercetin from quercetin aglycone and rutin in healthy volunteers. Eur. J. Clin. Pharmacol. 56, 545-553.

Fang, J.Y., Tsai, T.H., Lin, Y.Y., Wong, W.W., Wang, M.N., Huang, J.F., 2007. Transdermal delivery of tea catechins and theophylline enhanced by terpenes: a mechanistic study. Biol. Pharm. Bull. 30, 343-349.

Fang, J.Y., Wang, H.T.L., Huang, Y.L., Fang, C.L., 2006. Enhancement of the transdermal delivery of catechins by liposomes incorporating anionic surfactants and ethanol. Int. J. Pharm. 310, 131-138.

Yen, F.L., Wu, T.H., Lin, L.T., Cham, T.M., Lin, C.C., Naringenin-loaded nanoparticles improve the physicochemical properties and the hepatoprotective effects of naringenin in orally-administered rats with CCl(4)-induced acute liver failure.2009. Pharm. Res. 26, 893-902.

Ferruzzi, M.G., Lobo, J.K., Janle, E.M., Cooper, B., Simon, J.E., Wu, Q.L., Welch, C., Ho, L., Weaver, C., Pasinetti, G.M., 2009. Bioavailability of gallic acid and catechins from grape seed polyphenol extract is improved by repeated dosing in rats: implications for treatment in Alzheimer's disease. J. Alzheimers Dis. 18, 113-124.

Fong, Y.K., Li, C.R., Wo, S.K., Wang, S., Zhou, L., Zhang, L., Lin, G., Zuo, Z., 2012. In vitro and in situ evaluation of herb-drug interactions during intestinal metabolism and absorption of Baicalein. J. Ethnopharmacol.141, 742-753.

Forgiarini, A., Esquena, J., Gonzalez, C., Solans, C. 2001. Formation of nano-emulsions by low-energy emulsification methods at constant temperature. Langmuir 17, 2076-2083.

Freag, M.S., Elnaggar, Y.S.R., Abdallah, O.Y., 2013. Lyophilized phytosomal nanocarriers as platforms for enhanced diosmin delivery: optimization and ex vivo permeation. Int. J. Nanomed. 8, 2385-2397.

Fu, R.Q., He, F.C., Meng, D.S., Chen, L., 2006. Preparation of paclitaxel-loaded poly(d,l-lacticacid) nanoparticles. Acta Acad. Med. Mil. Tertiae 28, 1573-1574.

Fuhr, U., 1998. Drug interactions with grapefruit juice: extent, probable mechanism and clinical relevance. Drug Saf. 18, 251-272.

Fung, S.T., Ho, C.K., Choi, S.W., Chung, Iris, W.Y., Benzie, F.F., 2013. Comparison of catechin profiles in human plasma and urine after single dosing and regular intake of green tea (*Camellia sinensis*). Br. J. Nutr.109, 2199-2207.

Gannu, R., Palem, C.R., Yamsani, V.V., Yamsani, S.K., Yamsani, M.R., 2010. Enhanced bioavailability of lacidipine via microemulsion based transdermal gels: formulation optimization, ex vivo and in vivo characterization. Int. J. Pharm. 388, 231-241.

Gao, S., Zhan, Q., Li, J., Yang, Q., Li, X., Chen, W., Sun, L., 2010. LC-MS/MS method for the simultaneous determination of ethyl gallate and its major metabolite in rat plasma. Biomed. Chromatogr. 24, 472-478.

Garduño, A.C., Flores, A.A.O., Niño, J.C.S., Sanchez, C.E.M., Beristain, C.I., García, H.S., 2015. Preparation of betulinic acid nanoemulsions stabilized by ε-3 enriched phosphatidylcholine. Ultrason. Sonochem. 24, 204-213.

Ge, L.J., Fan, S.Y., Yang, J.H., Wei, Y., Zhu, Z.H., Lou, Y.J., Guo, Y., Wan, H.T., Xie, Y.Q., 2015. Pharmacokinetic and pharmacodynamic analysis of ferulic acid puerarin-astragaloside in combination with neuroprotective in cerebral ischemia/reperfusion injury in rats. Asian Pac. J. Trop. Med. 299-304.

Godin, B., Touitou, E., 2004. Mechanism of bacitracin permeation enhancement through the skin and cellular membranes from an ethosomal carrier. J. Control Release 94, 365-79.

Goldberg, D.M., Yan, J., Soleas, G.J., 2003. Absorption of three wine-related polyphenols in three different matrices by healthy subjects. Clin. Biochem. 36, 79-87.

González-Vallinas, M., Molina, S., Vicente, G., de la Cueva, A., Vargas, T., Santoyo, S., García-Risco, M.R., Fornari, T., Reglero, G., Ramírez de Molina, A. 2013. Antitumor effect of 5-fluorouracil is enhanced by rosemary extract in both drug sensitive and resistant colon cancer cells. Pharmacol. Res. 72, 61-8.

Graefe, E.U., Wittig, J., Mueller, S., Riethling, A.K., Uehleke, B., Drewelow, B., Pforte, H., Jacobasch, G., Derendorf, H., Veit, M., 2001. Pharmacokinetics and bioavailability of quercetin glycosides in humans. J. Clin. Pharmacol. 41, 492-499.

Graf, E., 1992. Antioxidant potential of ferulic acid. Free Radic. Biol. Med. 13, 435-48.

Grant, S., 2008. Is the focus moving toward a combination of targeted drugs? Best Pract. Res., Clin. Haematol. 21, 629-637.

Graves, S., Meleson, K., Wilking, J., 2005. Structure of concentrated nanoemulsions. J. Chem. Phys. 122, Article ID 134703. doi:10.1063/1.1874952.

Guengerich, F.P., Wu, Z.L., Bartleson, C.J., 2005. Function of human cytochrome P450s: characterization of the orphans. Biochem. Biophys. Res. Commun. 338, 465-9.

Gunasekaran, T., Haile, T., Nigusse, T., Dhanaraju, M.D., 2014. Nanotechnology: an effective tool for enhancing bioavailability and bioactivity of phytomedicine. Asian Pac. J. Trop. Biomed. 4, S1-S7.

Gupta, S., Kesarla, R., Omri, A., 2013. Formulation strategies to improve the bioavailability of poorly absorbed drugs with special emphasis on self-emulsifying systems. ISRN Pharmaceutics, Article ID 848043, 1-16. http://dx.doi.org/10.1155/2013/848043.

Hamad, A.W.R., Al-Momani, W.M., Janakat, S. Oran, S.A., 2009. Bioavailability of ellagic acid after single dose administration using HPLC. Pak. J. Nutr. 8, 1661-1664.

Hamaguchi, T., Matsumura, Y., Suzuki, M., Shimizu, K., Goda, R., Nakamura, I., Nakatomi, I., Yokoyama, M., Kataoka, K., Kakizoe, T., 2005. NK105, a paclitaxel incorporating micellar nanoparticle formulation, can extend in vivo antitumour activity and reduce the neurotoxicity of paclitaxel. Br. J. Cancer 92, 1240-1246.

Han, B.H., Park, M.H., Han, Y.N., Woo, L.K., Sankawa, U., Yahara, S., Tanaka, O., 1982. Degradation of ginseng saponins under mild acidic conditions. Planta Med. 44,146-149.

Harder, H., Tetens, I., Let, M.B., Meyer, A.S., 2004. Rye bran bread intake elevates urinary excretion of ferulic acid in humans, but does not affect the susceptibility of LDL to oxidation ex vivo. Eur. J. Nutr. 43, 230–236.

Harwansh, R.K., Mukherjee, P.K., Bahadur, S., Biswas, R., 2015. Enhanced permeability of ferulic acid loaded nanoemulsion based gel through skin against UVA mediated oxidative stress. Life Sci. 141, 202-211.

Harwansh, R.K., Patra, K.C., Pareta, S.K., 2011a. Nanoemulsion as potential vehicles for transdermal delivery of pure phytopharmaceuticals and poorly soluble drug. Int. J. Drug Delivery 3, 209-218.

Harwansh, R.K., Patra, K.C., Pareta, S.K., Singh, J., Rahman, M.A., 2011b. Nanoemulsions as vehicles for transdermal delivery of glycyrrhizin. Braz. J. Pharm. Sci. 47, 769-778.

Hasegawa, H., Sung, J.H., Matsumiya, S., Uchiyama, M., 1996. Main ginseng metabolites formed by intestinal bacteria. Planta Med. 62:453-455.

He, Y.Q., Liu, Y., Zhang, B.F., Liu, H.X., Lu, Y.L., Yang, L., Wang, Z.T. 2010. Identificationof theUDPglucuronosyltransferase isozyme involved in senecionine glucuronidation in human liver microsomes. Drug Metab. Dispos. 38, 626-34.

He, Z.F., Liu, D.Y., Zeng, S., Ye, J.T., 2008. Study on preparation of ampelopsin liposomes. J. Chine. Mat. Med. 33, 27-30.

Holder, G.M., Plummer, J.L., Ryan, A.J., 1978. The metabolism and excretion of curcumin (1,7-bis-(4-hydroxy-3-methoxyphenyl)-1,6- heptadiene-3,5-dione) in the rat. Xenobiotica 8, 761-768.

Hollman, P.C., Bijsman, M.N., van Gameren, Y., Cnossen, E.P., De Vries, J.H., Katan, M.B., 1999. The sugar moiety is a major determinant of the absorption of dietary flavonoid glycosides in man. Free Radic. Res. 31, 569-573.

Hollman, P.C., de Vries, J.H.M., van Leeuwen, S.D., Mengelers, M.J., Katan, M.B., 1995. Absorption of dietary quercetin glycosides and quercetin in healthy ileostomy volunteers. Am. J. Clin. Nutr. 62, 1276-1282.

Hou, J., Zhou, S.W., 2008. Formulation and preparation of glycyrrhizic acid solid lipid nanoparticles. Acta Acad. Med. Mil. Tertiae 30, 1043-5.

Hou, P., Zeng, Y., Ma, B., Wang, X., Liu, Z., Li, L., Qu, K., Bi, K., Chen, X., 2013. A fast, sensitive, and high-throughput method for the simultaneous quantitation of three ellagitannins from *Euphorbiae pekinensis* Radix in rat plasma by ultra-HPLC-MS/MS. J. Sep. Sci. 36, 2544-2551.

Howells, L.M., Berry, D.P., Elliott, P.J., Jacobson, E.W., Hoffmann, E., Hegarty, B., Brown, K., Steward, W.P., Gescher, A.J., 2011. Phase I randomized, double-blind pilot study of micronized resveratrol (SRT501) in patients with hepatic metastases-safety, pharmacokinetics, and pharmacodynamics. Cancer Prev. Res. 4, 1419-1425.

Hu, L., Jia, H,, Luo, Z., Liu, C., Xing, Q., 2010. Improvement of digoxin oral absorption in rabbits by incorporation into solid lipid nanoparticles. Pharmazie 65,110-113.

Huang, X., Su, S., Cui, W., Liu, P., Duan, J., Guo, J., Li, Z., Shang, E., Qian, D., Huang, Z., 2014. Simultaneous determination of paeoniflorin, albiflorin, ferulic acid, tetrahydropalmatine, protopine, typhaneoside, senkyunolide I in Beagle dogs plasma by UPLC–MS/MS and its application to a pharmacokinetic study after oral administration of Shaofu Zhuyu Decoction. J. Chromatogr. B 962, 75-81.

Huo, Y., Zhang, Q., Li, Q., Geng, B., Bi, K., 2016. Development of a UFLC-MS/MS method for the simultaneous determination of seven tea catechins in rat plasma and its application to a pharmacokinetic study after administration of green tea extract. J. Pharm. Biomed. Anal. 125, 229-235.

Hüsch, J., Bohnet, J., Fricker, G., Skarke, C., Artaria, C., Appendino, G., Schubert-Zsilavecz, M., Abdel-Tawab, M., 2013. Enhanced absorption of boswellic acids by a lecithin delivery form (Phytosome®) of boswellia extract. Fitoterapia 84, 89-98.

ICH, 1994. ICH harmonized tripartite guideline on validation of analytical procedures: text and methodology Q2 (R1). In: Proceedings of the International Conference on Harmonisation.

Igarashi, T., Nishino, K., Nayar, S.K., 2007. The appearance of human skin: a survey, found. Trends. Comput. Graph. Vis. 3, 1-95.

Imai, Y., Tsukahara, S., Asada, S., Sugimoto, Y., 2004. Phytoestrogens/flavonoids reverse breast cancer resistance protein/ABCG2-mediated multidrug resistance. Cancer Res 64, 4346-52.

Ioku, K., Pongpiriyadacha, Y., Konishi, Y., Takei, Y., Nakatani, N., Terao, J., 1998. beta-Glucosidase activity in the rat small intestine toward quercetin monoglucosides. Biosci. Biotechnol. Biochem. 62, 1428-1431.

Izquierdo, P., Feng, J., Esquena, J., Tadros, T.F., Dederen, J.C., Garcia, M.J., 2005. The influence of surfactant mixing ratio on nano-emulsion formation by the pit method. J. Colloid Interf. Sci. 285, 388-394.

Jafari, S.M., He, Y., Bhandari, B., 2007 Optimization of nanoemulsion production by microfluidization. Eur. Food Res. Tech. 225, 733-741.

Jain, N.K., Gupta, U., 2008. Application of dendrimer-drug complexation in the enhancement of drug solubility and bioavailability. Expert Opin. Drug Metab. Toxicol. 4, 1035-52.

Joo, K.M., Lee, J.H., Jeon, H.Y., Park, C.W., Hong, D.K., Jeong, H.J., Lee, S.J., Lee, S.Y., Lim, K.M., 2010. Pharmacokinetic study of ginsenoside Re with pure ginsenoside Re and ginseng berry extracts in mouse using ultra performance liquid chromatography/mass spectrometric method. J Pharm Biomed. 51, 278-083.

Junyaprasert, V.B., Singha, P., Suksiriworapong, J., Chantasart, D., 2012. Physicochemical properties and skin permeation of Span 60/Tween 60 niosomes of ellagic acid. Int. J. Pharm. 423, 303-311.

Kakkar, B., Das, P.N., Viswanathan, A., 1984. Modified spectrophotometer assay of SOD. Ind. J. Biochem. Biophys. 21, 130-132.

Karakaya, S., 2004. Bioavailability of phenolic compounds. Crit. Rev. Food Sci. Nutr. 44, 453-464.

Karikura, M., Miyase, T., Tanizawa, H., Takino, Y., Taniyama, T., Hayashi, T., 1990. Studies on absorption, distribution, excretion and metabolism of ginseng saponins. V. The decomposition products of ginsenoside Rb2 in the large intestine of rats. Chem. Pharm. Bull. 38, 2859-2861.

Ke, X., Xu, Y., Yan, F., Ping, Q.N., 2007. Preparation and rats in vivo pharmacokinetics Wogonin liposomes dynamics J. China. Pharm. Univ. 38, 502-6.

Kern, S.M., Bennett, R.N., Mellon, F.A., Kroon, P.A., Garcia-Conesa, M.T., 2003. Absorption of hydroxycinnamates in humans after high-bran cereal consumption. J. Agric. Food Chem. 51, 6050-6055.

Kesarwani, K., Gupta, R., 2013. Bioavailability enhancers of herbal origin: an overview. Asian Pac. J. Trop. Biomed. 3, 253-266.

Khurana, S., Jain, N.K., Bedi, P.M.S., 2013. Nanoemulsion based gel for transdermal delivery of meloxicam: physicochemical, mechanistic investigation. Life Sci. 92, 383-393.

Kidd, P.M., 2009. Bioavailability and activity of phytosome complexes from botanical polyphenols: the silymarin, curcumin, green tea, and grape seed extracts. Altern. Med. Rev.14, 226-246.

Kim, J., Lee, Y.S., Kim, C.S., Kim, J.S., 2012. Betulinic acid has an inhibitory effect on pancreatic lipase and induces adipocyte lipolysis. Phytother. Res. 26, 1103-1106.

Kim, Y.J., Houng, S., Kim, J.H., Kim, Y., Ji, H.G., Lee, S., 2012. Nanoemulsified green tea extract shows improved hypocholesterolemic effects in C57BL/6 mice. J. Nutr. Biochem. 23, 186-191.

Kind, P.R.N., King, E.J., 1954. Estimation of plasma phosphatase by determination of hydrolysed phenol with amino-antipyrine. J. Clin. Pathol. 7, 322-326.

Kitagawa, S., Yoshii, K., Morita, S., Teraoka, R., 2011. Efficient topical delivery of chlorogenic acid by an oil-in-water microemulsion to protect skin against UV-induced damage. Chem. Pharm. Bull. 59, 793-796.

Kitistis, G., Niopas, I., 1998. A study on the in vitro percutaneous absorption of propranolol from disperse system. J. Pharm. Pharmacol. 50, 413-419.

Kommuru, T.R., Gurley, B., Khan, M.A., Reddy, I.K., 2001. Self-emulsifying drug delivery systems (SEDDS) of coenzyme Q10: formulation development and bioavailability assessment. Int. J. Pharm. 212, 233-246.

Konishi, Y., Kobayashi, S., 2004. Transepithelial transport of chlorogenic acid, caffeic acid, and their colonic metabolites in intestinal caco-2 cell monolayers. J. Agric. Food Chem. 5, 2518-26.

Korsmeyer, R.W., Gurny, R., Doelker, E., Buri, P., Peppas, N.A., 1983. Mechanisms of solute release from porous hydrophilic polymers. Int. J. Pharm. 15, 25.

Kosugi, Y., Yamamoto, S., Sano, N., Furuta, A., Igari, T., Fujioka, Y., Amano, N., 2015. Evaluation of acid tolerance of drugs using rats and dogs controlled for gastric acid secretion. J. Pharm. Sci. 104, 2887-2893.

Kreilgaard, M., Pedersen, E.J., Jaroszewski, J.W., 2000. NMR characterization and transdermal drug delivery potential of microemulsion systems. J. Control. Rel. 69, 421-433.

Kwon, S.H., Kang, M.J., Huh, J.S., Ha, K.W., Lee, J.R., Lee, S.K., Lee, B.S., Han, I.H., Lee, M.S., Lee, M.W., Lee, J., Choi, Y.W., 2007. Comparison of oral bioavailability of genistein and genistin in rats. Int. J. Pharm. 337,148-154.

Lala, R.R., Awari, N.G., 2014. Nanoemulsion-based gel formulations of COX-2 inhibitors for enhanced efficacy in inflammatory conditions, Appl. Nanosci. 4, 143-151.

Lamaallam, S., Bataller, H., Dicharry, C., Lachaise, J., 2005. Formation and stability of mini-emulsions produced by dispersion of water/oil/surfactants concentrates in a large amount of water. Colloid. Surf. A: Physicochem. Eng. Aspects. 270-271, 44-51.

Lawrence, M.J., 1994. Surfactant systems: microemulsions and vesicles as vehicles for drug delivery. Eur. J. Drug Metab. Pharmacokinet. 3, 257-269.

Lawrence, M.J., 1996. Microemulsions as drug delivery vehicles. Curr. Opin. Colloid Interface Sci. 1, 826-832.

Lawrence, M.J., Rees, G.D., 2000. Microemulsion-based media as novel drug delivery systems. Adv. Drug Deliv. Rev. 45, 89-121.

Lawrence, M.J., Rees, G.D., 2002. Microemulsion based media as a novel drug delivery system. Adv. drug delivery. Rev. 45, 89-121.

Lennemas, H., 2007. Modeling gastrointestinal drug absorption requires more in vivo biopharmaceutical data: experience from in vivo dissolution and permeability studies in humans. Curr. drug metab. 8, 645-657.

Levin, C., Maibach, H., 2002. Exploration of alternative and natural drugs in dermatology. Arch. Dermatol. 138, 207-211.

Lewis, D.F.V., Dickins, M., Weaver, R.J., Eddershaw, P.J., Goldfarb, P.S., Tarbit, M.H., 1998. Molecular modeling of human CYP2C subfamily enzymes CYP2C9 and CYP2C19: rationalization of substrate specificity and site directed mutagenesis experiments in the CYP2C subfamily. Xenobiotica 28, 235-268.

Li, D., Martini, N., Wu, Z., Wen, J., 2012. Development of an isocratic HPLC method for catechin quantification and its application to formulation studies. Fitoterapia 83, 1267-1274.

Li, D.C., Zhong, X.K., Zeng, Z.P., Jiang, J.G., Li, L., Zhao, M.M., Yang, X.Q., Chen, J., Zhang, B.S., Zhao, Q.Z., Xie, M.Y., Xiong, H., Deng, Z.Y., Zhang, X.M., Xu, S.Y., Gao, Y.X., 2009. Application of targeted drug delivery system in Chinese medicine. J. Control Release 138, 103-112.

Li, H., Zhao, X., Ma, Y., Zhai, G., Li, L., Lou, H., 2009. Enhancement of gastrointestinal absorption of quercetin by solid lipid nanoparticles. J. Control Release 133, 238-244.

Li, H.F., Liu, M.X., Liu, Q.F., Luo, G.A., Wang, C., Wang, Y.M., Chen, Q., 2007. Preparation of pharmacokinetics of breviscapine-loaded poly (d, l-lactic acid) nanoparticles. Chin. J. New Drugs 16, 614-618.

Li, Y., Liu, C., Zhang, Y., Mi, S., Wang, N., 2011. Pharmacokinetics of ferulic acid and potential interactions with Honghua and clopidogrel in rats. J. Ethnopharmacol. 137, 562-567.

Li, Y., Zheng, J., Xiao, H., McClements, D.J., 2012. Nanoemulsion-based delivery systems for poorly water-soluble bioactive compounds: Influence of formulation parameters on polymethoxyflavone crystallization. Food Hydrocolloids 27, 517-528.

Li, Y.C., Dong, L., Jia, K., Chang, X.M., Xue, H., 2006. Comparison of two methods of preparation of tetrandrine solid lipid nanoparticles. J. Chin. Med. Mater. 29, 483-485.

Li, Y.C., Dong, L., Jia, K., Chang, X.M., Xue, H., 2007. Preparation and anti-fibrotic effects of solid lipid nanoparticles loaded with silibinin. J. Xi'an Jiaotong Univ. 28, 517-520.

Liang, L., Liu, X., Wang, Q., Cheng, S., Zhang, S., Zhang, M., 2013. Pharmacokinetics, tissue distribution and excretion study of resveratrol and its prodrug 3,5,4-tri-O-acetylresveratrol in rats. Phytomedicine 20, 558-563.

Lin, A.H., Li, H.Y., Liu, Y.M., Qiu, X.H., 2007. Preparation and release characteristics of berberine chitosan nanoparticles in vitro. China Pharm. 18, 755-757.

Lin, F.H., Lin, J.Y., Gupta, R.D., Tournas, J.A., Burch, J.A., Selim, M.A., Monteiro-Riviere, N.A., Grichnik, J.M., Zielinski, J., Pinnell, S.R. 2005. Ferulic acid stabilizes a solution of vitamins C and E and doubles its photoprotection of skin. J. Invest. Dermatol. 125, 826-32.

Lipinski, C.A., Lombardo, F., Dominy, B.W., Feeney, P.J., 2001. Experimental and computational approaches to estimate solubility and permeability in drug discovery and development settings. Adv. Drug Delivery Rev. 46, 3-26.

Lira, M.C.B., Ferraz, M.S., da Silva, D.G.V.C., Cortes, M.E., Teixeira, K.I., 2009. Caetano, N.P., Santos-Magalhães, N.S., J. Incl. Phenom. Macrocycl. Chem. 64, 215-24.

Liu, C., Cao, Y.F., Fang, Z.Z., Zhang, Y.Y., Hu, C.M., Sun, X.Y., Huang, T., Zeng, J., Fan, X.R., Mo, H. 2012. Strong inhibition of deoxyschizandrin and schisantherin A toward UDPglucuronosyltransferase (UGT) 1A3 indicating UGT inhibition-based herb-drug interaction. Fitoterapia 83, 1415-9.

Liu, C.H., Wu, C.T., 2010. Optimization of nanostructured lipid carriers for lutein delivery. Colloids and Surfaces A: Physicochem. Eng. Aspects 353, 149-156.

Lowry, O.H., Rosebrough, N.J., Forr, A.L., Ramdall, R.J., 1951. Protein measurement with the Folins phenol reagent. J. Biol. Chem. 193, 265-275.

Lu, Y.P., Lou, Y.R., Xie, J.G., Peng, Q.Y., Liao, J., Yang, C.S., Huang, M.T., 2002. Topical applications of caffeine or (-)-epicatechin gallate (EGCG) inhibit carcinogenesis and selectively increase apoptosis in UVB-induced skin tumours in mice. Proc. Natl. Acad. Sci. 99, 12455-12460.

Machida, Y., Onishi, H., Kurita, A., Hata, H., Morikawa, A., Machida, Y., 2000. Pharmacokinetics of prolonged-release CPT-11-loaded microspheres in rats. J. Control Release 66, 159-75.

Madrigal-Carballo, S., Lim, S., Rodriguez, G., Vila, A.O., Krueger, C.G., Gunasekaran, S., Reed, J.D., 2010. Biopolymer coating of soybean lecithin liposomes via layer-by-layer self-assembly as novel delivery system for ellagic acid. J. Funct. Foods 2, 99-106.

Mahale, N.B., Thakkar, P.D., Mali, R.G., Walunj, D.R., Chaudhari, S.R., 2012. Niosomes: novel sustained release nonionic stable vesicular systems - an overview. Adv. Colloid Interface Sci. 183, 46-54.

Mainardes, R.M., Evangelista, R.C. 2005. PLGA nanoparticles containing praziquantel: effect of formulation variables on size distribution. Int. J. Pharm. 290, 137-44.

Maiti, K., Mukherjee, K., Gantait, A., Ahamed, K.F.H., Saha, B.P., Mukherjee, P.K., 2005. Enhanced therapeutic benefit of quercetin-phospholipid complex in carbon tetrachloride-induced acute liver injury in rats: a comparative study. Iran. J. Pharmacol. Ther. 4, 84-90.

Maiti, K., Mukherjee, K., Gantait, A., Saha, B.P., Mukherjee, P.K., 2007. Curcumin-phospholipid complex: preparation, therapeutic evaluation and pharmacokinetic study in rats. Int. J. Pharm. 330, 155-163.

Maiti, K., Mukherjee, K., Gantait, A., Saha, B.P., Mukherjee, P.K., 2006. Enhanced therapeutic potential of naringenin-phospholipid complex in rats. J. Pharm. Pharmacol. 58, 1227-1233.

Maiti, K., Mukherjee, K., Murugan, V., Saha, B.P., Mukherjee, P.K., 2010. Enhancing bioavailability and hepatoprotective activity of andrographolide from *Andrographis paniculata*, a well-known medicinal food, through its herbosome. J. Sci. Food Agric. 90, 43-51.

Malloy, H.T., Evelyn, K.A., 1973. The determination of bilirubin with the photoelectric colorimeter, J. Biol. Chem. 119, 481-490.

Manach, C., Scalbert, A., Morand, C., Remesy, C., Jimenez, L., 2004. Polyphenols: food sources and bioavailability. Am. J. Clin. Nutr. 79, 727-747.

Manach, C., Williamson, G., Morand, C., Scalbert, A., Rémésy, C., 2005. Bioavailability and bioefficacy of polyphenols in humans. I. Review of 97 bioavailability studies. Am. J. Clin. Nutr. 81, 230S-242S.

Manconi, M., Sinico, C., Valenti, D., Loy, G., Fadda, A.M., 2002. Niosomes as carriers for tretinoin. I. Preparation and properties. Int. J. Pharm. 234, 237-248.

Manthena, V.S., Varma, A., Ashokraj, Y., Chinmoy, S., Dey, B., Panchagnula, R., 2003. P-glycoproein inhibitors and their screening: a perspective from bioavailability enhancement. Pharmacol. Res., 48, 347-359.

Marczylo, T.H., Verschoyle, R.D., Cooke, D.N., Morazzoni, P., Steward, W.P., Gescher, A.J., 2007. Comparison of systemic availability of curcumin with that of curcumin formulated with phosphatidylcholine. Cancer Chemother. Pharmacol. 60, 171-177.

Marianecci, C., Rinaldi, F., Mastriota, M., Pieretti, S., Trapasso, E., Paolino, D., Carafa, M., 2012. Anti-inflammatory activity of novel ammonium glycyrrhizinate/niosomes delivery system: human and murine models. J. Control Release 164, 17-25.

Mason, T.G., Graves, S.M., Wilking, J.N., Lin, M.Y., 2006. Extreme emulsification: formation and structure of nanoemulsions. J. Phy. Cond. Matter. 9, 193-199.

Mauludin, R., Müller, R.H., Keck, C.M., 2009. Development of an oral rutin nanocrystal formulation. Int. J. Pharm. 370, 202-209.

Melo, C.L.L.D., Queiroz, M.G.R., Filho, A.C.V.A., Rodrigues, A.M., Sousa, D.F.D., Almeida, J.G.L., Pessoa, O.D.N.L., Silveira, E.R., Menezes, D.B., Melo, T.S., Santos, F.A., Rao, V.S., 2009. Betulinic acid, a natural pentacyclic triterpenoid, prevents abdominal fat accumulation in mice fed a high-fat diet. J. Agric. Food Chem. 57, 8776-81.

Mikhail, A.S., Allen, C., 2009. Block copolymer micelles for delivery of cancer therapy: transport at the whole body, tissue and cellular levels. J. Control Release 138, 214-223.

Min, K.H., Park, K., Kim, Y.S., Bae, S.M., Lee, S., Jo, H.G. Park, R.W., Kim, I.S., Jeong, S.Y., Kim, K., Kwon, I.C. 2008. Hydrophobically modified glycol chitosan nanoparticles-encapsulated camptothecin enhance the drug stability and tumor targeting in cancer therapy. J. Control Release 127, 208-18.

Mishra, B., Patel, B.B., Tiwari, S., 2010. Colloidal nanocarriers: a review on formulation technology, types and applications toward targeted drug delivery. Nanomedicine 6, 9-24.

Mitri, K., Shegokar, R., Gohla, S., Anselmi, C., Müller, R.H., 2011. Lipid nanocarriers for dermal delivery of lutein: preparation, characterization, stability and performance. Int. J. Pharm. 414, 267-275.

Miyake, K., Arima, H., Hirayama, F., Yamamoto, M., Horikawa, T., Sumiyoshi, H., Noda, S., Uekama, K., 2000. Improvement of solubility and oral bioavailability of rutin by complexation with 2-hydroxypropyl-beta-cyclodextrin. Pharm. Dev. Technol. 5, 399-407.

Morand, C., Manach, C., Crespy, V., Remesy, C., 2000. Quercetin 3-O-beta-glucoside is better absorbed than other quercetin forms and is not present in rat plasma. Free Radic. Res. 33, 667-676.

Morand, C., Manach, C., Crespy, V., Remesy, C., 2000. Respective bioavailability of quercetin aglycone and its glycosides in a rat model. Biofactors 12,169-174.

Mukherjee, P.K., Harwansh, R.K., Bhattacharyya, S., 2015. Bioavailability of herbal products: approach toward improved pharmacokinetics, in: Mukherjee, P.K. (Ed.), Evidence-based validation of herbal medicine, Elsevier, Amsterdam, pp. 217-245.

Mukherjee, D., Kumar, N.S., Khatua, T., Mukherjee, P.K., 2010. Rapid validated HPTLC method for estimation of betulinic acid in *Nelumbo nucifera* (Nymphaeaceae) rhizome extract. Phytochem. Anal. 21, 556-560.

Mukherjee, K., Venkatesh, M., Venkatesh, P., Saha, B.P., Mukherjee, P.K., 2011. Effect of soy phosphatidyl choline on the bioavailability and nutritional health benefits of resveratrol. Food Res. Int. 44, 1088-1093.

Mukherjee, P.K., Das, J., Saha, K., Pal, M., Saha, B.P., 1997. Investigation on the steroidal anti-inflammatory activity of betulinic acid from rhizomes of *Nelumbo nucifera* Gaertn. (Family - Nymphaeaceae). Planta Med. 63, 367-370.

Mukherjee, P.K., Maity, N., Nema, N.K., Sarkar, B.K., 2011. Bioactive compounds from natural resources against skin aging. Phytomedicine 19, 64-73.

Mukherjee, P.K., Ponnusankar, S., Pandit, S., Hazam, P.K., Ahmmed, M., Mukherjee, K., 2011. Botanicals as medicinal food and their effects on drug metabolizing enzymes. Food Chem. Toxicol. 49, 3142-3153.

Mukherjee, P.K., Venkatesh, M., Maiti, K., Mukherjee, K., Saha, B.P., 2009. Value added herbal drug delivery systems - perspectives and developments. Indian J. Pharm. Educ. Res. 43, 329-337.

Murakami, A., Nakamura, Y., Koshimizu, K., Takahashi, D., Matsumoto, K., Hagihara, K., Taniguchi, H., Nomura, E., Hosoda, A., Tsuno, T., Maruta, Y., Kim, H.W., Kawabata, K., Ohigashi, H., 2002. FA15, a hydrophobic derivative of ferulic acid, suppresses inflammatory responses and skin tumor promotion: comparison with ferulic acid. Cancer Lett. 180, 121-9.

Murota, K., Terao, J., 2003. Antioxidative flavonoid quercetin: implication of its intestinal absorption and metabolism. Arch. Biochem. Biophys. 417, 12-17.

Murugan, V., Mukherjee, K., Maiti, K., Mukherjee, P.K. 2009. Enhanced oral bioavailability and antioxidant profile of ellagic acid by phospholipids. J. Agric. Food Chem. 57, 4559-4565.

Muzzio, M., Huang, Z., Hu, S.C, Johnson, W.D., McCormick, D.L., Kapetanovic, I. M., 2012. Determination of resveratrol and its sulfate and glucuronide metabolites in plasma by LC-MS/MS and their pharmacokinetics in dogs. J. Pharm. Biomed. Anal. 59, 201-208.

Nishikawa, M., Ariyoshi, N., Kotani, A., Ishii, I., Nakamura, H., Nakasa, H., Ida, M., Nakamura, H., Kimura, N., Kimura, M., Hasegawa, A., Kusu, F., Ohmori, S., Nakazawa, K., Kitada, M., 2004. Effects of continuous ingestion of green tea or grape seed extracts on the pharmacokinetics of midazolam. Drug Metab. Pharmacokinet. 19, 280-289.

Odani, T., Tanizawa, H., Takino, Y., 1983. Studies on the absorption, distribution, excretion and metabolism of ginseng saponins. II. The absorption, distribution and excretion of ginsenoside Rg1 in the rat. Chem. Pharm. Bull. 31, 292-298.

Ohkawa, H., Hash, N., Yagi, K., 1979. Assay for lipid peroxide for animal tissue by thiobarbituric acid reaction. Ann. Biochem. 95, 351-358.

Okur, N.Ü., Apaydın, S., Yavaşlu, N.Ü., Yavaso˘glu, A., Karasulu, H.Y., 2011. Evaluation of skin permeation and anti-inflammatory and analgesic effects of new naproxen microemulsion formulations. Int. J. Pharm. 416, 136-144.

Olthof, M.R., Hollman, P.C.H., Vree, T.B., Katan, M.B., 2000. Bioavailabilities of quercetin-3-glucoside and quercetin-4'-glucoside do not differ in humans. J. Nutr. 130, 1200-1203.

Ososki, A.L., Kennelly, E.J., 2003. Phytoestrogens: a review of the present state of research. Phytother. Res.17, 845-869.

Paglia, D.E., Valentine, W.N., 1967. Studies on the quantitative and qualitative characterisation of erythrocyte glutathione peroxidase. J. Lab. Clin. Med. 70, 158-169.

Pan, M.H., Huang, T.M., Lin, J.K. 1999. Biotransformation of curcumin through reduction and glucuronidation in mice. Drug Metab. Dispos. 27, 486-494.

Pan, Y., Abd-Rashid, B.A., Ismail, Z., Ismail, R., Mak, J.W., Pook, P.C., et al. 2011. In vitro modulatory effects of *Andrographis paniculata*, *Centella asiatica* and *Orthosiphon stamineus* on cytochrome P450 2C19 (CYP2C19). J. Ethnopharmacol. 133, 881-7.

Paolino, D., Lucania G., Mardente, D., Alhaique, F., Fresta, M., 2005. Ethosomes for skin delivery of ammonium glycyrrhizinate: in vitro percutaneous permeation through human skin and in vivo anti-inflammatory activity on human volunteers. J. Control Release 106, 99-110.

Parveen, R., Baboota, S., Ali, J., Ahuja, A., Vasudev, S.S., Ahmad, S., 2011. Oil based nanocarrier for improved oral delivery of silymarin: In vitro and in vivo studies. Int. J. Pharm. 413, 245-253.

Paudel, K.S., Milewski, M., Swadley, C.L., Brogden, N.K., Ghosh, P., Stinchcomb, A.L., 2010. Challenges and opportunities in dermal/transdermal delivery. Ther. Deliv. 1, 109-131.

Pey, C.M., Maestro, A., Solé, I., González, C., Solans, C., Gutiérrez, J.M., 2006. Optimization of nano-emulsions prepared by low-energy emulsification methods at constant temperature using a factorial design study. Colloids Surf. A: Physicochem. Eng Aspects. 288, 144-150.

Pinnell, S.R., 2003. Cutaneous photodamage, oxidative stress, and topical antioxidant protection. J. Am. Acad, Dermatol. 48, 1-22.

Pomponio, R., Gotti, R., Luppi, B., Cavrini, V., 2003. Microemulsion electrokinetic chromatography for the analysis of green tea catechins: effect of the cosurfactant on the separation selectivity. Electrophoresis 24, 1658-1667.

Pool, H., Mendoza, S., Xiao, H., McClements, D.J., 2013. Encapsulation and release of hydrophobic bioactive components in nanoemulsion-based delivery systems: impact of physical form on quercetin bioaccessibility. Food Funct. 4, 162.

Porras, M., Solans, C., González, C., Gutiérrez, J.M. 2008. Properties of water-in-oil (W/O) nano-emulsions prepared by a low-energy emulsification method. Colloids Surf. A: Physicochem. Eng. Aspects. 324, 181-188.

Porter, C.J.H., Pouton, C.W., Cuine, J.F., Charman, W.N., 2008. Enhancing intestinal drug solubilization using lipid-based delivery systems. Adv. Drug Delivery Rev. 60, 673-691.

Prasad, N.R., Ramachandran, S., Pugalendi, K.V., Menon, V.P., 2007. Ferulic acid inhibits UV-B induced oxidative stress in human lymphocytes. Nutrition Research. 27, 559-564.

Prausnitz, M.R., Mitragotri, S., Langer, R., 2004. Current status and future potential of transdermal drug delivery. Nat. Rev. Drug Discov. 3, 115-124.

Priprem, A., Watanatorn, J., Sutthiparinyanont, S., Phachonpai, W., Muchimapura, S., 2008. Anxiety and cognitive effects of quercetin liposomes in rats. Nanomed. Nanotechnol. Biol. Med. 4, 70-78.

Qian, C., Decker, E.A., Xiao, H., McClements, D.J., 2012. Nanoemulsion delivery systems: Influence of carrier oil on β-carotene bioaccessibility. Food Chem. 135, 1440-1447.

Qian, C., Decker, E.A., Xiao, H., McClements, D.J., 2013. Impact of lipid nanoparticle physical state on particle aggregation and β-carotene degradation: potential limitations of solid lipid nanoparticles. Food Res. Int. 52, 342-349.

Qin, S.H., Liu, H.G., 2006. Pharmacokinetics study on yinhuang compound microenema in rabbits. Zhongguo Zhongyao Zazhi 31, 54-56.

Quin, C., McClement, D.J. 2011. Formation of nanoemulsions stabilized by model food grade emulsifiers using high pressure homogenization: factors affecting particle size. Food Hydrocolloids. 25. 1000-1008.

Rahman, M.A., Harwansh, R., Mirza, M.A., Hussain, S., Hussain, A., 2011. Oral lipid based drug delivery system (LBDDS): formulation, characterization and application: a review. Curr. Drug Deliv. 8, 1-16.

Rahman, M.A., Hussain, A., Iqbal, Z., Harwansh, R.K., Singh, L.R. Ahmad, S., 2013. Nanosuspension: a potential nanoformulation for improved delivery of poorly bioavailable drug. Micro Nanosyst. 5, 273-287.

Ramassamy, C., 2006. Emerging role of polyphenolic compounds in the treatment of neurodegenerative diseases: a review of their intracellular targets. Eur. J. Pharmacol. 545, 51-64.

Ravi, T.P.U, Padma, T., 2011. Nanoemulsions for drug delivery through different routes. Research in Biotechnol. 2, 1-13.

Ravindranath, V., Chandrasekhara, N., 1980. Absorption and tissue distribution of curcumin in rats. Toxicology 16, 259-265.

Reitman, S., Frankel, S., 1957. A colourimetric method for the determination of serum oxaloacetatic and glutamic pyruvic transaminases. Am. J. Clin. Pathol. 28, 56-63.

Ren, J., Jiang, X., Li, C., 2007. Investigation on the absorption kinetics of chlorogenic acid in rats by HPLC. Arch. Pharmacal. Res. 30, 911-916.

Riviere, J.E., Papich, M.G., 2001. Potential and problems of developing transdermal patches for veterinary applications. Adv. Drug Deliv. Rev. 50, 175-203.

Rukkumani, R., Aruna, K., Varma, P.S., Menon, V.P., 2004. Ferulic acid, a natural phenolic antioxidant modulates altered lipid profiles during alcohol and thermally oxidized sunflower oil induced toxicity. Neutraceutic. Funct. Med. Foods. 4, 119-32.

Saberi, A.H., Fang, Y., McClements, D.J., 2013. Fabrication of vitamin E-enriched nanoemulsions: Factors affecting particle size using spontaneous emulsification. J. Colloid Interface Sci. 391, 95-102.

Saija, A., Tomaino, A., Trombetta, D., Pasquale, A.D, Uccella, N., Barbuzzi, T., Paolino, D., Bonina, F., 2000. In vitro and in vivo evaluation of caffeic and ferulic acids as topical photoprotective agents. Int. J. Pharm. 199, 39-47.

Seeram, N.P., Lee, R., Heber, D., 2004. Bioavailability of ellagic acid in human plasma after consumption of ellagitannins from pomegranate (*Punica granatum* L.) juice. Clin. Chim. Acta 348, 63-68.

Serra, A., Macià, A., Romero, M.P., Reguant, J., Ortega, N., Motilva, M.J., 2012. Metabolic pathways of the colonic metabolism of flavonoids (flavonols, flavones and flavanones) and phenolic acids. Food Chem. 130, 383-393.

Sessa, M., Balestrieri, M.L., Ferrari, G., Servillo, L., Castaldo, D., D'Onofrio, N., Donsì, F., Tsao, R., 2014. Bioavailability of encapsulated resveratrol into nanoemulsion-based delivery systems. Food Chem. 147, 42-50.

Sessa, M., Casazza, A.A., Perego, P., Tsao, R., Ferrari, G., Donsì, F., 2013. Exploitation of polyphenolic extracts from grape marc as natural antioxidants by encapsulation in lipid-based nanodelivery systems. Food Bioprocess Technol. 6, 2609-2620.

Setchell, K.D., Brzezinski, A., Brown, N.M., Desai, P.B., Melhem, M., Meredith, T., Zimmer-Nechimias, L., Wolfe, B., Cohen, Y., Blatt, Y., 2005. Pharmacokinetics of a slow-release formulation of soybean isoflavones in healthy postmenopausal women. J. Agric. Food Chem. 53, 1938-1344.

Shafiq, S., Shakeel, F., Talegaonkar, S., Ahmad, F.J., Khar, R.K., Ali, M., 2007. Development and bioavailability assessment of ramipril nanoemulsion formulation. Eur. J. Pharm. Biopharm. 66, 227-243.

Shah, K.A., Date, A.A., Joshi, M.D., Patravale, V.B., 2007. Solid lipid nanoparticles (SLN) of tretinoin: potential in topical delivery. Int. J. Pharm. 345, 163-171.

Shahrzad, S., Aoyagi, K., Winter, A., Koyama, A., Bitsch, I., 2001. Pharmacokinetics of gallic acid and its relative bioavailability from tea in healthy humans. J. Nutr. 131, 1207-1210.

Shakeel F., Ramadan, W., 2010. Transdermal delivery of anticancer drug caffeine from water-in-oil nanoemulsions. Colloids Surf. B 75, 356-362.

Shakeel, F., Haq, N., Alanazi, F.K., Alsarra, I.A., 2013. Impact of various nonionic surfactants on self-nanoemulsification efficiency of two grades of Capryol (Capryol-90 and Capryol-PGMC). J. Mol. Liq. 182, 57-63.

Shanmugam, S., Park, J., Kim, K.S., Piao, Z.Z., Yong, C.S., Choi, H., Woo, J. S., 2011. Enhanced bioavailability and retinal accumulation of lutein from self-emulsifying phospholipid suspension (SEPS). Int. J. Pharm. 412, 99-105.

Shargel, L., Yu, A.B., 1999. Applied biopharmaceutics & pharmacokinetics, 4th edition, New York: McGraw-Hill.

Sharma, G., Italia, J.L., Sonaje, K., Tikoo, K., Ravi, K.M.N.V., 2007. Biodegradable in situ gelling system for subcutaneous administration of ellagic acid and ellagic acid loaded nanoparticles: Evaluation of their antioxidant potential against cyclosporine induced nephrotoxicity in rats. J. Control Release 118, 27-37.

Sharma, R.A., Euden, S.A., Platton, S.L., Cooke, D.N., Shafayat, A., Hewitt, H.R., Marczylo, T.H., Morgan, B., Hemingway, D., Plummer, S.M., Pirmohamed, M., Gescher, A.J., Steward, W.P., 2004. Phase I clinical trial of oral curcumin: biomarkers of systemic activity and compliance. Clin. Cancer Res.10, 6847-6854.

Sharom, F.J., 2008. ABC multidrug transporters: structure, function and role in chemoresistance. Pharmacogenomics 9, 105-27.

Shimada, S., 2008. Composition comprising nanoparticle *Ginkgo biloba* extract with the effect of brain function activation IPC8 Class-AA61K914FI, USPC Class-424489.

Shinoda, K., Saito, H., 1968. The effect of temperature on the phase equilibria and the types of dispersions of the ternary system composed of water, cyclohexane, and non-ionic surfactant. J. Colloid Interf. Sci. 26, 70-74.

Shoba, G., Joy, D., Joseph, T., Majeed, M., Rajendran, R., Srinivas, P.S., 1998. Influence of piperine on the pharmacokinetics of curcumin in animals and human volunteers. Planta Med. 64, 353-356.

Shoji, Y., Nakashima, H., 2006. Glucose-lowering effect of powder formulation of African black tea extract in KK-A(y)/TaJcl diabetic mouse. Arch. Pharm. Res. 29, 786-794.

Silva, H.D., Cerqueira, M.A., Souza, B.W.S., Ribeiro, C., Avides, M.C., Quintas, M. A.C., Coimbra, J.S.R., Carneiro-da-Cunha, M.G., Vicente, A.A., 2011. Nanoemulsions of β-carotene using a high-energy emulsification evaporation technique. J. Food Eng. 102, 130-135.

Silva, H.D., Cerqueira, M.Â., Vicente, A.A., 2012. Nanoemulsions for food applications: development and characterization. Food Bioprocess Technol. 5, 854-867.

Singh, H.P., Utreja, P., Tiwary, A.K., Jain, S., 2009. Elastic liposomal formulation for sustained delivery of colchicine: in vitro characterization and in vivo evaluation of anti-gout activity. AAPS J. 11, 54-64.

Solans, C., Esquena, J., Forgiarini, A.M., Uson, N., Morales, D., Izquierdo, P., 2002 Nanoemulsions: formation and properties. In: Mittal, K.L., Shah, D.O., (Eds). Surfactants in Solution: Fundamentals and Applications. New York: Marcel Dekker. pp. 525.

Solans, C., Izquierdo, P., Nolla, J., Azemar, N., Garcia-Celma, M.J. 2005. Nano-emulsions. Curr. Opin. Colloid Interf. Sci. 10, 102-110.

Sole, I., Maestro, A., Pey, C.M., Gonzalez, C., Solans, C., Gutierrez, J.M., 2006. Nanoemulsions preparation by low energy methods in an ionic surfactant system. Colloids Surf. A: Physiochem. Eng. Aspects. 288, 138-143.

Sole, I., Pey, C.M., Maestro, A., Gonzalez, C., Porras, M., Solans, C., Gutierrez, J.M. 2010. Nanoemulsions prepared by phase inversion composition method: preparation variables and scale up. J. Colloid Interf. Sci. 344, 417-423.

Mei, S., Ping, I.C., Hung, W., 2005. Silybin milk preparation and pharmacokinetics in rabbits. J. China Pharm. Univ. 36, 427-31.

Sonneville-Aubrun, O., Simonnet, J.T., L'Alloret, F., 2004. Nanoemulsions: a new vehicle for skincare products. Adv. Colloids Interf. Sci. 108-109, 145-149.

Srinivasan, M., Ram-Sudheer, A., Raveendran Pillai, K., Raghu Kumarc, P., Sudhakaran, P.R., Menon, V.P., 2006. Influence of ferulic acid on gamma radiation induced DNA damage, lipid peroxidation and antioxidant status in primary culture of isolated rat hepatocytes. Toxicology. 228, 249-58.

Srinivasan, M., Rukkumani, R., Ram Sudheer, A., Menon, V.P., 2005. Ferulic acid, a natural protector against carbon tetrachloride induced toxicity. Fundam. Clin. Pharmacol. 19, 491-6.

Srinivasan, M., Sudheer, A.R., Menon, V.P., 2007. Ferulic acid: therapeutic potential through its antioxidant property. J. Clin. Biochem. Nutr. 40, 92-100.

Staniforth, V., Huang, W.C., Aravindaram, K., Yang, N.S., 2012. Ferulic acid, a phenolic phytochemical, inhibits UVB-induced matrix metalloproteinases in mouse skin via posttranslational mechanisms. J. Nutr. Biochem. 23, 443-451.

Stoner, G.D., Sardo, C., Apseloff, G., Mullet, D., Wargo, W., Pound, V., Singh, A., Sanders, J., Aziz, R., Casto, B., Sun, X., 2005. Pharmacokinetics of anthocyanins and ellagic acid in healthy volunteers fed freeze-dried black raspberries daily for 7 days. J. Clin. Pharmacol. 45, 1153-1164.

Stro¨mbom, J., Sandberg, F., Dencker, L., 1985. Studies on absorption and distribution of ginsenoside Rg1 by whole-body autoradiobiography and chromatography. Acta Pharm. Suec. 22, 113-122.

Subramanyam, R., Gollapudi, A., Bonigala, P., Chinnaboina, M., Amooru, D.G., 2009. Betulinic acid binding to human serum albumin: a study of protein conformation and binding affinity. J. Photochem. Photobiol., B 94, 8-12.

Sun, H., Dong, T., Zhang, A., Yang, J., Yan, G., Sakurai, T., Wu, X., Han, Y., Wang, X., 2013. Pharmacokinetics of hesperetin and naringenin in the Zhi Zhu Wan, a traditional chinese medicinal formulae, and its pharmacodynamics study. Phytother. Res. 27, 1345-1351.

Sun, H.W., Ouyang, W.Q., 2007. Preparation, quality and safety evaluation of berberine nanoemulsion for oral application. J. Shanghai Jiaotong Univ. 1, 60-5.

Suo, X.B., Zhang, H., Wang, Y.Q., 2007. HPLC determination of andrographolide in rat whole blood: study on the pharmacokinetics of andrographolide incorporated in liposomes and tablets. Biomed. Chromatogr. 21, 730-734.

Suppasrivasuseth, J., Bellantone, R.A., Plakogiannis, F.M., Stagni, G., 2006. Permeability and retention studies of (-)epicatechin gel formulations in human cadaver skin. Drug Dev. Ind. Pharm. 32, 1007-1017.

Tada, Y., Ikeda, T., Takahashi, H., Yano, N., Yuzawa, K., Nagasawa, A., et al. 2001. Subchronic toxicity test of ferulic acid, natural food additive, in F344 rats. Tokyo Metrop. Res. Lab. Public Health 52, 267–271.

Tada, Y., Tayama, K., & Aoki, N., 1999. Acute oral toxicity of ferulic acid, natural food additive, in rats. Tokyo Metrop. Res. Lab. Public Health 50, 311-313.

Tang, D.W., Yu, S.H., Ho, Y.C., Huang, B.Q., Tsai, G.J., Hsieh, H.Y., Sung, H.W., Mi, F.L., 2013. Characterization of tea catechins-loaded nanoparticles prepared from chitosan and an edible polypeptide. Food Hydrocolloids 30, 33-41.

Tawab, M.A., Bahr, U., Karas, M., Wurglics, M., Schubert-Zsilavecz, M., 2003. Degradation of ginsenosides in humans after oral administration. Drug Metab. Dispos. 31, 1065-1071.

Tenjarla, S., 1999. Microemulsions: an overview and pharmaceutical applications. Crit. Rev. Ther. Drug Carrier Systems. 16, 461-521.

Tiyaboonchai, W., Tungpradit, W., Plianbangchang, P., 2007. Formulation and characterization of curcuminoids loaded solid lipid nanaparticles. Int. J. Pharm. 337, 299-306.

Trotta, M., Peira, E., Debernardi, F., Gallarate, M., 2002. Elastic liposomes for skin delivery of dipotassium glycyrrhizinate. Int. J. Pharm. 241 319-327.

Tsai, Y., Lee, K., Huang, Y., Huang, C., Wu, P., 2010. In vitro permeation and in vivo whitening effect of topical hesperetin microemulsion delivery system. Int. J. Pharm. 388, 257-262.

Udeani, G.O., Zhao, G.M., Shin, Y.G., Cooke, B.P., Graham, J., Beecher, C.W.W., Kinghorn, A.D., Pezzuto, J.M., 1999. Pharmacokinetics and tissue distribution of betulinic acid in CD-1 mice. Biopharm. Drug Dispos. 20, 379-383.

Umathe, S.N., Dixit, P.V., Bansod, K.U., Wanjari, M.M., 2008. Quercetin pretreatment increases the bioavailability of pioglitazone in rats: involvement of CYP3A inhibition. Biochem. Pharmacol.75, 1670-6.

Panda, V.S., Naik, S.R., 2008. Cardioprotective activity of *Ginkgo biloba* Phytosomes in isoproterenol-induced myocardial necrosis in rats: a biochemical and histoarchitectural evaluation. Exp. Toxicol. Pathol. 60, 397-404.

Vemulapalli, V., Khan, N.M., Jasti, B.R., 2007. Physicochemical characteristics that influence the transport of drugs across intestinal barrier. AAPS news magazine 18-21.

Wahlstrom, B., Blennow, G., 1978. A study on the fate of curcumin in the rat. Acta Pharmacol. Toxicol. 43, 86-92.

Wakerly, M.G., Pouton, C.W., Meakin, B.J., Morton, F.S., 1986. Self-emulsification of vegetable oil nonionic surfactant mixture: a proposed mechanism of action. ACS Symp. Ser. 311, 242-255.

Walle, T., Otake, Y., Walle, U.K., Wilson, F.A., 2000. Quercetin glucosides are completely hydrolyzed in ileostomy patients before absorption. J. Nutr. 130, 2658-2661.

Wan, Y., Jiang, S., Lian, L.H., Bai, T., Cui, P.H., Sun, X.T., Jin, X.J., Wu, Y.L., Nan, J.X., 2013. Betulinic acid and betulin ameliorate acute ethanol-induced fatty liver via TLR4 and STAT3 in vivo and in vitro. Int. Immunopharmacol. 17, 184-190.

Wang, D., Wang, X., Li, X., Ye, L., 2008. Preparation and characterization of solid lipid nanoparticles loaded with α-asarone. PDA J. Pharm. Sci. Technol. 62, 56-65.

Wang, L., Li, X., Zhang, G., Dong, J., Eastoe, J., 2007. Oil-in-water nanoemulsions for pesticide formulations. J. Colloid Interf. Sci. 314, 230-235.

Wang, Y.N., Wu, W., Chen, H.C., Fang, H., 2010. Genistein protects against UVB-induced senescence-like characteristics in human dermal fibroblast by p66Shc down-regulation. J. Dermatol. Sci. 58, 19-27.

Warisnoicharoen, W., Lansley, A.B., Lawrence, M.J., 2000. Light scattering investigations on dilute non-ionic oil-in-water microemulsions. AAPS Pharm. Sci. 2, 429-448.

Wu, L., Zhang, Q.L., Zhang, X.Y., Lv, C., Li, J., Yuan, Y., Yin, F.X., 2012. Pharmacokinetics and blood-brain barrier penetration of (+)-catechin and (-)-epicatechin in rats by microdialysis sampling coupled to high-performance liquid chromatography with chemiluminescence detection. J. Agric. Food Chem. 60, 9377-9383.

Xiao, L., Zhang, Y.H., Xu, J.C., Jin, X.H., 2008. Preparation of floating rutin-alginate-chitosan microcapsule. Chin. Trad. Herb Drugs 2, 209-12.

Long, X.Y., Luo, J.B., Li, L.R., Lin, D., Rong, H.S., Huang, W.M. 2006. Preparation and in vitro evaluations of topically applied capsaicin transfersomes. Zhongguo Zhong Yao Za zhi 31, 981-4.

Xie, L., Li, X., Jiang, D., Zhang, D., 2011. Determination and pharmacokinetic study of catechins in rat plasma by HPLC. J. Pharm. Anal. 1, 297-301.

Yang, C.P., Liu, M.H., Zou, W., Guan, X.L., Lai, L., Su, W.W., 2012b. Toxicokinetics of naringin and its metabolite naringenin after 180-day repeated oral administration in beagle dogs assayed by a rapid resolution liquid chromatography/tandem mass spectrometric method. J. Asian Nat. Prod. Res. 14, 68-75.

Yang, C.Y., Hsiu, S.L., Wen, K.C., Lin, S.P., Tsai, S.Y., Hou, Y.C., Chao, P.D.L., 2005. Bioavailability and metabolic pharmacokinetics of rutin and quercetin in rats. J. Food Drug Anal. 13, 244-250.

Yang, H., Yuan, B., Li, L., Chen, H., Li, F., 2004. HPLC determination and pharmacokinetics of chlorogenic acid in rabbit plasma after an oral dose of *Flos lonicerae* extract. J. Chromatogr. Sci. 42, 173-176.

Yang, K.Y., Lin, L.C., Tseng, T.Y., Wang, S.C., Tsai, T.H., 2007. Oral bioavailability of curcumin in rat and the herbal analysis from *Curcuma longa* by LC-MS/MS. J. Chromatogr. B: Anal. Technol. Biomed. Life Sci. 853, 183-9.

Yang, Y., Zhang, Z., Li, S., Ye, X., Li, X., He, K., 2014. Synergy effects of herb extracts: pharmacokinetics and pharmacodynamic basis. Fitoterapia 92, 133-147.

Yang, Z., Wang, J.R., Niu, T., Gao, S., Yin, T., You, M., et al. 2012a. Inhibition of pglycoprotein leads to improved oral bioavailability of compound k, an anticancer metabolite of red ginseng extract produced by gut microflora. Drug Metab. Dispos. 40, 1538-44.

Yanyu, X., Yunmei, S., Zhipeng, C., Quineng, P., 2006. The preparation of silybin-phospholipid complex and the study on its pharmacokinetics in rats. Int. J. Pharm. 307, 77-82.

Ye, L., Wang, T., Tang, L., Liu, W., Yang, Z., Zhou, J., Zheng, Z., Cai, Z., Hu, M., Liu, Z., 2011. Poor oral bioavailability of a promising anticancer agent andrographolide is due to extensive metabolism and efflux by P glycoprotein. J. Pharm. Sci. 100, 5007-5017.

Yeung, J.H., Or, P.M., 2012. Polysaccharide peptides from *Coriolus versicolor* competitively inhibit model cytochrome P450 enzyme probe substrates metabolism in human liver microsomes. Phytomedicine19, 457-63.

Yi, J., Xia, W., Wu, J., Yuan, L., Wu, J., Tu, D., Fang, J., Tan, Z., 2014. Betulinic acid prevents alcohol-induced liver damage by improving the antioxidant system in mice. J. Vet. Sci. 15, 141-148.

Yi, J., Zhu, R., Wu, J., Wu, J., Tan, Z., 2015. Ameliorative effect of betulinic acid on oxidative damage and apoptosis in the splenocytes of dexamethasone treated mice. Int. Immunopharmacol. 27, 85-94.

Yilmaz, E., Borchert, H.H., 2006. Effect of lipid-containing, positively charged nanoemulsions on skin hydration, elasticity and erythema - an in vivo study. Int. J. Pharm. 307, 232-238.

Yogeeswari, P., Sriram, D., 2005. Betulinic acid and its derivatives: a review on their biological properties. Curr. Med. Chem. 12, 657-666.

Yoshida, N., Takada, T., Yamamura, Y., Adachi, I., Suzuki, H., Kawakami, J., 2008. Inhibitory effects of terpenoids on multidrug resistance-associated protein 2-and breast cancer resistance protein-mediated transport. Drug Metab. Dispos. 36,1206-11.

Chen, Y., Lin, X., Park, H., Greever, R., 2009. Study of artemisinin nanocapsules as anticancer drug delivery systems. Nanomedicine 5, 316-22.

Zeng, M., Zhang, J., Yang, Y., Jin, Y., Xiao, W., Wang, Z., Ding, G., Yan, R., 2014. An automated dual-gradient liquid chromatography–MS/MS method for the simultaneous determination of ferulic acid, ligustrazine and ligustilide in rat plasma and its application to a pharmacokinetic study. J. Pharm. Biomed. Anal. 88, 354-363.

Zhan, X.Y., Zhu, Q.Y., 2008. Advance of the research on targeting drug delivery system. China Prac. Med. 3, 471-474.

Zhang, J., Tang, Q., Xu, X., Li, N., 2013. Development and evaluation of a novel phytosome-loaded chitosan microsphere system for curcumin delivery. Int. J. Pharm. 448, 168-174.

Zhang, L., Yao, J., Zhou, J., Wang, T., Zhang, Q., 2013. Glycyrrhetinic acid-graft-hyaluronic acid conjugate as a carrier for synergistic targeted delivery of antitumor drugs. Int. J. Pharm. 441, 654-64.

Zhang, L.W., Al-Suwayeh, S.A., Hsieh, P.W., Fang, J.Y., 2010. A comparison of skin delivery of ferulic acid and its derivatives: evaluation of their efficacy and safety. Int. J. Pharm. 399, 44-51.

Zhang, Q.H., Wang, W.B., Li, J., Chang, Y.X., Wang, Y.F., Zhang, J., Zhang, B.L., Gao, X.M., 2012. Simultaneous determination of catechin, epicatechin and epicatechin gallate in rat plasma by LC–ESI-MS/MS for pharmacokinetic studies after oral administration of *Cynomorium songaricum* extract. J. Chromatogr. B 880, 168-171.

Zhang, Y., Wang, G.J., Song, T.T., Murphy, P.A., Hendrich, S., 1999. Urinary disposition of the soybean isoflavones daidzein, genistein and glycitein differs among humans with moderate fecal isoflavone degradation activity. J. Nutr. 129, 957-62.

Zhao, L.X., Liu, A.C., Yu, S.W., Wang, Z.X., Lin, X.Q., Zhai, G.X., Zhang, Q.Z., 2013. The permeability of puerarin loaded poly(butylcyanoacrylate) nanoparticles coated with polysorbate 80 on the blood-brain barrier and its protective effect against cerebral ischemia/reperfusion injury. Biol. Pharm. Bull. 36,1263-70.

Zhao, Y., Wang, C., Albert H.L., Chow, K.R., Gong, T., Zhang, Z and Zheng, Y., 2010. Self-nanoemulsifying drug delivery system (SNEDDS) for oral delivery of Zedoary essential oil: formulation and bioavailability studies. Int. J. Pharm. 383, 170-177.

Zhao, Z., Egashira, Y., Sanada, H., 2005. Phenolic antioxidants richly contained in corn bran are slightly bioavailable in rats. J. Agric. Food Chem. 53, 5030-5035.

Zhao, Z., Moghadasian, M.H., 2008. Chemistry, natural sources, dietary intake and pharmacokinetic properties of ferulic acid: a review. Food Chem. 109, 691-702.

Zhaohui, Z., Taotao, W., Jingwu, H., Gengshan, L., Shaozu, Y., Wenjuan, X., 2003. Iron-induced oxidative damage and apoptosis in cerebellar granule cells: attenuation by tetramethylpyrazine and ferulic acid. Eur J Pharmacol. 467, 41-7.

Zhaowu, Z., Xiaoli, W., Yangdel, Z., Nianfeng, L., 2009. Preparation of matrine ethosome, its percutaneous permeation in vitro and anti-inflammatory activity in vivo in rats. J. Liposome Res. 19, 155-62.

Zheng, D., Duan, C., Zhang, D., Jia, L., Liu, G., Liu, Y., Wang, F., Li, C., Guo, H., Zhang Q., 2012. Galactosylated chitosan nanoparticles for hepatocyte-targeted delivery of oridonin. Int J Pharm. 15, 379-86.

Zheng, Y., Hou, S.X., Chen, T., Lu, Y., 2006. Preparation and characterization of transfersomes of three drugs in vitro. China J. Chin. Mater. Med. 31, 728-31.

Mei, Z., Li, X., Wu, Q., Hu, S., Yang, X., 2005. The research on the anti-inflammatory activity and hepatotoxicity of triptolide-loaded solid lipid nanoparticle. Pharmacol. Res. 51, 345-51.

Zhong, H., Deng, Y., Wang, X., Yang, B., 2005. Multivesicular liposome formulation for the sustained delivery of breviscapine. Int. J. Pharm. 301, 15-24.

Zhou, S., Gao, Y., Jiang, W., Huang, M., Xu, A., Paxton, J.W., 2003. Interactions of herbs with cytochrome P450. Drug Metabol. Rev. 35, 35-98.

Zhou, W., Liu, S., Ju, W., Shan, J., Meng, M., Cai, B., Di, L., 2013. Simultaneous determination of phenolic acids by UPLC-MS/MS in rat plasma and its application in pharmacokinetic study after oral administration of *Flos Lonicerae* preparations. J. Pharm. Biomed. Anal. 86, 189-197.

Zou, L., Harkey, M., Henderson, G., 2002. Effects of herbal components on cDNA-expressed cytochrome P450 enzyme catalytic activity. Life Sci. 1, 1579-89.

## Acknowledgement

I take this opportunity to express my deep gratitude to all of them who have supported and helped to make this thesis successfully. First of all I would like to pay obeisance to the almighty for giving me ability, courage & strength to face and cope up with the barriers & hurdles that came by my way of PhD journey.

It is moment of great pleasure and immense satisfaction for me to express my reverence, deep gratitude and respect to my esteemed guide Prof. Pulok K Mukherjee, Director, School of Natural Product Studies, Department of Pharmaceutical Technology, Jadavpur University, who was continuous source of inspiration throughout the course of my PhD thesis work. I don't have words to express my feelings about his dedication, hard work and passion for the research. His deep involvement, logical and analytical thinking has made a big difference towards the research. I consider myself to be fortunate to work under his supervision and I am indebted for shaping my research life. I am grateful to him for seeking support to improve by all means. It was an immense pleasure working under his guidance.

I am thankful to Dr. (Mrs.) Kakali Mukherjee, for her admiration and encouragement during my PhD work. I also thank Prof. Tuhinadri Sen, Prof. Sanmoy Karmakar and Dr. P. Haldar for their support in completing this work effectively. I would like to express my gratitude to Dr. Jagadish Singh and Dr. Partha Pratim Roy, Assistant Professor, Institute of Pharmaceutical Science, Guru Ghasidas Vishwavidyalaya, Bilaspur for their conscientious support and encouragement throughout my thesis work. I pen down my sincere gratitude to my Ex-colleague Dr. Akhlaquer Rahman, Faculty of Pharmacy, Integral University, Lucknow and Mr. Mrityunjoy Kundu, Bose Institute, Kolkata for their active help and motivation for my works. They helped me particularly for analysis and characterization of my formulations. I am very grateful to my wife Mrs. Sangeeta Harwansh for her love, support and sacrifice during my PhD work.

I gratefully acknowledge the help and support rendered by my co-research fellow Dr. Subrata Pandit, Dr. Santanu Bhadra, Dr. Neelesh K. Nema, Dr. Niladri Maity, Dr. Sushil K. Chaudhary, Dr. Manoj Kumar Dalai, Dr. Sauvik Bhattacharya, Mr. Rajarshi Biswas, Sk. Milan Ahmmed, Mr. Mrinmoy Nag, Mr. Debayan Goswami, Mr. Amit Kar, Mr. Shiv Bahadur, Mr. Joydeb Chanda, Dr. (Mrs.) Kasturi Basu, Mr. Sayan Biswas, Mr. Subhadip Banerjee, Mr. Logesh Rajan, Mr. Bhaskar Das, Mr. Amrendra Tiwari, Mr. Arpan, Mr. Pritorthi from School of Natural Product Studies, Jadavpur University, Kolkata. It would not be possible to complete this work without the active help from my research fellow.

I am highly obliged to my entire family and friends for standing by me in low time. I express my sincere gratitude to my Late Grandfather who blessed and encouraged me in all aspects throughout my career.

**Ranjit K. Harwansh,** ***M. Pharm***

Life Sciences 141 (2015) 202–211

Contents lists available at ScienceDirect

Life Sciences

journal homepage: www.elsevier.com/locate/lifescie

# Enhanced permeability of ferulic acid loaded nanoemulsion based gel through skin against UVA mediated oxidative stress

Ranjit K. Harwansh, Pulok K. Mukherjee *, Shiv Bahadur, Rajarshi Biswas

*School of Natural Product Studies, Department of Pharmaceutical Technology, Jadavpur University, Kolkata 700032, India*

ARTICLE INFO

*Article history:*
Received 2 May 2015
Received in revised form 24 August 2015
Accepted 1 October 2015
Available online 5 October 2015

*Keywords:*
Nanoemulsion
Ferulic acid
Permeability
Oxidative stress
UVA protection activity
Nano-gel

ABSTRACT

*Aims:* The study was aimed to develop a ferulic acid (FA) loaded nanoemulsion based gel in order to ensure the enhanced permeability and maximum antioxidant activity against UVA induced oxidative stress in rat.
*Main methods:* The optimized ferulic acid loaded nanoemulsion 3 (FA-NE3) was prepared by spontaneous nanoemulsification method with an appropriate ratio (20:30:50% *w/w*) of the oil (isostearyl isostearate), aqueous system and Smix [surfactant (labrasol) and co-surfactant (plurol isostearique)] respectively. FA-NE3 was characterized by measuring their droplet size, zeta potential, refractive index, transmission electron microscopy (TEM), ultraviolet (UV), fourier transform infrared spectroscopy (FTIR) and rheological characteristics. *Ex vivo* skin permeation and *in vivo* UVA protection activity of FA-NE3 based nano-gels (FA-NG3) along with placebo were studied through the rat skin.
*Key findings:* FA-NE3 exhibited sustained-release profile, better permeability and ultraviolet A (UVA) protection activity as compared to conventional dosage form. This phenomenon may be attributed towards increased solubility of the drug and enhanced permeability from nanoemulsion. FA-NE3 based nanogel (FA-NG3) could elevate the level of skin marker enzymes against oxidative stress mediated by UVA.
*Significance:* The gel formulation exhibited significant ($P < 0.01$) skin permeability and antioxidant activity in the current investigations. The nanogel could be promising nanocarriers for topical delivery of FA in response to better skin protection activity against UVA rays in a sustained manner.



## 1. Introduction

The emergence of new technologies has a great interest in developing a nanocarrier system to improve the therapeutic properties of a drug [1]. The nanocarriers ideally fulfill prerequisites that it should deliver the drug at a controlled rate as directed by the needs within the body [2]. The goal of the nanocarrier system is to enhance the permeability and bioavailability of low bioavailable drug by increasing its solubility through the nanoemulsion (NE) like carrier system [3]. Nanoemulsions (NEs) are transparent, liquid isotropic dispersions composed of water, oil and surfactants/co-surfactants (Smix). They are thermodynamically stable, which has typically a droplet diameter of approximately 20–200 nm [4].

Photo-damage of skin is the most occurring dermatological problems worldwide [5]. A majority of UVB is absorbed through the epidermis of the skin, but UVA reaches the dermal layer and also the circulating blood, tissues and produces reactive oxygen species (ROS) [6,7]. ROS can influence lipid peroxidation in membranes [8] which leads to the melanoma, dermatitis, aging, inflammations and other severe problems [9]. Endogenous antioxidant capability of the skin is a major determinant in its response to oxidative stress-mediated damage involving reduced level of antioxidant enzymes, including glutathione [10], superoxide dismutase, catalase, glutathione peroxidase and increased levels of thiobarbituric acid reactive substances [11]. The topical antioxidant lotions may be beneficial, but they cannot protect the skin on long-term exposure of sun rays and need to be applying frequently [12].

Ferulic acid (FA) [4-hydroxy-3-methoxycinnamic acid] (Fig. 1) is present in many functional foods, including wheat, rice, barley, oats, citrus fruits, tomatoes, etc. [12]. FA proved to afford significant protection to the skin against UV induced oxidative stress [13]. Several studies have been established that FA has shown to inhibit the expression of cytotoxic and inflammation-associated enzymes [14], matrix metalloproteinases and attenuates the degradation of collagen fibers [15].

Several studies have been demonstrated that FA possesses potent antioxidant, antiaging, hepatoprotective, antiatherogenic, antimutagenic, anti-inflammatory, anticancer, antidiabetic, neuroprotective and cardioprotective activities [16]. FA undergoes a marked first-pass metabolism, which limits its oral bioavailability

* Corresponding author.
*E-mail address:* naturalproductm@gmail.com (P.K. Mukherjee).

http://dx.doi.org/10.1016/j.lfs.2015.10.001
0024-3205/

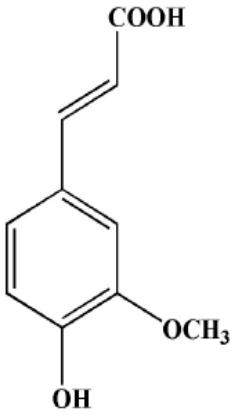


**Fig. 1.** Ferulic acid.

(9–20%) and also have very fast biotransformation [17,18]. Merely, the conventional topical formulations of FA get the desired skin protective effect on long exposure to sunlight, because FA has lower elimination half life and higher rate of distribution and elimination. Therefore, present study was aimed to develop NE based gel (nanogel) of FA and to evaluate its therapeutic efficacy against oxidative stress induced by UVA irradiation.

## 2. Materials and methods

### 2.1. Chemicals and excipients

Ferulic acid [assay 99%] was obtained from Sigma-Aldrich Chemicals, Bangalore. Labrafac™ lipophile WL1349 (LLW), labrasol®, plurol oleique®, plurol isostearique®, isostearyl isostearate® (ISIS), lauroglycol™ 90 and transcutol CG® were gift samples from Gattefossé (Saint Priest, Cedex France). Acconon® CC-6 was procured from ABITEC Corporation, Columbus, USA. All other chemicals and reagents used were of analytical grade obtained from Merck, Mumbai. Water was obtained from Milli-Q water purification system (Millipore, MA).

### 2.2. RP-HPLC analysis of FA

Estimation of FA content in the formulations was analyzed by RP-HPLC (Waters 600, Milford, MA, USA) at a flow rate of 1 mL/min with 15 min run time at 321 nm wavelengths at 25 ± 0.5 °C using a Spherisorb $C_{18}$ column (250 mm × 4.6 mm, 5 μm; Waters, Ireland) fitted with a $C_{18}$ guard column (10 × 3.0 mm). The samples were injected through 20 μL micro-syringe (Hamilton Microliter®; Switzerland). The standard stock solution was prepared by dissolving the known amount of FA in methanol to get a concentration of 1000 μg/mL. Different aliquots were prepared by subsequent dilution with the same solvent. Samples were stored at 4 °C and protected from light before using. In this analysis, mobile phase of acetonitrile and deionized water was used as a proportion of 35:65, 30:70 and 25:75 *v/v* (1% glacial acetic acid; pH 2.2) which were sonicated for 15 min and degassed prior to use. Before applying all samples were also filtered through 0.45 μm (NYL) syringe filter.

The method was validated in terms of linearity, repeatability, intermediate precision, sensitivity and recovery as per the guideline of International Conference on Harmonization (ICH) [19]. The assay precision was calculated in terms of percentage of the relative standard deviation (% RSD) of determinations. Sensitivity of the system was determined by the limit of detection (LOD) and limit of quantification (LOQ) based on the standard deviation of the response (σ) and the slope (S) of the standard curve using the following equations.

$$LOD = 3.3\sigma/S \text{ and } LOQ = 10\sigma/S \quad (1)$$

The recoveries of standard compounds from various samples and formulation at three concentration levels were determined by measuring the percentages of detecting concentrations over additional concentrations. The quantitative analysis was repeated about three times (n = 3) by comparing and interpolating the peak area (response) of the sample with the standard.

### 2.3. Development and evaluation of the nanoemulsion

#### 2.3.1. Solubility study of FA in oils

The solubility of FA in various oils; including labrafac lipophile WL1349, ethyl oleate, IPM, ISIS, oleic acid, olive oil, and soybean oil was performed by adding an excess amount of the drug in 1 mL of each of the selected oils and distilled water separately in 2 ml capacity Eppendorf tube and mixed using a vortex mixer (Spinix, Tarson, India). Then the mixture tubes were kept at 25 ± 1.0 °C in an isothermal shaker for 72 h to get equilibrium [20]. The equilibrated samples were taken out from the shaker and centrifuged at 13,500 rpm (Spinwin MC-02, Tarson, India) for 5 min wherein the supernatant was taken and filtered through a 0.45 μm membrane filter. The concentration of FA was individually analyzed by RP-HPLC method at $\lambda_{max}$ 321 nm.

#### 2.3.2. Pseudo-ternary phase diagram study

On the basis of drug excipient solubility studies, oil phase (ISIS), surfactants (labrasol and acconon CC-6), cosurfactants (transcutol CG and plurol isostearique) and Milli-Q water was selected for further study. These were grouped in four different combinations for phase diagram studies (Table 1). Surfactant and cosurfactant mixture (Smix) in each group (Table 1) were used in different weight ratios (1:0, 1:1, 2:1, 3:1, 1:2, 1:3). These Smix ratios were chosen in increasing concentrations of surfactant with respect to cosurfactant and vice versa for the development of various phase diagrams.

For the construction of the phase diagrams, aqueous titration method was adopted where water was added by drop-wise in the mixture of Smix and oil. According to transparency and flowability, NE (o/w) phase was recognized. Fourteen various combinations of oil and Smix (*w/w*) (1:9, 1:8, 1:7, 1:6, 1:5,1:4, 1:3.5, 1:3, 1:2.5, 1:2, 1:1, 6:4, 7:3, 9:1) were selected to cover maximum ratios for the study to delineate the boundaries of each phase diagram. Water was added at every 5% interval to find the range of 5–95% of total volume. The physical state of the NE was illustrated in a pseudo-three component phase diagram where the three axes denoted oil, aqueous phase and Smix in that order [21].

#### 2.3.3. Thermodynamic stability study

Thermodynamic stability of the selected formulations was performed in order to assess the physical stability as per the method described by Choudhury et al. [21]. In brief, centrifugation test (Cent.), heating-cooling cycle (H & C) and freeze–thaw cycles (Freez Tha.) were carried out in these tests. Furthermore, FA loaded NEs were prepared by incorporating 1 mg/mL concentration into selected oil phase at 10–30% (*w/w*) along with respective Smix ratios using the spontaneous nano-emulsification method.

**Table 1**
Oil, surfactant and cosurfactant grouped in different combinations.

| Group | Oil | Surfactant | Cosurfactant |
|---|---|---|---|
| I | ISIS | Labrasol | Transcutol CG |
| II | ISIS | Labrasol | Plurol isostearique |
| III | ISIS | Acconon CC-6 | Transcutol CG |
| IV | ISIS | Acconon CC-6 | Plurol isostearique |

### 2.4. Characterization of nanoemulsion formulations

#### 2.4.1. Electrical conductivity

The conductivity of the NE was performed by applying electrical current through the formulation to find the formulation type. A measurement in the conductivity meter (Systronic Conductivity meter 306, Systronic Ltd., India) was anticipated for o/w emulsion type [22].

#### 2.4.2. Percentage transmittance

Percentage transmittances of the diluted samples of NEs (100 times in water) were analyzed at 450 nm using a spectrophotometer (SpectraMax® M5, USA).

#### 2.4.3. Viscosity

The viscosity of the selected NE was measured by using a Brookfield Viscometer with spindle CPE 41 (Brookfield Engineering Laboratories, Inc., MA) [21].

#### 2.4.4. pH

The pH of the NE was measured using a digital pH meter (Orion 3 Star, Thermo Scientific) at 25 ± 0.5 °C.

#### 2.4.5. Refractive index

An Abbe refractometer was used for measurement of the refractive index of NE along with placebo (NE without FA) at 25 ± 0.5 °C [21].

#### 2.4.6. Drug percentage entrapment efficiency (%EE) and drug loading (%DL)

%EE and %DL of FA loaded NEs were estimated as per the procedure established by Bu et al. In brief, content of free FA was separated from FA loaded NE (FA-NE) by the ultrafiltration method (10,000 Da, Millipore) with centrifugation at 13,500 g for 5 min [23].

#### 2.4.7. Droplet size, polydispersity index and zeta potential analysis

The average droplet size (Z-average) and polydispersity indexes (PDI) of selected formulations were measured by photon correlation spectroscopy (PCS) using a Malvern Zetasizer (Nano ZS90, Malvern instruments Ltd., UK) with a 50 mV laser. Each droplet size value was reported the average of at least three independent measurements. Zeta potential (ξ) measurements were also carried out on the same diluted sample using the same equipment and operating conditions and the zeta potential values were calculated.

#### 2.4.8. Transmission electron microscopy (TEM)

TEM analysis was performed to determine the morphology of FA-NE3. It was performed by using TEM (JEOL JEM 2100, USA) with a working voltage of 200 kV. The diluted and filtered NE sample was placed on 300 mesh size carbon coated copper grid. The filled, copper grid was negatively stained with 2% (w/v) phosphotungstic acid (PTA) for 30 s. Excess of PTA was removed by absorbing on a filter paper and dried overnight at room temperature (25 ± 0.5 °C). Photo-micrographs of the sample from the TEM were taken at different magnification.

#### 2.4.9. UV-spectrophotometry study

In this assay, diluted sample was scanned at 321 nm at room temperature (25 °C) through a spectrophotometer (Multiskan-Go, Thermo Scientific, USA) and the result was recorded.

#### 2.4.10. High performance thin layer chromatography (HPTLC) analysis

The HPTLC (CAMAG, Switzerland) analysis of the FA-NE3 along with standard FA was performed using a solvent system containing toluene:ethyl acetate:formic acid at a ratio of (6:3:0.8 v/v/v). The sample was spotted onto the plate through the applicator (Linomat 5). UV densitometry scanning of developed HPTLC plate (Silica gel 60 F254) was done at wavelength 315 nm and data was analyzed by software (WINCATS).

#### 2.4.11. Fourier transforms infrared (FTIR) study

FTIR studies were performed to detect any chemical interactions between FA and excipients in the formulation, for followings: (A) pure FA, (B) FA-NE3 and (C) placebo NE (FA-NE3 without FA). The FTIR measurements were done in the range of 4000–450 $cm^{-1}$ using FTIR (Perkin Elmer, USA).

#### 2.4.12. Stability study

The optimized NE formulation (FA-NE3) was subjected to stability studies at long term and accelerated conditions (40 ± 2 °C/75 ± 5% RH) as per the ICH guidelines. The formulation was kept in air tight glass vials and assayed periodically at the time interval of 0, 1, 3 and 6 months for any change in appearance, precipitation, clarity, pH, droplet size, zeta potential and drug content. Drug content in the NE was analyzed using RP-HPLC method at 321 nm. Logarithm of percentage of the drug remained to be decomposed was plotted against time in a month to determine the predicted shelf life ($t_{90}$) of the formulation.

#### 2.4.13. Preparation of the gel formulation

The conventional gel of ferulic acid (FA-CG, ~0.1 g of FA) was prepared by dispersing the carbopol 940 (1 g) in distilled water up to 100 mL. The dispersion medium was stored in the dark place at room temperature (25 °C) for 24 h to swell completely. Other components like polyethylene glycol 400 (PEG 400)—10 g, propylene glycol (PG)—10 g, isopropyl alcohol (IPA)—10 g and triethanolamine (TEA)—0.5 g was incorporated to obtain a homogeneous dispersion of gel [24]. The NE gel (FA-NG3, ~0.1 g of FA) was developed by adding 1 g of an already swollen dispersion system of carbopol 940 into the optimized FA-NE3 to get the homogenous mass.

#### 2.4.14. Rheological studies

The flow behavior of FA-NG3 formulations and the corresponding placebo were evaluated through Anton Paar, Modular Compact Rheometer-MCR 102. A stress/rate with a temperature controller was employed to measure the rheological properties of the formulations. The measurements were performed at a temperature of 25 ± 0.5 °C with a 4°/40 mm cone and plate geometry and gap of 0.100 mm. The steady rheological behaviors of the FA-NG3 and placebo were measured at a controlled rate varying from 0.001–100 and 0.0001–100 $s^{-1}$ respectively. After being loaded onto the plate, the samples were allowed to rest about 10 min prior to measurement.

#### 2.4.15. Spreadability test

The spreadability of the FA-NG3 and placebo was evaluated as per the method described by Khurana et al. [25].

### 2.5. Animals

Wistar male rats (180–220 g) were selected in this study. Animals were housed in groups (n = 6) at ambient temperature (25 ± 0.5 °C and 45–55% RH) and conditions with 12 h light/dark cycles. They had free access to pellet chow (Brook Bond, Lipton India) and water *ad libitum*. The experiment was performed as approved by the Institutional Animal Ethical Committee with the ethical guidelines as provided by the committee (approval number: AEC/PHARM/1501/05/2015) for the purpose of control and supervision of experiment on animals (CPCSEA), India.

#### 2.5.1. Ex vivo skin permeation study

Hairless abdominal skin was mounted in the *Franz diffusion* cell with the *stratum corneum* side faced towards the donor compartment and the dermal side towards the receptor compartment with an effective diffusion surface area of 1.766 $cm^2$. The receptor compartment was filled with phosphate buffer saline (PBS—pH 7.4). The diffusion cell was maintained at 37 ± 0.5 °C with constant stirring. FA-NE1-5, FA-NG3 and FA-CG (1 mL equivalent to 0.1 g of FA) were evenly spread

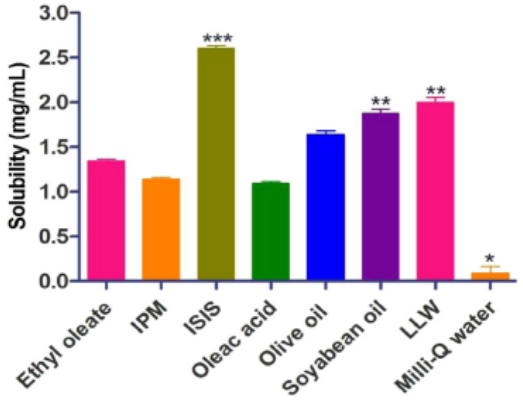


**Fig. 2.** Solubility studies of FA in several excipients. Values were mean ± SEM (n = 6). *P & **P < 0.05, ***P < 0.01.

over the skin in donor compartment and sealed with paraffin film to provide occlusive conditions. 200 μL sample of the receptor medium was withdrawn at predetermined time intervals over a period of 24 h, and an equivalent volume of fresh PBS was replenished to maintain the sink conditions. All experiments were performed in triplicate. All samples were filtered, suitably diluted and analyzed by RP-HPLC.

*2.5.2. Efficacy study of the FA loaded gel formulations as a photoprotective agent against UVA exposure*

The UV protective effect of the FA loaded gel formulations were evaluated based upon the method established by Bhattacharyya et al. [6]. A thin and uniform layer of gel formulation was applied to the demarcated shaved area on the dorsal skin of the rats. Group I (Control) and Group II (UV irradiated) were treated with placebo formulation. Group III was applied for FA conventional gel (FA-CG1 equivalent to 0.1% FA). Group IV was applied to FA-NE3 loaded nanogel (FA-NG1 equivalent to 0.1% FA). Group V was applied to FA conventional gel (FA-CG2 equivalent to 0.1% FA). Group VI was applied to FA-NE3 loaded nanogel (FA-NG2 equivalent to 0.1% FA). Group VII was applied to NG (NE3 loaded nanogel containing

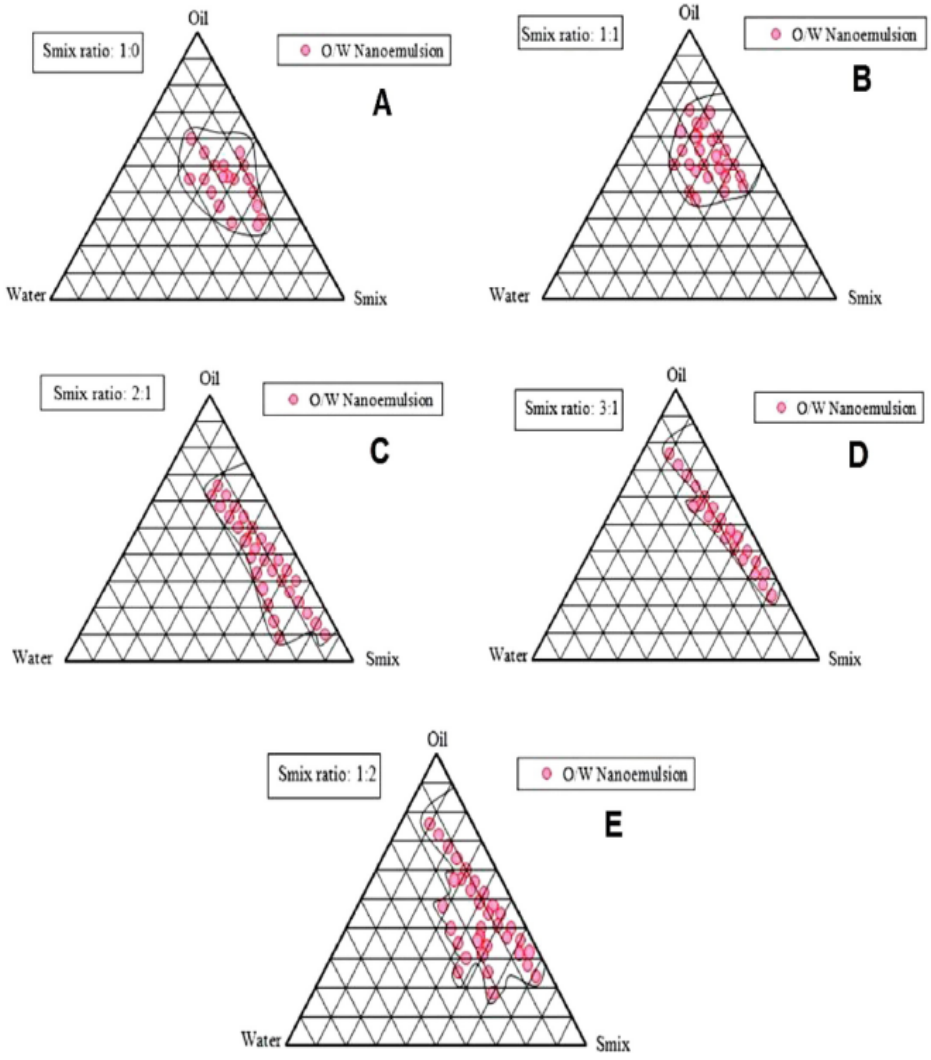


**Fig. 3.** (A–E) Pseudo-ternary phase diagrams of Group II, indicating an o/w nanoemulsion region at different Smix ratios.

**Table 2**
Composition of optimized nanoemulsion formulations selected from Group II.

| NE Code | Smix (S:Cos) | Ingredients in nanoemulsion formulation (% w/w) | | | | Oil:Smix ratio |
|---|---|---|---|---|---|---|
| | | Oil | Water | S | Cos | |
| FA-NE1 | 1:1 | 10 | 35 | 27.5 | 27.5 | 1:5.5 |
| FA-NE2 | 2:1 | 15 | 35 | 33.33 | 16.67 | 1:3.3 |
| FA-NE3 | 1:1 | 20 | 30 | 25 | 25 | 1:2.5 |
| FA-NE4 | 1:2 | 25 | 28 | 15.67 | 31.33 | 1:1.8 |
| FA-NE5 | 2:1 | 30 | 26 | 29.33 | 14.67 | 1.47 |

0.1% NE3 without FA). Exposure of UVA radiation was done to UVA irradiated, FA-CG1, FA-NG1 and NG groups immediately after topical application while to FA-CG2 and FA-NG2 groups after 4 h of topical application for seven days. On the eighth day, all the animals were anesthetized using diethyl ether and sacrificed by cervical dislocation. The UVA treated portion of cutaneous (epidermis and dermis) tissues was quickly dissected in ice-cold saline, washed with ice-cold saline and the homogenate were prepared in 0.1 M PBS (pH 7.4).

*2.5.3. Estimation of antioxidant biochemical marker enzymes in cutaneous tissue*

The glutathione peroxidase (GPX) level was estimated according to the method proposed by Paglia and Valentine [26] and the level of superoxide dismutase (SOD) were determined based on the procedure suggested by Kakkar et al. [27]. Antioxidant level of catalase (CAT) was estimated using the method of Beers and Seizer [28] and thiobarbituric acid reactive substances (TBARS) was calculated according to the procedure of Ohkawa et al. [29]. Estimation of total protein was performed in a procedure described by Lowry et al. [30]. Data were expressed as units/mg of protein. All the enzyme estimations were performed by using a spectrophotometer (Spectramax® M5, USA).

*2.6. Statistical analysis*

The data were statistically analyzed by one-way analysis of variance (ANOVA) followed by Dunnet's post hoc test using Graph Pad Prism software-5.0 (San Diego, CA, USA). The differences between means were considered to be significant when the $P < 0.05$.

## 3. Results

*3.1. Method validation of RP-HPLC-PDA*

The optimum separation of FA was achieved by using the mobile phase at ratio of 30:70 *v/v* (1% glacial acetic acid; pH 2.2) at a flow rate of 1 mL/min at 25 ± 0.5 °C under the isocratic conditions. The retention time (Rt) of FA was found to be 8.083 ± 0.01 min. A good linear precision relationship between the concentrations (200–1000 ng/mL) and peak areas was obtained as the correlation coefficient ($r^2$) of 0.9992 ± 0.01. Intra-assay precision was performed at four different concentrations and measured the %RSD. The %RSD of both instrumental precision and intra-assay precision was estimated to be <1.00. The precision to the method was optimized by calculating intra-day and inter-day repeatability at four subsequent concentrations ranging from 250–1000 ng/mL. The RSD values in all tested groups were found less than 3%, which was significant. The LOD and LOQ of were estimated to be 0.023 and 0.072 ng/mL, relatively, which indicated that the proposed method can be used for detection and quantification of FA. The recovery rates of FA from low, middle and high concentrations were 100.07, 100.01 and 100% respectively.

*3.2. Solubility studies of FA in various oils*

The solubility of FA was performed in various oils and maximum solubility of FA in ISIS was found to be 2.60 ± 0.04 mg/mL while in water; it was 0.09 ± 0.14 mg/mL (Fig. 2). Therefore, ISIS was selected as oil phase for the development of the formulations.

*3.3. Pseudo-ternary phase diagram study*

The individual pseudo-ternary phase diagrams were plotted to get the maximum o/w NE regions for each group. Results have been shown in the Supplementary Tables S1–S4 and Figs. S1–S3A–E. Among the four groups, the maximum widespread region and stability of NE were found for the group II (Supplementary Table S2). NE region was found to be very less at Smix 1:0 (Fig. 3A). After addition of cosurfactant along with a surfactant in equal proportion Smix (1:1) (Fig. 3B), a stable and flowable NE region was obtained. In Smix ratio of 2:1, 3:1 and 1:2 (Fig. 3C, D, E), the lower NE regions were found in comparison with Smix ratio (1:1). Therefore, Smix (1:1) was further selected for the development of various formulations.

*3.4. Thermodynamic stability study*

The selected formulations were subjected to different thermodynamic stability by using heating-cooling cycle, centrifugation and freeze thaw cycle stress tests. There was no obvious event seen during these tests, although some formulations were unstable as represented in Supplementary Tables S1–S4.

*3.5. Selection of formulations from phase diagrams and development of FA nanoemulsions*

From pseudo-ternary phase diagrams (Fig. 3A–E) it is revealed that oil could be solubilized up to 25% (*w/w*). Thus from each phase diagram, a different concentrations of oil was selected within the range of 10–30% so that maximum formulations could be selected to cover the NE area on the phase diagram (Supplementary Table S2). For each portion of oil selected, only those preparations with minimal concentration of Smix were studied. No event was observed about the phase behavior and the NE region of phase diagrams after inclusion of FA (1 mg) in the formulations, which was likely as the formation of stable NE. Composition of optimized FA loaded nanoemulsion has been explained in Table 2.

**Table 3**
Characterization of various nanoemulsions.

| NE code | pH | Viscosity (cP) | Cond. (ms/cm) | P.T. | R.I. | %EE | %DL | Z-average (nm) | PDI | Z.P. (mV) |
|---|---|---|---|---|---|---|---|---|---|---|
| FA-NE1 | 6.92 ± 0.06 | 8.42 ± 0.02 | 0.67 ± 0.34 | 80.89 ± 0.12 | 1.416 ± 0.16 | 90.89 ± 0.21 | 0.91 ± 0.04 | 185.8 ± 1.38 | 0.612 ± 0.01 | −63.4 ± 0.85 |
| FA-NE2 | 6.96 ± 0.04 | 7.65 ± 0.02 | 0.60 ± 0.21 | 67.80 ± 1.23 | 1.429 ± 0.38 | 92.78 ± 0.18 | 0.93 ± 0.05 | 158.5 ± 1.19 | 0.508 ± 0.04 | −58.8 ± 0.65 |
| FA-NE3 | 6.98 ± 0.02 | 5.36 ± 0.03 | 0.56 ± 0.10 | 99.21 ± 0.89 | 1.401 ± 0.18 | 98.88 ± 0.12 | 1.03 ± 0.02 | 102.3 ± 1.14 | 0.158 ± 0.02 | −35.2 ± 0.41 |
| FA-NE4 | 6.97 ± 0.03 | 6.11 ± 0.01 | 0.70 ± 0.48 | 78.34 ± 1.78 | 1.408 ± 0.21 | 95.68 ± 0.15 | 0.96 ± 0.06 | 138.4 ± 1.01 | 0.189 ± 0.01 | −47.1 ± 0.48 |
| FA-NE5 | 7.04 ± 0.02 | 7.87 ± 0.01 | 0.63 ± 0.57 | 75.88 ± 2.10 | 1.420 ± 0.44 | 93.87 ± 0.25 | 0.94 ± 0.03 | 154.6 ± 1.12 | 0.234 ± 0.06 | −48.2 ± 0.52 |

Cond.: conductivity; P.T.: percentage transmittance; R.I.: refractive index; %EE: percentage entrapment efficiency; %DL: percentage drug loading; PDI: polydispersity index; Z.P.: zeta potential. Value was represented as (mean ± SD) (n = 3).

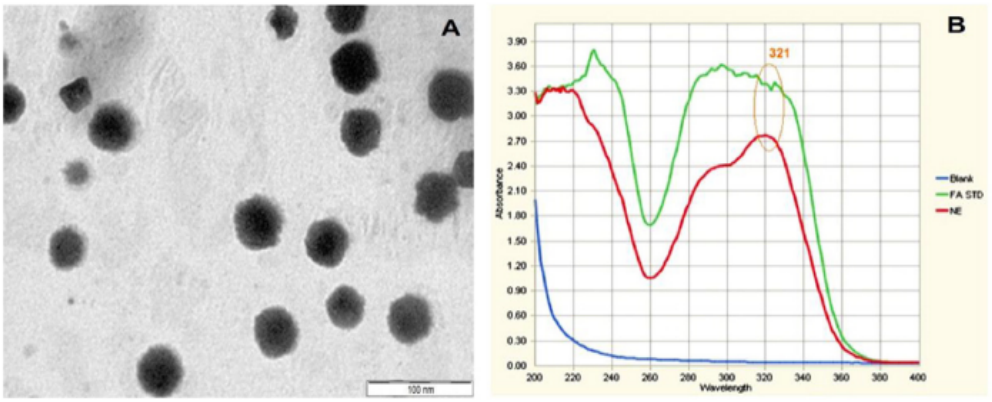


**Fig. 4.** Transmission electron microscope photograph (A) and UV spectra of FA-NE3 nanoemulsion (B).

### 3.6. Characterization of developed nanoemulsion

Developed NEs were characterized by measuring different parameters, including electrical conductivity, percentage transmittance, viscosity, pH, refractive index, drug entrapment efficiency and drug loading, droplet size, PDI and zeta potential. The observed results have been shown in Table 3.

### 3.7. TEM and UV-spectrum analysis

The morphology and surface structure of the optimized FA-NE3 has been shown in Fig. 4A where the droplets appeared as dark spot due to the dispersed oil droplets. The size of droplet was similar to that obtained by a Zetasizer.

UV spectrum showed that FA was present in the formulation (FA-NE3), when scanned through 321 nm wavelength as like as the pure FA (321 nm). Detail has been shown in Fig. 4B.

### 3.8. HPTLC analysis

The optimized solvent system [toluene–ethyl acetate–formic acid at a ratio of (6:3:0.8, v/v/v)] produced a sharp and well-defined symmetrical peak with $R_f$ in 0.38 for FA, when the chamber was saturated with the mobile phase for 30 min at room temperature (25 °C). HPTLC chromatogram of standard FA and the FA-NE3 showed the $R_f$ value of 0.38 and 0.39 respectively (Fig. 5). The result indicated that the FA was quite compatible with their excipient, which was used for development of NE.

### 3.9. FTIR study

The chemical interactions among the excipients and FA were confirmed further in order to understand the compatibility of FA-NE3 formulation (Fig. 6), for pure FA (curve A), FA-NE3 (curve B) and placebo (curve C). The characteristic sharp peak of FA was found at 3436.6 $cm^{-1}$ (carboxylic acid O-H stretching), 1690.7 $cm^{-1}$ (carboxylic acid C=O stretching), 1276.6 $cm^{-1}$ (carboxylic acid C–O stretching); 1517 and 1620.1 $cm^{-1}$ (aromatic C=C) which confirm the skeleton of FA. These peaks were found with slight variation even after the nano-formulations, thus indicating the absence of chemical interactions between FA and the excipients. This confirmed that FA was compatible with other excipients used in formulations.

### 3.10. Stability study

The FA-NE3 when subjected to stability study based on ICH guidelines, there was no substantial alteration observed with its droplet size, zeta potential and pH at 40 °C (Table 4). A first order degradation of FA content in the FA-NE3 was found to be 1.76% at the remainder of

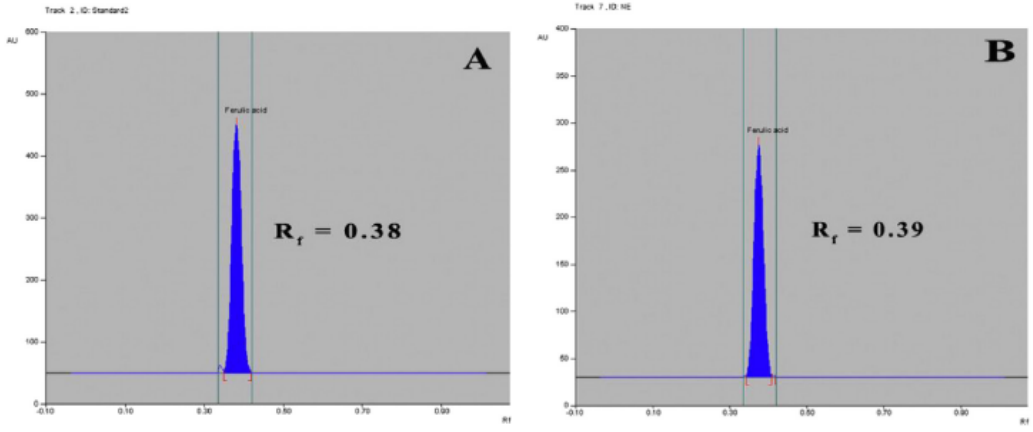


**Fig. 5.** HPTLC chromatogram of standard FA (A) and FA-NE3 formulation (B).

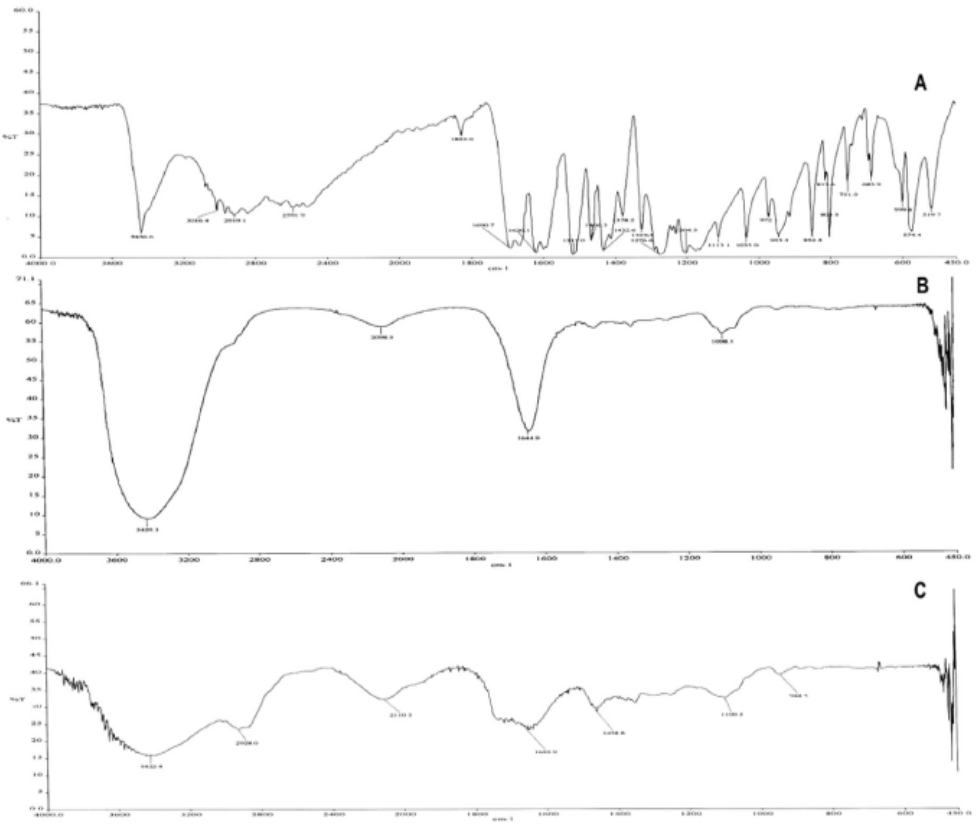


**Fig. 6.** FTIR spectrum of ferulic based formulation (A) pure ferulic acid, (B) FA-NE3 and (C) placebo formulation.

6 months at 40 °C. First order degradation kinetics at 40 °C was graphically represented in Fig. 7. From the stability studies, it can be anticipated that the FA-NE3 was stable at 40 °C for longer periods. Shelf life of the formulation was estimated to be 2.06 years.

### 3.11. Rheological studies

The viscosity of the placebo and FA-NG3 were found in the range of 600 to 0.68 and 3790 to 1.83 Pa·s respectively and represented in Supplementary Fig. S4.

### 3.12. Spreadability test

The placebo and FA-NG3 were found to exhibit good spreadability (63.18 ± 1.08 and 65.86 ± 0.82% *w/w* respectively) that would assure the practicability to skin administration. There was no significant difference ($P < 0.05$) between the spreadability of placebo and FA-NG3 formulations.

### 3.13. Skin permeation studies

The percentage cumulative permeation of FA from different FA-NE1-5, FA-NG3 and FA-CG were studied through rat skin (Fig. 8A & B). The cumulative permeation of FA-NE3 for 24 h was significantly higher (91.33%) than that of other formulations; this may be due to low viscosity, nanodroplet size and appropriate pH of FA-NE3, when compared with FA-NE1, FA-NE2, FA-NE4 and FA-NE5. Further, the comparative studies between FA-CG, FA-NE3 and FA-NG3 were performed. In case of FA-NG3, nanogel formulation exhibited better permeation profile (96.95%) in comparison with FA-CG conventional gel (61%) at 24 h. A significant difference was observed with percentage cumulative permeation profile of FA from FA-NG3 and FA-CG; this could be due to the average size of internal phase droplets (o/w), which were significantly smaller in NEs.

Flux *Jss* (μg/h/cm$^2$) and permeability *Kp* (cm/h) of FA from various formulations across the skin has been shown in Fig. 8C. Maximum flux and permeability of FA were achieved with FA-NG3 compared to others. The result stated that *Jss*, lag time and *Kp* were estimated to be 2.319 ± 0.19 μg/h/cm$^2$, 0.256 h and 0.519 ± 0.09 cm/h respectively.

**Table 4**
Degradation study of optimized ferulic acid loaded NE formulation, FA-NE3.

| Time (month) | Temperature (°C) | Droplet size (nm) | Zeta potential (mV) | pH | % Drug remained | Log% drug remained |
|---|---|---|---|---|---|---|
| 0 | 40 ± 2 (75 ± 5% RH) | 105 ± 0.14 | −35 ± 0.21 | 6.96 ± 0.13 | 100 | 2 |
| 1 | | 106 ± 2.07 | −35 ± 0.57 | 6.98 ± 0.21 | 99.54 | 1.9979 |
| 3 | | 104 ± 1.10 | −34 ± 1.08 | 6.92 ± 2.04 | 98.40 | 1.9928 |
| 6 | | 106 ± 1.04 | −34 ± 1.11 | 6.95 ± 1.00 | 96.59 | 1.9849 |

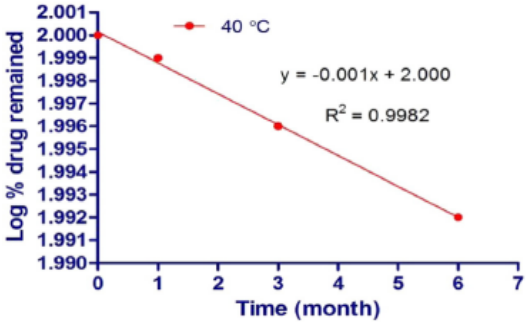


**Fig. 7.** First order degradation kinetics of ferulic acid from FA-NE-3 at 40 °C.

### 3.14. The consequence of UVA exposure on the skin antioxidant biochemical marker enzymes

The antioxidant enzyme levels in the UVA irradiated rat skin was reduced significantly in comparison to the control group (without UVA exposure) ($P < 0.01$). The levels of skin antioxidant enzymes (GPX, SOD and CAT) were significantly higher in case of the groups pre-treated with FA-CG1 and FA-NG1, than UVA irradiated group ($P < 0.01$) (Fig. 9A–C)). The group pre-treated with NG did not produce any effect on the skin antioxidant enzymes as compared to the UVA irradiated group, which may be due to the placebo NG (Fig. 9A–C).

Significant increase in the level of SOD, GPX and CAT was observed with FA-NG2 group (***$P < 0.01$) comparing to FA-CG2 group (**$P < 0.05$), after 4 h of UVA irradiation and treatment with FA loaded nanogel and FA conventional gel respectively as shown in Fig. 9A–C.

The raised level of TBARS was significantly reduced with FA-CG1, FA-NG1 and FA-NG2 treated groups compared to the UVA irradiated group (***$P < 0.01$). FA-CG2 group reduced the TBARS to the minimum extent compared to FA-NG2 (**$P < 0.05$), after 4 h of UVA irradiation (Fig. 9D). This may be due to less permeability of FA conventional gel. FA-NG2 showed the better therapeutic effect because of its enhanced permeability than the conventional gel. Thus, FA encapsulated nanogel formulations could enhance UV protective activity of the skin for longer periods rather than conventional topical formulations.

## 4. Discussion

The objective of the study was to develop an FA incorporated NE based nano-gel for enhancing the drug solubility and permeability through skin. Surfactants, labrasol (HLB = 14) and acconon CC-6 (HLB = 12.5) and cosurfactants, transcutol CG (HLB = 4.2) and plurol isostearique (HLB = 10.8) could work better along with its Smix [31,32]. The formation of free energy during nano-emulsification mainly depends on the concentration of the surfactant used that lowers the surface tension at the oil–water interface [33] and resulting in the thermodynamically stable system [34]. High amount of surfactant may lead to untoward effect to the skin [35,36]. Therefore, the minimum amount of Smix (1:1) was used for formulation (FA-NE3).

Homogeneous droplet size distribution was studied in the formulation with the help of diversity in the intensity of light scattering by the oil droplets which expressed as PDI. The uniformity of the droplet size in the formulation was indicated by the PDI value. PDI values of all formulations were found to be low, indicating uniformity of droplet size within each formulation. The lowest PDI value for FA-NE3 indicated that the system was homogenous.

Suitable droplet size (100–200 nm) and zeta potential was found for the FA-NE3. Zeta potential (ξ) is an important parameter to check the stability of the formulation. It is very well known that the zeta potential indicates the degree of repulsion between adjacent charged droplets in a colloidal dispersion such as NE, which is related to the stability of the formulation. Usually, −30 mV or +30 mV should consider as high zeta potential value [37]. The zeta potential of the FA-NE3 was negatively charged, and was within the range of −35.2 ± 0.41 to −63.4 ± 0.85 as shown in Table 3. This was due to the smallest droplet size of the formulations. The high negative charge of the optimized NE is probably influenced by the anionic groups of the fatty acids, and glycols present in the oil and Smix. The nanosize range of droplets with higher zeta potential in the formulation is generally attributed to prevent coalescence between droplets. Thus ξ sustains the homogeneity as well as the stability to the system [37]. Therefore, it can be concluded that there were least chances of coagulation or flocculation of the system in the biological environment and during its storage condition.

In the rheological study of gel, FA-NG3 expressed high viscosity as compared to placebo, which may be due to the drug integrated into the gel matrix and leads to increase in viscosity. Thus the nano-gel may be suitable for topical administration. The FA-NG3 exhibited non-Newtonian shear thinning phenomenon when viscosity decreases with the rate of shear stress. Carbopol-940 was used as a gelling agent and results in improved skin permeability [38].

FA-NG3 nanogel showed enhanced drug permeability across the skin, which may be due to quick diffusion of water from the formulation to the skin membrane and easy drug release [39]. In the oil phase, ISIS was selected as an effective penetration enhancer. The Smix (labrasol/

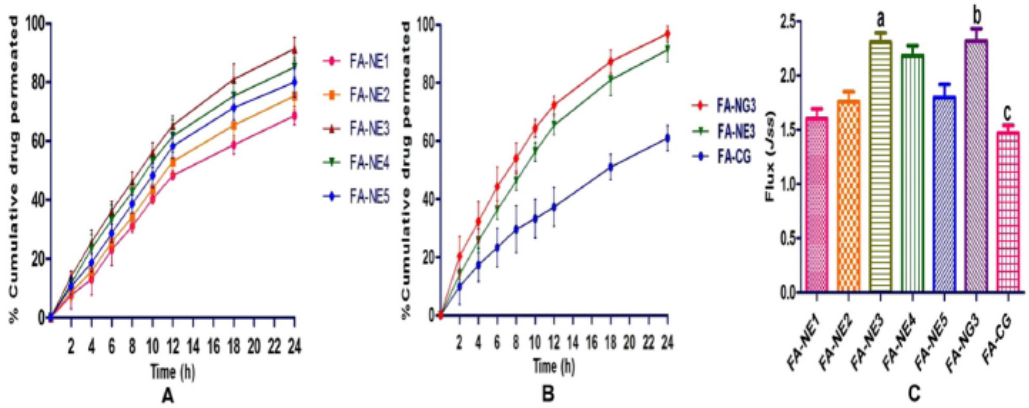


**Fig. 8.** Permeation study of ferulic acid from various nanoemulsions (A) FA-NE (1–5), (B) FA-CG, FA-NE3 and FA-NG3 through rat skin and (C) steady state flux of various formulations across rat skin. Values were mean ± SEM (n = 6). $^{a}P < 0.05$, $^{a,b}P < 0.01$.

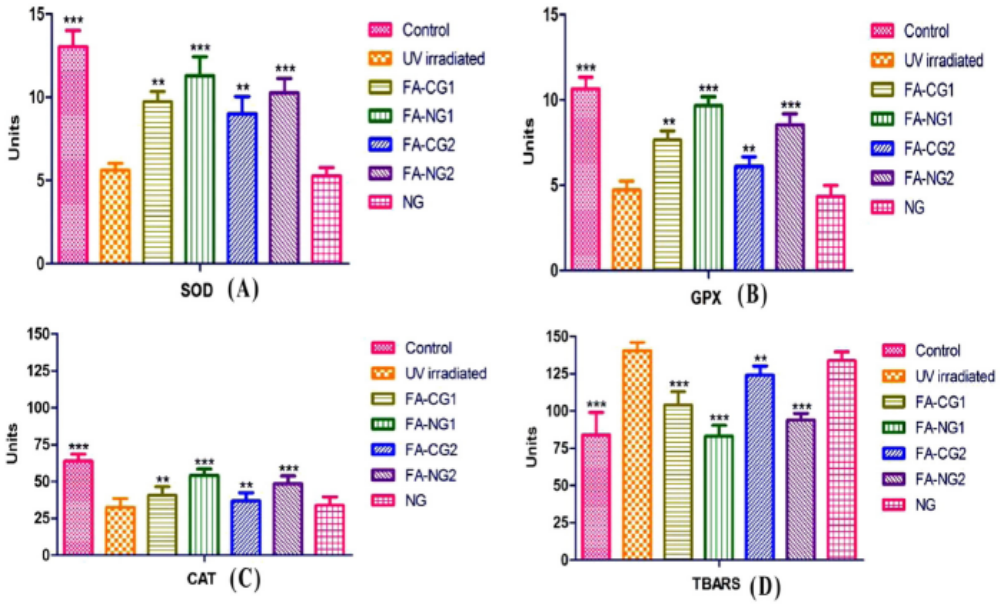


**Fig. 9.** Effect of FA loaded different gel formulations on (A) SOD, (B) GPX, (C) CAT and (D) TBARS levels in rat skin. Values were mean ± SEM (n = 6). $^{**}P < 0.05$, $^{***}P < 0.01$.

plurol isostearique) in the NE based gel may reduce the diffusion barrier of the stratum corneum by acting as permeation enhancers.

Drug release model of FA-CG and FA-NG3 was fitted with Zero order, First order, Higuchi's model, and Korsmeyer–Peppas model. This demonstrated that the higher coefficient of correlation ($r^2$) was found to be 0.996 for FA-NG3. Assuming highest $r^2$, the best fit was shown by zero-order drug release for nanogel formulation. The optimized FA-NG3 formulation was suitable for non-*Fickian* pattern ($0.5 < Kp < 1$) of drug release through diffusion and matrix erosion.

In the UV protective activity, level of the skin antioxidant enzyme was not elevated significantly by UVA irradiation on application of FA conventional gel after 4 h, which may be due to less permeability of conventional formulation. Chaudhary et al. reported that the novel nanocarrier gel of diclofenac diethylamine and curcumin showed superior biological activity due to its enhanced permeability [40]. The topical delivery route can avoid hepatic first pass metabolism resulting in the possible prolongation of the $t_{1/2}$ and a sufficient concentration in the systemic circulation [16]. FA loaded nanogel exhibited better UVA protection activity even after 4 h of application to the skin surface due to its improved permeability and sustained-release profile compared to conventional gel.

## 5. Conclusion

A topical nanogel of ferulic acid was developed, which showed sustained-release effect against UVA exposure in skin. The optimized gel formulation showed improved drug permeability and enhanced UV protection activity, which might be due to the potent antioxidant activity of FA in opposition to oxidative stress mediated by UVA. It significantly elevates the level of the antioxidant markers and arrested the unwanted effects generated by ultraviolet radiation. This phenomenon attributed towards the encapsulated FA in NE having a nanosize range of droplets provided large surface area, which possess superior skin penetration potential when compared with its conventional gel. The nanoemulsion based FA nanogel was found to be stable, safe and effective for topical application against UV. Therefore, the FA nanogel formulation could be explored further as a promising nanocarrier for skin delivery.

### Conflict of interest statement

The authors declare no conflicts of interest.

## Acknowledgment

The authors are thankful to the Department of Biotechnology, Govt. of India New Delhi, India for financial support through Tata Innovation fellowship (D.O. No. BT/HRD/35/01/04/2014) to Dr. Pulok K. Mukherjee. Thanks are due to the University Grant Commission, Govt. of India New Delhi, India for providing research fellowship to the first author.

## Appendix A. Supplementary data

Supplementary data to this article can be found online at http://dx.doi.org/10.1016/j.lfs.2015.10.001.

## References

[1] P.K. Mukherjee, R.K. Harwansh, S. Bhattacharyya, Bioavailability of herbal products: approach toward improved pharmacokinetics, in: P.K. Mukherjee (Ed.), Evidence-based Validation of Herbal Medicine, Elsevier, Amsterdam 2015, pp. 217–245.
[2] Y. Li, J. Zheng, H. Xiao, D.J. McClements, Nanoemulsion-based delivery systems for poorly water-soluble bioactive compounds: influence of formulation parameters on polymethoxyflavone crystallization, Food Hydrocoll. 27 (2012) 517–528.
[3] R.K. Harwansh, K.C. Patra, S.K. Pareta, Nanoemulsion as potential vehicles for transdermal delivery of pure phytopharmaceuticals and poorly soluble drug, Int. J. Drug Deliv. 3 (2011) 209–218.
[4] H.D. Silva, M.Â. Cerqueira, A.A. Vicente, Nanoemulsions for food applications: development and characterization, Food Bioprocess Technol. 5 (2012) 854–867.
[5] P.K. Mukherjee, N. Maity, N.K. Nema, B.K. Sarkar, Bioactive compounds from natural resources against skin aging, Phytomedicine 19 (2011) 64–73.
[6] S. Bhattacharyya, S. Majhi, B.P. Saha, P.K. Mukherjee, Chlorogenic acid–phospholipid complex improve protection against UVA induced oxidative stress, J. Photochem. Photobiol. B 130 (2014) 293–298.
[7] M.V. Butnariu, C.V. Giuchici, The use of some nanoemulsions based on aqueous propolis and lycopene extract in the skin's protective mechanisms against UVA radiation, J. Nanobiotechnol. 9 (2011) 1–9.
[8] F. Afaq, H. Mukhtar, Botanical antioxidants in the prevention of photocarcinogenesis and photoaging, Exp. Dermatol. 15 (2006) 678–684.
[9] C. Couteau, A. Faure, J. Fortin, E. Paparis, L.J.M. Coiffard, Study of the photostability of 18 sunscreens in creams by measuring the SPF in vitro, J. Pharm. Biomed. Anal. 44 (2007) 270–273.

[10] M.Z. Campanini, F.A. Pinho-Ribeiro, A.L.M. Ivan, V.S. Ferreira, F.M.P. Vilela, F.T.M.C. Vicentini, R.M. Martinez, A.C. Zarpelon, M.J.V. Fonseca, T.J. Faria, M.M. Baracat, W.A. Verri, S.R. Georgetti, R. Casagrande, Efficacy of topical formulations containing *Pimenta pseudocaryophyllus* extract against UVB-induced oxidative stress and inflammation in hairless mice, J. Photochem. Photobiol. B 127 (2013) 153.
[11] A. Saija, A. Tomaino, D. Trombetta, A.D. Pasquale, N. Uccella, T. Barbuzzi, D. Paolino, F. Bonina, In vitro and in vivo evaluation of caffeic and ferulic acids as topical photoprotective agents, Int. J. Pharm. 199 (2000) 39.
[12] N.R. Prasad, S. Ramachandran, K.V. Pugalendi, V.P. Menon, Ferulic acid inhibits UV-B induced oxidative stress in human lymphocytes, Nutr. Res. 27 (2007) 559–564.
[13] L.M. Alias, S. Manoharan, L. Vellaichamy, S. Balakrishnan, C.R. Ramachandran, Protective effect of ferulic acid on 7,12-dimethylbenz[a]anthracene-induced skin carcinogenesis in Swiss albino mice, Exp. Toxicol. Pathol. 61 (2009) 205–214.
[14] E. Barone, V. Calabrese, C. Mancuso, Ferulic acid and its therapeutic potential as a hormetin for age-related diseases, Biogerontology 10 (2009) 97–108.
[15] V. Staniforth, W.C. Huang, K. Aravindaram, N.S. Yang, Ferulic acid, a phenolic phytochemical, inhibits UVB-induced matrix metalloproteinases in mouse skin via post-translational mechanisms, J. Nutr. Biochem. 23 (2012) 443–451.
[16] L.W. Zhang, S.A. Al-Suwayeh, P.W. Hsieh, J.Y. Fang, A comparison of skin delivery of ferulic acid and its derivatives: evaluation of their efficacy and safety, Int. J. Pharm. 399 (2010) 44–51.
[17] L.C. Bourne, C. Rice-Evans, Bioavailability of ferulic acid, Biochem. Biophys. Res. Commun. 253 (1998) 222–227.
[18] N.M. Anson, R.V.D. Berg, R. Havenaar, A. Bast, G.R.M.M. Haenen, Bioavailability of ferulic acid is determined by its bioaccessibility, J. Cereal Sci. 49 (2009) 296–300.
[19] ICH, ICH harmonized tripartite guideline on validation of analytical procedures: text and methodology Q2 (R1), Proceedings of the International Conference on Harmonisation, October 1994.
[20] S. Shafiq, F. Shakeel, S. Talegaonkar, F.J. Ahmad, R.K. Khar, M. Ali, Development and bioavailability assessment of ramipril nanoemulsion formulation, Eur. J. Pharm. Biopharm. 66 (2007) 227–243.
[21] H. Choudhury, B. Gorain, S. Karmakar, E. Biswas, G. Dey, R. Barik, M. Mandal, T.K. Pal, Improvement of cellular uptake, in vitro antitumor activity and sustained release profile with increased bioavailability from a nanoemulsion platform, Int. J. Pharm. 460 (2014) 131–143.
[22] N.Ü. Okur, S. Apaydın, N.Ü. Yavasoğlu, A. Yavasoğlu, H.Y. Karasulu, Evaluation of skin permeation and anti-inflammatory and analgesic effects of new naproxen microemulsion formulations, Int. J. Pharm. 416 (2011) 136–144.
[23] H. Bu, X. He, Z. Zhang, Q. Yin, H. Yu, Y. Li, A TPGS-incorporating nanoemulsion of paclitaxel circumvents drug resistance in breast cancer, Int. J. Pharm. 471 (2014) 206–213.
[24] R.K. Harwansh, K.C. Patra, S.K. Pareta, J. Singh, M.A. Rahman, Nanoemulsions as vehicles for transdermal delivery of glycyrrhizin, Braz. J. Pharm. Sci. 47 (2011) 769–778.
[25] S. Khurana, N.K. Jain, P.M.S. Bedi, Nanoemulsion based gel for transdermal delivery of meloxicam: physicochemical, mechanistic investigation, Life Sci. 92 (2013) 383–393.
[26] D.E. Paglia, W.N. Valentine, Studies on the quantitative and qualitative characterisation of erythrocyte glutathione peroxidase, J. Lab. Clin. Med. 70 (1967) 158–169.
[27] B. Kakkar, P.N. Das, A. Viswanathan, Modified spectrophotometer assay of SOD, Ind. J. Biochem. Biophys. 21 (1984) 130–132.
[28] R.F. Beers, I.W. Seizer, A spectrophotometric method for measuring breakdown of hydrogen peroxide by catalase, J. Biol. Chem. 115 (1952) 130–140.
[29] H. Ohkawa, N. Hash, K. Yagi, Assay for lipid peroxide for animal tissue by thiobarbituric acid reaction, Anal. Biochem. 95 (1979) 351–358.
[30] O.H. Lowry, N.J. Rosebrough, A.L. Forr, R.J. Ramdall, Protein measurement with the Folins phenol reagent, J. Biol. Chem. 193 (1951) 265–275.
[31] W. Warisnoicharoen, A.B. Lansley, M.J. Lawrence, Light scattering investigations on dilute non-ionic oil-in-water microemulsions, AAPS PharmSci. 2 (2000) 429–448.
[32] T.R. Kommuru, B. Gurley, M.A. Khan, I.K. Reddy, Self-emulsifying drug delivery systems (SEDDS) of coenzyme Q10: formulation development and bioavailability assessment, Int. J. Pharm. 212 (2001) 233–246.
[33] M.J. Lawrence, G.D. Rees, Microemulsion-based media as novel drug delivery systems, Adv. Drug Deliv. Rev. 45 (2000) 89–121.
[34] D.Q.M. Craig, S.A. Barker, D. Banning, S.W. Booth, An investigation into the mechanisms of self-emulsification using particle size analysis and low frequency dielectric spectroscopy, Int. J. Pharm. 114 (1995) 103–110.
[35] F. Shakeel, W. Ramadan, Transdermal delivery of anticancer drug caffeine from water-in-oil nanoemulsions, Colloids Surf. B 75 (2010) 356–362.
[36] M. Butnariu, C. Bostan, Antimicrobial and anti-inflammatory activities of the volatile oil compounds from *Tropaeolum majus* L. (Nasturtium), Afr. J. Biotechnol. 10 (2011) 5900–5909.
[37] V. Bali, M. Ali, J. Ali, Nanocarrier for the enhanced bioavailability of a cardiovascular agent: in vitro, pharmacodynamic, pharmacokinetic and stability assessment, Int. J. Pharm. 403 (2011) 46–56.
[38] R.R. Lala, N.G. Awari, Nanoemulsion-based gel formulations of COX-2 inhibitors for enhanced efficacy in inflammatory conditions, Appl. Nanosci. 4 (2014) 143–151.
[39] E. Yilmaz, H.H. Borchert, Effect of lipid-containing, positively charged nanoemulsions on skin hydration, elasticity and erythema—an in vivo study, Int. J. Pharm. 307 (2006) 232–238.
[40] H. Chaudhary, K. Kohli, V. Kumar, A novel nano-carrier transdermal gel against inflammation, Int. J. Pharm. 465 (2014) 175–186.

Journal of Photochemistry & Photobiology, B: Biology 160 (2016) 318–329

Contents lists available at ScienceDirect

Journal of Photochemistry & Photobiology, B: Biology

journal homepage: www.elsevier.com/locate/jphotobiol

# Enhancement of photoprotection potential of catechin loaded nanoemulsion gel against UVA induced oxidative stress

Ranjit K. Harwansh [a], Pulok K. Mukherjee [a,*], Amit Kar [a], Shiv Bahadur [a], Naif Abdullah Al-Dhabi [b], V. Duraipandiyan [b]

[a] School of Natural Product Studies, Department of Pharmaceutical Technology, Jadavpur University, Kolkata 700032, India
[b] Department of Botany and Microbiology, Addiriyah Chair for Environmental Studies, College of Science, King Saud University, Riyadh 11451, Saudi Arabia

ARTICLE INFO

*Article history:*
Received 25 August 2015
Received in revised form 14 March 2016
Accepted 15 March 2016
Available online 12 April 2016

*Keywords:*
Photoprotection
Nanoemulsion
Catechin
Nano-gel
Bioavailability
UVA exposure

ABSTRACT

The present study was aimed to develop a catechin (CA) loaded nanoemulsion based nano-gel for the protection of skin against ultraviolet radiation (UV) induced photo-damage and to ensure its enhanced skin permeability as well as bioavailability through transdermal route. The optimized nanoemulsion (CA-NE4) was prepared by spontaneous nano-emulsification method. It was composed of oil (ethyl oleate), $S_{mix}$ [surfactant (span 80) and co-surfactant (transcutol CG)] and aqueous system in an appropriate ratio of 15:62:23% w/w respectively. The CA-NE4 was characterized through assessment of droplet size, zeta potential, refractive index, transmission electron microscopy (TEM), UV, high performance thin layer chromatography (HPTLC) and Fourier transform infrared spectroscopy (FTIR) analysis. The average droplet size and zeta potential of CA-NE4 were found to be 98.6 ± 1.01 nm and −27.3 ± 0.20 mV respectively. The enhanced skin permeability was better with CA-NE4 based nano-gel (CA-NG4) [96.62%] compared to conventional gel (CA-CG) [53.01%] for a period of 24 h. The enhanced % relative bioavailability (*F*) of CA (894.73), $C_{max}$ (93.79 ± 6.19 ng mL$^{-1}$), $AUC_{0-t\infty}$ (2653.99 ± 515.02 ng h mL$^{-1}$) and $T_{max}$ (12.05 ± 0.02 h) was significantly obtained with CA-NG4 as compared to oral suspension for extended periods (72 h). CA-NG4 could improve the level of cutaneous antioxidant enzymes like superoxide dismutase (SOD), glutathione peroxidase (GPX) and catalase (CAT) and reduce the level of thiobarbituric acid reactive substances (TBRAS) against oxidative stress induced by UVA. Nano-gel formulation of CA showed sustained release profile and enhanced photoprotection potential due to its improved permeability as well as bioavailability ($P < 0.05$) compared to the conventional gel. Therefore, transdermal administration of nano-gel (CA-NG4) of CA offers a better way to develop the endogenous cutaneous protection system and thus could be an effective strategy for decreasing UV-induced oxidative damage in the skin tissues.



*Abbreviations:* ANOVA, analysis of variance; CA, catechin; CA-CG, conventional gel of catechin; CA-NE, catechin encapsulated nanoemulsion; CA-NG, nanoemulsion (CAT-NE4) based nano-gel; CMC, sodium carboxymethyl cellulose; CAT, catalase; DL, drug loading; DNA, deoxyribonucleic acid; EE, drug entrapment efficiency; ELO, eucalyptus oil; EO, ethyl oleate; FTIR, Fourier transform infrared spectroscopy; GPX, glutathione peroxidase; GSH, glutathione; HLB, hydrophilic lipophilic balance; HPTLC, high performance thin layer chromatography; ICH, International Conference on Harmonization; IPM, isopropyl myristate; ISIS, Isostearyl Isostearate®; *Jss*, stead state transdermal flux; *Kp*, permeability coefficient; LLW, Labrafac™ Lipophile WL1349; LOD, limit of detection; LOQ, limit of quantification; LPO, liquid paraffin oil; MED, minimally erythemogenic dose; MMPs, matrix metalloproteinases; NDDS, novel drug delivery system; NE, nanoemulsion; OA, oleic acid; OL, olive oil; PBS, phosphate buffer saline; PDA, photo diode array detector; PDI, polydispersity index; PEG 400, polyethylene glycol 400; Placebo-NG4, nano-gel formulation without catechin; PTA, phosphotungstic acid; QC, quality control; ROS, reactive oxygen species; RP-HPLC, reverse phase-high performance liquid chromatography; RSD, relative standard deviation; SBO, soybean oil; SD, standard deviation; SEM, standard error of mean; $S_{mix}$, surfactant and cosurfactant mixture; SO, sesame oil; SOD, superoxide dismutase; $t_{1/2}$, half life; $t_{90}$, shelf life; TBARS, thiobarbituric acid reactive substances; TEM, transmission electron microscopy; UV, ultraviolet ray; w/o, water in oil nanoemulsion.

* Corresponding author.
*E-mail addresses:* harwanshranjeet@gmail.com (R.K. Harwansh), naturalproductm@gmail.com (P.K. Mukherjee), amit.kar2@gmail.com (A. Kar), shiv.pharma17@gmail.com (S. Bahadur), alharbinaif@hotmail.com (N.A. Al-Dhabi), avdpandiyan@yahoo.co.in (V. Duraipandiyan).

http://dx.doi.org/10.1016/j.jphotobiol.2016.03.026
1011-1344/

## 1. Introduction

Intemperate exposure of skin to sunlight [ultraviolet radiation (UV: UVA and UVB)] is the cause of several dermatological problems [1]. Most of the UVB (315–280 nm) is absorbed in the epidermis, while UVA (400–315 nm) reaches to the deeper dermal layer that interacts with endogenous antioxidant defense system of the skin. Reactive oxygen species (ROS) are produced as the consequence of the exposure to UV rays [2]. The oxidative processes into structural damages result in changing the function of proteins and lipids through peroxidation. This UV-mediated oxidative stress can cause to unwanted and serious skin effect like sunburn, aging, wrinkle, dermatitis, inflammation, DNA damages, mutagenesis, and cancer (melanoma) [3]. Interaction of UV rays with DNA leads to strand breaks, oxidation of nucleic acid and photoreaction between adjacent pyrimidine bases leading to the formation of dimeric photoproducts [4,5].

Modification of the cellular antioxidant system is a major consequence of the oxidative stress. It involves reduced level of the glutathione (GSH) [6], superoxide dismutase (SOD), catalase (CAT), glutathione peroxidase (GPX) and increased level of the thiobarbituric acid reactive substances (TBARS) [7]. Conventional topical antioxidant lotions may be helpful, but they cannot protect the skin from long-term exposure to UV irradiation and need to be applied frequently [7].

Catechin (CA) is a flavanol type of polyphenolic antioxidant molecule which is present in green tea, red wine, coffee, apple, chocolate and several nutritional and functional food products [8,9]. CA possesses potent antioxidant potential and is capable of scavenging free reactive oxygen radicals by virtue of its reducing properties arising from the multiple hydroxyl groups attached to the aromatic rings [10]. CA has been proven to afford significant photoprotection to the skin against UV-mediated oxidative stress [11], photo-damage, basal cell carcinoma, melanoma and sunburn [12]. Several research reports suggested that CA has shown to exhibit cytostatic properties and induce apoptosis in many tumor cells [13]. It inhibits the expression of inflammation-associated enzymes, matrix metalloproteinases (MMPs) and restores levels of cutaneous antioxidant enzymes [14]. Other different activities of CA have been reported including antiaging [15], antidiabetic [16], neuroprotective [17], anti-obesity, antibacterial, hypolipidemic [10], anti-HIV [18] and anti-inflammatory [19]. Despite their exciting array of therapeutic effects, CA has a short (1.25 h) half-life ($t_{1/2}$) [20] and less than 5% oral bioavailability because of their extensive first-pass hepatic metabolism and elimination [21]. Poor oral bioavailability of CA is also associated with its digestive instability and poor intestinal uptake [22].

The emergence of novel drug delivery system (NDDS) has a great interest in developing a nanocarrier system to improve the therapeutic efficacy of a drug [23]. The nanocarrier ideally fulfills prerequisites that it should deliver the drug at a controlled rate as directed by the needs of the body. The goal of the NDDS is to enhance the permeability or bioavailability of poor bioavailable drugs by improving their solubility through the nanoemulsion (NE) like nanocarrier system [23]. NE is defined as an optical isotropic, transparent, low viscous and stable system of oil, surfactant/cosurfactant ($S_{mix}$) and aqueous system in an appropriate ratio with droplet size that varies from 20 to 200 nm. Nanoemulsions (NEs) prevent decomposition of drugs and improve their physical stability. They have advantages of simplicity in production and their feasibility to be easily scaled-up [24].

The conventional topical formulations of CA provide desired photoprotective effect on long exposure to UV irradiation, but CA has limited bioavailability due to lower elimination $t_{1/2}$ and a higher rate of biotransformation process. Thus, the present study was aimed to develop a NE based gel (nano-gel) of CA and to investigate its therapeutic potential against oxidative stress mediated by excessive UVA exposure and also to ensure enhanced skin permeability as well as the bioavailability of CA after transdermal administration of its nano-gel formulation.

## 2. Materials and Methods

### 2.1. Chemicals and Excipients

(+) catechin (assay 98%) was purchased from Sigma-Aldrich Chemicals, St. Louis, MO. Labrafac™ Lipophile WL1349 (LLW), Labrasol®, Plurol Oleique®, Plurol Isostearique®, Isostearyl Isostearate® (ISIS), Lauroglycol™ 90 and Transcutol CG® were provided as gift samples from Gattefossé (Saint Priest, France). Acconon® CC-6 was supplied from ABITEC Corporation, Columbus, USA. All other chemicals and reagents used were of analytical grade and procured from Merck, Mumbai. Purified water was obtained from Milli-Q water purification system (Millipore, MA).

### 2.2. Reverse Phase-High Performance Liquid Chromatography (RP-HPLC) Analysis of CA

RP-HPLC method was used to estimate the CA content in the excipients and their formulations. The HPLC system (Waters 600, Milford, MA, USA) equipped with the injection valve (rheodyne-7725i) with 20 μL sample loop, vacuum degasser, quaternary pump and photodiode array detector (PDA) was used for this analysis. The data were analyzed by Empower™-2 software. Chromatographic separation of the sample was done at a 1 mL/min flow rate, 280 nm wavelengths and 15 min run time at controlled temperature (25 ± 0.5 °C). The sample was eluted through a Spherisorb $C_{18}$ column (250 mm × 4.6 mm, 5 μm; Waters, Ireland) attached to a $C_{18}$ guard column (10 × 3.0 mm).

The samples were injected into the valve by using a microsyringe (20 μL) [Hamilton Microliter®; Switzerland]. The stock solution was prepared by dissolving the weighed amount of CA in methanol to get 1000 μg/mL concentration in each case. Aliquots were prepared by dilution of the stock using the same solvent and kept in the refrigerator at 2 to 8 °C for further uses. To obtain good resolution different mobile system composed of methanol and water at the ratio of 65:35, 70:30, 75:25 v/v (1% glacial acetic acid; pH 2.5) was used in isocratic mode. Prior to use, the mobile system was sonicated for 15 min and degassed. Before analysis, all samples were properly filtered through the syringe filter (0.45 μm; NYL).

The method validation of CA was performed in terms of linearity, repeatability, intermediate precision, sensitivity and recovery according to the recommended guideline of the International Conference on Harmonization (ICH). The assay's precision was analyzed in terms of % relative standard deviation (%RSD) of determinations. Sensitivity was determined by estimating the limit of detection (LOD) and limit of quantification (LOQ) based on the standard deviation of the response (σ) and the slope (S) of the standard curve by using the following equations: $LOD = 3.3\sigma/S$ and $LOQ = 10\sigma/S$.

The % recoveries of CA from quality control (QC) samples and formulations at three different concentrations were analyzed by calculating the % of detecting concentrations over additional concentrations. The quantitative analysis was repeated for three times ($n = 3$) by comparing and interpolating the QC sample peak area with the standard CA area.

### 2.3. Development and Evaluation of the Nanoemulsion

#### 2.3.1. Screening of CA in Oils, Surfactants and Cosurfactants

Screening of CA in different oil phase [LLW, ethyl oleate (EO), isopropyl myristate (IPM), isostearyl isostearate (ISIS), oleic acid (OA), olive oil (OL), soybean oil (SBO), liquid paraffin oil (LPO), sesame oil (SO) and eucalyptus oil (ELO)] was studied by dissolving an excess amount of the CA in 1 mL of each of the selected oils in Eppendorf tube (2 mL capacity) and mixed by a vortex mixer (Spinix, Tarson, India). Different mixture tubes were agitated in an isothermal shaker for 72 h at 25 ± 1.0 °C to reach equilibrium [25]. The equilibrated samples were removed and centrifuged at 13,500 rpm for 5 min using Spinwin MC-02,

Tarson, India. The supernatant was taken and filtered through a 0.45 μm membrane filter. The CA concentration was analyzed from each sample through RP-HPLC method at 280 nm wavelength.

The surfactants (Labrasol, Acconon CC-6, Lauroglycol 90, Span 80, Tween 80 and Brij 35) and cosurfactants (Transcutol CG, PEG 400, Plurol Isostearate and Plurol Oleique) were screened for development of NEs. Surfactant solution (2.5 mL of 15 wt.%) was prepared. Initially, 5 μL of the selected oil was added into the surfactant solution with vigorous vortexing until a clear solution was seen. Different excipients like EO, span 80 and transcutol CG were selected as oil phase, surfactant and cosurfactant respectively for development of the formulation.

*2.3.2. Construction of Ternary Phase Diagram*

The oil phase (EO), surfactants (span 80), cosurfactants (transcutol CG) and aqueous system (Milli-Q) were selected for the construction of pseudo-ternary phase diagrams. Surfactant and cosurfactant mixtures ($S_{mix}$) were used in different ratios (1:0, 1:1, 2:1, 3:1, 1:2, 1:3 w/w). This $S_{mix}$ ratio was prepared in an increasing amount of surfactant with respect to cosurfactant and vice versa. For the construction of phase diagram, water was added drop-wise to the mixture of $S_{mix}$ and oil by aqueous titration method. NE (w/o) region was developed based on the observation of its transparency and flowability. Various combinations of oil and $S_{mix}$ [1:9, 1:8, 1:7, 1:6, 1:5, 1:4, 1:3.5, 1:3, 1:2.5, 1:2, 1:1, 6:4, 7:3 and 9:1 w/w] were chosen to cover maximum ratios to delineate the boundaries of each phase diagram. The aqueous system was added at every 5% interval to obtain the range of 5–95% of total volume. Physical states of the formulations were observed through the pseudo-ternary phase diagrams where triangle apexes represented by the oil, $S_{mix}$ and aqueous phase respectively [26].

*2.3.3. Thermodynamic Stability Study and Selection of Formulations from Phase Diagrams*

Thermodynamic stability of the NE was performed in order to assess the physical stability as per the procedure described by Choudhury et al. [26]. Briefly, centrifugation (Cent.), heating–cooling cycle (H & C) and freeze–thaw cycle (Freeze Tha.) tests were evaluated to find out suitable formulations. Then, CA based NEs were prepared by incorporating 1 mg/mL amount into optimized oil phase at 10, 15, 20, 25 and 30% with respective $S_{mix}$ ratio using spontaneous nano-emulsification method.

*2.4. Characterization of Formulations*

*2.4.1. Conductivity*

The conductivity of the NE was measured by applying an electrical potential through the conductometer (Systronic Conductivity meter 306, Systronic Ltd., India) to find the type of formulation.

*2.4.2. Percentage Transmittance*

Percentage transmittance of the diluted sample of NE (100 times in water) was recorded at 450 nm using a spectrophotometer (SpectraMax® M5, USA).

*2.4.3. Viscosity*

The viscosity of NE was measured at 25 ± 0.5 °C by using a Brookfield viscometer with spindle CPE 41 (Brookfield Engineering Laboratories, Inc., MA).

*2.4.4. pH*

The pH of NE was analyzed through a digital pH meter (Orion 3 Star, Thermo Scientific, India) at controlled temperature (25 ± 0.5 °C).

*2.4.5. Refractive Index*

Refractive index (R.I.) of the NE along with placebo (NE without CA) was analyzed through an Abbe refractometer at 25 ± 0.5 °C.

*2.4.6. Drug Entrapment Efficiency and Drug Loading*

Drug entrapment efficiency (%EE) and drug loading (%DL) of CA loaded NEs were carried out according to the method established by Bu et al. [27]. Briefly, free CA content was separated from CA loaded NE (CA-NE) by ultrafiltration method (10,000 Da, Millipore) with centrifugation at 13,500 × *g* for 5 min. CA content was analyzed by using RP-HPLC method at 280 nm.

*2.4.7. Droplet Size, Polydispersity Index and Zeta Potential Analysis*

The droplet size (Z-average), polydispersity indexes (PDI) and zeta potential of diluted NEs were determined by Zetasizer (Nano ZS90, Malvern instruments Ltd., UK) with a 50 mV laser. Analysis was carried out at working condition of 25 ± 0.5 °C.

*2.4.8. Transmission Electron Microscopy (TEM)*

Morphology and surface structure of optimized CA-NE4 was analyzed by using TEM (JEOL JEM 2100, USA) with a working voltage of 200 kV. The diluted and filtered NE sample was carefully placed on carbon-coated copper grid (300 mesh size). The filled copper grid was negatively stained with phosphotungstic acid [PTA 2% (w/v)] for 30 s. Extra PTA was removed by absorbing it on a filter paper and dried overnight at room temperature (25 ± 0.5 °C). Photomicrograph of the sample was taken at different magnification.

*2.4.9. UV — Spectrophotometry Study*

Diluted sample of CA-NE4, placebo and pure CA was scanned together at 280 nm at 25 ± 0.5 °C through a spectrophotometer (Multiskan-Go, Thermo Scientific, USA) and the spectrum was recorded. 96-well microplate (Quartz) was used for this study.

*2.4.10. High Performance Thin Layer Chromatography (HPTLC) Analysis*

The chromatographic study of the CA-NE4 and pure CA was performed through HPTLC (CAMAG, Switzerland) using a solvent system of toluene: ethyl acetate: formic acid in a ratio of 7:5:1 v/v/v. The sample was applied onto the HPTLC plate (Silica gel 60 F254) through the Linomat-5 applicator. UV-densitometry scanning of developed HPTLC plate was carried out at $\lambda_{max}$ 280 nm and data acquisition was made by software (WINCATS).

*2.4.11. Fourier Transform Infrared Spectroscopy (FTIR) Study*

FTIR study was performed for assessment of drug-excipient compatibility in the formulation. FTIR spectrum of the pure CA (A), placebo-NE4 (B) and CA-NE4 (C) was analyzed in the range of 4000–450 $cm^{-1}$ by using FTIR (Perkin Elmer, USA).

*2.4.12. Stability Study*

Accelerated stability study of the optimized CA-NE4 was performed at 40 ± 2 °C/75 ± 5% RH according to recommended ICH guidelines. The formulation was packed in an air-tight glass vial and kept in a stability chamber for 0, 30, 60 and 90 days. Formulation was observed periodically for any change in its droplet size, zeta potential, drug content, appearance, precipitation, clarity and pH. Drug content was analyzed by using RP-HPLC method at 280 nm. Logarithm of percentage of the drug remained to be decomposed was plotted against time (days) to estimate shelf life ($t_{90}$) of the CA-NE4.

*2.4.13. Preparation of the Gel Formulation*

CA based gel formulation was prepared as per the method reported by the Harwansh et al. [28]. In brief, the conventional gel of catechin (CA-CG, equivalent to 0.1 g of CA) was prepared by dispersing the carbopol 940 (1 g) in distilled water, and volume made up to 100 mL. This gel medium was stored in a dark place at controlled temperature (25 ± 0.5 °C) for 24 h to equilibrium. After that other ingredients such as PEG 400 — 10 g, propylene glycol — 10 g, isopropyl alcohol — 10 g and triethanolamine — 0.5 g were added to get a conventional gel. The nanoemulsion-based gel (CA-NG4, equivalent to 0.1 g of CA) was

prepared by mixing 1 g of previously swollen dispersion system of carbopol-940 into CA-NE4 to produce the homogenous mass. Placebo-NG4 (nano-gel without CA) was prepared with CA-NE4 (blank).

#### 2.4.14. Rheological Behavior

The flow behaviors of CA-NG4 and placebo-NG4 formulations were studied through a rheometer (Anton Paar, Modular Compact Rheometer-MCR 102). A stress/rate with a temperature controller was applied to analyze the rheological property of the gel formulation. The analysis was done at a temperature of 25 ± 0.5 °C with a 4°/40 mm cone and plate geometry and a gap of 0.100 mm. The steady rheological property of CA-NG4 and placebo-NG4 was measured at a controlled rate varying from 0.001–100 and 0.0001–100 $s^{-1}$ respectively. Sample was allowed to rest for 10 min before applying stress onto the plate.

#### 2.4.15. Spreadability Test

The spreadability of gel formulations CA-NG4 and placebo-NG4 was tested according to the procedure reported by Khurana et al. [29].

### 2.5. Animals

Adult male Wistar rats weighing between 180–220 g were selected for animal experiments. Animals were housed in groups (n = 6) at an ambient conditions of temperature 25 ± 0.5 °C and 45–55% RH with 12 h light/dark cycles. They were fed with pellet chow (Brook Bond, Lipton, India) and water ad libitum. The experiment was conducted as approved by the Institutional Animal Ethical Committee with the ethical guidelines as provided by the committee (approval numbers: AEC/PHARM/1501/05/2015) for the purpose of control and supervision of an experiment on animals (CPCSEA, India).

#### 2.5.1. In Vitro Skin Permeation Study

The abdominal rat skin was used after removing the hairs using a soft hair removing lotion. The rats were anesthetized and sacrificed by cervical dislocation after that full-thickness abdominal skin was excised. Any adhered subcutaneous tissue on the visceral side of the skin was removed surgically, wiped with isopropyl alcohol to remove adhered fat and washed with phosphate buffer saline (PBS) of pH 7.4. The skin was then carefully checked through a magnifying glass to ensure about any surface irregularity.

After verification, the skin was mounted in the Franz diffusion cell with the *stratum corneum* side faced towards the donor compartment and the dermal side towards the receptor compartment with an effective diffusion surface area of 1.766 $cm^2$. The receptor compartment was filled with PBS (pH 7.4). The sink condition was maintained at 37 ± 0.5 °C with constant stirring with a magnetic stirrer. Formulations of CA-NE1–5, CA-NG4 and CA-CG (500 mg equivalent to 5 mg of CA) were evenly spread on the skin in donor compartment and sealed with paraffin film to provide occlusive conditions. Sample (200 μL) of the receptor medium was taken at predetermined time intervals over a period of 24 h and an equivalent volume of fresh PBS was replenished to maintain the sink conditions. The experiments were performed in triplicate. All samples were analyzed by RP-HPLC after suitable dilution and filtration.

#### 2.5.2. Skin Irritation Study

The skin irritation study was performed on the dorsal side of the rats (Wistar) (n = 6). 500 mg of each gel formulations of CA-CG, CA-NG4 and placebo-NG4 were applied on the rat skin. Animals were observed and evaluated for any sign/symptom of erythema and edema for a period of 7 days.

#### 2.5.3. Efficacy Evaluation of CA Loaded Gel Formulations Against UVA Exposure

*2.5.3.1. UVA Exposure to Animals.* The photoprotective activity of CA loaded different gel formulations against UVA exposure was evaluated as per the method described by Bhattacharyya et al. [4]. Briefly, Philips UV lamps (TL 100 W, Philips, India) were used as a UVA source (400–315 nm) with an emission spectrum of 370 nm. The UV lamp was equipped with the UVX digital UV intensity meter (Cole-Parmer, India) for measurement of the incident light intensity of 508.3 nW/$cm^2$. Distance between the UV lamps and dorsal skin was 40 cm. A distinguished area of about 2 × 3 $cm^2$ on the dorsal rat skin was removed using a soft hair-removing lotion. The rats were observed for 48 h to exclude rats showing abnormal hair growth or a reaction to the depilatory preparation. Application of a dose of 138 mJ/$cm^2$ of UVA radiation (obtained by UV exposure for 4.30 min from a distance of 40 cm) produced a minimally perceptible erythema. This dose was considered as the minimally erythemogenic dose (MED). UVA irradiation (610 mJ/$cm^2$; 4.42 times MED) was applied to the rats for 20 min in this experiment [4].

*2.5.3.2. Application of Gel Formulations.* The rats were divided into 5 groups (n = 6). Thin and uniform layers of gel formulations (500 mg equivalent to 5 mg of CA) were applied on the dorsal surface of the rat's skin. Group I was control (untreated UV irradiation) and Group II was irradiated with UVA. Groups III–V were treated with CA-CG, CA-NG4 and placebo-NG4 respectively. All the animals of groups II–V (except group I) were exposed to UVA radiation immediately after application of the different gel formulations for seven days.

On the eighth day, all the animals were anesthetized and sacrificed as per the protocols of CPCSEA. The UVA treated portion of cutaneous (epidermis and dermis) tissues was dissected and quickly put in ice-cold saline solution. The homogenate of skin tissue was prepared in 0.1 M PBS (pH 7.4) and centrifuged at 13,500 rpm for 5 min (Spinwin MC-02, Tarson, India). Then the supernatant was collected and stored at −20 °C for further use.

*2.5.3.3. Estimation of Skin Antioxidant Marker Enzymes in Cutaneous Tissue*

*2.5.3.3.1. Glutathione Peroxidase (GPX).* The level of GPX was estimated as per the method described by Paglia and Valentine [30]. In brief, the reaction mixture was composed of 400 μL (0.25 M) potassium phosphate buffer (pH 7.0), 200 μL supernatant (obtained from homogenate), 100 μL reduced glutathione (10 mM), 100 μL nicotinamide adenine dinucleotide phosphate reduced (2.5 mM) and 100 μL glutathione reductase (6 U/mL). 100 μL hydrogen peroxide (12 mM) was used for initiation of reaction and absorbance recorded at 340 nm (SpectraMax® M5, USA).

*2.5.3.3.2. Superoxide Dismutase (SOD).* The SOD level was measured according to the procedure proposed by Kakkar et al. [31]. The assay mixture was 0.1 mL of supernatant (from homogenate), 1.2 mL of sodium pyrophosphate buffer (pH 8.3; 0.052 M), 0.1 mL of phenazine methosulfate (186 μm), 0.3 mL of nitro blue tetrazolium (300 μM) and 0.2 mL of reduced nicotinamide adenine di-nucleotide (750 μM). The reaction was started by incorporating reduced nicotinamide adenine di-nucleotide and incubated at 30 °C for 90 s. Finally, the reaction was stopped by using 0.1 mL of glacial acetic acid. The reaction mixture was agitated vigorously with 4.0 mL n-butanol and the color intensity of the chromogen in the butanol layer was recorded spectrophotometrically at 560 nm (SpectraMax® M5, USA).

*2.5.3.3.3. Catalase (CAT).* CAT level was determined by using the procedure of Beers and Seizer [32]. Briefly, the 0.1 mL supernatant (from homogenate) was added in to test the tube containing 1.9 mL of 50 mM phosphate buffer (pH 7.0) and the reaction was initiated by adding 1.0 mL of freshly prepared 30 mM hydrogen peroxide. The decomposition rate of $H_2O_2$ was recorded spectrophotometrically at 240 nm (SpectraMax® M5, USA).

*2.5.3.3.4. Thiobarbituric Acid Reactive Substances (TBARS).* TBARS level was quantified according to the procedure of Ohkawa et al. [33]. In brief, 1.5 mL acetic acid (20%; pH 3.5), 1.5 mL of thiobarbituric acid (0.8%) and 0.2 mL of sodium dodecyl sulfate (8.1%) were incorporated to 0.1 mL of supernatant (from homogenate) and heated at 100 °C for 1 h. The mixture was cooled to room temperature and 5 mL of n-butanol-pyridine (15:1) mixture, 1 mL of distilled water was added with vigorous shaking. After that, the mixture was centrifuged at 1200 ×*g* for 10 min for separation of an organic layer, and absorbance was recorded at 532 nm (SpectraMax® M5, USA).

Total protein was estimated according to the procedure of Lowry et al. [34]. Briefly, 0.01 mL of tissue homogenate (2.5%) was diluted to 1.2 mL and mixed with 6 mL of solution-A (1 mL copper sulfate (1%) + 1 mL sodium potassium tartrate (2%) + 98 mL 2% sodium carbonate in 0.1 N sodium hydroxide). The mixture was incubated at room temperature for 10 min and 0.3 mL of solution-B (phosphomolybdate-phosphotungstate reagent) was incorporated and mixed properly. The mixture was stored at room temperature for 30 min. Absorbance was measured at 750 nm using a spectrophotometer (SpectraMax® M5, USA). Data were expressed as units/mg of protein.

### 2.6. In Vivo Bioavailability Study in Rats

The bioavailability of CA (500 mg of CA-NG4 equivalent to 5 mg CA) was studied after transdermal administration of CA-NG4 compared with an oral suspension of pure CA. The oral suspension was prepared by mixing 5 mg of CA in 5 mL of water containing 0.5% (w/v) of sodium carboxymethyl cellulose (CMC). The animals were allowed free access to food and water, until the night prior to dosing they fasted for 10 h. Latin square crossover design was followed; the animals were divided into two groups (n = 6). In group I, oral suspension (5 mg/5 mL) was administered through a feeding tube followed by rinsing with 10 mL of purified water and group II was applied with CA-NG4 (~5 mg CA) in phase I. In phase II vice versa was followed and conducted after 15 days of the washout period. The uniform layer of CA-NG4 was applied over a surface area of 1.766 $cm^2$ and covered with a water impermeable membrane and further fixed with the help of adhesive membrane. 2.5 mL of blood samples were withdrawn from retro-orbital plexus of rats after administration of CA oral suspension and CA-NG4 at pre-determined intervals of time 0.0, 0.5, 1, 2, 4, 8 and 12 h; 0.0, 1, 2, 4, 6, 8, 12, 18, 24, 36, 48 and 72 h respectively. All blood samples were allowed to clot and centrifuged at 13,500 rpm for 10 min (Spinwin MC-02, Tarson, India). Plasma was separated and kept at −20 °C prior to analysis. The CA contents in the samples were estimated by RP-HPLC method at 280 nm.

### 2.7. Analysis of Pharmacokinetic Parameters

The pharmacokinetic parameters of CA were determined with the help of a computer designed program, Phoenix WinNonlin® 6.4 (Certara, USA) after administration of CA-NG4 and CA-oral suspension to each rat. The non-compartmental model was used for calculating the pharmacokinetic parameters. Maximum concentration ($C_{max}$) and time to reach maximum concentration ($T_{max}$) are the values obtained directly from plasma concentration vs time curve. Area under the concentration–time curve ($AUC_{0-t}$), area under the concentration–time curve until infinite observation ($AUC_{0-t\infty}$), mean residence time ($MRT_{0-t}$), mean residence time to the infinite observation ($MRT_{0-t\infty}$) and elimination half-life ($t_{1/2}$el), elimination rate constant (Kel), clearance (Cl), and volume of distribution (Vd) were determined. The relative bioavailability (*F*) of CA was calculated as a ratio of the plasma $AUC_{0-t}$ of the CA-NG4 and CA-oral suspension.

### 2.8. Statistical Analysis

Statistical comparisons of data were made by one-way ANOVA followed by Dunnett's multiple comparison tests by using Graph Pad Prism software-5.0 (San Diego, CA, USA). All the data were expressed as mean ± standard deviation (SD) except the estimation of antioxidant enzyme levels in rat skin where data are expressed as mean ± standard error of means (SEM). The differences between means were considered to be significant at the $P < 0.05$.

## 3. Results

### 3.1. RP-HPLC-PDA Method Validation of CA

The RP-HPLC chromatographic separation of CA was carried out with the mobile phase in a ratio of 65:35 v/v (1% glacial acetic acid; pH 2.5) at a flow rate of 1 mL/min at 25 ± 0.5 °C under the isocratic conditions. The retention time (Rt) of CA was found to be 9.45 ± 0.02 min. A good linear precision relationship between the concentrations (20–100 μg/mL) and peak areas was obtained for the correlation coefficient ($r^2$) of 0.9993 ± 0.001. Intra-assay precision was performed at four different concentrations, and the %RSD of both instrumental precision and intra-assay precision was estimated to be <2.00. The precision of the method was optimized by calculating intra-day and inter-day repeatability at four subsequent concentrations ranging from 10–25 μg/mL. The RSD values in all tested groups were found to be <3%, which was significant. The LOD and LOQ were estimated to be 0.042 and 0.129 μg/mL respectively, which indicated that the proposed method can be used for detection and quantification of CA. The recovery rates of CA after spiking the additional standard drug concentrations at the different level (low: 20 μg/mL, middle: 30 μg/mL and high: 40 μg/mL) to the previously analyzed QC samples were estimated to be 19.94 ± 0.15 (99.70%), 29.94 ± 0.07 (99.80%) and 39.81 ± 0.12 μg/mL (99.52%) respectively.

### 3.2. Solubility Studies of CA in Oils

The solubility studies of CA were carried out in the different oil phase and maximum solubility of CA was found to be 2.68 ± 0.29 mg/mL in EO (Table 1). Therefore, EO was selected as an oil phase for the development of the formulations.

### 3.3. Pseudo-Ternary Phase Diagram Study

The pseudo-ternary phase diagram was plotted to get the maximum oil in water (w/o) NE regions, which consists of EO, span 80, transcutol CG and aqueous system. This formulation was appropriate due to its widespread NE (w/o) region. Individual phase diagrams were plotted and observed for each $S_{mix}$ (1:0–1:2) as shown in Fig.1 (A–E) and Supplementary Table 1.

In Fig. 1A, a small area was found at $S_{mix}$ (1:0) without cosurfactant but the w/o NE region was too preliminary towards aqueous and $S_{mix}$ rich apex. After addition of cosurfactant along with a surfactant in

**Table 1**
Solubility profile of catechin in different oils, mean ± SD (n = 3).

| Oil phase | Solubility (mg/mL) |
|---|---|
| Labrafac Lipophile WL1349 [LLW] | 1.89 ± 0.19 |
| Ethyl oleate (EO) | 2.68 ± 0.29 |
| Isopropyl myristate (IPM) | 0.72 ± 0.29 |
| Isostearyl isostearate (ISIS) | 1.29 ± 0.27 |
| Oleic acid (OA) | 1.21 ± 0.13 |
| Olive oil (OL) | 1.51 ± 0.15 |
| Soybean oil (SBO) | 1.17 ± 0.09 |
| Liquid paraffin oil (LPO) | 0.96 ± 0.17 |
| Sesame oil (SO) | 1.44 ± 0.18 |
| Eucalyptus oil (ELO) | 1.13 ± 0.23 |

equal proportion $S_{mix}$ (1:1), a stable and flowable NE region was obtained which, was optimized for selection of various formulations from this region as depicted in Fig. 1B. In this area, the oil was solubilized up to 30% along with 30% (w/w) $S_{mix}$ respectively.

The surfactant amount was increased to double at the $S_{mix}$ ratio (2:1) and NE area was smaller with the $S_{mix}$ ratio (1:1) (Fig. 1C). NE region was narrowed at a $S_{mix}$ ratio (3:1) in comparison with $S_{mix}$ (1:1) (Fig. 1D). A gel area was also observed at higher concentration of surfactant which was unfavorable for development of NE. When cosurfactant was increased at $S_{mix}$ (1:2) (Fig. 1E), oil was solubilized up to 15% (w/w). A little NE region was obtained in comparison to $S_{mix}$ (1:1).

### 3.4. Thermodynamic Stability Study

The formulations were subjected to heating–cooling cycle, centrifugation and freeze–thaw cycle stress tests to assess their thermodynamic stability. No obvious consequence was observed during the test. However, some formulations were unstable as represented in Supplementary Table 1.

### 3.5. Development of CA Based Nanoemulsions

From each phase diagram, a different amount of oil was selected between the ranges of 10–30% (w/w) so that maximum formulations could be selected, covering the maximum NE region. The amount of oil was selected at a low amount of $S_{mix}$ from each phase diagram. The favorable event was observed in the NE region of phase diagram after incorporation of CA (1 mg). Compositions of CA encapsulated nanoemulsions have been explained in Table 2.

### 3.6. Characterization of Nanoemulsions

Different NEs were characterized by using different parameters including droplet size, zeta potential (Supplementary Fig. 1.), conductivity, %transmittance, viscosity, pH, R.I., %EE and %DL. The results have been shown in Table 3.

### 3.7. TEM and UV — Spectrum Analysis

The TEM morphology of the optimized CA-NE4 has been shown in Fig. 2A. The surface of the droplet was observed as a dark spot in a photograph, which may be due to the dispersed oil droplets. Droplet size produced by TEM was quite similar to that obtained by Zetasizer.

UV spectrum showed that CA was present in the formulation (CA-NE4), when scanned at 280 nm wavelength as like as the pure CA (280 nm). The peak of UV spectra (CA-NE4) has been very slightly

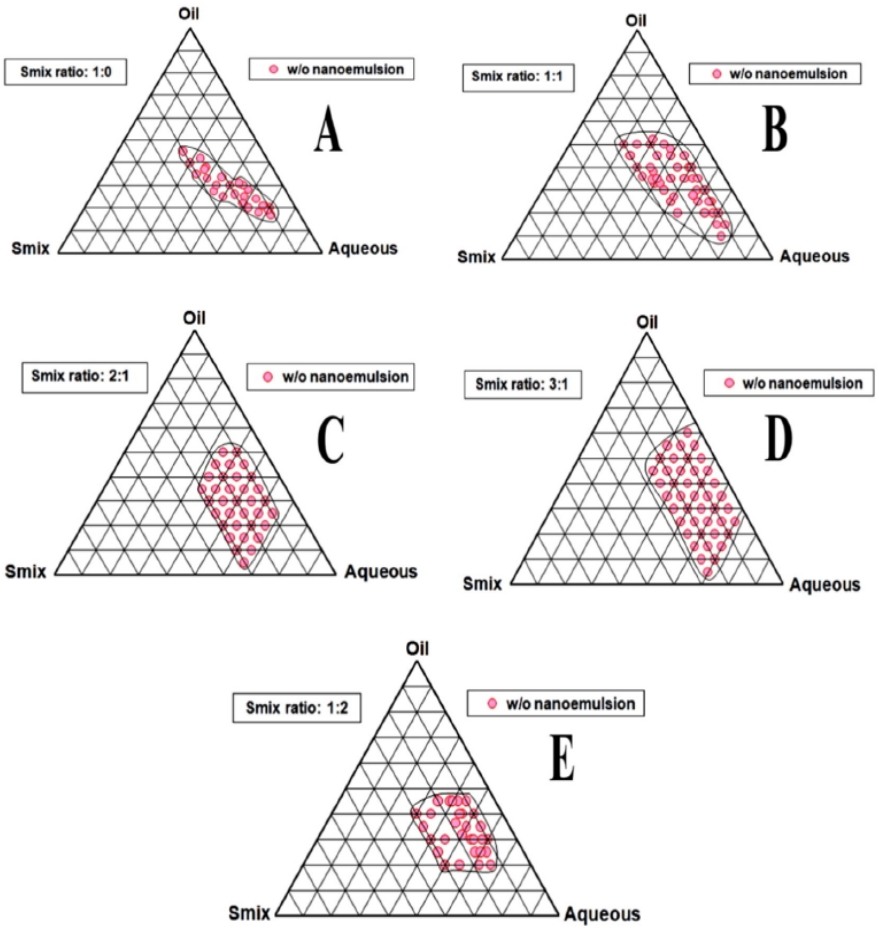


**Fig. 1.** Pseudo-ternary phase diagrams indicating a w/o nanoemulsion region at different $S_{mix}$ ratio (1:0–1:2 w/w). [(A): w/o NE at $S_{mix}$ (1:0) without using cosurfactant; (B): w/o NE at equal ratio of surfactant and cosurfactant (1:1); (C): w/o NE at $S_{mix}$ (2:1) using double amount of surfactant; (D): w/o NE at $S_{mix}$ (3:1) using triple amount of surfactant; (E): w/o NE at $S_{mix}$ (1:2) using double amount of cosurfactant].

**Table 2**
Compositions of different nanoemulsion formulations.

| NE code | $S_{mix}$ | Ingredients in nanoemulsion formulation (% w/w) | | | | Oil:$S_{mix}$ ratio |
|---|---|---|---|---|---|---|
| | | Oil | Water | Surfactant | Cosurfactant | |
| CA-NE1 | 1:1 | 10 | 17 | 36.5 | 36.5 | 1:7.3 |
| CA-NE2 | 2:1 | 20 | 27 | 35.32 | 17.66 | 1:2.6 |
| CA-NE3 | 3:1 | 15 | 29 | 42 | 14 | 1:3.7 |
| CA-NE4 | 1:1 | 15 | 23 | 31 | 31 | 1:4.1 |
| CA-NE5 | 1:2 | 15 | 25 | 20 | 40 | 1:4 |

shifted due to drug entrapment with NE matrix. Detail has been graphically shown in Fig. 2B.

### 3.8. HPTLC Analysis

HPTLC chromatogram produced a sharp and well-defined symmetrical peak when the chamber was saturated with the mobile phase for 30 min at a controlled temperature (25 ± 0.5 °C). HPTLC chromatogram of pure CA (A) and CA-NE4 (B) confirmed the $R_f$ value of 0.20 and 0.21 respectively (Fig. 3). The result stated that the CA found quite compatible with their excipient, which was used for NE formulation.

### 3.9. FTIR Study

The chemical compatibility of catechin with the excipients was analyzed by FTIR study which was used in the formulation (CA-NE4). Details of FTIR spectrum have been shown in Fig. 4 (A–C). The wave numbers of FTIR spectra of pure catechin at 965.3, 1020.1, 1144.1, 1285.0,1474.4, 1514.5 and 1610.5 $cm^{-1}$ were assigned to C—H alkenes, —C—O alcohols, —OH aromatic, C—O alcohols, C—H alkanes, C═C aromatic ring and C═C alkenes respectively. Stretching of O—H was found at 3412.0 $cm^{-1}$. In case of CA-NE4 formulation, the wave numbers at 965.3, 1020.1, 1285.0, 1474.4, 1610.5 $cm^{-1}$ and 3412.0 $cm^{-1}$ were shifted to 947.0, 1115.6, 1249.6, 1455.9, 1702.2 and 3454.8 respectively. Other wave numbers at 1364.9 and 1864.2 were also shifted to 1351.7 and 2088.1 $cm^{-1}$ respectively. It may be due to the coordination bonding of several —OH groups of parent ring with the water content of the nanoemulsion (w/o). This result confirms that CA was pretty compatible with their excipients used in the formulations.

### 3.10. Stability Study

The optimized CA-NE4 was evaluated during the period of 0, 30, 60 and 90 days at 40 °C. No changes were observed in the droplet size, zeta potential and pH of the CAT-NE4 formulation and results have been shown in Supplementary Table 2. A first order degradation of CA content in the formulation was found to be 0.71% for the remainder of 90 days at 40 °C (Supplementary Fig. 2). From the results, it can be concluded that the CA-NE4 was stable at 40 °C. Shelf life ($t_{90}$) of CA based nano-gel was found to be 3.23 years.

### 3.11. Rheological Behavior

The viscosities were calculated in a range of 37.1–0.123 and 46.1–0.0784 Pa s for placebo-NG4 and CA-NG4 formulation respectively. Higher viscosity attributed to the CA-NG4 was due to the drug which integrated into the gel matrix and leads to close proximity hence viscosity increased. The CA-NG4 showed non-Newtonian shear thinning and viscosity decreases with the rate of shear stress. Thus, the nano-gel formulation may be suitable for skin administration. Details have been shown in Supplementary Fig. 3.

### 3.12. Spreadability Test

The placebo-NG4 (58.43 ± 0.85% w/w) and CA-NG4 (59.87 ± 0.59% w/w) showed good spreadability that would assure practicability to the skin administration. No significant difference ($P < 0.05$) between the spreadability of placebo-NG4 and CA-NG4 was observed in this study.

### 3.13. Skin Permeation Studies

The percentage cumulative skin permeation profile of CA from different CA-NE1–5, CA-NG4 and CA-CG were studied as shown in Fig. 5 (A & B). The best release profile (93.76%) has been exhibited by the CA-NE4 compared to other formulation for 24 h. CA-NG4 and CA-CG showed skin permeability of 96.62 and 53.01% respectively for 24 h. CA-NG4 demonstrated better drug permeability, which may be due to enhanced solubility, low viscosity, nano-droplet size, favorable zeta potential and an appropriate pH comparatively to others. While a significant difference between skin permeation profile of CA-CG and CA-NG4 was observed. This may be due to the poor permeability of conventional formulation because of its non-uniform droplet size distribution and low solubility.

The transdermal flux [*Jss* (μg/h/$cm^2$)] and permeability coefficient [*Kp* (cm/h)] of CA from different formulations across the skin have been explained in Fig. 5 (C). Significantly maximum flux (2.25 ± 0.11 μg/h/$cm^2$) and permeability (0.450 ± 0.05 cm/h) of CA were achieved with CA-NG4 (***$P < 0.01$) compared to other formulations. The lag time was found to be 0.25 h for CA-NG4.

### 3.14. Skin Irritation Study

There were no substantial clinical signs of irritation, erythema or edema observed throughout the study period. These results indicated that the gel formulation of CA (CA-NG4) was non-irritant and safe for skin application.

### 3.15. Efficacy Evaluation of Gel Formulations Against UVA Exposure

In group II (UVA irradiated), the antioxidant enzyme level of rat skin was elevated significantly compared to the control group (untreated UV irradiation) (***$P < 0.01$) (Fig. 6A & B). In test groups (III and IV), the levels of cutaneous antioxidant enzymes (SOD, GPX and CAT) were significantly increased when treated with CA-CG and CA-NG4 respectively compared to UVA irradiated group. The placebo-NG4 group did not

**Table 3**
Characterization of different catechin loaded nanoemulsions.

| NE code | Z-average (nm) | PDI | Z.P. (mV) | pH | Visco. (cP) | Cond. (ms/cm) | P.T. | R.I. | (%EE) | (%DL) |
|---|---|---|---|---|---|---|---|---|---|---|
| CA-NE1 | 181.8 ± 1.12 | 0.231 ± 0.16 | −43.6 ± 0.90 | 6.85 ± 0.04 | 12.34 ± 0.05 | 21.58 ± 1.20 | 88.78 ± 0.82 | 1.436 ± 0.02 | 97.72 ± 0.11 | 1.01 ± 0.02 |
| CA-NE2 | 253.7 ± 1.10 | 0.305 ± 0.14 | −52.5 ± 0.95 | 6.89 ± 0.02 | 15.89 ± 0.12 | 22.99 ± 1.15 | 82.74 ± 1.12 | 1.443 ± 0.03 | 95.73 ± 0.16 | 0.98 ± 0.01 |
| CA-NE3 | 382.7 ± 1.08 | 0.430 ± 0.07 | −39.5 ± 0.73 | 6.83 ± 0.03 | 17.24 ± 0.03 | 24.89 ± 1.52 | 81.31 ± 1.56 | 1.484 ± 0.08 | 93.61 ± 0.33 | 0.93 ± 0.03 |
| CA-NE4 | 98.6 ± 1.05 | 0.120 ± 0.03 | −27.3 ± 0.20 | 6.80 ± 0.01 | 10.18 ± 0.01 | 19.59 ± 0.70 | 99.88 ± 1.09 | 1.421 ± 0.01 | 99.02 ± 0.13 | 1.12 ± 0.02 |
| CA-NE5 | 314.7 ± 1.15 | 0.187 ± 0.09 | −24.5 ± 0.35 | 7.34 ± 0.10 | 18.56 ± 0.04 | 27.56 ± 1.25 | 79.98 ± 1.21 | 1.450 ± 0.04 | 94.37 ± 0.46 | 0.96 ± 0.01 |

PDI: polydispersity index; Z.P.: zeta potential; Visco.: viscosity; Cond.: conductivity; P.T.: percentage transmittance; R. I.: refractive index; %EE: percentage entrapment efficiency; %DL: percentage drug loading. Values were mean ± SD (n = 3).

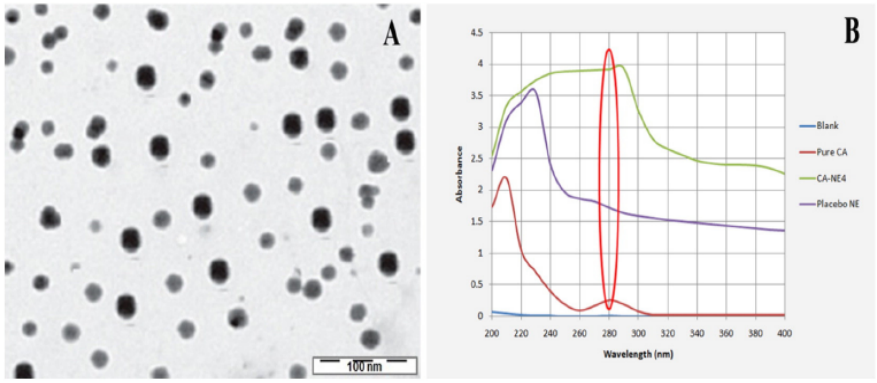


**Fig. 2.** TEM photograph (A) and UV spectra of CA-NE4 formulation (B).

produce any significant effect on the skin antioxidant system in comparison to group II, which may be due to placebo-NG (nano-gel formulation without catechin). The high level of TBARS has been significantly improved with CA-CG and CA-NG4 treated groups compared to the UVA irradiated group. Details have been explained in Fig. 6 (A & B).

The CA-CG group showed less cutaneous protection efficacy than the CA-NG4 due to less availability of CA to the blood circulation and associated tissue. CA-NG4 showed enhanced photoprotective potential because of its improved permeability than its conventional gel. Thus, CA loaded transdermal nano-gel formulations could enhance UV protective activity for longer periods than the conventional dosage form.

### 3.16. In Vivo Bioavailability Study

The bioavailability study of CA was performed after administration of its oral suspension and CA-NG4. Results have been represented in Fig. 7 and Table 4. CA has been well released and permeated from CA-NG4 as compared to the oral suspension for longer periods (72 h). Statistically significant $C_{max}$, $T_{max}$, MRT and AUC profiles were observed with oral suspension and CA-NG4 ($P < 0.05$). The $C_{max}$ of CA was found to be 87.52 ± 8.56 and 93.79 ± 6.19 ng $mL^{-1}$ after administration of oral suspension and CA-NG4 respectively. The $AUC_{0-t\infty}$ (2653.99 ± 515.02 ng h $mL^{-1}$), $T_{max}$ (12.05 ± 0.02 h) and $MRT_{0-t\infty}$ (35.98 ± 10.34 h) were higher for CA-NG4 comparatively to the oral suspension ($P < 0.05$). The $t_{1/2}$el of CA was increased when it was in the nano-gel (24.75 ± 13.60 h) form and eventually the Kel (0.028 ± 0.02 $h^{-1}$) and Cl (0.0021 ± 0.04 L $h^{-1}$) of the molecule in nano-gel form were also lowered. The mean value of $AUC_{0-t}$ by transdermal route was 8.94 times higher than that of oral route, and the difference was found to be statistically significant ($P < 0.05$). This could be due to avoidance of first-pass hepatic metabolism by the transdermal route. The reported oral bioavailability of CA was 5% [21] because of hepatic first-pass metabolism. In the current investigation, the relative bioavailability ($F$) of CA (CA-NG4) by transdermal route was found to be 894.73. This indicated enhanced bioavailability of CA (nano-gel) through transdermal route. This may be due to the CA-NG4 that releases drug in a sustained manner for extended periods (72 h). For transdermal route, *stratum corneum* acts as a permeation barrier and thereby the sustained-release activity of CA was found with CA-NG4 in comparison to orally administered suspension which is an immediate release dosage form. Therefore, CA based nano-gel could provide an effective treatment for the management of skin damage mediated by the UV exposure.

## 4. Discussion

Long-term exposure to UV irradiation to the human skin is a cause of several dermatological disorders induced by oxidative stress. ROS formed as a consequence of UV irradiation can target cellular antioxidant defense systems like GPX, SOD and CAT and reduce their levels. UVA contributes only to a minor extent to the induction of skin cancer that is mostly explained by the formation of pyrimidine dimmers produced by UVB [35]. However, UVA-induced oxidative stress plays a key role in other deleterious processes such as skin aging of immunosuppression. A polyphenolic antioxidant is suitable as an effective alternative in cosmetic formulations as they can protect the skin from harmful UV rays [2]. Catechin is a potent polyphenolic antioxidant which is capable of protecting the living tissue from the oxidative stress by scavenging the ROS [10]. It can also induce the cellular antioxidant response element pathway, which is able to stimulate and restore the

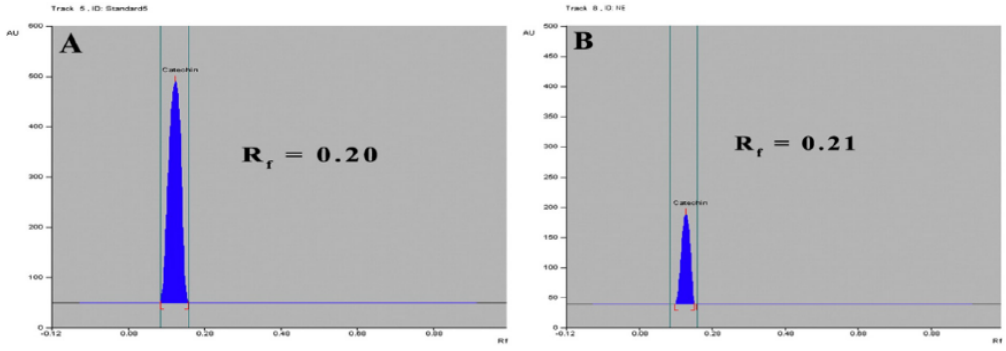


**Fig. 3.** HPTLC chromatogram of pure CA (A) and catechin loaded nanoemulsion, CA-NE4 (B).

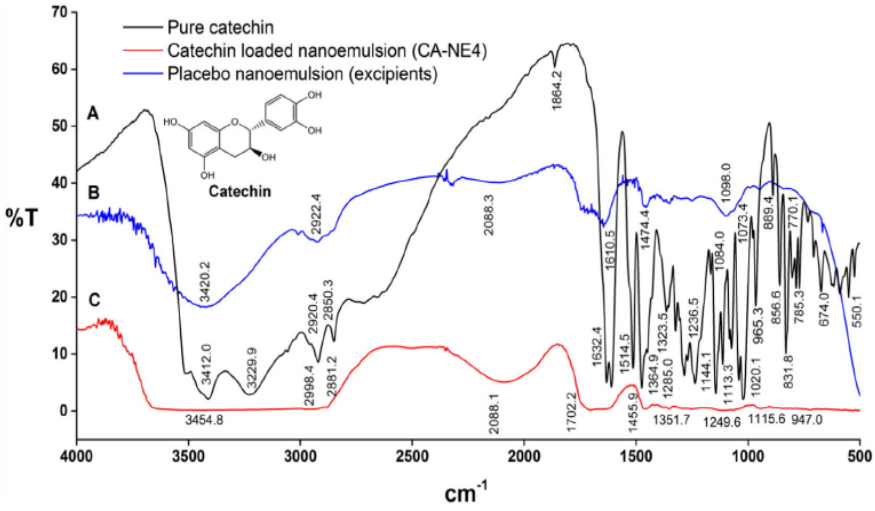


**Fig. 4.** FTIR spectrum of pure CA (A), placebo nanoemulsion (B) and CA-NE4 (C).

activity of the antioxidant enzyme system under oxidative stress condition [11]. Catechin is an ideal photo-protective or sun-screening agent that can be used to UV radiation for photo-damage [2]. Transdermal delivery is an attractive route for local and systemic treatment. Transdermal application of drug offers the potential advantage of delivering the drug directly to the site of action and acting for an extended period of time.

The present study was aimed to develop a catechin loaded nanoemulsion (CA-NE4) and its nano-gel (CA-NG4) for transdermal application in order to ensure the enhanced permeability and maximum photoprotective and sunscreen activity against UVA-mediated oxidative stress in the rat. In vivo bioavailability study of catechin has also been performed through the transdermal administration of optimized nano-gel formulation. For the development of nanoemulsion (w/o), span 80 (HLB = 4.3) and transcutol CG (HLB = 4.2) were chosen as surfactant and cosurfactant respectively, and that could work better in a $S_{mix}$ ratio. Nanoemulsions were prepared through self nanoemulsification process and resulting into the thermodynamically stable system [36]. A formulation containing the higher amount of surfactant may lead to unwanted effect to the skin [37]. Thus, the lower amount of $S_{mix}$ (1:1) was selected for development of optimized formulation, CA-NE4.

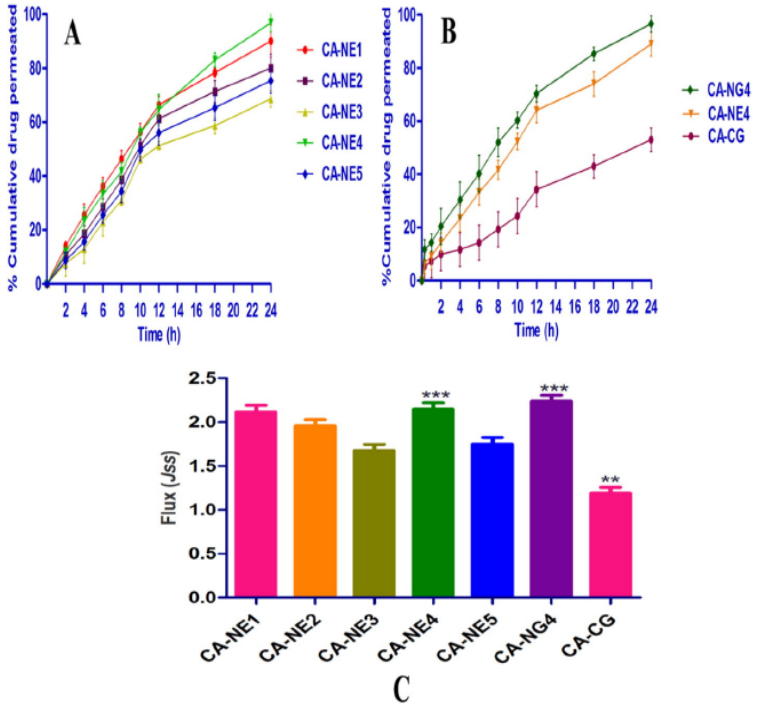


**Fig. 5.** Transdermal skin permeation profiles of CA from different nanoemulsions (A) CA-NE (1–5), (B) CA-CG, CA-NE4 and CA-NG4 through rat skin and (C) steady state flux of different formulations across rat skin. Values were mean ± SD (n = 3). $^{**}P < 0.05$, $^{***}P < 0.01$ when compared to the conventional group.

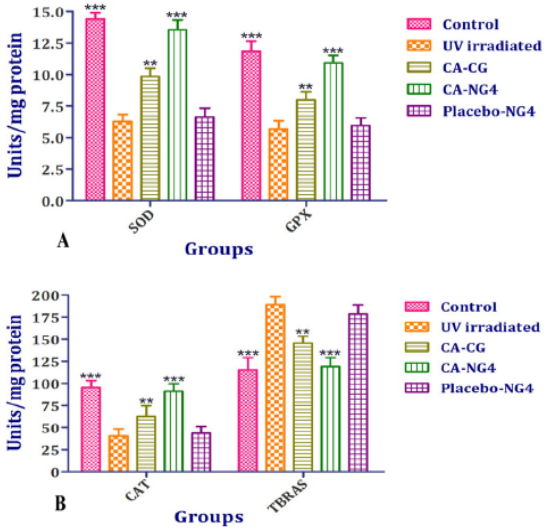


**Fig. 6.** Effect of transdermal gel formulations of CA on different cutaneous antioxidant enzyme levels (A) SOD and GPX, and (B) CAT and TBARS. Values are mean ± SEM (n = 6). $^{**}P < 0.05$, $^{***}P < 0.01$ when compared to the control and UVA irradiated group.

**Table 4**
Pharmacokinetic parameters of CA in rats after administration of oral suspension and CA-NG4, values represented were mean ± SD (n = 6).

| Pharmacokinetic parameter | Oral suspension (≈5 mg CA) | CA-NG4 (≈5 mg CA) |
|---|---|---|
| $C_{max}$ (ng $mL^{-1}$)[a] | 87.52 ± 8.56 | 93.79 ± 6.19 |
| $T_{max}$ (h)[b] | 2.02 ± 0.01 | 12.05 ± 0.02 |
| $AUC_{0-t}$ (ng h $mL^{-1}$)[c] | 256.70 ± 37.16 | 2296.78 ± 293.39 |
| $AUC_{0-t\infty}$ (ng h $mL^{-1}$)[d] | 256.86 ± 37.14 | 2653.99 ± 515.02 |
| ($t_{1/2}$el) (h)[e] | 1.71 ± 0.24 | 24.75 ± 13.60 |
| Kel ($h^{-1}$)[f] | 0.405 ± 0.06 | 0.028 ± 0.02 |
| Cl ($Lh^{-1}$)[g] | 0.019 ± 0.02 | 0.0021 ± 0.04 |
| Vd (L)[h] | 0.047 ± 0.01 | 0.0745 ± 0.03 |
| %F[i] | – | 894.73 |

[a] Peak of maximum concentration ($C_{max}$).
[b] Time of peak concentration ($T_{max}$).
[c] Area under the concentration-time curve until last observation ($AUC_{0-t}$).
[d] Area under the concentration-time curve until infinite observation ($AUC_{0-t\infty}$).
[e] Elimination half-life ($t_{1/2}$el).
[f] Elimination rate constant (Kel).
[g] Clearance (Cl).
[h] Volume of distribution (Vd).
[i] Relative bioavailability (%F) of catechin.

Uniform droplets may enhance the drug solubility and stability in the formulation. The uniformity of the droplet size was indicated by polydispersity index (PDI) value. The low PDI value (0.120) has been observed for the optimized formulation that indicates uniformity of droplet size. The best droplet's uniformity was concerned with CA-NE4, and the formulation was a homogenous system. Appropriate nano droplet (~100 nm) and zeta potential (−27.3 mV) were obtained with CA-NE4. Zeta potential plays an important role in the stability of the formulation. It is very well known that the zeta potential indicated by the degree of repulsion between adjacent charged droplets in a dispersion system such as nanoemulsion, which deals with the stability of the system. Generally, −30 mV or +30 mV is considered as high zeta potential value [38]. The high negative charge of CA-NE4 is probably influenced by the anionic groups of the fatty acids present in the oil and $S_{mix}$. The nano size range of droplets with a higher zeta potential of CA-NE4 is generally attributed to prevent coalescence between droplets. Thus, zeta potential sustains the homogeneity as well as the stability to the system.

In the rheological behavior of gel formulation, CA-NG4 showed high viscosity than the placebo due to drug integration into the gel matrix of carbopol 940. Therefore, the catechin based nano-gel may be suitable for transdermal administration. The CA-NG4 has expressed non-Newtonian shear thinning property. Its viscosity decreases with the rate of shear stress. Carbopol-940 was used as a viscosity modifier resulting in improved membrane permeability. Nano-gel has been showed to enhance drug permeability across the rat skin after transdermal application, which may be due to diffusion of water content from the formulation and improved drug release. Transcutol CG could also play a role in the drug permeation by reducing the diffusion barrier of the *stratum corneum*, which is known as permeation enhancers.

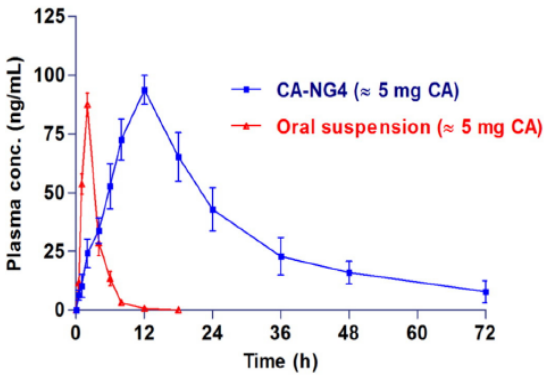


**Fig. 7.** Plasma concentration profiles of CA in rats, after administration of oral suspension (~5 mg of CA) and CA-NG4 (~5 mg of CA). Values were mean ± SD (n = 6).

Permeation profiles of CA-CG and CA-NG4 were fitted with zero order, First order, Higuchi's model, and Korsmeyer–Peppas model. The best release pattern of CA-CG ($r^2 = 0.937$) and CA-NG4 ($r^2 = 0.992$) was achieved with Korsmeyer–Peppas model. The CA-NG4 showed a non-Fickian pattern ($0.5 < Kp < 1$) of drug release by diffusion and matrix erosion. The conventional gel was prepared by simple mixing of all ingredients along with the added drug. It was known as conventional gel because there was no nano-carrier (nanoemulsion) system used in this formulation. Generally, the conventional formulation is frequently applied because it produces instant drug release and action for a short span of time. It could not produce sustained release pattern of drug permeability. The dimensions of the droplets in the conventional formulation were micro rather than nano size. It scantily diffused the skin layer and could not follow the zero order drug release profile for longer periods, which may be due to their bigger droplet size and lack of permeation enhancer in the formulation.

Solubility plays an important role in enhancing the permeability as well bioavailability of the low lipid soluble drug (catechin) by increasing their solubilization through nanoemulsion like carrier system. For poor lipid soluble molecule like catechin, nanoemulsion could be a nano-carrier for enhancing their therapeutic efficacy. The catechin based nano-gel formulation exhibited enhanced skin permeability comparatively to the conventional gel when transdermally applied. These may be due to nanosize droplets of the formulation and significantly diffusion of drug content from gel formulation that was carried out for extended periods. Mechanism of sustained release was achieved with nano-gel by drug diffusion and matrix erosion. The conventional gel has resulted in poor activity due to rapid drug release for a shorter period of time. The poor diffusion process and low availability of drug concentration into systemic circulation were also attributed towards the less therapeutic efficacy of the conventional gel.

In vivo antioxidant potential of catechin based transdermal nano-gel formulations was found significantly against UVA exposure except placebo formulation. CA-NG4 exhibited better UV protective activity after its transdermal administration. This activity may be due to its improved

permeability and sustained-release profile compared to conventional gel. This result indicated that the use of catechin in transdermal nano-gel formulation might increase its penetration or absorption capacity inside the skin layers and that the presence of a higher concentration may be responsible for better sun protection.

Different pharmacokinetic parameters of catechin were evaluated and found significant after transdermal and oral administration of their CA-NG4 and suspension respectively. The enhanced relative bioavailability of catechin was found to be 894.73 by the transdermal route. It may be due to avoidance of hepatic first-pass metabolism. Nano-gel exhibited sustained release profile and maintained the blood concentrations for longer periods. In an earlier reported work the oral bioavailability of CA was 5% because of hepatic first-pass effect [21]. Hence, the transdermal delivery system of catechin is an alternative approach to enhance their bioavailability and therapeutic efficacy.

The skin permeability of catechins from tea extract has been studied by Batchelder et al. and assumed that sufficient amount of catechins were permeated across skin through transdermal route [39]. This result encourages the transdermal routes for catechin delivery. Enhancement of the transdermal delivery of catechins by liposomes has been performed by Fang et al. [40]. A gel formulation of epicatechin has been developed and evaluated for their skin permeability and stability for topical use [41]. Topical application of (−)-epicatechin gallate and caffeine has also been shown to decrease the number of non-malignant and malignant skin tumors in mice [42].

Enhanced bioavailability of lacidipine through microemulsion based gel has been achieved after transdermal administration [43]. In a different study, enhanced permeability and biological activity of nano-carrier gel of diclofenac diethylamine and curcumin have been achieved by transdermal route [44]. Recently, Harwansh et al. have reported that ferulic acid loaded nano-gel showed better skin protection activity against UVA-mediated oxidative stress due to its improved permeability and sustained-release profile compared to conventional gel [45]. Transdermal route eliminates the side effect, increases patient compliance, avoids first-pass metabolism, enhances bioavailability and maintains the plasma drug level for longer periods resulting in improved $t_{1/2}$. Nano-gel formulation of catechin could serve as an effective formulation for photoprotection of the skin against extreme exposure to UV radiation.

## 5. Conclusion

Excessive UV exposure interferes with the cellular defense system of human skin and causes oxidative stress. ROS as a result of UV irradiation may oxidize and damage cellular lipids, proteins and DNA. This leads to the destruction of skin structures and results in hindrance of regular function of the cutaneous antioxidant defense system of the skin. The enhanced relative bioavailability of catechin (894.73%) was achieved with nano-gel formulation after its transdermal application for 72 h. The nano-gel increased antioxidant potential of catechin against UVA-induced oxidative stress in a sustained manner. Nano-gel formulation of catechin was developed with nanoemulsion that could be useful as an effective strategy for photoprotection against UVA-induced oxidative stress. The CA-NG4 formulation was found to be stable, safe and effective for transdermal delivery. Thus, nanoemulsion based gel formulation of catechin may be a promising nanocarrier for skin delivery.

## Conflict of Interest Statement

The authors have no conflicts of interest.

## Acknowledgement

The authors are thankful to the Department of Biotechnology (DBT), Govt. of India New Delhi, India for the financial support through Tata Innovation Fellowship (D.O. No. BT/HRD/35/01/04/2014) to Dr. Pulok K. Mukherjee. Thanks are due to the University Grant Commission (UGC), Govt. of India New Delhi, India for providing research fellowship to Mr. Ranjit K Harwansh.

## Appendix A. Supplementary Data

Supplementary data to this article can be found online at http://dx.doi.org/10.1016/j.jphotobiol.2016.03.026.

## References

[1] N.K. Nema, N. Maity, B. Sarkar, P.K. Mukherjee, *Cucumis sativus* fruit-potential antioxidant, anti-hyaluronidase, and anti-elastase agent, Arch. Dermatol. Res. 303 (2011) 247–252.
[2] E. Gregoris, S. Fabris, M. Bertelle, L. Grassato, R. Stevanato, Propolis as potential cosmeceutical sunscreen agent for its combined photoprotective and antioxidant properties, Int. J. Pharm. 405 (2011) 97–101.
[3] P.K. Mukherjee, N. Maity, N.K. Nema, B.K. Sarkar, Bioactive compounds from natural resources against skin aging, Phytomedicine 19 (2011) 64–73.
[4] S. Bhattacharyya, S. Majhi, B.P. Saha, P.K. Mukherjee, Chlorogenic acid-phospholipid complex improve protection against UVA induced oxidative stress, J. Photochem. Photobiol. B 130 (2014) 293–298.
[5] M. Ichihashi, A. Ueda, T. Budiyanto, M. Bito, M. Oka, K. Fukunaga, T. Tsuru, Horikawa, UV-induced skin damage, Toxicology 189 (2003) 21–39.
[6] M.Z. Campanini, F.A. Pinho-Ribeiro, A.L.M. Ivan, V.S. Ferreira, F.M.P. Vilela, F.T.M.C. Vicentini, R.M. Martinez, A.C. Zarpelon, M.J.V. Fonseca, T.J. Faria, M.M. Baracat, W.A. Verri, S.R. Georgetti, R. Casagrande, Efficacy of topical formulations containing Pimenta pseudocaryophyllus extract against UVB-induced oxidative stress and inflammation in hairless mice, J. Photochem. Photobiol. B 127 (2013) 153–160.
[7] A. Saija, A. Tomaino, D. Trombetta, A.D. Pasquale, N. Uccella, T. Barbuzzi, D. Paolino, F. Bonina, In vitro and in vivo evaluation of caffeic and ferulic acids as topical photoprotective agents, Int. J. Pharm. 199 (2000) 39–47.
[8] R. Pomponio, R. Gotti, B. Luppi, V. Cavrini, Microemulsion electrokinetic chromatography for the analysis of green tea catechins: effect of the cosurfactant on the separation selectivity, Electrophoresis 24 (2003) 1658–1667.
[9] A. Dube, K. Ng, J.A. Nicolazzo, I. Larson, Effective use of reducing agents and nanoparticle encapsulation in stabilizing catechins in alkaline solution, Food Chem. 122 (2010) 662–667.
[10] D. Li, N. Martini, Z. Wu, J. Wen, Development of an isocratic HPLC method for catechin quantification and its application to formulation studies, Fitoterapia 83 (2012) 1267–1274.
[11] C. Levin, H. Maibach, Exploration of alternative and natural drugs in dermatology, Arch. Dermatol. 138 (2002) 207–211.
[12] J.Y. Fang, T.H. Tsai, Y.Y. Lin, W.W. Wong, M.N. Wang, J.F. Huang, Transdermal delivery of tea catechins and theophylline enhanced by terpenes: a mechanistic study, Biol. Pharm. Bull. 30 (2007) 343–349.
[13] A.A. Al-Hazzani, A.A. Alshatwi, Catechin hydrate inhibits proliferation and mediates apoptosis of SiHa human cervical cancer cells, Food Chem. Toxicol. 49 (2011) 3281–3286.
[14] S.R. Pinnell, Cutaneous photodamage, oxidative stress, and topical antioxidant protection, J. Am. Acad. Dermatol. 48 (2003) 1–22.
[15] R. Cooper, D.J. Morr'e, D.M. Morr'e, Medicinal benefits of green tea: part I. Review of noncancer health benefits, J. Altern. Complement. Med. 11 (2005) 521–528.
[16] Y. Shoji, H. Nakashima, Glucose-lowering effect of powder formulation of African black tea extract in KK-A(y)/TaJcl diabetic mouse, Arch. Pharm. Res. 29 (2006) 786–794.
[17] C. Ramassamy, Emerging role of polyphenolic compounds in the treatment of neurodegenerative diseases: a review of their intracellular targets, Eur. J. Pharmacol. 545 (2006) 51–64.
[18] L. Wu, Q.L. Zhang, X.Y. Zhang, C. Lv, J. Li, Y. Yuan, F.X. Yin, Pharmacokinetics and blood–brain barrier penetration of (+)-catechin and (−)-epicatechin in rats by microdialysis sampling coupled to high-performance liquid chromatography with chemiluminescence detection, J. Agric. Food Chem. 60 (2012) 9377–9383.
[19] P. Chatterjee, S. Chandra, P. Dey, S. Bhattacharya, Evaluation of anti-inflammatory effects of green tea and black tea: a comparative in vitro study, J. Adv. Pharm. Technol. Res. 3 (2012) 136–138.
[20] C. Manach, G. Williamson, C. Morand, A. Scalbert, C. Rémésy, Bioavailability and bioefficacy of polyphenols in humans. I. Review of 97 bioavailability studies, Am. J. Clin. Nutr. 81 (2005) 230S–242S.
[21] C.H. Chen, M.F. Hsieh, Y.N. Ho, C.M. Huang, J.S. Lee, C.Y. Yang, Y. Chang, Enhancement of catechin skin permeation via a newly fabricated mPEG-PCL-graft-2-hydroxycellulose membrane, J. Membr. Sci. 371 (2011) 134–140.
[22] D.W. Tang, S.H. Yu, Y.C. Ho, B.Q. Huang, G.J. Tsai, H.Y. Hsieh, H.W. Sung, F.L. Mi, Characterization of tea catechins-loaded nanoparticles prepared from chitosan and an edible polypeptide, Food Hydrocoll. 30 (2013) 33–41.
[23] P.K. Mukherjee, R.K. Harwansh, S. Bhattacharyya, Bioavailability of herbal products: approach toward improved pharmacokinetics, in: P.K. Mukherjee (Ed.), Evidence-Based Validation of Herbal Medicine, Elsevier, Amsterdam 2015, pp. 217–245.
[24] R.K. Harwansh, K.C. Patra, S.K. Pareta, Nanoemulsion as potential vehicles for transdermal delivery of pure phytopharmaceuticals and poorly soluble drug, Int. J. Drug Deliv. 3 (2011) 209–218.

[25] S. Shafiq, F. Shakeel, S. Talegaonkar, F.J. Ahmad, R.K. Khar, M. Ali, Development and bioavailability assessment of ramipril nanoemulsion formulation, Eur. J. Pharm. Biopharm. 66 (2007) 227–243.
[26] H. Choudhury, B. Gorain, S. Karmakar, E. Biswas, G. Dey, R. Barik, M. Mandal, T.K. Pal, Improvement of cellular uptake, in vitro antitumor activity and sustained release profile with increased bioavailability from a nanoemulsion platform, Int. J. Pharm. 460 (2014) 131–143.
[27] H. Bu, X. He, Z. Zhang, Q. Yin, H. Yu, Y. Li, A TPGS-incorporating nanoemulsion of paclitaxel circumvents drug resistance in breast cancer, Int. J. Pharm. 471 (2014) 206–213.
[28] R.K. Harwansh, K.C. Patra, S.K. Pareta, J. Singh, M.A. Rahman, Nanoemulsions as vehicles for transdermal delivery of glycyrrhizin, Braz. J. Pharm. Sci. 47 (2011) 769–778.
[29] S. Khurana, N.K. Jain, P.M.S. Bedi, Nanoemulsion based gel for transdermal delivery of meloxicam: physicochemical, mechanistic investigation, Life Sci. 92 (2013) 383–393.
[30] E. Paglia, W.N. Valentine, Studies on the quantitative and qualitative characterisation of erythrocyte glutathione peroxidase, J. Lab. Clin. Med. 70 (1967) 158–169.
[31] B. Kakkar, P.N. Das, A. Viswanathan, Modified spectrophotometer assay of SOD, Ind. J. Biochem. Biophys. 21 (1984) 130–132.
[32] R.F. Beers, I.W. Seizer, A spectrophotometric method for measuring breakdown of hydrogen peroxide by catalase, J. Biol. Chem. 115 (1952) 130–140.
[33] H. Ohkawa, N. Hash, K. Yagi, Assay for lipid peroxide for animal tissue by thiobarbituric acid reaction, Ann. Biochem. 95 (1979) 351–358.
[34] O.H. Lowry, N.J. Rosebrough, A.L. Forr, R.J. Ramdall, Protein measurement with the Folin phenol reagent, J. Biol. Chem. 193 (1951) 265–275.
[35] F. Chainiaux, J. Magalhaes, F. Eliaers, J. Remacle, O. Toussaint, UVB-induced premature senescence of human diploid skin fibroblasts, Int. J. Biochem. Cell Biol. 34 (2002) 1331–1339.
[36] D.Q.M. Craig, S.A. Barker, D. Banning, S.W. Booth, An investigation into the mechanisms of self-emulsification using particle size analysis and low frequency dielectric spectroscopy, Int. J. Pharm. 114 (1995) 103–110.
[37] F. Shakeel, W. Ramadan, Transdermal delivery of anticancer drug caffeine from water-in-oil nanoemulsions, Colloids Surf. B 75 (2010) 356–362.
[38] V. Bali, M. Ali, J. Ali, Nanocarrier for the enhanced bioavailability of a cardiovascular agent: in vitro, pharmacodynamic, pharmacokinetic and stability assessment, Int. J. Pharm. 403 (2011) 46–56.
[39] R.J. Batchelder, R.J. Calder, C.P. Tomas, C.M. Heard, In vitro transdermal delivery of the major catechins and caffeine from extract of *Camellia sinensis*, Int. J. Pharm. 283 (2004) 45–51.
[40] J.Y. Fang, H.T.L. wang, Y.L. Huang, C.L. Fang, Enhancement of the transdermal delivery of catechins by liposomes incorporating anionic surfactants and ethanol, Int. J. Pharm. 310 (2006) 131–138.
[41] J. Suppasrivasuseth, R.A. Bellantone, F.M. Plakogiannis, G. Stagni, Permeability and retention studies of (−)epicatechin gel formulations in human cadaver skin, Drug Dev. Ind. Pharm. 32 (2006) 1007–1017.
[42] Y.P. Lu, Y.R. Lou, J.G. Xie, Q.Y. Peng, J. Liao, C.S. Yang, M.T. Huang, Topical applications of caffeine or (−)-epicatechin gallate (EGCG) inhibit carcinogenesis and selectively increase apoptosis in UVB-induced skin tumours in mice, Proc. Natl. Acad. Sci. 99 (2002) 12455–12460.
[43] R. Gannu, C.R. Palem, V.V. Yamsani, S.K. Yamsani, M.R. Yamsani, Enhanced bioavailability of lacidipine via microemulsion based transdermal gels: formulation optimization, ex vivo and in vivo characterization, Int. J. Pharm. 388 (2010) 231–241.
[44] H. Chaudhary, K. Kohli, V. Kumar, A novel nano-carrier transdermal gel against inflammation, Int. J. Pharm. 465 (2014) 175–186.
[45] R.K. Harwansh, P.K. Mukherjee, S. Bahadur, R. Biswas, Enhanced permeability of ferulic acid loaded nanoemulsion based gel through skin against UVA mediated oxidative stress, Life Sci. 141 (2015) 202–211.